Amine Functionalized and Cation-Exchanged Zeolites for Selective Adsorption of Carbon Dioxide over Nitrogen and Methane

Thesis

Submitted in partial fulfillment of the
requirements for the degree of

DOCTOR OF PHILOSOPHY

by

Geetanjali Bhati

Roll No. 166107117

Department of Chemical Engineering

Indian Institute of Technology Guwahati

Guwahati 781039, INDIA

March, 2025

Department of Chemical Engineering
Indian Institute of Technology Guwahati
Guwahati 781039 (INDIA)

STATEMENT

I hereby declare that the work presented in this thesis, titled "**Amine Functionalized and Cation-Exchanged Zeolites for Selective Adsorption of Carbon Dioxide over Nitrogen and Methane**," is the result of original research carried out by me at the Department of Chemical Engineering, Indian Institute of Technology Guwahati, North Guwahati, India, under the guidance of Prof. Bishnupada Mandal and Prof. Ramagopal V. S. Uppaluri. Following the standard practices of scientific reporting, I acknowledge all sources and references that have contributed to this work.

March, 2025 **Geetanjali Bhati**

Department of Chemical Engineering Indian Institute of Technology Guwahati
Guwahati 781039 (INDIA)

CERTIFICATE

It is certified that the work contained in the thesis entitled **"Amine Functionalized and Cation-Exchanged Zeolites for Selective Adsorption of Carbon Dioxide over Nitrogen and Methane"**, by Geetanjali Bhati has been carried out under our supervision and that this work has not been submitted elsewhere for a degree.

(Prof. Bishnupada Mandal)
Department of Chemical Engineering
IIT Guwahati, Guwahati – 781039, India

(Prof. Ramagopal V. S. Uppaluri)
Department of Chemical Engineering
IIT Guwahati, Guwahati – 781039, India

Dedicated to

My Daughter, Husband,

Parents, Sister, and In-laws

ACKNOWLEDGMENTS

I am deeply indebted to everyone who contributed directly or indirectly to my tenure in the Ph.D. curriculum at IIT Guwahati. To each of you, I offer my heartfelt gratitude.

First and foremost, I wish to express my deepest appreciation to my Ph.D. thesis Co-ordinating Supervisor, Prof. Bishnupada Mandal, whose unwavering guidance, insightful discussions, and steadfast support have been invaluable. I consider myself incredibly fortunate to have had the privilege of working under Your supervision. You have not only guided me through the complexities of academic life but have also prepared me for the career I have always aspired for in the future journey of my life. Along with the invaluable lessons taught to me in your able guidance, Your patience and continuous encouragement will forever be cherished. I hope to pass on the wisdom You've imparted to many others in the future.

I am equally grateful to my other Ph.D. thesis Supervisor, Prof. Ramgopal V. S. Uppaluri, for his invaluable suggestions and his extraordinarily motivational and supportive attitude. Beyond the technical guidance, I have learned from You the importance of approaching the stiffer challenges in the research problem with calmness and steadiness. Your kind words and positivity-enhancing enthusiasm have been a source of confidence and inspiration. With all these, it has been a true pleasure to have You as my Ph. D. thesis Supervisor.

I would also like to extend my sincere appreciation to all members of my doctoral committee for their very useful comments that enhanced the diversity and subjective depth in the technical content of my Ph.D. thesis research works. A special thanks to Prof. Animes Kumar Golder, Prof. G. Pugazhenthi, and Prof. Lalit Mohan Pandey for providing very useful suggestions during annual

progress seminars. These enhanced productivities in my research engagements, and thereby enhanced the subjectivity and depth in the addressed characterization studies.

I wholeheartedly express my thanks and gratitude to the faculty of the Department of Chemical Engineering at IIT Guwahati for their continuous guidance and encouragement. I am also thankful to the staff members for ensuring a conducive working environment at the Department.

I am profoundly thankful to the Central Instruments Facility, Centre for the Environment, Central Workshop, and Analytical Lab Facility at the Department of Chemical Engineering at IIT Guwahati. The high-end resources at these entities were instrumental in conducting BET, FESEM, FETEM, XRD, XPS, FTIR, and TGA analyses. Special thanks to Mr. Rupjyoti Dutta from MSTD, CSIR-North East Institute of Sciences and Technology, Jorhat, and Dr. Atul Kumar Singh from the Central Research Facilities (CRF) at IIT Delhi for their assistance with the XPS analysis.

Next, I extend my deepest gratitude to my senior colleagues, Dr. Satyannaryana Edubilli, Dr. Babul Prasad, Dr. Ramesh Tellagorla, Dr. Prudhviraj Medikonda, Dr. Pradip Das, Dr. Sushma Chakraborty, Dr. Imdadul H. Mandal, Dr. Aritra Das, and Dr. Sukanya Kundu, for their invaluable advice and mentorship. With my lab mates — Dr. Khalid Mehmood Wani, Dr. Preetisagar Talukdar, Dr. Thangsei Nengneilhing Baite, Dr. Udaratta Bhattacharjee, Dr. Prabhat Patel, Dr. Tinka Singh, Dr. Shika Singh, Dr. Aviti Katare, Dr. Amit Kumar, Ms. Paushali Mukherjee, Mr. Nuruzzaman Choudhury, Mr. Shubham Kumar, Ms. Tchummegne Koum Ida, Ms. Kumudhini Akasapu, Mr. Kamal Narayan Baruah, Mr. Dharanikota Nagaphani Sai Kumar, Mr. Shashi Bhushan Singh, Ms. Ahana Dutta, Ms. Sneha Singh, Mr. Tapas Das, and Mr. Bhrigu Talukdar— it has been an incredible journey of shared knowledge and collaboration. I wholeheartedly appreciate such friendly environment at both labs of Prof. Bishnupada Mandal and Prof. Uppaluri.

To my friends (Mrs. Subratee Das, Dr. Dipti Kanika Mahato, Dr. Dipa, Dr. Shivani Gupta, and Dr. Jenasree Hazarika), who have been a constant source of support and camaraderie during my time here, I am immensely grateful. Your friendships have enriched my life beyond measure.

Lastly, my deepest thanks and love go to my Daughter, Husband, Parent, Sister, and In-laws. Your unwavering love, support, and blessings have been my greatest strength. I am truly blessed to have such a wonderful family, and I am forever grateful to God for this gift.

Date: 17 March 2025

Place: IIT Guwahati **(Geetanjali Bhati)**

Vitae

Geetanjali Bhati

Guwahati, Assam, Assam | +91-8769112979

geetbhati@iitg.ac.in

Experience

- IIT Guwahati, Assam, Guwahati
  Teaching Assistant (01/2017 – 12/2021)
- Global Institute of Technology, Jaipur, Rajasthan
  Assistant Professor (02/2016 – 05/2016)
- Reliance Industries Limited, Navi Mumbai, Maharashtra
  Trainee (05/2014 – 05/2015)

Skills

Teamwork, Qualitative Research, Research Writing

Education

- IIT Guwahati, North Guwahati, Assam
  Ph.D. (Chemical Engineering, Pursuing)
- Nirma University, Ahmedabad, Gujarat
  M.Tech. (Chemical Engineering, 2015)
- Jaipur National University, Jaipur, Rajasthan
  B. Tech. (Chemical Engineering, 2013)
- Kendriya Vidyalaya, Beawar, Rajasthan
  Senior Secondary (2009)
- Kendriya Vidyalaya, Beawar, Rajasthan
  Secondary (2007)

Awards

Best Oral Presentation in CHEMCON 2022 (Ph.D.), Gold Medalist in Chemical Engineering Department (B. Tech.)

Certificates

May 2014 to May 2015 - Trainee (Reliance Industries Limited), June 2012 - Summer Trainee (Indian Oil Corporation Limited), June 2011 - Summer Trainee (Hindustan Zinc Limited)

Publications

- **G. Bhati**, D. N. P. Sai Kumar, B. Mandal, and R. Uppaluri, "Investigating the synergistic effects of various amine groups on Zeolite-Y for CO_2 capture" Environmental Science and Pollution Research (**Springer, Impact Factor 5.8**)

- G. Bhati, D. N. P. Sai Kumar, B. Mandal, and R. Uppaluri, "CO_2 selectivity and adsorption performance of K_2CO_3-modified zeolite: a temperature-dependent study" Environmental Science and Pollution Research (**Springer, Impact Factor 5.8**).
- G. Bhati, D. N. P. Sai Kumar, B. Mandal, and R. Uppaluri, "Influence of Cation Exchange on the Selective CO_2 Adsorption Performance of Zeolite-Y Over CH_4 and N_2" (**Elsevier, Impact Factor 4.8**).

Research Output

Thesis Publications

1. **G. Bhati**, D. N. P. Sai Kumar, B. Mandal, and R. Uppaluri, Investigating the synergistic effects of various amine groups on Zeolite-Y for CO_2 capture, Environmental Science and Pollution Research, (2024) https://doi.org/10.1007/s11356-024-33869-8.
2. **G. Bhati**, D. N. P. Sai Kumar, B. Mandal, and R. Uppaluri, Influence of Cation Exchange on the Selective CO_2 Adsorption Performance of Zeolite-Y Over CH_4 and N_2, Microporous and Mesoporous Materials, 387 (2025) 113537, https://doi.org/10.1016/j.micromeso.2025.113537.
3. **G. Bhati**, D. N. P. Sai Kumar, B. Mandal, and R. Uppaluri, CO_2 selectivity and adsorption performance of K_2CO_3-modified zeolite: a temperature-dependent study, Environmental Science and Pollution Research**,** 31 (2024) 65051–65065, https://doi.org/10.1007/s11356-024-35493-y.

Conferences

1. **G. Bhati**, R. Uppaluri and B. P. Mandal. Synthesis of Amine-Functionalized Zeolites for Carbon Dioxide Separation. AIChE Annual Meeting 2019, Orlando, Florida, USA, Nov 12 (2019) (**Poster presentation**)
2. **G. Bhati**, B. Mandal, and R. Uppaluri, Effect of amine groups on Zeolite-Y for carbon dioxide adsorption, CHEMCON 2023, HIT Kolkata, Dec 27-30 (2023) (**Oral Presentation**)
3. **G. Bhati**, B. Mandal, and R. Uppaluri, Role of primary, secondary, and tertiary amines on carbon dioxide capture, ICPHD 2023, IIT Guwahati, Nov 03-05 (2023) (**Oral Presentation**)
4. **G. Bhati**, B. Mandal, and R. Uppaluri, Synthesis, and characterization of amine-functionalized Zeolite-Y to enhance the carbon dioxide adsorption capacity, CHEMCON, HBTU Kanpur, Dec 27-30 (2022) (**Oral Presentation**)

Workshop Attended

1. **Grow A Future Proof Green-Career**

   A one-day workshop titled "Valuable insights and tools to build a sustainable and fulfilling career in the green industry" Mar 05, 2024 at IIT Guwahati, North Guwahati, Assam (Jointly organized by Carbon Mandal and IIT Guwahati, India)

Abstract

Global warming issues are exacerbated with the ever-increasing concentrations of CO_2 in the atmosphere. For quite some time, considerable efforts have been directed to suppress this challenging issue. The ever-increasing atmospheric CO_2 concentrations caused by human activity have prompted researchers to develop and apply separation processes to reduce CO_2 emissions from large-point emitters. Among alternate separation technologies, the adsorption-based processes are viable and promising options.

The Ph.D. thesis research works involved the adsorption-based gas adsorption with Zeolite-Y as a support material. The zeolites are inorganic crystals with uniform pores of molecular dimension. Thereby, they have numerous applications in terms of adsorption, purification, separation, and pollution control. Various industrial applications utilize zeolites and this is due to their superior cation-exchange ability, catalytic capabilities, and molecular sieve.

The adsorption characteristics of modified Zeolite-Y adsorbents have been extensively studied in this Ph.D. thesis. The gases deployed were carbon dioxide (CO_2), methane (CH_4), and nitrogen (N_2). Due to its good performance, the Zeolite-Y adsorbent was eventually modified with the amines or cations and the loaded adsorbents being achieved with the impregnation method demonstrated their efficacy in terms of the carbon dioxide adsorptive capacity.

The thesis research work constitutes four hierarchical phases or parts. The first part of the conducted studies focused on converging upon the identification of the best commercial adsorbent as a support material among three chosen alternate commercial zeolites (Zeolite-Y, Beta, and ZSM-5). The best support was identified in terms of the highest carbon dioxide adsorption capacity which is being conducted through the gravimetric analysis. Thereafter, in the second part of the

study, the best-performing Zeolite-Y has been loaded with monoethanolamine, diethanolamine, and triethanolamine. Thereafter, the ability of the functionalized zeolites was assessed in terms of their ability to adsorb carbon dioxide. Further characterization such as XRD, BET, FTIR, and FESEM were also conducted to corroborate the measured adsorption capacities with the morphological analysis. Adsorbents containing 1, 5, and 10 wt.% amine groups have been shown to adsorb carbon dioxide between 1.14 and 2.26 mmol g^{-1} at 303 K up to 1 bar. The gas (CO_2, CH_4, and N_2) adsorption studies were conducted on optimized material According to a thermodynamic perspective, the experimental results for CO_2 adsorption were well concordant with the Virial adsorption isotherm. The Ideal Adsorbed Solution Theory (IAST) was utilized to determine the selectivity of 5 mol% of CO_2 for CO_2/CH_4 and 13 mol% of CO_2 for CO_2/N_2 at 303K for optimized material. The cyclic adsorption-desorption study (up to 4^{th} cycles) of MEOH5 has performed well. This affirmed that the adsorbent may be used for longer-term processes and without major adsorption capacity loss. In summary, among the considered synthetic amine-loaded adsorbents, it was found that the monoethanolamine-loaded Zeolite-Y is a promising adsorbent for carbon dioxide adsorption applications.

The third part of the research involved the synthesis and characterization of cation-loaded Zeolite-Y sorbents and the subsequent assessment of their potential for enhanced CO_2 capture. The synthesized adsorbents were characterized through FTIR, XRD, BET, TEM, and XPS. The characterization assessments were conducted for the wet impregnation-based lithium or sodium or potassium cations-loaded Zeolite-Y adsorbents (5 wt.% loadings). Thereafter, gravimetric analysis was conducted for the evaluation of the best adsorbent. Adsorbents containing cations have been shown to selectively adsorb CO_2 to CH_4, and N_2 in the temperature range of 303-343 K and up to 1 bar pressure. It was assessed that the higher basicity enhanced gas adsorption capacity (i.e. Li^+

< Na^+ < K^+). The modeling studies showed that the Viral adsorption isotherm model is the best fit for CO_2 and Langmuir is the best fit for CH_4 and N_2 adsorption. The heat of adsorption is higher for CO_2 in comparison to the CH_4 and N_2. This is due to the higher quadrupole moment and polarizability. The selectivity prediction of CO_2 gas from IAST for two binary gas mixtures (CO_2/CH_4 and CO_2/N_2) was also addressed in the temperature range of 303-343 K. The KYZC exhibited the highest CO_2 uptake (2.89 mmol g^{-1}) among all synthesized adsorbents and relatively superior CO_2 sorption capacity with respect to both CH_4 and N_2 at 303 K and 1 bar process conditions.

The fourth and final part of the Ph.D. thesis work involved the examination of the influence of several parameters such as loading, temperature, and pressure for the potassium-loaded zeolite sorbent. The K_2CO_3-impregnated Zeolite-Y adsorbents were characterized by FTIR, XRD, TGA, BET, FETEM, and XPS. The synthesized adsorbents were assessed for their adsorptive efficacy for three alternate gases (CO_2, CH_4, and N_2). It was assessed that a variation in K_2CO_3 loading from 5-15 wt.% did result in a reduced CO_2 adsorption capacity from 3.61-1.73 mmol g^{-1}. The modeling studies were conducted. Thereby, it was affirmed that the Virial adsorption isotherm model has been the best fit for CO_2 adsorption and the Langmuir adsorption isotherm model is the best fit for CH_4 and N_2. The equilibrium modeling studies also conveyed that the K_2CO_3-loaded adsorbent is economically feasible for commercial carbon dioxide capture applications as the sorbent is stable and optimally loaded with potassium-carbonate. Based on the experimental single-component adsorption isotherms, the Ideal Adsorbed Solution Theory (IAST) was utilized to determine the selectivity of 5 mol% of CO_2 for CO_2/CH_4 (selectivity = 280) and 13 mol% of CO_2 for CO_2/N_2 (selectivity = 6) at lower pressure. Such investigations were conducted in the 303-343 K temperature range up to 1 bar to mimic the condition of natural gas and flue gas streams.

The KYZC10 exhibited excellent cyclic (up to 8th cycles) adsorption-desorption performance and thermal stability among all synthesized materials.

The novelty of the PhD research works is in the dual approach based on carbon dioxide adsorption capacity enhancement. This has been addressed for the Zeolite-Y through the dual role of carbonate loading and cation exchange in the cation-loaded carbonate exchanged Zeolite-Y adsorbent. Such adsorbent's performance has been assessed in the PhD thesis to be superior to even the best amine-functionalized Zeolite-Y sorbent. Thus, the thesis research work is distinguished in terms of the development and comparative assessment of two distinct types of adsorbents i.e. amine-functionalized Zeolite-Y and cation-loaded carbonate exchanged Zeolite-Y. Thus, the utility of carbonates in cation exchange-based sorbents not only significantly propels CO_2 adsorption capacity but also provides a cost-effective alternative to the expensive amines that are traditionally used in industrial applications. The demonstrated innovative strategy for the cation-loaded carbonate exchanged zeolite provides an innovative strategy for large-scale carbon capture's practical, viable, and economical solution. Further efforts in this direction can be conveniently targeted through the advances in materials science and engineering approaches. Accordingly, versatile and highly efficient sorbents for CO_2 capture in various applications can be sought and realized.

List of Figures

Figure No.	Figure Caption	Page No.
Figure 1.1	Schematic diagram depicting carbon capture, and storage (CCS) technology	4
Figure 2.1	Schematic representation of gravimetric adsorption system for gas adsorption studies.	68
Figure 3.1	(a) XRD pattern and (b) FTIR spectra of commercial zeolites	99
Figure 3.2	FESEM images of (a) YZC, (b) Beta, and (c) ZSM-5 at 20kX magnification	101
Figure 3.3	N_2 adsorption-desorption isotherm plot of commercial zeolites	103
Figure 3.4	(a) CO_2, (b) CH_4, and (c) N_2 adsorption capacities at 303K for commercial zeolites	105
Figure 3.5	(a) TGA curve and (b) XRD pattern of amine-functionalized Zeolite-Y samples	107
Figure 3.6	Nitrogen adsorption isotherms at 77 K of the amine-functionalized Zeolite-Y	108
Figure 3.7	FTIR spectra of Zeolite-Y and amine-functionalized Zeolite-Y adsorbents	110
Figure 3.8	FESEM image of pure Zeolite-Y adsorbent	111
Figure 3.9	FESEM images of (a) MEOH1, (b) MEOH5, and (c) MEOH10 adsorbents	112
Figure 3.10	FESEM images of (a) DEOH1, (b) DEOH5, and (c) DEOH10 adsorbents	113
Figure 3.11	FESEM images of (a) TEOH1, (b) TEOH5, and (c) TEOH10 adsorbents	114
Figure 3.12	Adsorption mechanism of CO_2 with (a) MEOH, and (b) DEOH	116
Figure 3.13	High-resolution XPS spectra of C1s for (a) monoethanolamine, (b) diethanolamine, and (c) triethanolamine-loaded adsorbents	117
Figure 3.14	(a) Effect of primary, secondary, and tertiary amine groups CO_2	119

	adsorption at 303K, (b) Effect of 1 wt.%, 5 wt.%, and 10wt.% monoethanolamine loading on CO_2 adsorption at 303K, and (c) CO_2, CH_4, and N_2 adsorption of MEOH5 adsorbent at 303K	
Figure 3.15	(a) Monoethanolamine, (b) Diethanolamine, (c) Triethanolamine adsorption isotherms for (▲) 1 wt.%, (●) 5 wt.%, and (◆) 10 wt.%. Symbols are experimental data; lines are fits obtained using the Virial model parameter	122
Figure 3.16	(a) CO_2 adsorption isotherms, (b) CH_4 adsorption isotherms, (c) N_2 adsorption isotherms on MEOH5 at 303 K. Symbols are experimental data; lines are fits obtained using Virial and Langmuir model parameters.	124
Figure 3.17	Heat of adsorption at zero loading of amine-functionalized Zeolite-Y	126
Figure 3.18	IAST predicted binary adsorption isotherms with pressure on MEOH5 for (a) 5 mol% for the CO_2/CH_4 mixture and (b) 13 mol% for the CO_2/N_2 mixture	128
Figure 3.19	Cyclic adsorption-desorption performance of MEOH5 adsorbent	129
Figure 4.1	FTIR spectra of commercial Zeolite-Y and cation-loaded Zeolite Y adsorbents	136
Figure 4.2	XRD pattern of commercial Zeolite-Y and cation-loaded ZeoliteY	137
Figure 4.3	(a) N_2 adsorption-desorption isotherm, and (b) Pore size distribution of commercial Zeolite-Y and cation-loaded Zeolite-Y	138
Figure 4.4	FETEM images of (a) Zeolite-Y, (b) LiYZC, (c) NaYZC, and (d) KYZC	140
Figure 4.5	High-resolution XPS spectrum of (a) YZC, (b) LiYZC, (c) NaYZC, and (d) KYZC	141
Figure 4.6	Carbon dioxide adsorption isotherm of commercial Zeolite-Y and cation-loaded Zeolite-Y at 303K	143
Figure 4.7	Carbon dioxide adsorption isotherm of (a) HYZC, (b) LiYZC, (c) NaYZC, and (d) KYZC at (●) 303 K, (▲) 323 K, and (◆) 343 K	145
Figure 4.8	Methane adsorption isotherm of (a) HYZC, (b) LiYZC, (c)	146

	NaYZC, and (d) KYZC at (●) 303 K, (▲) 323 K, and (◆) 343 K	
Figure 4.9	Nitrogen adsorption isotherm of (a) HYZC, (b) LiYZC, (c) NaYZC, and (d) KYZC at (●) 303 K, (▲) 323 K, and (◆) 343 K	147
Figure 4.10	Heat of adsorption at zero loading of cation-loaded adsorbents for three different gases	149
Figure 4.11	IAST predicted binary adsorption isotherms at 303K with pressure on cation-loaded Zeolite-Y for (a) 5 mol% for the CO_2/CH_4 mixture and (b) 13 mol% for the CO_2/N_2 mixture	151
Figure 5.1	Attenuated total reflection (ATR) spectra of potassium carbonate loaded Zeolite-Y	160
Figure 5.2	XRD patterns of Zeolite-Y, pure K_2CO_3, and synthesized adsorbents	161
Figure 5.3	TGA analysis of Zeolite-Y, and different loading of K_2CO_3 on Zeolite-Y	162
Figure 5.4	(a) Adsorption-desorption isotherm of commercial Zeolite-Y and potassium carbonate loaded Zeolite-Y with N_2 at 77K, (b) BJH pore size distribution curve for pure and loaded adsorbents	164
Figure 5.5	TEM images of (a) YZC, (b) KYZC5, (c) KYZC10, and (d) KYZC15	166
Figure 5.6	XPS spectra of (a) YZC, (b) KYZC5, (c) KYZC10, and (d) KYZC15	167
Figure 5.7	(a) CO_2 adsorption capacities at 303 K for three different K_2CO_3 loaded Zeolite-Y, and (b) Effect of KYZC10 material for CO_2 adsorption at three different temperatures	170
Figure 5.8	(a) CO_2 adsorption isotherms, (b) CH_4 adsorption isotherms, (c) N_2 adsorption isotherms on KYZC10 at (●) 303 K, (▲) 323 K, and (◆) 343 K. Symbols are experimental data; lines are fits obtained using Virial and Langmuir model parameters	173
Figure 5.9	(a) Comparison of enthalpy of adsorption at zero loading of KYZC10 for three different gases, (b) Variation Henry constant with temperature for three different gases (●) CO_2, (▲) CH_4, and	175

(◆) N_2

Figure 5.10 IAST predicted binary adsorption isotherms with pressure on KYZC10 for (a) 5 mol% for the CO_2/CH_4 mixture and (b) 13 mol% for the CO_2/N_2 mixture 177

Figure 5.11 Cyclic adsorption/desorption performance of KYZC10 adsorbent for carbon dioxide adsorption 178

List of Tables

Table No.	Table Caption	Page No.
Table 1.1	A summary of CO_2 adsorption data of the commercial zeolites at 1 bar pressure	20
Table 1.2	A summary of CO_2 adsorption data of amine-functionalized zeolites at 1 bar and 348 K	24
Table 1.3	A summary of CO_2 adsorption data of alternate cation-loaded zeolites at 1 bar and 298 K	29
Table 1.4	A summary of CO_2 adsorption data of alternate cation exchanges and carbonate-loaded adsorbents	33
Table 2.1	A summary of second-virial coefficients of various gases	72
Table 2.2	A summary of deployed gases and their purities in the conducted experimental investigations	73
Table 2.3	A summary of various investigated adsorbents in the Ph.D. thesis and their range of operating conditions	75
Table 2.4	A summary of the adsorption-related molecular properties of various gases	76
Table 3.1	Textural properties of amine-functionalized Zeolite-Y	109
Table 3.2	Comparative evaluation of amine loading adsorbents for pure CO_2 adsorption at atmospheric pressure	120
Table 4.1	Physiochemical properties of adsorbents	139
Table 5.1	Thermal decomposition of pure Zeolite-Y and synthesized adsorbents	163
Table 5.2	Physical properties of different adsorbents.	165
Table 5.3	Gas adsorption properties	172
Table 5.4	A comparison of the CO_2 adsorption capacities and selectivity of selected commercial zeolites and best synthetic adsorbents at 303 K and 1 bar conditions	182

Notations

N_{t0}	Evacuated sample weight (g)
N_t	Excess amount adsorbed (g)
N_{eq}	Excess amount adsorbed for helium (g)
V_{buo}	Buoyancy volume (m^3)
V_B	Volume of the bucket (m^3)
V_s	Volume of the impenetrable solid (m^3)
B^{gas}	Second virial coefficient of the gas phase (m^3 K mol^{-1})
P	Pressure (bar)
R	Gas constant (J K^{-1} mol^{-1})
T	Temperature (K)
B_1, B_2, B_3, B_4, B_5	Parameters used for describing temperature dependency of second virial coefficient of gas (see Eq. 2.15)
M_w	Molar mass of the gas
N	Adsorbed gas amount (mmol g^{-1})
N^{max}	Saturation adsorption capacity (mmol g^{-1})
b	Second virial coefficient ($mmol^{-1}$ g)
c	Third virial coefficients ($mmol^{-2}$ g^2)
b^0 and b^1	Temperature independent parameters of second virial coefficients, ($mmol^{-1}$ g and $mmol^{-1}$ g K), respectively

c^0 and c^1	Temperature independent parameters of third virial coefficients, (mmol^{-1} g and mmol^{-1} g K), respectively
Δh_{ads}	Enthalpy of adsorption (kJ mol^{-1})
A	Specific surface area of the adsorbent (m^2 g^{-1})
n_i	Adsorption amount of component "i" (mmol g^{-1})
P_i	Partial pressure of a component "i" (bar)
P_i^0	Standard state pressure of component 'i' (bar)
N_0	Number of components in the mixture
n_i^0	Standard loading state (mmol g^{-1})
n_i	Number of moles of component "i" (mol)
n_T	Total number of moles (mol)
S_{ij}	Adsorption selectivity
x_i	Mole fraction of components "i" in the adsorbed phase
x_j	Mole fraction of components "j" in the adsorbed phase
y_i	Mole fraction of component "i" in the gas phase
y_j	Mole fraction of component "j" in the gas phase

Greek Letters

ρ^{gas}	Bulk density (g m^{-3})
β	Henry's constant (mmolg^{-1} bar^{-1})
β^0	Parameter related to entropy used for describing temperature dependency of Henry's constant (mmol g^{-1} bar^{-1})

β^1	Parameter related to enthalpy used for describing temperature dependency of Henry's constant (K)
π	Spreading pressure (N m^{-1})

Abbreviations

YZC	Zeolite-Y
MEOH1	1 wt.% loading of monoethanolamine loaded on Zeolite-Y
MEOH5	5 wt.% loading of monoethanolamine loaded on Zeolite-Y
MEOH10	10 wt.% loading of monoethanolamine loaded on Zeolite-Y
DEOH1	1 wt.% loading of diethanolamine loaded on Zeolite-Y
DEOH5	5 wt.% loading of diethanolamine loaded on Zeolite-Y
DEOH10	10 wt.% loading of diethanolamine loaded on Zeolite-Y
TEOH1	1 wt.% loading of triethanolamine loaded on Zeolite-Y
TEOH5	5 wt.% loading of triethanolamine loaded on Zeolite-Y
TEOH10	10 wt.% loading of triethanolamine loaded on Zeolite-Y
HYZC	H^+ cation-loaded Zeolite-Y
LiYZC	Li^+ cation-loaded Zeolite-Y
NaYZC	Na^+ cation-loaded Zeolite-Y
KYZC	K^+ cation-loaded Zeolite-Y
KYZC5	5 wt.% loading of K^+ cation on Zeolite-Y
KYZC10	10 wt.% loading of K^+ cation on Zeolite-Y
KYZC15	15 wt.% loading of K^+ cation on Zeolite-Y

List of Contents

	Page No.
Statement	ii
Certificate	iii
Dedication	iv
Acknowledgments	v-vii
Vitae	viii-ix
Research Output	x-xi
Abstract	xii-xv
List of Figures	xvi-xix
List of Tables	xx
Nomenclature	xxi-xxiii
Chapter 1: Introduction, Literature Review, and Objectives	1-58
1.1 Orientation	3
1.1.1 Impacts of Global Warming	3
1.1.2 Modes of Carbon Capture and Storage Systems	3
1.1.3 Post-combustion Methods	4
1.1.4 Introduction to Adsorption	5
1.1.5 General characteristics of adsorbents	6
1.1.6 Adsorbents for CO_2 Capture	10
1.1.7 Zeolite as a promising CO_2 capture adsorbent	13
1.2 Background for the Ph.D. thesis work	15
1.3 Prior Art	18
1.3.1 Commercial zeolite performance for CO_2 capture	18

1.3.2 Performance of amine-functionalized zeolites for CO_2 Capture 21

1.3.3 Cation-exchanged and non-carbonate-loaded zeolites for CO_2 capture 25

1.3.4 Cation-exchanged and carbonate-loaded zeolites for CO_2 capture 30

1.4 Lacunae and Possible Scope for Further Research 34

1.4.1 Identification of a commercial zeolite with enhanced CO_2 adsorption capacity 34

1.4.2 Selection of amines for functionalization of the best identified commercial zeolite 38

1.4.3 Identification of cation exchanges zeolites with enhanced CO_2 capture characteristics 42

1.4.4 Identification of cation-exchanged and carbonate-loaded zeolites with enhanced CO_2 capture characteristics 45

1.5 Objectives of the Ph.D. thesis 47

1.6 Organization of the Ph.D. Thesis 48

Chapter 2: Materials and Methods, Theories, and Models 58-95

2.1 Selection of commercial zeolite 59

2.1.1 Precursors 59

2.1.2 Characterization Techniques 60

2.1.3 Assessment of Gas Adsorption Capacity 65

2.1.3.1 Gravimetric Adsorption Setup 67

2.1.3.2 Adsorption Measurements 70

2.1.3.3 Adsorption Calculations 71

2.1.3.4 Purity of Gases 73

2.1.3.5 Adsorption process conditions 74

2.1.3.6 Physical properties of gases 75

2.1.4 Ranking methodology for the selection of the best commercial adsorbent 76

2.2 Synthesis and characterization of amine-functionalized Zeolite-Y adsorbents 77
2.2.1 Base Materials 77
2.2.2 Adsorbent Synthesis 77
2.2.3 Adsorbent Characterization 78
2.2.4 Gas Adsorption Studies 79
2.3 Synthesis and characterization of cation-loaded Zeolite-Y adsorbents 80
2.3.1 Raw Materials 80
2.3.2 Material Synthesis 80
2.3.3 Material Characterization 81
2.3.4 Evaluation of Best Isotherm Model for Pure Gas 82
2.3.5 Ideal Adsorbed Solution Theory for Gas Mixture Selectivity Estimation 86
2.3.6 Gas Adsorption Assessment Inference 88
2.4 Influence of Potassium Carbonate Loading on the Cation-Loaded Zeolite-Y Adsorbent CO_2 Capture Characteristics 88
2.4.1 Materials 88
2.4.2 Synthesis 84
2.4.3 Characterization 89
2.4.4 Modelling Studies 90
2.4.5 Application of IAST for Selectivity Prediction 91
2.4.6 Gas Adsorption Studies 91
2.5 Summary 91
Chapter 3: Exploring the Synergistic Impact of Amine-Functionalization on Zeolite-Y for Gas Adsorption 96-132
3.1 Background 97
3.2 Commercial Zeolite Assessment 98

3.2.1 Characterization 98

3.2.2 Adsorption Study 103

3.3 Amine-functionalized Zeolite 106

3.3.1 Characterization 106

3.3.2 Parameters Effect for CO_2 Adsorption 115

3.32.1 Effect of amine group 115

3.3.2.2 Effect of amine loading 118

3.3.2.3 Adsorption isotherm 120

3.3.2.4 Adsorption enthalpy 125

3.3.2.5 IAST Application 127

3.3.2.6 Cyclic Study 128

3.3.3 Summary 130

Chapter 4: Influence of Cation Exchange on the Gas Adsorption Efficiency of Zeolite-Y 133-156

4.1 Background 134

4.2 Characterization 135

4.3 Gas adsorption performance 141

4.3.1 Effect of Cation Loading 142

4.3.2 Effect of temperature 144

4.3.3 Adsorption isotherm model 145

4.3.4 Heat of Adsorption 148

4.3.5 IAST Applications 150

4.4 Summary 152

Chapter 5: Exploring CO_2 Selectivity in K_2CO_3-Modified Zeolite-Y: Loading and Temperature Effects on Adsorption Performance 157-187

5.1 Background 158

5.2 Adsorbents Characterization 159

5.3 Role of various Parameters on gas adsorption 167

5.3.1 Effect of K_2CO_3 loading 168

5.3.2 Effect of temperature 169

5.3.3 Isotherm Model 171

5.3.4 Adsorption enthalpy and Henry constant variation 174

5.3.5 Henry's Constant Calculation 174

5.3.6 IAST Applications 176

5.3.7 Cyclic Performance 178

5.4 Comparison of synthesized adsorbents for gas adsorption 180

5.5 Summary 184

Chapter 6: Conclusions and Future Scope 189-195

6.1 Conclusions 190

6.1.1 Selection of Zeolite-Y as the best commercial sorbent 190

6.1.2 Amine-functionalized Zeolite-Y characteristics 191

6.1.3 Cation-loaded Zeolite-Y 192

6.1.4 Optimally loaded potassium-exchanged Zeolite-Y sorbent characteristics 193

6.2 Future Scope 194

Appendix 196-206

CHAPTER 1

Introduction, Literature Review, and Objectives

CHAPTER 1

Introduction, Literature Review, and Objectives

In the past three decades, porous materials have captured the interest of chemists, physicists, and material scientists. This is due to their versatile applications in key areas such as adsorption, separation, purification, and catalysis. Such materials' ability to interact with gases and liquids at the molecular level makes them particularly valuable for industrial applications. Despite extensive research, synthesizing novel porous materials and evaluating their performance in these applications remain vital areas of scientific inquiry. This chapter details a comprehensive overview of carbon capture and storage (CCS) methods. The emphasis is on adsorption and developing industrially relevant adsorbents for CO_2 capture from flue and natural gases. Such details underscore the significance of research targeted in the Ph.D. thesis and the development of novel adsorbents customized for enhanced CO_2 adsorption. The chapter also outlines the key objectives of this work. These include the synthesis, characterization, and evaluation of the gas adsorption performance of the synthesized adsorbents. Relevant knowledge gaps in the mentioned research sub-themes have been detailed to coverage upon the objectives being set and stated in the last but one section of this chapter. Such discussion laid the groundwork for the detailed investigations and the findings elucidated in the subsequent chapters of the Ph.D. thesis.

Carbon dioxide (CO_2), the well-known and prominent greenhouse gas with ever-increasing atmospheric concentration, contributes to global warming, ice caps melting, and extreme weather events. Carbon capture and storage (CCS) technologies minimize such adverse effects. This is achieved through the capture of emissions from industrial sources. Among CCS technologies, adsorption is an effective process for the entrapping of CO_2 molecules onto solid materials called adsorbents. In the due course of adsorbent selection, several factors such as surface area, pore size distribution, and selectivity for CO_2 to other gases shall be considered. To date, notable adsorbents for CO_2 separation are well-known as activated carbon, metal-organic frameworks (MOFs), and

zeolites. Among these, adsorbents such as zeolites have outstanding performance. This is due to their high adsorption capacity, robust structural integrity, and ability to be engineered at the molecular level to enhance CO_2 selectivity and adsorption capacity. Thus, zeolites serve as a potent material for the mitigation of global warming effects due to their unique aluminosilicates-based microporous structure.

1.1 Orientation

1.1.1 Impacts of Global Warming

Global warming is potentially contributed by the serious issue of the ever-increasing CO_2 emissions in the environment. Thereby, the greenhouse effect occurs in which water vapor, carbon dioxide (CO_2), methane, and other such atmospheric gases absorb the outgoing infrared radiation. Thus, to counter this effect, it is important to reduce CO_2 emissions through environmentally friendly and cleaner industrial processes [1].

1.1.2 Modes of Carbon Capture and Storage Systems

The CCS systems simultaneously reduce CO_2 emissions, mitigate global climate change, enhance feasible for large-scale CO_2 sources, and reduce excess CO_2 in the atmosphere while providing society with a low-emission energy source, prioritizing efficient, environmentally friendly, and cost-effective energy systems [2]. As depicted in Figure 1, the CCS involves the sequestration of CO_2 emissions. Such an option eliminates the release of CO_2 emissions into the environment.

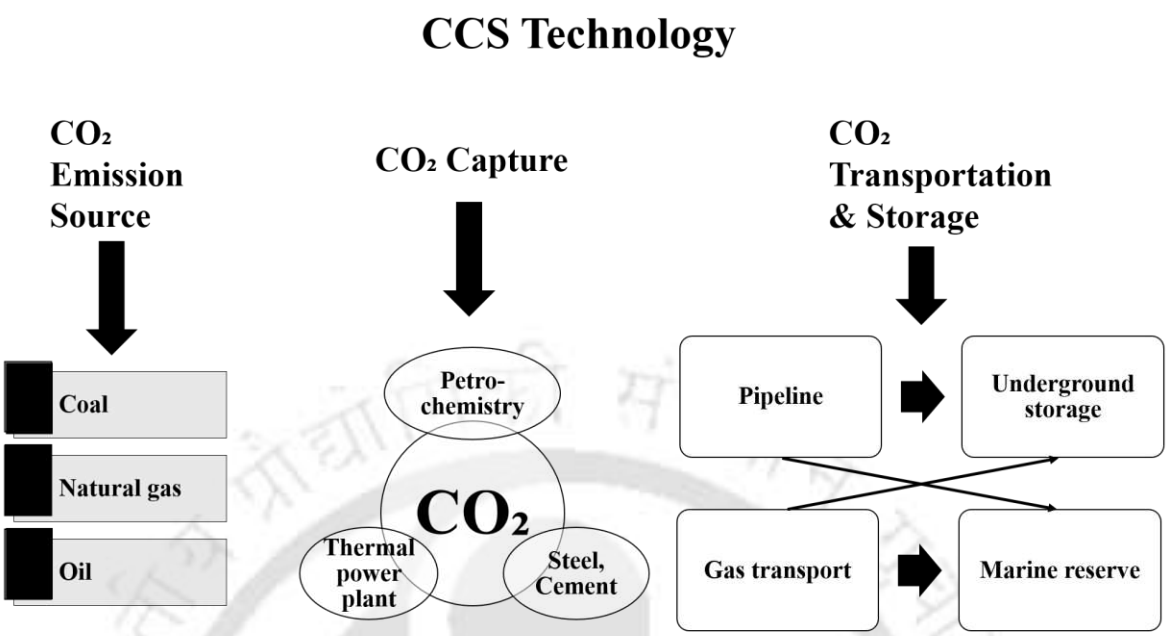

Figure 1.1: Schematic diagram depicting carbon capture, and storage (CCS) technology.

The most common technologies for CO_2 capture are post-combustion, pre-combustion, and oxy-fuel. CCS is essentially a technology that captures CO_2 and represents 70-80% of its overall costs. Various factors influence the selection of capture technology [3]. Notable among these are the state of the maturity or development of the technology, the contextual application, customization to an existing facility, retrofitting ability, and capital and operating costs [4].

Among the above-mentioned technologies, post-combustion CO_2 capture has been proven to be convenient from the perspectives of compatibility with existing infrastructure, flexibility, proven effectiveness, ease of integration, and lower initial investment costs.

1.1.3 Post-combustion methods

The post-combustion CO_2 capture technologies have been developed from the point sources. Based on their process mechanism, these processes are generally classified into absorption, adsorption,

membrane separation, cryogenic distillation, and chemical looping technologies. Among these alternate technologies, the usage of solid adsorbents for adsorption is considered to be a very promising choice. This is due to lesser energy requirements and retrofitted easily to existing plants. Adsorption is a straightforward method for the selective removal of process gases. Adsorption-based CO_2 capture is favorable due to its beneficial aspects such as quicker adsorption, higher capacity for CO_2 uptake, appropriately good selectivity, stability, and recycling ability. Other promising aspects include lower heat capacity, mitigation or no production of liquid waste, and the ability to operate over a wider range of temperatures [5].

1.1.4 Introduction to Adsorption

Adsorptive separation facilitates the separation of a gaseous mixture through the working principle of the variant adsorption and desorption properties of the gaseous constituents. Adsorption refers to the selective separation of ions, atoms, or molecules of a liquid, gas, or dissolved solid onto the surface of a material. While the ions, atoms, or molecules that are attached to the surface of materials form a layer and are referred to as adsorbate, the material to which they get attached to the surface of materials is referred to as adsorbent. The desorption is the opposite or reverse reaction of adsorption. In an adsorbent material, the atoms on the surface are different from those inside the bulk of the material. Surface atoms are exposed and not surrounded by other atoms or molecules like inside the material. This lack of surrounding atoms leaves these surface atoms with unsatisfied or unbalanced forces, making them more reactive or capable of interacting with other substances. Because these surface atoms have these unsatisfied bonds or forces, they can attract and hold onto molecules (like gases or liquids) that come into contact with the surface. This is the basic mechanism of adsorption, where molecules from a fluid phase (gas or liquid) adhere to the

surface of a solid (the adsorbent). Instead, adsorption creates surface energy through the satisfaction of the bonding needs of the adsorbent with the adsorbate entities or atoms [6]. Such a bonding is dependent upon the involved species. In the physisorption process, the adsorption occurs physically through the weak van der Waals forces. On the other hand, chemisorption involves both covalent bonding and electrostatic attraction as the principal mechanisms of adsorption.

The CO_2 adsorption process involves selective adsorption of CO_2 onto a solid surface. Subsequently, the spent adsorbent can be regenerated through either pressure reduction or temperature enhancement. Accordingly, either physical or chemical adsorption or both can occur. In the physical adsorption process, physical sorbents and inorganic porous materials (e.g., carbonaceous materials and zeolites) consume less energy than that consumed by the chemical sorbents. Since no new bond is formed between the sorbate and sorbent, much less energy is required for CO_2 regeneration. Chemical adsorption in carbon capture or separation is mostly carried out through the chemical interactions that alter existent molecular structures through the interaction with CO_2. The spent adsorbent can be regenerated through the elevation of temperature [7].

1.1.5 General characteristics of adsorbents

The selection of the right adsorbent for a contextual and customized application is tedious and difficult. Several factors such as the application, process design, desired performance, and location of the gaseous path in the capture technique are not able to ascertain upon the right choice of an adsorbent. Thus, it is vital to ensure that the adsorbent for CO_2 capture has specific desirable qualities. These are briefly stated as follows:

a. Good performance: The sorbent should be able to achieve CO_2 separation in the temperature window and pressure range of the intended application. For instance, in the case of post-combustion CO_2 capture, the sorbent should capture CO_2 from the flue gas that constitutes a low concentration of CO_2 (13-15 wt.%) at atmospheric pressure and a temperature lower than 50°C. To achieve separation, some conventional CO_2 separation processes might require compression of the entire process stream. Often, sorbents with a wide range of tunable properties are desirable as they could be tailored and customized to appropriately fit various operating environments.

b. High working capacity: In general, for a given throughput, high working capacity reduces the required volume of sorbent. This in turn reduces sorbent bed height and related equipment size, capital costs, and energy requirements. A sorbent with a steep adsorption isotherm ascertains a specified working capacity system for the lowest pressure or temperature swing. Henceforth, it is promising due to the lowest energy penalty.

c. High selectivity: The high selectivity for CO_2 to other CCS-relevant gases is essential for an efficient adsorption/desorption cycle. Thus, the selectivity determines the purity of the produced CO_2-enriched stream. This in turn plays an important role in CO_2 transportation and storage economics. Further, pre-treatment processes are also important to eliminate impurities. This often requires additional equipment and would henceforth increase capital and operating costs.

d. Dimensionless breakthrough time: The selectivity and working capacity metrics do not go hand in hand. Henceforth, a new metric called dimensionless breakthrough time (t_{break}) has been proposed. Thereby, the parameter combines both selectivity and working capacity. It is

more useful for sorbent evaluation in pressure swing adsorption (PSA) units. For an adsorbent, a high value of t_{break} is desirable as it reduces the frequency of the required regeneration.

Breakthrough time (t_{break}) is the time taken for the concentration of adsorbate (e.g., CO_2) at the outlet of an adsorption column to reach a predefined threshold, making it a critical metric for evaluating adsorbent performance. It depends on adsorption capacity, which determines how much gas the adsorbent can retain, and selectivity, which indicates the adsorbent's preference for the target gas in a mixture. Higher adsorption capacity and selectivity both extend t_{break}, as more adsorbate is retained, and competition from other gases is reduced. The formula for t_{break} encapsulates these dependencies and is grounded in mass transfer and adsorption kinetics, often modeled using isotherms (e.g., Langmuir, Freundlich) and transport equations, with inputs like equilibrium data, IAST-predicted selectivity, and column flow rates. The dimensionless breakthrough time, t_{break}, is calculated as:

$$t_{break} = f(selectivity, adsorption\ capacity)$$

where f represents a functional relationship that accounts for the simultaneous influence of selectivity and adsorption capacity on the breakthrough behavior of the sorbent.

The t_{break} is a practical metric for PSA processes as it directly reflects the time taken for the adsorbed gas to breakthrough the adsorbent under operating conditions. A higher t_{break} indicates better performance, as it reduces the frequency of regeneration cycles. Thereby, improved process efficiency and reduced operational costs can be facilitated.

Through the combination of selectivity and adsorption capacity into a single metric, the t_{break} provides a holistic evaluation of the adsorbent's suitability for PSA applications. It addresses the limitations of the independent utility of selectivity and adsorption capacity, as these metrics often optimize at different points for a given adsorbent. A high t_{break} is desirable as it implies

enhanced adsorption efficiency due to high selectivity and extended operational time between regeneration cycles due to high adsorption capacity.

e. Regeneration energy: The spent adsorbent regeneration process must be energy efficient. Therefore, CO_2 capture can be facilitated through appropriate cost-reduction strategies. For spent sorbent regeneration, several techniques including pressure swing adsorption (PSA), vacuum swing adsorption (VSA), thermal swing adsorption (TSA), electric swing adsorption (ESA), pressure-vacuum swing adsorption (PVSA), pressure-thermal swing adsorption (PTSA), and vacuum-temperature swing adsorption (VTSA) are available. It is vital to take into account both the regeneration energy and the costs of generated compressed CO_2 for the selection of a particular regeneration technique. Further, the regeneration conditions will significantly affect material performance, stability, lifetime, and sorbent make-up rate. Materials with high CO_2 loading (L), low specific heat capacity (C_S), and lower heat of adsorption (Q_r) can lead to the desired lower regeneration energy (as in the TSA case). However, the trade-off between CO_2 loading (L) and the heat of adsorption (Q_r) necessitates upon a finer balance.

f. Reaction kinetics: The working capacity in a dynamic system is a function of adsorption rate and equilibrium capacity. Henceforth, fast reaction kinetics lead to a more efficient capture technology for a post-combustion flue gas being characterized with a large volumetric flow rate. This minimizes the required sorbent quantity. Besides, it also controls the cycle time of a fixed-bed adsorption system. However, there will always be a trade-off between adsorption kinetics and regeneration energy. Henceforth, process design studies prompt upon the careful consideration of alternate options.

g. Mechanical strength: In the multicycle operation, the sorbent bed configuration such as circulating fluidized bed and severe operating conditions may cause appreciable attrition and disintegration of sorbent particles. Henceforth, sorbents should exhibit microstructural and morphological stability for the ascertaining of non-depreciable working capacity and high kinetics. This is essential to minimize the sorbent makeup rate and to ascertain upon the cost-effectiveness of the CO_2 capture process. Besides, they should also have adequate mechanical strength and ability to transform into pellets or beads.

h. Chemical stability/tolerance to impurities: The adsorbent must be tolerant to impurities that exist in the gas stream. Impurities can significantly reduce the CO_2 sorption capacity and can even degrade the sorbent crystal structure. A sorbent's ability to capture CO_2 can be negatively affected by moisture (water vapor). When moisture is present, it can occupy the active sites on the sorbent surface that would otherwise be available for CO_2, leading to a reduction in CO_2 adsorption capacity.

i. Cyclic stability: The lifetime of adsorbents, which determines the frequency of their replacement, has a significant influence on the economics of any commercial-scale adsorptive operation. Thus, the ideal sorbent should exhibit excellent cyclic stability [8].

1.1.6 Adsorbents for CO_2 Capture

For an adsorbent to be a suitable option for carbon capture and storage, it must meet certain important criteria. These include large surface area (500–1500 m^2g^{-1}), high porosity (0.3–1.5 cm^3g^{-1}), minimal thermal degradation (up to 300–800°C), chemical stability (stable in mildly acidic to neutral environments), a strong ability to selectively capture carbon dioxide (>100 or higher), low synthesis costs (<$5–10/kg), and a suitable loading capacity (2-6 mmol g^{-1}). To date, several alternate adsorbents have been synthesized for carbon capture and sequestration. These primarily

refer to zeolites, activated carbons, metal-organic frameworks, and covalent organic frameworks. Below, a brief account of these adsorbents has been presented.

Zeolites

Zeolites are aluminosilicates and constitute a framework composed of interconnected SiO_4 and AlO_4 tetrahedra that form a three-dimensional structure. The inclusion of Aluminium (Al^{3+}) ascertains a negative charge in the zeolite system. This is due to the difference in the valence states of silicon and aluminum. In such a Zeolite framework, silicon (Si^{4+}) atoms are partially replaced by aluminum (Al^{3+}) atoms. Such a substitution reduces the overall positive charge at that site as aluminum has one positive charge lower than silicon Thus, each substitution of Si^{4+} with Al^{3+} introduces a net negative charge (−1) in the framework. Such a charge imbalance is inherent to the structure and shall be optimized to maintain the stability of the Zeolite framework. To do so, the negative charge is compensated with the added (exchanged) cations into the Zeolite pores. Due to being weakly bound, the cations do have a significant role in the adsorption processes, especially for acidic gases such as CO_2. The negative charge in the framework enhances the electrostatic interaction between the framework and acidic gases such as CO_2. Thus, the exchangeable cations further strengthen the pertinent interactions and render the zeolites to function as effective adsorbents [9]. The CO_2 adsorption in the zeolites occurs primarily through the aluminum constituent in the silicate structure. The introduction of aluminum results in a negative charge in the structure. This is balanced with exchangeable cations, such as alkali metals, in the pores. These alkali cations allow zeolites to adsorb acidic gases such as CO_2. Further, it is preferable to have a low silicon (Si) to aluminum (Al) ratio (between 2 and 5) for the enhanced cation numbers in the system The inclusion of Al^{3+} in the zeolite structure is fundamental to its adsorption characteristics.

This is due to the aluminum cation creating a capable charged framework for electrostatic interactions. The resultant negative charge is a direct consequence of the lower valence of Al^{3+} in comparison to the Si^{4+}. Eventually, it is balanced with the cations in the pores. The charge imbalance is central to the good ion exchange capacity and adsorption behavior of the zeolites [10].

Activated carbon

Carbon-rich materials, such as those with well-organized porosity and carbon networks, are treated with activated carbon. High surface area, well-organized macro-, meso-, and micropores, and a variety of chemical functional groups on the surface of the sample render their suitability for a wide range of applications. Despite certainly affirming such benefits, significant alternatives need to be explored due to the alterations in the pore distribution, pore structure, and pore size. Such features are due to the wider range of the starting materials. As a result, the adsorbent performance frequently alters among various alternate activated carbon sorbents. To further enhance their CO_2 adsorption performance, carbon molecular sieves and carbon nanotubes have been developed as new-generation adsorbents [11].

Metal-organic frameworks (MOFs)

A developing type of microporous crystalline structure known as a metal-organic framework constitutes molecules with core cations being connected with the organic linkers, or ligands. Thereby, a three-dimensional structure is formed for desirable efficacy towards gas storage, nonlinear optics, CO_2 separation, and catalysis. With proven utility, the MOFs have gained their late prominence in the application domain. Since MOFs can be easily tuned for pore size and topography, they are of greater interest as CO_2 adsorbents [12].

Covalent-organic frameworks (COFs)

Constituting highly porous polymers, the COFs are crystalline with organic components being connected with covalent connections through the π-structure forms. Thus, the COFs have adaptable constituent materials that can be tailored to alter pore size and thermal and chemical stability parameters. Accordingly, with a high surface area, and good structural density, the COFs can be variegated to adopt tunable functional group alternations. They also follow a repeating pattern of the organic constituents [13].

On the other hand, the adsorption of CO_2 through zeolites is an excellent option for post-combustion gas streams. This is due to their favorable kinetics and capacities under moderate operating environments or processes. However, while deploying zeolites, the flue gas stream must be eliminated with contaminants such as NO_x, SO_x, and H_2O. Thereby, the best adsorbent performance can be ascertained. In other words, pre-treatment is mandatory for such adsorbents.

1.1.7 Zeolite as a promising CO_2 capture adsorbent

In comparison to other materials, zeolites are often considered to be superior adsorbents for carbon dioxide (CO_2) adsorption. This is due to their unique properties. Under moderate working circumstances, zeolites exhibit a high adsorption capacity. Zeolites exhibit very fast CO_2 adsorption rates. Thus, they enable the equilibrium state within very little time (a few minutes). With strong mechanical and cyclic stability, they can be transformed into granules, spheres, and extrudates. All major factors namely basicity, pore size, and the strength of the electric field generated by the exchangeable cations in the zeolites' cavities do significantly influence their sorption characteristics. During active adsorption, basicity is created along with an electric field in

the cavities. Through the enhancement of the electron density of the oxygen framework, the fundamental characteristics of zeolites being brought about by the cations enable a strong capitalization of acidic molecules [14]. Other key reasons for the consideration of zeolites for CO_2 capture are as follows:

a. Highly Ordered Porous Structure: Zeolites have a well-defined crystalline structure with uniform and highly ordered micropores. This facilitates precise control over pore size and shape. Such features are highly desired feature for the selective adsorption of CO_2 molecules. The consistent pore size distribution enhances the efficiency and capacity of CO_2 adsorption.

b. High Surface Area: The extensive internal surface area provided by the microporous structure of zeolites offers numerous active sites for CO_2 adsorption. Such a high surface area enhances the amount of CO_2 being adsorbed per unit mass of the zeolite.

c. Selectivity for CO_2: Zeolites exhibit excellent selectivity for CO_2 with respect to other gases such as nitrogen (N_2) and methane (CH_4). This selectivity is due to the specific interactions between CO_2 molecules and the framework of the zeolite. These interactions refer to electrostatic forces, van der Waals interactions, and at times chemical interactions with cations within the zeolite structure.

d. Thermal and Chemical Stability: From both thermal and chemical stability perspectives, zeolites are promising for application in a wide range of operating conditions. They can also withstand high temperatures and are resistant to degradation by various chemicals. This ensures long-term performance and durability in CO_2 capture processes.

e. Regenerability: Zeolites can be easily regenerated through the temperature swing adsorption (TSA) or pressure swing adsorption (PSA) processes. Such a promising regenerability feature allows for multiple cycles of adsorption and desorption without significant performance

loss. This renders the zeolites to be a cost-effective choice for continuous CO_2 capture applications.

f. Hydrophilic Properties: Many zeolites possess hydrophilic properties. For this reason, they are beneficial to capture CO_2 from humid gas streams. The ability to adsorb water alongside CO_2 can be beneficial in certain applications. However, such a property may also demand careful management strategies for the prevention of competitive adsorption.

g. Availability and Customizability: With their relative abundance, the zeolites can be synthesized with various compositions and with properties tailored to specific applications. Such a versatility of the features facilitates the optimal design of zeolites with the best performance characteristics for CO_2 capture. For example, the tuning of the Si/Al ratio in the zeolites adjusts its acidity and associated adsorption capacity.

In summary, the combination of higher selectivity, excellent thermal and chemical stability, ease of regeneration, and economic viability renders zeolites to be one of the best adsorbents for CO_2 capture.

1.2 Background for the Ph.D. thesis work

In the past three decades, the research and development activity in the gas adsorption characteristics has been gaining significant attention. About one-fifth of air separation is presently carried out with the adsorption technologies. Adsorbent material performance is the most important factor for ascertaining the most efficient commercial separation and purification operations in a wider range of industries. While zeolites have been used for adsorption from the 18^{th} century, their utility for gas removal gained attention in the mid-20^{th} century. Zeolites were

originally used in water softening and catalysis applications. However, in a short period, their potential for gas adsorption and purification has been demonstrated.

Amine-loaded zeolites have been emerging as promising gas adsorbents, especially for CO_2 capture applications. With improved selectivity and lower energy requirements for regeneration, the systems are promising for the traditional CO_2-capturing methods. Amine-loaded zeolites in industrial CO_2 storage and mitigation contribute to the reduction of global warming and greenhouse gas emissions. Thus, amine-loaded zeolites could be effectively utilized for CO_2 capture. Accordingly, technological advances can be achieved for the reduction of the global warming effects of CO_2.

In addition, the ion-exchange properties of the zeolites enhance their ability to adsorb specific gases, as different cations within the structure do affect adsorption performance. Various zeolite types being developed with optimized pore structures and surface chemistries reflect upon their maximum effectiveness for the capture of greenhouse gases.

In general, adsorption is primarily governed by the adsorption of high-binding energy sites and under pressure conditions. Furthermore, the adsorption characteristics of flexible adsorbents are also influenced by their structural configuration (i.e. their phase). Also, several physical properties of adsorbate, such as polarizability, polarity, and kinetic diameter have an important role in accelerating selective CO_2 adsorption. The development of zeolite-based adsorbents with tailored structures for targeted applications necessitates a systematic investigation for greater insight into the role of adsorbate properties, adsorbent structure, pores, pore volume, and the availability of cavities and channels.

In the recent past, several studies have been addressed on the efficacy of amine-functionalized adsorbents for effective CO_2 adsorption. A comparison of mesoporous adsorbents such as activated carbon, silica, alumina, and zeolites affirms that zeolites are promising candidates for CO_2 capture. Zeolites exhibit unique features such as uniform pore sizes (typically ranging from 0.4 to 1.2 nm for microporous materials), strong selective adsorption capacities (e.g., CO_2 adsorption capacities ranging from 0.04 to 2.11 mmol g^{-1} under specific conditions), excellent thermal and chemical stability (stability upto 700–800°C in some cases), and easy regeneration in multiple cycles.

Limited research activity was devoted to the utility of cation-loaded adsorbents for CO_2 adsorption and desorption. Thus, various alkali cation-loaded adsorbents can be prepared and assessed for their efficacy in terms of fabrication costs and CO_2 capture performance. For this reason, it is important to conduct systematic studies on different types of adsorbents and for similar operating conditions. Their ability to adsorb CO_2 can be assessed for their potential in terms of reusability and reduced processing costs. Zeolites loaded with alkali cations have recently received good attention for their sorption capacity to capture greenhouse gases [14].

Also, presently, alkali carbonates are being used for CO_2 capture in aqueous and dry conditions. The primary advantage of carbonate sorbents to amine-based sorbents is in terms of the lower energy requirement for spent sorbent regeneration [15]. Carbonates decompose at higher temperatures. This renders them to be suitable for multi-cycle CO_2 capture processes [16]. Several factors contribute to the effective usage of alkali metal carbonates in CO_2 capture systems. This includes higher absorption capacity, favorable thermodynamics, regenerability, cost-effectiveness, chemical stability, and operational versatility. All these properties render them to be suitable for enhanced CO_2 capture technology efficiency and for pragmatic applications. Considering these

aspects, the Ph.D. thesis aims to assess upon the alternate cation-loaded zeolites, carbonate-loaded zeolites, and amine-loaded zeolites for CO_2 sorption. Thereby, their performance shall be assessed and compared with the conventional sorption materials. Needless to say, the most competent and effective commercial zeolite must be chosen for the subsequent efforts. Henceforth, this shall be addressed as the first aim or goal of the PhD thesis.

1.3 Prior art

The prior art in the field of zeolites-based CO_2 adsorption can be broadly categorized into four sub-themes namely identification of competent commercial zeolites based on CO_2 sorption efficiency, performance assessment of amine-functionalized, cation-loaded, and cation-carbonate loaded zeolite sorbents. A brief account of these has been presented in the following sub-sections.

1.3.1 Commercial zeolite performance for CO_2 capture

Microporous crystalline aluminum-silicate zeolites have been widely used for gas adsorption applications. Zeolites produce negative charges due to the substitution of silicon with aluminum in their frameworks. This can be compensated with the cations within their pore structures. Zeolites, with variegated performance, are the recommended choice for CO_2 sorption from flue gas streams. This is dependent on several factors, such as their composition, framework structure, pore size distribution, shape, type of cations, and associated purity. Till date, several articles have been published for the assessment of the CO_2 adsorption capacity of different types of zeolites.

Choudhary et al. [17] studied the sorption isotherms of methane, ethane, ethene, and carbon dioxide on NaX (Si/Al: 1.3), NaY (Si/Al: 2.4), and NaM zeolites (Si/Al: 5.5) and with gravimetric sorption. The CO_2 adsorption capacity of NaX, NaY, and NaM zeolites are in the range of 5-6 mmol g^{-1}, 3.5-6 mmol g^{-1}, and 1.5-3.5 mmol g^{-1}, respectively for the temperature and pressure

range of 305-353K and 0-200 kPa. While the Dubinin-Polanyi equation has been the best fit for the methane sorption data for all three zeolites, the Langmuir equation has been the best fit for the CO_2 sorption data. No specific sorption equation fits with the sorption data of ethane and ethene in any of the three mentioned zeolites. Additionally, the isosteric heat of sorption for the sorption of methane, ethane, ethene, and carbon dioxide is strongly dependent upon sorbate types and zeolite sorbents.

Gomes et al. [18] reported that the Zeolite 13X can efficiently separate CO_2 from N_2/CO_2 mixtures (10 mol% CO_2, 30 mol% N_2, and balance Helium) with a packed bed column. The adsorption studies were performed in terms of both experimental and theoretical (binary-component simulation) investigations.

Ko et al. [19] improved CO_2 capture from a binary mixture of N_2/CO_2 (15% CO_2 and balance N_2) with the FVPSA (Fractionated Vacuum Pressure Swing Adsorption). The Langmuir adsorption isotherm parameters were determined from the experimental data. The high-temperature FVPSA exhibited good performance for the achievement of high purities (~90%) and recoveries of both components. This was primarily achieved due to the characteristic features of the zeolite 13X and the adopted operating conditions.

Harlick et al. [20] studied thirteen zeolite-based adsorbents in a packed column. The authors determined adsorption heats and Henry's Law constants (concentration pulse method) for CO_2 in a balanced N_2 atmosphere. The studied zeolites were 5A, 13X, NaY, NaY-10, H-Y-5, H-Y-30, H-Y-80, HiSiv 1000, H-ZSM-5-30, H-ZSM-5-25-50, H-ZSM-5-80, and HiSiv 3000. The temperature and isotherm shape profoundly influenced upon the adsorbents' working capacity in the column. Temperature enhancement in the local column reduced the adsorption capacity of the

adsorbents. According to the reported experimental findings, the zeolite-based adsorbents had the heat of adsorption in the following order: 5A > 13X > NaY > NaY-10 > HiSiv 1000 > H-ZSM-5-30 > HiSiv 3000 > H-ZSM-5-50 = H-Y-5 > H-ZSM-5-80 > H-ZSM-5-280 > H-Y-80 > H-Y-30. In the conducted study, the CO_2 adsorption capacity (1.5-2 mmol g^{-1}) of several adsorbents was evaluated in the pressure range of 0.001-1 atm. The findings were prominent for 13X, NaY, H-Y-5, ZSM-5-30, and HiSiv 3000. Among these adsorbents, the 13X had the highest capacity (~1.8 mmol g^{-1}) at 1 atm to adsorb CO_2. This is followed by NaY, H-ZSM-5-30, HiSiv 3000, and H-Y-5.

The relevant references in the thesis overview section refer to literature that reported commercial zeolite sorbents for CO_2 capture. The available information in this prior art provides useful information and supports the discussion related to the selection and application of commercial zeolites in CO_2 adsorption studies. Table 1.1 summarizes the carbon dioxide adsorption data for commercial zeolites and for alternate adsorption measurement methodologies.

Table 1.1: A summary of CO_2 adsorption data of the commercial zeolites at 1 bar pressure.

Zeolite	**T**	**N**	**Adsorption Methodology**	**Reference**
	(K)	**(mmol g^{-1})**		
H-ZSM-5	313	1.08	Gas Chromatography	[21]
Beta	303	1.76	Volumetric	[22]
NaX	273	1.14	Volumetric	[23]
Zeolite-13X	298	2.27	Gravimetric	[24]
NaUSY	303	1.2	Gravimetric	[25]
Zeolite A	293	0.2	Volumetric	[26]

1.3.2 Performance of amine-functionalized zeolites for CO_2 capture

For a long time, researchers investigated zeolites as an alternative option for CO_2 capture from the flue gases. Despite affirming numerous advantages, zeolite-based sorbents suffer from drawbacks that may profoundly limit their practical usage in the industry. These are sensitivity to high temperatures and inhibition of CO_2 adsorption under humid conditions. For this reason, few researchers modified zeolites with various amines. Till date, few articles investigated the sorption characteristics of amine-functionalized Zeolite-Y60 (AFZ). According to Jadhav et al. [27], the zeolite 13X was modified with monoethanolamine (MEA). A loading of 2, 10, and 50 wt% was considered for the impregnation method-based synthesis. The CO_2 adsorption capacity was evaluated in a packed column and for a temperature range of 30-120ºC. The feed gas constituted 15 vol% CO_2 and 85 vol% He. 13X-MEA-10, with a 10 wt% MEA loading, demonstrated the highest breakthrough (BT) adsorption capacity of 44 mLg^{-1} (0.0019 mmol g^{-1}) and surpassed the 28 mLg^{-1} (0.0012 mmol g^{-1}) capacity of unmodified zeolite 13X. This result indicated enhanced adsorption of the acidic gas CO_2 and has been due to the introduction of basicity in various matrices. At 120°C, 13X-MEA-50, with a 50 wt% MEA loading, achieved the highest adsorption capacity of 14 mLg^{-1} (0.0006 mmol g^{-1}) in comparison to 4 mLg^{-1} (0.00018 mmol g^{-1}) for unmodified zeolite and 6.6 mLg^{-1} (0.0003 mmol g^{-1}) for 13X-MEA-10. The increased adsorption capacity at 50% loading, despite the reduced pore volume and lower surface area, suggests the significance of a hybrid mechanism at higher temperatures. This is in contrast to the dominant physisorption at 30 °C.

Asuldoss et al. [28] modified ZSM-5 with amine functional groups and with a wet impregnation method. The considered amine loadings varied as 20-60 wt%. The adsorption studies were

conducted at a temperature range of 65-75°C. The sorbents loaded with primary amines exhibited much lower adsorption capacities in comparison to those loaded with secondary and tertiary amines. Grafting with a less saturated amine might facilitate better CO_2 adsorption. The study found that the TETA-modified ZSM-5 (40 wt%) exhibited the highest CO_2 adsorption capacity (60 mg g^{-1} or 1.36 mmol g^{-1}). On the other hand, the TEA-modified ZSM-5 sample exhibited the lowest CO_2 adsorption (47 mg g^{-1} or 1.06 mmol g^{-1}).

Babaei et al. [29] synthesized a new Y-type zeolite with a Si/Al molar ratio of 2.5 (NaY). The sorbent was subsequently modified with 10 wt% amines and with the wet-impregnation method. Thereby, the pure CO_2 (99.999%) adsorption capacity was measured volumetrically at 298 K and 348 K. At 298 K, the modified zeolites exhibited lower adsorption capacities than the unmodified zeolites. This is likely due to physisorption being the predominant process at this temperature. Thus, the adsorption capacity is directly proportional to the adsorbent's surface area. Thereby, the feature elucidates upon the reduced adsorption capacity of the modified zeolites at 298 K and even in the presence of amines. However, at 348 K, the modified zeolites adsorbed more CO_2. With an increase in the temperature, chemical reactions between the amino groups and CO_2 occurred and thereby carbamate species were formed. Such a behavior suggests a strongly diffusion-controlled process. In this process, more internal sites can react with CO_2 that diffuses into the particles. At lower temperatures, the slow diffusion of CO_2 in amine-loaded adsorbents results in unusually lower uptake. However, at higher temperatures, the reaction kinetics improve and thereby increase the adsorption capacity. For CO_2 capture from flue gas, which is at a higher temperature, it is important to achieve a high adsorption capacity. The amine-modified NaY zeolite exhibited promising results (CO_2 adsorption capacity of unmodified zeolites as 73.51 mg g^{-1} or 1.67 mmol g^{-1} and that of modified zeolites as 92.90 mg g^{-1} or 2.11 mmol g^{-1} at 348 K).

Dinda et al. [30] used fixed-bed flow reactors for CO_2 adsorption studies with a simulated gas mixture system (15 vol.% CO_2, balance N_2). Zeolites ZSM-5 (Si/Al: 30), Zeolite-Y, and Zeolite-13X were used as support materials. To investigate the performance of the adsorbents for CO_2 adsorption in the temperature range of 25-60°C, four different types of amines (MEA, EDA, DETA, and TETA) were impregnated (5-40 wt.%) onto various support materials. Upto an amine loading of 30 wt%, the CO_2 adsorption capacity increased, and thereafter, a decreasing trend was observed. Such reduction in CO_2 capture capacity beyond 30% amine impregnation is due to pore blockage, which hinders CO_2 molecules from gaining access to the active sites for adsorption. The CO_2 uptake capacity of MEA-, EDA-, and DETA-loaded adsorbents decreased with increasing adsorption temperature. No significant alteration in adsorption capacity was observed for the MEA-loaded adsorbent. The highest CO_2 uptake capacity for the EDA-impregnated adsorbent occurred at 25°C. For the DETA-impregnated adsorbent, the maximum adsorption capacity was at 30°C and for similar conditions. The TETA-impregnated adsorbent exhibited the highest CO_2 uptake capacity at 60°C. These results indicate that the maximum CO_2 capture capacity shifts to a higher temperature for the case in which the number of amine groups increases in the homologous series (in this regard, it shall be noted that the EDA, DETA, and TETA contain two, three, and four amine groups, respectively). Thus, TETA-loaded adsorbents exhibit their maximum capacity at 50°C, and the 30-TETA-ZSM-5 sorbent has a capture capacity of 53 g of CO_2 per kg or 1.20 mmol g^{-1} of adsorbent. In the presence of amine compounds, more basic sites are available for the chemisorption of CO_2. This observation corroborates with the surface area and pore volume analysis.

Tejavath et al. [31] conducted CO_2 adsorption studies on 40, 50, and 60 wt% amine-impregnated zeolite 13X, Zeolite 4A, and Zeolite 5A sorbents. For this purpose, 99.99% pure CO_2 gas at

temperatures ranging from 25 to 100°C was assessed for the adsorption properties of four different amines (MEA, EDA, TEA, and DETA). The DETA-loaded Zeolite 13X adsorbent (40-DETA-13X) exhibited the highest CO_2 adsorption capacity (1.054 mmol g^{-1}) in comparison to the adsorption capacity of Zeolite 13X (0.417 mmol g^{-1}). The behavior of highly loaded adsorbents up to 75°C is primarily attributed to a diffusion-controlled mechanism. Accordingly, the pores of zeolites are filled with the DETA and other amine moieties. This limits the porosity and enhances the availability of CO_2 adsorption sites loaded with the amines. The CO_2 adsorption capacities (40−60 wt%) of highly loaded adsorbents are associated with reduced diffusion resistance at higher temperatures. However, at approximately 100°C, the CO_2 adsorption capacity reduces due to the exothermic nature of the reaction. The CO_2 adsorption kinetics data were analyzed by comparing the data with the Lagergren pseudo-first- and pseudo-second-order models. This conveyed CO_2 adsorption capacities of 1.055 and 1.058 mmol g^{-1} and activation energies of 86 and 76 $kJmol^{-1}$ for 40 wt% DETA zeolite 13X, respectively.

Table 1.2 summarizes the carbon dioxide adsorption data for various amine groups and various amine loading cases.

Table 1.2: A summary of CO_2 adsorption data of amine-functionalized zeolites at 1 bar and 348 K.

Zeolite	**Amine group**	**Amine loading**	**N**	**Reference**
		(wt.%)	**(mmol g^{-1})**	
NaY	TEPA	50	2.11	[32]
NaY	DEA	50	1.77	[32]
NaY	2-MAE	50	1.94	[32]
Zeolite-13X	DETA	40	1.05	[31]

Zeolite-13X	TEA	40	0.11	[31]
Zeolite-13X	MEA	40	0.37	[31]
Zeolite 4A	TEA	40	0.37	[31]
Zeolite 4A	MEA	40	0.24	[31]
Zeolite 5A	TEA	40	0.24	[31]
Zeolite 5A	MEA	40	0.04	[31]

1.3.3 Cation-exchanged and non-carbonate-loaded zeolites for CO_2 capture

The impregnation process for zeolite modification involves the replacement of the original cations in the structure with electropositive cations that enhance acidic gas adsorption. In addition, an exchange of the alkali metal ions results in a significant increase in CO_2 adsorption. Thus, the cations that can be used for ion exchange reactions include H^+, Li^+, Na^+, K^+, Mg^{2+}, Ca^{2+}, Ba^{2+}, Fe^{3+}, and NH^{4+}. These cations enhance CO_2 adsorption through the alteration of the surface properties and structure of the zeolite. Various factors affect the ion exchange. These include the concentration, type, and time of exchanged cations.

Walton et al. [33] investigated ion exchange on NaY (Si/Al: 2.35) and NaX (Si/Al: 1.23) zeolites and with alkali metal cations such as Li^+, K^+, Rb^+, and Cs^+. Gravimetric measurements of adsorption equilibrium data for pure CO_2 (99.8%) on each material were conducted at 298 K and 1 atm. The sodium forms were subjected to cation exchange with 1.0 molar chloride solutions of Li^+, K^+, Rb^+, and Cs^+. Thereby, the 1.0 M NaCl system was the control case. The conducted study represents the first examination of adsorption equilibrium isotherms and capacities of CO_2 on the alkali metal series for both Y and X zeolites under mild conditions. Generally, it was observed that the monolayer capacity reduces with increasing cation size for both X and Y zeolites. Such a trend

suggests that the capacities are predominantly controlled by ion-quadrupole interactions. Also, steric factors restricted the acid-base effects. The highest CO_2 adsorption capacity was achieved for Li-exchanged Zeolites NaX and NaY and about 5.7 mmol g^{-1} and 5.2 mmol g^{-1}, respectively. Lithium cations, being the smallest among the studied alkali metal series, exhibit stronger ion-quadrupole interactions. This is due to their larger charge density. This is even for the case considered to be the least basic among the ion-exchanged forms.

Hudson et al. [34] considered SSZ-13 zeolites with SiO_2/Al_2O_3 = 12, and a copper derivative with Cu^{2+}/Al = 0.35 in their investigations. SSZ-13 is composed of a corner-sharing Al/SiO_4 tetrahedral structure that forms double six-membered-ring cages. Thereby, the cages stack in an ABC-type sequence. These cages connect to form a cavity with 8-membered windows (consisting of 8 oxygen and 8 Si/Al) and with approximately 3.8 Å pore diameter. Such windows provide size exclusion for gas molecule adsorption. Low-pressure adsorption of carbon dioxide and nitrogen was studied in both acidic and copper-exchanged forms of the SSZ-13 adsorbent. For low gas coverage, the isosteric heat of adsorption for CO_2 was found to be 33.1 $kJmol^{-1}$ for Cu-SSZ-13 and 34.0 $kJmol^{-1}$ for H-SSZ-13. The study included an investigation of low-pressure CO/N_2 sorption in these derivatives and henceforth provided deeper insights into site-specific adsorption properties. Such properties were accessed with neutron powder diffraction (NPD) and in combination with the in situ CO_2 and N_2 adsorption. At 1 bar and 298K, the maximum uptake was lower for the Cu^{2+}-exchanged derivative (3.75 mmol g^{-1} or 14.2 wt.%) and in comparison to the acidic form (3.98 mmol g^{-1} or 14.9 wt.%). This is due to the fact that there is only one location for the copper cation in the host framework. The NPD data were collected at sequential in-situ loadings of 0.5, 0.75, 1.0, 1.5, and 4.0 CO_2 molecules per Cu^{2+} cation. These findings demonstrated that the supercage site can accommodate a maximum of approximately 4.5 CO_2 molecules per Cu^{2+} or 12 wt.% CO_2.

The NPD of CO_2 loaded in H-SSZ-13 with 2.0 CO_2 per H^+ (about 3.0 CO_2 per Cu^{2+}) also exhibited CO_2 adsorption at the window site. The case was similarly canted into the pore. In SSZ-13, while the 3.8 Å pore window is too small for easy diffusion of N_2 (kinetic diameter 3.64 Å), the CO_2 (3.30 Å) can more freely diffuse into the pores. The ideal distance for adsorption in the window sites based on van der Waals radii leads to very high CO_2 selectivity in SSZ-13. The use of Cu^+ but not Cu^{2+} has been suggested to be the most advantageous choice, as a copper-cation-based zeolite should offer practical benefits. Cu-SSZ-13 has been inferred to be a separation material as water can significantly influence upon the overall uptake of the sieving media.

Mortazavi et al. [35] modified clinoptilolite zeolite and through a straightforward method for an enhanced CO_2 adsorption. Ion exchange through precipitation was employed to synthesize adsorbents such as clinoptilolite/Mg^{2+}, clinoptilolite/Ca^{2+}, and clinoptilolite/Li^+. CO_2 adsorption was evaluated with the volumetric method (25°C, 0-5 bar pressure range). For all cation-exchanged samples, the results demonstrated an enhancement in CO_2 adsorption capacity and altered as 4-6 mmol g^{-1} which is higher in comparison to the ~2 mmol g^{-1} of the pure zeolite. The adsorption isotherms exhibited the highest capacity for clinoptilolite/Li^+. This is attributed to the high basicity of lithium and its small atomic radius. The higher capacity observed for clinoptilolite/Ca^{2+} in comparison to clinoptilolite/Mg^{2+} would have resulted from the greater initial relative amount of calcium to magnesium in the zeolite structure.

Tobarameekul et al. [36] developed zinc-loaded NaY adsorbents with Zn loadings of 1, 3, and 5 wt.% and with the ion exchange method. Na^+ cations in the NaY zeolite structure can be readily replaced by other cations. These tend to balance excess negative charges. In this modification, two monovalent Na^+ cations were replaced by a single divalent Zn^{2+} cation. Thereby, the surface

charge characteristics were altered and this resulted in a higher surface area and an electric field gradient within the zeolite pores and frameworks. Such a modification enhanced the interaction between Zn^{2+} cations and CO_2 molecules, and lead to stronger CO_2 adsorption. The Zn/Y zeolites were tested in a packed bed reactor at various temperatures (373.15, 573.15, and 873.15 K) and CO_2 flow rates (1, 3, and 5 Lh^{-1}) and at 1 atm pressure. For the 5 wt.% Zn loading case, the maximum CO_2 adsorption capacities observed were 9.37 mmol g^{-1} and 8.99 mmol g^{-1} for zeolites derived from bagasse ash and rice husk ash, respectively. The results demonstrated that the enhanced Zn loading from 1 to 5 wt.% did enhance the CO_2 adsorption capacity. This is attributed to improved physical properties, such as the increased surface area and total pore volume. Such an effect subsequently enhanced the number of desorption sites. The highest CO_2 adsorption capacity for the bagasse ash-derived zeolite (5 wt.% Zn) was 9.45 mmol g^{-1} at 373.15 K. The study also indicated that the CO_2 adsorption capacity was reduced at higher adsorption temperatures. The lower temperatures favored physical adsorption in comparison to chemical adsorption. At a CO_2 flow rate of 1 Lh^{-1}, the maximum adsorption capacities of the zeolites developed with bagasse ash (5 wt.% Zn at 373.15 K) and rice husk ash (5 wt.% Zn at 573.15 K) were 10.33 mmol g^{-1} and 9.91 mmol g^{-1}, respectively. Furthermore, CO_2 adsorption at a flow rate of 1 Lh^{-1} was more than 0.25 times higher than the value assessed at 5 Lh^{-1}. The lower flow rates resulted in sustained CO_2 adsorption for the experimented operating time case. However, the higher flow rates increased the outflow CO_2 concentration and significantly reduced the total adsorption operating time. The longer residence time at a flow rate of 1 Lh^{-1} allowed more time for CO_2 molecules to bind. This resulted in enhanced CO_2 uptake.

Jin et al. [37] used NaX zeolite (Si/Al: 2.3) for cation exchange with a 1 mol/L LiCl solution and with the precipitation method. Li^+, being an alkali metal cation with a smaller radius than Na+, has

a higher electrostatic surface charge accumulation. Therefore, Li^+ can generate stronger electrostatic interactions with CO_2 and N_2 molecules, which have quadrupole moments. The polarizability of cations is inversely proportional to their ionic radius. Henceforth, after cation exchange, the polarizability of the zeolite increases. This leads to an increased adsorption capacity. The CO_2 adsorption process, whether in NaX or LiX, involves physical adsorption through microporous adsorption and quadrupole interactions between cations and CO_2. The adsorbent can release the adsorbed gases during desorption. This operation allows the recycling and reduced cost of CO_2 adsorption to a certain extent. The maximum adsorption capacities of CO_2 for NaX and LiX zeolites were 5.04 mmol g^{-1} and 5.57 mmol g^{-1} at 298.15 K, respectively. The adsorption isotherms of CO_2 and N_2 for NaX and LiX zeolites were well-fit with the Sip model. Such fitness is confirmed by the inhomogeneous surface properties of the adsorbents and the exothermic nature of the adsorption process. Table 1.3 summarizes CO_2 adsorption data of the cation exchange resin at 298 K and for alteration in the type of cation and loading of the cation.

Table 1.3: A summary of CO_2 adsorption data of alternate cation-loaded zeolites at 1 bar and 298 K.

Zeolite	Cation	Cation loading (wt.%)	N (mmol g^{-1})	Reference
Zeolite 13X	Li^+	4.0	1.1	[38]
Zeolite 13X	K^+	4.0	1.2	[38]
Zeolite 13X	Ca^+	4.0	1.7	[38]
RHO	Cu^{2+}	3.5	3.2	[39]
SSZ-13	Cu^{2+}	2.8	2.3	[39]
SAPO-34	Cu^{2+}	3.5	1.6	[39]
CHA	Cu^{2+}	3.5	2.5	[39]

1.3.4 Cation-exchanged and carbonate-loaded zeolites for CO_2 capture

The integration of organic amines into porous supports is considered to be a promising approach for CO_2 capture. However, the low utilization efficiency of amines and their volatilization during the regeneration process presents significant challenges. Consequently, there is a need to explore alternative sorbents. Potassium-based sorbents, such as potassium carbonate (K_2CO_3), exhibit greater thermal stability in comparison to organic amines. This renders them to be less prone to decomposition. Therefore, potassium-based sorbents may offer a more effective solution for CO_2 removal in confined environments.

Zeolite structures with carbonate groups provide additional active sites that are capable of interacting chemically with CO_2. Such an interaction is typically stronger than the physical adsorption that exists in the unmodified zeolites. CO_2 reacts with carbonate-loaded zeolites to form bicarbonate species. This effectively prompts CO_2 capture in a stable form. A carbonate-loaded zeolite excels as a CO_2 adsorbent. This is due to its improved adsorption capacity and high selectivity as well as its stability and cost-effectiveness. Carbonates of alkali metals (M_2CO_3; M = Li, Na, K), one of the possible candidates for CO_2 capture, are suitable for CO_2 separation from flue gases and for temperatures below 200ºC.

In the study conducted by Zhao et al. [40], various supports, including activated carbon (AC), Al_2O_3, zeolite 5A, zeolite 13X, and silica aerogels (SG), were utilized with K_2CO_3 as the active component to develop potassium-based sorbents. The sorbents were prepared by impregnating K_2CO_3 onto the aforementioned supports and for a theoretical loading of 30% K_2CO_3 by weight. The CO_2 sorption performances of these sorbents were evaluated under conditions of 5000 ppm CO_2, 1.8% H_2O, and balance N_2, and with a modified fixed bed reactor system coupled with a gas

analyzer at 20ºC. The measured CO_2 sorption capacities were 0.87, 1.18, 0.34, 0.53, and 0.15 mmol CO_2/g for K_2CO_3/AC, K_2CO_3/Al_2O_3, K_2CO_3/5A, K_2CO_3/13X, and K_2CO_3/SG, respectively. The results indicate that the potassium-based sorbents are capable of removing CO_2 at ambient temperature and through the chemical reaction-assisted sorption scheme. Specifically, one mole of K_2CO_3 reacts with one mole of CO_2 and one mole of H_2O to form two moles of $KHCO_3$.

Lee et al. [41] investigated the effects of calcination temperature (300ºC, 400ºC, 500ºC, 600ºC, and 700ºC) under nitrogen and air environments and for potassium-based sorbents. These sorbents were prepared with the impregnation method for the 30 wt.% K_2CO_3 loading case. The CO_2 sorption characteristics of the potassium-based sorbents, supported on ZrO_2 or TiO_2, were evaluated in a fixed bed reactor and for conditions of 9 vol.% H_2O, 1 vol.% CO_2, and balance N_2 at 60ºC. For the KZrI30 sorbents, the CO_2 capture capacities were 83–93 mg CO_2 g^{-1} sorbent (1.88-2.11 mmol g^{-1}) and irrespective of the calcination temperature and atmosphere. Such consistent performance was attributed to the formation of only K_2CO_3 and ZrO_2 phases, and without any new alloy species. In contrast, potassium-based sorbents using TiO_2 supports formed inactive K–Ti alloy species, such as $K_2Ti_2O_5$ and $K_2Ti_6O_{13}$, during calcination. Thermogravimetric analysis of the KTiI30 and KZrI30 sorbents revealed initial weight losses in the 40–150ºC range. This is due to the loss of adsorbed water. Notably, the KZrI30 sorbent exhibited no weight loss between 200ºC and 800ºC in the air. However, the KTiI30 sorbent exhibited a weight loss of approximately 9 wt.% between 500ºC and 800ºC. These findings indicate that potassium-based ZrO_2 sorbents possess excellent thermal stability below 800ºC. In conclusion, the thermal stability of potassium-based sorbents can be significantly enhanced with the ZrO_2 but not the TiO_2 as a support. The thermal stability of potassium-based sorbents supported on ZrO_2 and TiO_2 differs due to their distinct behaviors during calcination. ZrO_2-supported sorbents (KZrI30) maintained stable K_2CO_3

and ZrO_2 phases and ensured consistent CO_2 capture (1.88-2.11 mmol g^{-1}) and excellent thermal stability up to 800°C (confirmed by the TGA analysis). In contrast, TiO_2-supported sorbents (KTiI30) formed inactive K–Ti alloy phases, which compromised their CO_2 adsorption and thermal stability. In this case, the stability can be attributed to its ability to resist phase transformations and maintain structural integrity. Further, its lower sorbent performance can be attributed to its tendency to promote undesirable chemical interactions at high temperatures.

Varghese et al. [42] conducted a study that focused on three different hydrogel-derived carbon samples (CA_2U, CA_2U_2, and CA_2U_3). These samples were activated through a single-step pyrolysis process that utilized a minimal amount of environmentally friendly K_2CO_3 (CA_2U-KC, CA_2U_2-KC, and CA_2U_3-KC). The adsorption experiments were carried out at temperatures of 25°C and 0°C and for a gas mixture consisting of 15% CO_2 and 85% N_2. The selective CO_2 adsorption capacities of the prepared carbons were investigated for various pressures (up to 1 bar) and with a Quantachrome Autosorb-iQ gas analyzer. Among various samples, the CA_2U_3-KC sample exhibited the highest CO_2 adsorption capacity at 0°C (measuring 8.2 mmol g^{-1}). This was followed by the CA_2U_2-KC sample. Activation of the carbons led to enhancements in pore volumes and surface areas. This was evident in the increased CO_2 adsorption capacities of the CA_2U_2-KC (0.37 g of K_2CO_3 per gram or 0.008 mmol g^{-1}) and CA_2U_3-KC (0.23 g of K_2CO_3 per gram or 0.005 mmol g^{-1}) samples. However, the CO_2 adsorption capacity of the CA_2U_1-KC sample at 0°C remained similar to that of the CA_2U_1 sample (0.44 g per gram or 0.01 mmol g^{-1} of hydrogel-CA_2U_1). This is due to the negligible impact of K_2CO_3 activation on the pore volume and surface area of CA_2U_1-KC. The interaction strength between CO_2 and the CA_2U_1-KC sample was notably lower than that of the CA_2U_2-KC and CA_2U_3-KC samples. This conveyed the profound dependency on carbon pore size distribution. An analysis of the prepared carbon materials using Langmuir and Freundlich

isotherm models revealed improvements in the maximum monolayer capacity (q_m) for all samples after K_2CO_3 activation. This suggested an increase in available surface sites for adsorption. The Freundlich adsorption isotherm indicated physisorption for all prepared samples at 25°C, and for a heterogeneity factor (n_F) greater than 1. The choice of aqueous K_2CO_3 as the activating agent was crucial, as it facilitated the formation of macro pores and micropores within the carbon network during pyrolysis. The CO_2 adsorption data of cation-loaded by carbonate on support material have been summarized in Table 1.4.

Table 1.4: A summary of CO_2 adsorption data of alternate cation exchanges and carbonate-loaded adsorbents.

Support	Carbonate	Carbonate loading (wt%)	T (K)	Experimental conditions	Cycles	N (mmol g^{-1})	Reference
Activated carbon	K_2CO_3	30	333	1% CO_2, 9% H_2O, Balance N_2	10	1.95	[43]
Sorb NX30	Na_2CO_3	30	323	14.4% CO_2, 5.4 O_2, 10% H_2O, Balance N_2	-	2.27	[44]
γ-alumina	K_2CO_3	16	373	5% CO_2, 12% H_2O, Balance N_2	7	1.70	[45]
γ-alumina	Na_2CO_3	35	315	10% CO_2, 10% H_2O, Balance N_2	-	2.70	[46]
ZrO_2	K_2CO_3	30	333	1% CO_2, 9% H_2O, Balance N_2	10	2.10	[41]
γ-alumina	K_2CO_3	35	328	8% CO_2, 15% H_2O, Balance N_2	11	2.38	[47]
Aerogel	K_2CO_3	40	333	1.71% CO_2, 2.14% H_2O, Balance N_2	-	2.88	[48]

Table 1.3 and Table 1.4 summarize the best-reported adsorption data of the cation-doped and carbonate-based zeolite sorbents as per the literature and the best-assessed data as per the research conducted. After an extensive literature survey, no data was found that perfectly matched the reported data in the Ph.D. thesis regarding the deployed experimental setup, temperature (303 K), pressure (1 bar), and specific cation loading conditions. This underscores the novelty of the research that was conducted. Accordingly, the provided data reduces the subjective research gap associated with CO_2 sorption in the cation-loaded Zeolite-Y sorbent and at the optimized experimental conditions. However, only for comparison purposes, adsorption capacities reported for similar systems have been mentioned in the respective tables. They are deviant due to the pertinent differences in the experimental conditions. Such contextualization demonstrates that while direct comparisons are not feasible, the performance of the reported adsorbents is highly competitive and novel in the field.

1.4 Lacunae and Possible Scope for Further Research

1.4.1 Identification of a commercial zeolite with enhanced CO_2 adsorption capacity

In the mentioned sub-research theme, the carried-out research requires further insights into the following perspectives. Choudhary et al. [17] performed the sorption of methane, ethane, ethene, and carbon dioxide in Zeolite X, Zeolite Y, and Mordenite zeolites (305–353 K, 0–200 kPa) was studied with the novel gravimetric sorption apparatus. While methane sorption followed the Dubinin-Polanyi equation, carbon dioxide adhered to the Langmuir model. However, no single isotherm could describe ethane and ethene sorption across all zeolites. The isosteric heat of sorption varied with surface coverage and depended upon the sorbate and sorbent. Except for

ethene in Mordenite, sorbed molecules exhibited high mobility due to the surface coverage and ethene for the case demonstrated restricted 2D translational motion. The study did not explore alternate adsorption isotherm models that account for the surface heterogeneity. Considering this limitation, the aimed research works of the Ph.D. thesis consider the fitness studies of the measured CO_2, CH_4, and N_2 adsorption data with alternate isotherm models such as Virial and Langmuir isotherms that account for surface heterogeneity. While this research focused on commercial zeolites for their large-pore features, the thesis research aims to functionalize Zeolite-Y with amines and cations for the realization of enhanced adsorption capacity and selectivity. Additionally, the study evaluates the long-term stability of synthesized materials in terms of the multiple adsorption-desorption cyclic adsorption capacities. The thesis also targets the prediction of CO_2 selectivity with the IAST for binary gas mixtures. Such analysis-based insights have not been addressed in earlier investigations. In summary, the Ph.D. thesis research works acknowledge and extend the findings of this work and thereby offer newer directions for the improved performance of the zeolite-based CO_2 adsorption systems.

Through a combination of simulations and experiments, another investigation (Gomes et al. [18]) demonstrated the feasibility of Pressure Swing Adsorption (PSA) for CO_2 removal and recovery from flue gases using Zeolite 13X, Zeolite 5A, a carbon molecular sieve, and alumina. Experiments with a CO_2-N_2-inert gas mixture on a two-column PSA unit revealed that Zeolite 13X had the best performance due to its high capacity and favorable sorption properties. A reduction in cycle time from 240 to 130s lowered the separation efficiency but did not significantly affect the cycles needed to reach a steady state. The study maintained conditions of 600 cm^3 min^{-1} flow rate, 0.80 purge ratio, and 1 atm pressure. Temperature Swing Adsorption was suggested as a

potential alternative for improved capacity and reduced adsorption time. Such systems may offer better adsorption capacities and lower time of the adsorption process.

Harlick et al. [20] developed a selection methodology for adsorbents targeting CO_2 removal from flue gas using Pressure Swing Adsorption (PSA). Thirteen zeolite-based adsorbents, including 5A, 13X, NaY, and ZSM-5, were evaluated based on Henry's Law constants and the heat of adsorption. Using the concentration pulse method (CPM) at 40°C and 1 atm, Henry's constants for CO_2 in an N_2 carrier ranged from 6.16–9.42 mol kg^{-1} atm^{-1} for ZSM-5, 0.57–0.781 mol kg^{-1} atm^{-1} for H-Y, and 41.9 mol kg^{-1} atm^{-1} for NaY. The heat of adsorption varied with the Si/Al ratio, with values of 32.3–34.6 kJ mol^{-1} for ZSM-5 and 25.3–33.1 kJ mol^{-1} for H-Y. The study highlighted that lower Si/Al ratios in faujasite-type zeolites enhanced adsorption, and pure component CO_2 isotherms and working capacity curves for PSA were provided for Zeolite 13X, NaY, and ZSM-5. However, the sensitive influence of heat effects and operating temperature on adsorption capacities was not addressed.

Xu et al. [22] investigated the equilibrium adsorption isotherms of CO_2, CH_4, and N_2 on the β-zeolite with a Si/Al ratio of 25 by utilizing a static volumetric adsorption system. The findings revealed that zeolite exhibited the highest CO_2 adsorption capacity (1.76 mmol g^{-1}) at 303 K and 1 atm. This is followed by CH_4 (0.38 mmol g^{-1}) and N_2 (0.14 mmol g^{-1}) at the same process condition. However, the study did not explore the influence of temperature on the gas adsorption characteristics.

Zhang et al. [24] investigated CO_2 adsorption on Zeolite 13X using gravimetric adsorption method at 298–328 K and 0–30 bar. At 298 K and 1 bar, the adsorption capacity was 2.27 mmol g^{-1}, and the kinetics were well described by the linear driving force (LDF) model, with mass transfer constantly increasing with temperature. Adsorption activation energy (E_a) decreased as the

pressure increased. While the study focused on the LDF model, the virial adsorption isotherm model might have offered better accuracy for the wider pressure and temperature range studied.

García et al. [25] studied CO_2 separation from CH_4 using pressure swing adsorption with FAU and LTA zeolites and with the breakthrough experiments conducted at 303 K and 1 bar with a 50/50 CO_2/CH_4 feed. Adsorption capacities ranged from 0.3–1.0 mmol g^{-1} for FAU and 0.1–0.7 mmol g^{-1} for LTA at 303 K and 1 bar, with selectivity of 5–61 and 6–306, respectively. Lower Si/Al ratios enhanced CO_2 selectivity due to increased polarity. The Langmuir model fits single-component isotherms, and the Ruthven statistical model (RSM) identified optimal trade-offs between selectivity and working capacity. The optimal Henry constant range for CO_2 altered as 5 × 10^{-3} and 50 × 10^{-3} molecules bar^{-1} $Å^{-3}$ and the heat of adsorption altered as 27–32 kJ mol^{-1}. Even though no temperature variation studies were conducted, EMC-1, SAPO-37, Na-USY, and LTA-5 zeolites were identified as the optimal zeolites.

Several important and subjective gaps in the existing literature have been identified for the evaluation of Zeolite-Y, β-Zeolite, and ZSM-5. Despite addressing extensive research on individual zeolites, studies do not exist for the simultaneous comparison of these three specific types of zeolites for CO_2 adsorption. Each zeolite has been individually studied in various contexts. However, no comprehensive research was undertaken to include the mentioned three zeolites in a comparative analysis framework for CO_2 adsorption. The existing literature provides insights into the CO_2 adsorption capacities and characteristics of Zeolite-Y, β-Zeolite, and ZSM-5. However, these studies are often isolated and do not address a direct comparison among the three adsorbents and for common conditions of assessment. Such an absence of comparative studies represents a significant gap in terms of the understanding of these zeolites for their relative performance to one another. This is important for the selection of the most effective support material for CO_2 capture

applications. Addressing this gap requires the conduct of a comparative study of Zeolite-Y, β-Zeolite, and ZSM-5 adsorbents. Thereby, CO_2 adsorption capacities can be assessed under identical experimental conditions. Such a study will provide valuable insights into their relative performance and suitability as competent support materials for subsequent research studies that aim to achieve high-end performing adsorbents for CO_2 adsorption.

In summary, the literature does not infer the best commercial adsorbents namely, Zeolite-Y, β-Zeolite, and ZSM-5. This is the need of the hour for further enhancing the CO_2 adsorption capacity of the best adsorbent among these three sorbents. Converging upon such a zeolite will be beneficial for synthesizing super-efficient adsorbents for CO_2 separation from flue gas systems.

1.4.2 Selection of amines for functionalization of the best identified commercial zeolite

Jadhav et al. [27]] enhanced the CO_2 adsorption capacity of Zeolite 13X through the modification with monoethanolamine (MEA) and achieved loadings of 0.5–25 wt.% via the impregnation method. Further, the methanol-based incorporation had been the most feasible. The MEA-modified adsorbent demonstrated improved CO_2 selectivity, which was further enhanced with the moisture. Characterization revealed high crystallinity, surface area, and thermal stability. Breakthrough adsorption studies on a packed column (feed gas containing 15 vol.% CO_2 in He balance) affirmed that the 13X-MEA-10 had the highest capacity (1.96 mmol g^{-1}) at 303 K and outperformed unmodified zeolite (1.25 mmol g^{-1}). Adsorption efficiency improved up to 3.5 times at 393 K, and the CO_2 selectivity over N_2 was optimized at 348 K. The mechanism, involving carbamate and bicarbonate formation, requires further exploration. However, the work conducted does not detail this aspect in a comprehensive framework.

In another study (Aruldoss et al. [28]), enhanced CO_2 adsorption in ZSM-5 through its wet-impregnation method based on grafting with amines (DETA, TETA, DEA, and TEA). The amines were selected as per their boiling points and balanced adsorption performance. Secondary and tertiary amines showed higher adsorption capacities in comparison with the primary amines. The TETA-loaded sorbent (40 wt.%) achieved the highest capacity of 1.36 mmol g^{-1}. Adsorption occurred at 338–348 K and the desorption was studied at 373–383 K. Such studies confirmed the thermal stability and regenerability of the sorbents. While the study highlights promising results, it lacks details on the parametric optimality and the influence of temperature and pressure on the adsorption mechanism.

Babaei et al. [29] synthesized amine-modified Y-type zeolite (NaY, Si/Al ratio of 2.5) for the analysis of the effect of surface modification on CO_2 adsorption. Amine modifiers—diethanolamine (DEA), tetraethylenepentamine (TEPA), and 2-methylaminoethanol (2-MAE) were chosen for their high-temperature performance, which is very important for flue gas CO_2 capture. The modification enhanced CO_2 adsorption capacity and shifted the dominant mechanism from physical to chemical interaction. Adsorption capacities of TEPA-NaY, DEA-NaY, and 2-MAE-NaY were measured at 298 K (1.38 mmol g^{-1}) and 348 K, and demonstrated increased values of 2.11, 1.77, and 1.94 mmol g^{-1}, respectively. Characterization techniques confirmed surface and structural changes and highlighted the potential of these sorbents for high-temperature applications. However, more detailed temperature studies are to be addressed soon.

Dinda et al. [30] investigated CO_2 adsorption on ZSM-5, Zeolite 13X, and Zeolite-Y (Si/Al ratios of 15.6, 5.2, and 1.5, respectively) sorbents after their modification with amines such as monoethanolamine (MEA), ethylenediamine (EDA), diethylenetriamine (DETA), and triethylenetetramine (TETA). The authors adopted a fixed-bed reactor configuration and simulated

flue gas condition (15±1 vol.% CO_2 in N_2, saturated with water vapor, at a flow rate of 50±3 cc min^{-1}). The adsorption capacity increased with the number of amine groups and peaked at 30 wt.% amine loading. Among all cases, the TETA-loaded ZSM-5 achieved the highest capacity (1.20 mmol g^{-1}). Across five cycles, TETA-ZSM-5 showed capacities of 1.07, 1.04, 1.01, and 1.00 mmol g^{-1}, and demonstrated thermal stability. While optimal performance for TETA-ZSM-5 occurred at 323 K, the MEA, EDA, and DETA adsorbents exhibited reduced uptake at higher temperatures. Chemisorption was identified as the dominant mechanism. However, the exact interaction between CO_2 and amine groups remains unexplored and unexplained.

Tejavath et al. [31] studied the CO_2 adsorption capacity of amine-impregnated zeolites, including 13X, 4A, and 5A, and with 99.99% pure CO_2-based thermogravimetric analysis. Amines such as monoethanolamine (MEA), ethylenediamine (EDA), diethylenetriamine (DETA), and triethanolamine (TEA) were selected based on their forms. Among these, primary amines offered high reactivity, combinations of primary and secondary amines provided "synergistic effect and stability, and tertiary amines were the best suited for high-temperature applications. Zeolite 13X loaded with 40 wt.% DETA (13X-DETA-40) affirmed the highest CO_2 adsorption capacity and ascertained 1.69 mmol g^{-1} in a lab-scale reactor and 1.055–1.058 mmol g^{-1} in kinetic studies, and activation energies of 76–86 kJ mol^{-1}. The adsorption process was rapid, with 0.8 mmol g^{-1} adsorbed in the first two minutes. A techno-economic analysis revealed an 84% reduction in cost per ton of CO_2 adsorbed from $49,830 at the microscale to $7,690 at the lab scale. However, the study did not clarify why Zeolite 13X was chosen for the detailed investigation.

Current research often addresses and assesses a diverse range of amine functional groups. These are primary, secondary, and combinations of primary and secondary amines. However, many studies do not follow a consistent approach to the amine structure. For instance, while some studies

use amine groups with hydroxyl groups attached, others use amine groups without such modifications. Additionally, there is a lack of standardized comparison among amine-functionalized zeolites that share a common amine structure. This hinders the ability to draw definitive conclusions with respect to the sensitive influence of different amine types on CO_2 adsorption. Moreover, the literature often fails to address CO_2 adsorption trends concerning the Si/Al ratio of the zeolite framework. There is insufficient information on the influence of variant Si/Al ratios on the effectiveness of various amine-functionalized zeolites and for CO_2 capture. Such a status limits the understanding of the influence of the structural properties of the zeolites on the CO_2 adsorption performance. Such gaps shall be addressed and this involves a systematically study of amine-functionalized zeolites with primary, secondary, and tertiary amines. Thereby consistency, can be assured in the amine structure and for various samples. Additionally, a focused comparison of CO_2 adsorption performance with variant Si/Al ratios of the zeolite framework is essential. Such a research strategy will provide valuable insights into optimizing amine-functionalized zeolites for CO_2 capture and can contribute to a more comprehensive understanding of the factors that influence adsorption efficiency.

In summary, the section delineated various criteria for the selection of various amines to functionalize zeolites. They aim to optimize and achieve the highest CO_2 adsorption capacity. Such a discussion lays the groundwork for a deeper understanding of the customized application of functional groups for enhanced adsorption properties. For the chosen best commercial zeolite in the first objective of this Ph.D. thesis, amine loading and the influence of temperature for the optimized and best choice of the amine for the synthesized zeolite shall be assessed.

1.4.3 Identification of cation exchanges zeolites with enhanced CO_2 capture characteristics

Walton et al. [33] investigated ion exchange on Zeolite X and Y and for various alkali metal cations (Li^+, K^+, Rb^+, and Cs^+). Thereby, their influence on CO_2 adsorption was assessed. The selection of base zeolites (Zeolite X and Zeolite Y) was based on their extensive commercial usage. This is attributed to their stable crystal structures, identical cage structures, and large pore volumes. The type of cation did influence available pore volume and electric field inside the pores and thereby provided a convenient means for tuning of the adsorptive properties of the porous materials. In general, it was found that the CO_2 capacities have been the highest for the Li-exchanged forms. In these, the ion–quadrupole interaction has been dominant. However, the investigations did not experimentally demonstrate the exchange of cations, the adsorption of cations in the supercages, or the CO_2 adsorption throughout the entire zeolite unit cell.

Hudson et al. [34] investigated low-pressure CO_2/N_2 sorption in acidic and copper-exchanged SSZ-13 zeolites using neutron powder diffraction (NPD) and in-situ CO_2 and N_2 adsorption methods. The SSZ-13 structure, composed of corner-sharing Al/SiO_4 tetrahedra and double six-membered-ring cages, allows size exclusion in gas adsorption. Cu-SSZ-13 showed minimal impact on CO_2 uptake but improved selectivity for CO_2 over N_2, and rendered it to be suitable for CO_2/N_2 flue-stack separations under humid conditions. Water vapor presence affects the CO_2 adsorption capacity in Cu-SSZ-13 and through the preferential adsorption at the Copper sites. Despite this, the overall CO_2 uptake is not significantly affected as the primary adsorption site responsible for CO_2 uptake is at the center of the 8-membered ring pore window and this is not occupied by copper. This renders the Cu-SSZ-13 relatively resistant to the effects of humidity in comparison to other materials such as MOF-74, which retains only 16% of its initial capacity after water exposure. However, the precise value of the CO_2 adsorption capacity in the presence of water vapor has not

been quantified in the article. The ideal adsorbed solution theory (IAST) selectivity for CO_2 over N_2 was >70 for both Cu- and H-SSZ-13, with selectivity of 72.0 and 73.6, respectively. The CO_2 binding mode at the center of the 8-membered-ring pore window was identified and contributed to the high selectivity. The SSZ-13 zeolites used in this study were determined to have SiO_2/Al_2O_3 = 12, with the copper derivative having Cu^{2+}/Al = 0.35. The study did not address how copper affects adsorption capacity in the presence of water.

Mortazavi et al. [35] studied the CO_2 adsorption characteristics of clinoptilolite modified by cation exchange (Li^+, Mg^{2+}, and Ca^{2+}) and with the volumetric method. Clinoptilolite, a natural zeolite, showed enhanced CO_2 adsorption after modification, with clinoptilolite/Li^+ exhibiting the best performance, and demonstrating a 4.18-fold increase in capacity. Other modifications, including amine (MEA, TEA, hexyl amine) and ionic liquid ($[b_{mim}]PF_6$), also improved CO_2 adsorption, with clinoptilolite/2% MEA and clinoptilolite/5% $[b_{mim}]PF_6$ showing enhancement by 3.58 and 4.35 times, respectively, at 4 bar CO_2 pressure. The study highlighted the strong interactions between modifiers and CO_2 molecules as a key to enhanced adsorption. However, no characterization data for the cation-loaded materials was provided by the authors.

Another study (Tobarameekul et al. [36]), investigated zinc-loaded NaY zeolites synthesized from bagasse ash and rice husk ash and focused on CO_2 adsorption performance. NaY zeolites, with a Si/Al ratio of 0.75 and a pore diameter of 7.4 Å, were modified via ion exchange with varying zinc loadings (0–5 wt.%). The optimal crystallization temperature (298.15 K) yielded zeolites with preserved crystalline structures, as confirmed by SEM, and enhanced CO_2 adsorption. The highest capacity (10.33 mmol g^{-1}) was achieved at 373.15 K and a CO_2 flow rate of 1 L h^{-1} using zeolite 5B298-373-1. BET analysis revealed that Zn-loaded zeolites had higher surface area and pore volumes, which improved adsorption. CO_2 adsorption was influenced by crystallization

temperature, flow rate, and Zn loading, with better performance at lower crystallization temperatures and flow rates. A factorial design using Minitab highlighted interactions between adsorbent type and temperature. The study demonstrated the eco-friendly, cost-effective potential of agricultural waste-derived zeolites for industrial CO_2 adsorption. However, the investigation did not examine other divalent cations or broader experimental conditions.

According to another investigation (Jin et al. [37]), prepared NaX zeolite from the co-combustion ash of rice husks and coal, reducing material costs for CO_2 adsorbents. The synthesized NaX zeolite, with a high-purity crystalline structure and a surface area of 583 m^2 g^{-1}, exhibited strong CO_2 adsorption properties due to its quadrupole moment. NaX zeolite was modified by Li^+ exchange to increase its specific surface area from 583.0 m^2 g^{-1} to 614.0 m^2 g^{-1}. Consequently, the CO_2 adsorption capacity at 298.15 K increased from 5.03 mmol g^{-1} (NaX) to 5.57 mmol g^{-1} (LiX). This represents an increase in the adsorption capacity of approximately 10%. Adsorption isotherms confirmed superior CO_2/N_2 selectivity for LiX zeolite. Despite these improvements, the study did not detail upon the Li^+ ion exchange mechanism in NaX.

While there has been substantial simulation-based research on CO_2 adsorption using alkali-cation-loaded Zeolite-Y, there is an absence of experimental studies that validate such simulation-based analysis. The conducted experimental research has often focused on the gas adsorption performance of alkali-cations (with +1 and +2 charges). However, such cations were at times, randomly selected. Henceforth, the findings are not consistent to enter upon the optimality of the Zeolite-Y commercial sorbent. Additionally, existing studies have primarily investigated alkali-cation-loaded natural zeolites. Thus, there is knowledge gap in the experimental exploration of alkali-cation-loaded Zeolite-Y for CO_2 adsorption. Such non-availability of empirical data conveys the uncertainty in the practical performance and efficiency of alkali-cation-loaded Zeolite-

Y in CO_2 capture. Addressing this gap requires experimental investigation into the CO_2 adsorption capabilities of alkali-cation-loaded Zeolite-Y. Such research should include a systematic evaluation of various alkali cations and their effects on CO_2 adsorption. Also, a comparative assessment of the findings with the outcome of the simulation studies can ensure the enhanced practical applicability and optimization of the performance of Zeolite-Y for CO_2 capture applications.

In summary, the literature on cation-loaded zeolites does not systematically highlight upon its enhanced CO_2 adsorption capabilities. Such studies can be addressed with the principles discussed in the previous section on amine-functionalized zeolites. Thereby, alternate modification techniques can be explored for improved CO_2 adsorption performance. In a nutshell, the efficiency of Zeolite-Y for Li^+, Na^+, and K^+ cation-loaded Zeolite-Y needs to be assessed for the ascertaining of the enhanced CO_2 adsorption capacity.

1.4.4 Identification of cation-exchanged and carbonate-loaded zeolites with enhanced CO_2 capture characteristics

Zhao et al. [40] investigated CO_2 sorption on K_2CO_3-loaded supports, including activated carbon (AC), Al_2O_3, zeolite 5A, zeolite 13X, and silica aerogels (SG), and under ambient temperature and 5000 ppm CO_2. While K_2CO_3/Al_2O_3 showed the highest CO_2 sorption capacity (1.18 mmol g^{-1}), K_2CO_3/AC exhibited the highest bi-carbonation efficiency and easy regeneration at 373–473 K. In contrast, other sorbents required higher regeneration temperatures (623 K). Moisture significantly reduced the sorption capacities of K_2CO_3/zeolites (0.34–0.53 mmol g^{-1}) and SG (0.12–0.31 mmol g^{-1}) and the impregnating process damaged the SG structure. K_2CO_3/AC emerged as a promising

candidate for CO_2 removal in confined spaces, offered high sorption capacity and efficient regeneration. Future research should explore the CO_2 sorption reaction rates in ambient conditions.

Lee et al. [41] investigated the effect of calcination temperature (573–973 K) and atmosphere (air and nitrogen) on K_2CO_3-loaded sorbents using ZrO_2 and TiO_2 supports. Potassium-based ZrO_2 sorbents exhibited superior CO_2 capture capacities (1.89–2.11 mmol CO_2 g^{-1}) and excellent thermal stability across all conditions, as only K_2CO_3 and ZrO_2 phases were formed. In contrast, potassium-based TiO_2 sorbents experienced reduced CO_2 capture above 773 K. This is due to the formation of inactive K–Ti alloy species. These results highlight ZrO_2 as superior support and maintenance of sorbent stability and structure during calcination. However, the study lacks detailed adsorption data and comprehensive material characterization.

Even though there has been extensive research on the application of potassium carbonate for CO_2 adsorption on various adsorbents, studies were not devoted to the investigations with the zeolite supports. The existing literature predominantly addresses the use of potassium carbonate on materials other than zeolites. Thus, there is a knowledge gap in the effectiveness of carbonate-loaded zeolite supports. Moreover, there are only two articles that explored CO_2 adsorption with potassium carbonate sorbents. Neither of these studies involved zeolite-based adsorbents. Such scarcity of research conveys no empirical data to infer upon the performance of potassium carbonate-loaded zeolites for CO_2 capture. To address these gaps, it is essential to conduct experimental studies on potassium carbonate-loaded zeolites. Such research should evaluate the CO_2 adsorption capacities and efficiencies of these materials. Thereby, valuable insights can be achieved into their potential advantages and limitations. Such studies will help to infer upon the sensitive influence of potassium carbonate on zeolite supports and thereby contribute to the development of more effective CO_2 capture technologies.

1.5 Objectives of the Ph.D. thesis

This Ph.D. thesis aims to assess upon an effective, porous, flexible, low-cost, sustainable, and environmentally friendly commercial adsorbent and its factionalized variant for the adsorption of higher adsorption characteristics of carbon dioxide and other greenhouse gases, such as methane. To do so, the following objectives have been set and stated:

a. Assessment of the best-performing zeolites among commercial zeolites (Zeolite-Y, Beta, and ZSM-5). This shall be targeted through a comparative analysis of the structural properties and CO_2 adsorption capacities. The assessed parameters refer to supercage characteristics, oxygen-member rings (OMRs), adsorption capacity, and other surface characterization data.
b. Wet-impregnation-based preparation and characterization of primary (monoethanolamine), secondary (diethanolamine), and tertiary (triethanolamine) amine-functionalized best commercial zeolite being determined as the finding of the first objective of this Ph.D. thesis. The relevant sub-objectives are:
   i. Effect of amine-loading on the synthesized adsorbents in terms of the characterization data
   ii. Assessment of the CO_2 adsorption capacity of alternate amine-functionalized zeolites in terms of the sensitive influence of pressure and temperature
c. Wet-impregnation based synthesis and characterization of cation-loaded (Li, Na, and K) best-performing zeolite being inferred from the first objective of this Ph.D. thesis. The study shall involve the realization of following three sub-objectives:
   i. Influence of type of alkali cations (Li, Na, and K) and loading on the characteristics (structural and textural properties) of cation-exchanged and carbonate-loaded for the best-performing zeolite

ii. Assess upon the gaseous (CO_2, CH_4, and N_2) adsorption capacity of the prepared zeolites at various combinations of pressure and temperatures

iii. Evaluate thermodynamic parameters such as enthalpy and Henry's constant for a greater understanding into the energetics of the adsorption process.

1.6 Organization of the Ph.D. Thesis

The Ph.D. thesis has been organized into six chapters. A brief account of the Ph.D. thesis chapters has been presented in the following paragraphs.

Chapter 1 (Introduction, Literature Review, and Objectives): This chapter provides a brief overview of CCS modes and technologies, the adsorption process for the post-combustion method, various types of adsorbents, and the importance of zeolites as an adsorbent. It also presents a literature review of the history and progress of commercial zeolites, amine-functionalized zeolites, cation-loaded zeolites, and the effect of carbonate loading on support material for carbon dioxide adsorption. The data of CO_2 adsorption capacity of various adsorbents has also been presented, in addition to the data of some functionalized adsorbents. Additionally, it includes an overview of the research background and stated objectives.

Chapter 2 (Materials and Methods, Theories, and Models): This chapter begins with an overview of the selection criteria for commercial zeolites, focusing on factors such as pore size and zeolite structure, which are critical for optimizing adsorption performance. The chapter details the raw materials used for the synthesis methods for the synthesis of amine-functionalized and cation-loaded zeolites. These methods involve precise procedures to incorporate functional groups and cations, and for enhanced CO_2 specific adsorbent properties. Characterization of the synthesized adsorbents is conducted through different techniques that provide comprehensive insights into

their structural and chemical characteristics. The chapter also describes the experimental setup for gas adsorption studies, including the apparatus and procedures used for measuring gas uptake and analyzing adsorption behavior. Theoretical frameworks, including adsorption models and the Ideal Adsorbed Solution Theory (IAST), were employed to interpret the data and predict adsorption performance.

Chapter 3 (Exploring the Synergistic Impact of Amine-Functionalization on Zeolite-Y for Gas Adsorption): This chapter focuses on the systematic selection and optimization of zeolites for CO_2 adsorption studies. Initially, three commercial zeolites were evaluated based on their characterization data and CO_2 adsorption performance for the identification of the most suitable support material for further research. Following this, the selected zeolite was functionalized with three different amine groups to enhance its adsorption properties. The chapter details upon the characterization and CO_2 adsorption studies conducted on these amine-functionalized zeolites for the assessment of the most effective adsorbent. Subsequently, modeling studies were performed to calculate key thermodynamic parameters, including the heat of adsorption and Henry's constant, which are crucial for understanding the adsorption process. Additionally, cyclic adsorption studies of optimized adsorbent were conducted to assess upon the stability and reusability of the optimized adsorbent.

Chapter 4 (Influence of Cation Exchange on the Gas Adsorption Efficiency of Zeolite-Y): The chapter details upon the synthesis and characterization of various cations (Li, Na, and K) loaded onto Zeolite-Y (5 wt.%). This section outlines the methods used to incorporate different cations into the zeolite structure and the subsequent characterization techniques that were employed to analyze the structural and chemical changes. Gas adsorption studies were conducted with CO_2, CH_4, and N_2 to evaluate the performance of the cation-loaded zeolites. The chapter includes a

comprehensive analysis of adsorption data using two distinct modeling approaches to interpret the adsorption behavior. Furthermore, the Ideal Adsorbed Solution Theory (IAST) was applied to assess upon the selectivity of the cation-loaded zeolites for CO_2 to other gases, and for providing insights into their potential applications in gas separation technologies.

Chapter 5 (Exploring CO_2 Selectivity in K_2CO_3-Modified Zeolite-Y: Loading and Temperature Effects on Adsorption Performance): The chapter explores the synthesis and characterization of Zeolite-Y loaded with varying weight percentages of potassium carbonate (5, 10, and 15 wt.%). The chapter begins with a detailed description of the preparation process and the characterization techniques used to analyze the structural and compositional changes in potassium carbonate-loaded zeolites. Gas adsorption studies were conducted for CO_2, CH_4, and N_2 and with a gravimetric system for the evaluation of the adsorption performance of these adsorbents. The resultant data were interpreted through modeling studies and for an assessment of the adsorption behavior. Additionally, the Ideal Adsorbed Solution Theory (IAST) was employed to determine the selectivity of potassium carbonate-loaded zeolites for CO_2 with respect to other gases. The chapter concludes with cyclic studies on optimized adsorbents for the evaluation of their stability and reusability in repeated adsorption cycles.

Chapter 6 (Conclusions and Future Scope): The chapter summarizes the key findings of the Ph.D. thesis and provides a critical assessment of the inferred conclusions. Also, recommendations for further research have been outlined.

References

[1] M. Karimi, M. Shirzad, J.A.C. Silva, A.E. Rodrigues, Carbon dioxide separation and capture by adsorption: a review, Environ. Chem. Lett. 21 (2023) 2041–2084. https://doi.org/10.1007/s10311-023-01589-z.

[2] F.A. Rahman, M.M.A. Aziz, R. Saidur, W.A.W.A. Bakar, M.. Hainin, R. Putrajaya, N.A. Hassan, Pollution to solution: Capture and sequestration of carbon dioxide (CO_2) and its utilization as a renewable energy source for a sustainable future, Renew. Sustain. Energy Rev. 71 (2017) 112–126. https://doi.org/10.1016/j.rser.2017.01.011.

[3] S.-Y. Lee, S.-J. Park, A review on solid adsorbents for carbon dioxide capture, J. Ind. Eng. Chem. 23 (2015) 1–11. https://doi.org/10.1016/j.jiec.2014.09.001.

[4] B.G. Miller, Carbon Dioxide Emissions Reduction and Storage, in: Clean Coal Eng. Technol., Elsevier, 2017: pp. 609–668. https://doi.org/10.1016/B978-0-12-811365-3.00013-2.

[5] R. Ben-Mansour, M.A. Habib, O.E. Bamidele, M. Basha, N.A.A. Qasem, A. Peedikakkal, T. Laoui, M. Ali, Carbon capture by physical adsorption: Materials, experimental investigations and numerical modeling and simulations – A review, Appl. Energy. 161 (2016) 225–255. https://doi.org/10.1016/j.apenergy.2015.10.011.

[6] B.P. Spigarelli, S.K. Kawatra, Opportunities and challenges in carbon dioxide capture, J. CO_2 Util. 1 (2013) 69–87. https://doi.org/10.1016/j.jcou.2013.03.002.

[7] C.-H. Yu, C.-H. Huang, C.-S. Tan, A Review of CO_2 Capture by Absorption and Adsorption, Aerosol Air Qual. Res. 12 (2012) 745–769. https://doi.org/10.4209/aaqr.2012.05.0132.

[8] T.O. Nelson, A. Kataria, P. Mobley, M. Soukri, J. Tanthana, RTI's Solid Sorbent-Based

CO_2 Capture Process: Technical and Economic Lessons Learned for Application in Coal-fired, NGCC, and Cement Plants, Energy Procedia. 114 (2017) 2506–2524. https://doi.org/10.1016/j.egypro.2017.03.1409.

[9] R. V. Siriwardane, M.-S. Shen, E.P. Fisher, Adsorption of CO_2, N_2, and O_2 on Natural Zeolites, Energy & Fuels. 17 (2003) 571–576. https://doi.org/10.1021/ef020135l.

[10] H.J. Choi, J.G. Min, S.H. Ahn, J. Shin, S.B. Hong, S. Radhakrishnan, C.V. Chandran, R.G. Bell, E. Breynaert, C.E.A. Kirschhock, Framework flexibility-driven CO_2 adsorption on a zeolite, Mater. Horizons. 7 (2020) 1528–1532. https://doi.org/10.1039/D0MH00307G.

[11] A.A. Abd, M.R. Othman, J. Kim, A review on application of activated carbons for carbon dioxide capture: present performance, preparation, and surface modification for further improvement, Environ. Sci. Pollut. Res. 28 (2021) 43329–43364. https://doi.org/10.1007/s11356-021-15121-9.

[12] T. Ghanbari, F. Abnisa, W.M.A. Wan Daud, A review on production of metal organic frameworks (MOF) for CO_2 adsorption, Sci. Total Environ. 707 (2020) 135090. https://doi.org/10.1016/j.scitotenv.2019.135090.

[13] H. Li, A. Dilipkumar, S. Abubakar, D. Zhao, Covalent organic frameworks for CO_2 capture: from laboratory curiosity to industry implementation, Chem. Soc. Rev. 52 (2023) 6294–6329. https://doi.org/10.1039/D2CS00465H.

[14] D.G. Boer, J. Langerak, P.P. Pescarmona, Zeolites as Selective Adsorbents for CO_2 Separation, ACS Appl. Energy Mater. 6 (2023) 2634–2656. https://doi.org/10.1021/acsaem.2c03605.

[15] Y. Duan, B. Zhang, D.C. Sorescu, J.K. Johnson, CO_2 capture properties of M–C–O–H (M=Li, Na, K) systems: A combined density functional theory and lattice phonon dynamics

study, J. Solid State Chem. 184 (2011) 304–311. https://doi.org/10.1016/j.jssc.2010.12.005.

[16] M.Z. Memon, X. Zhao, V.S. Sikarwar, A.K. Vuppaladadiyam, S.J. Milne, A.P. Brown, J. Li, M. Zhao, Alkali Metal CO_2 Sorbents and the Resulting Metal Carbonates: Potential for Process Intensification of Sorption-Enhanced Steam Reforming, Environ. Sci. Technol. 51 (2017) 12–27. https://doi.org/10.1021/acs.est.6b04992.

[17] V.R. Choudhary, S. Mayadevi, A.P. Singh, Sorption isotherms of methane, ethane, ethene and carbon dioxide on NaX, NaY and Na-mordenite zeolites, J. Chem. Soc. Faraday Trans. 91 (1995) 2935. https://doi.org/10.1039/ft9959102935.

[18] V.G. Gomes, K.W.K. Yee, Pressure swing adsorption for carbon dioxide sequestration from exhaust gases, Sep. Purif. Technol. 28 (2002) 161–171. https://doi.org/10.1016/S1383-5866(02)00064-3.

[19] D. Ko, R. Siriwardane, L.T. Biegler, Optimization of Pressure Swing Adsorption and Fractionated Vacuum Pressure Swing Adsorption Processes for CO2 Capture, Ind. Eng. Chem. Res. 44 (2005) 8084–8094. https://doi.org/10.1021/ie050012z.

[20] P.J.E. Harlick, F.H. Tezel, An experimental adsorbent screening study for CO_2 removal from N2, Microporous Mesoporous Mater. 76 (2004) 71–79. https://doi.org/10.1016/j.micromeso.2004.07.035.

[21] P.J.. Harlick, F.. Tezel, Adsorption of carbon dioxide, methane and nitrogen: pure and binary mixture adsorption for ZSM-5 with SiO_2/Al_2O_3 ratio of 280, Sep. Purif. Technol. 33 (2003) 199–210. https://doi.org/10.1016/S1383-5866(02)00078-3.

[22] X. Xu, X. Zhao, L. Sun, X. Liu, Adsorption separation of carbon dioxide, methane and nitrogen on monoethanol amine modified β-zeolite, J. Nat. Gas Chem. 18 (2009) 167–172. https://doi.org/10.1016/S1003-9953(08)60098-5.

[23] J. Zhang, R. Singh, P.A. Webley, Alkali and alkaline-earth cation exchanged chabazite zeolites for adsorption based CO_2 capture, Microporous Mesoporous Mater. 111 (2008) 478–487. https://doi.org/10.1016/j.micromeso.2007.08.022.

[24] Z. Zhang, W. Zhang, X. Chen, Q. Xia, Z. Li, Adsorption of CO_2 on Zeolite 13X and Activated Carbon with Higher Surface Area, Sep. Sci. Technol. 45 (2010) 710–719. https://doi.org/10.1080/01496390903571192.

[25] E.J. García, J. Pérez-Pellitero, G.D. Pirngruber, C. Jallut, M. Palomino, F. Rey, S. Valencia, Tuning the Adsorption Properties of Zeolites as Adsorbents for CO_2 Separation: Best Compromise between the Working Capacity and Selectivity, Ind. Eng. Chem. Res. 53 (2014) 9860–9874. https://doi.org/10.1021/ie500207s.

[26] P. Rzepka, Z. Bacsik, A.J. Pell, N. Hedin, A. Jaworski, Nature of Chemisorbed CO_2 in Zeolite A, J. Phys. Chem. C. 123 (2019) 21497–21503. https://doi.org/10.1021/acs.jpcc.9b04142.

[27] P.D. Jadhav, R. V. Chatti, R.B. Biniwale, N.K. Labhsetwar, S. Devotta, S.S. Rayalu, Monoethanol Amine Modified Zeolite 13X for CO_2 Adsorption at Different Temperatures, Energy & Fuels. 21 (2007) 3555–3559. https://doi.org/10.1021/ef070038y.

[28] D. Aruldoss, R. Saigoanker, J. Das Savarimuthu, J. R., Amine-grafted zeolites-mesoporous ceramics: Synthesis and adsorption characteristics, Ceram. Int. 40 (2014) 7583–7587. https://doi.org/10.1016/j.ceramint.2013.11.111.

[29] M. Babaei, M. Anbia, M. Kazemipour, Improving CO_2 adsorption with new amine-functionalized Y-type zeolite, J Adv. Env. Heal. Res. 5 (2017) 70–77. https://doi.org/https://doi.org/10.22102/jaehr.2017.71674.

[30] S. Dinda, P. Murge, B. Chakravarthy Paruchuri, A study on zeolite-based adsorbents for

CO2 capture, Bull. Mater. Sci. 42 (2019) 240. https://doi.org/10.1007/s12034-019-1936-8.

[31] V. Tejavath, V. Kasarabada, S. Gonuguntla, V. Perupoga, S. V. Nandury, S. Bojja, U. Pal, Technoeconomic Investigation of Amine-Grafted Zeolites and Their Kinetics for CO_2 Capture, ACS Omega. 6 (2021) 6153–6162. https://doi.org/10.1021/acsomega.0c05397.

[32] M.K. Majideh Babaei, Mansoor Anbia, Improving CO_2 adsorption with new amine-functionalized Y-type zeolite, J. Adv. Environ. Heal. Res. 5 (2017) 70–77. https://doi.org/https://doi.org/10.22102/jaehr.2017.71674.

[33] K.S. Walton, M.B. Abney, M. Douglas LeVan, CO_2 adsorption in Y and X zeolites modified by alkali metal cation exchange, Microporous Mesoporous Mater. 91 (2006) 78–84. https://doi.org/10.1016/j.micromeso.2005.11.023.

[34] M.R. Hudson, W.L. Queen, J.A. Mason, D.W. Fickel, R.F. Lobo, C.M. Brown, Unconventional, Highly Selective CO_2 Adsorption in Zeolite SSZ-13, J. Am. Chem. Soc. 134 (2012) 1970–1973. https://doi.org/10.1021/ja210580b.

[35] N. Mortazavi, M. Bahadori, A. Marandi, S. Tangestaninejad, M. Moghadam, V. Mirkhani, I. Mohammadpoor-Baltork, Enhancement of CO_2 adsorption on natural zeolite, modified clinoptilolite with cations, amines and ionic liquids, Sustain. Chem. Pharm. 22 (2021) 100495. https://doi.org/10.1016/j.scp.2021.100495.

[36] P. Tobarameekul, S. Sangsuradet, P. Worathanakul, Comparative Study of Zn Loading on Advanced Functional Zeolite NaY from Bagasse Ash and Rice Husk Ash for Sustainable CO_2 Adsorption with ANOVA and Factorial Design, Atmosphere (Basel). 13 (2022) 314. https://doi.org/10.3390/atmos13020314.

[37] Y. Jin, Q. Xu, F. Zheng, J. Lu, Enhancement in CO_2 adsorption by zeolite synthesized from co-combustion ash of coal and rice husk modified with lithium ion, J. Energy Inst. 110

(2023) 101348. https://doi.org/10.1016/j.joei.2023.101348.

[38] K.-M. Lee, Y.-H. Lim, C.-J. Park, Y.-M. Jo, Adsorption of Low-Level CO_2 Using Modified Zeolites and Activated Carbon, Ind. Eng. Chem. Res. 51 (2012) 1355–1363. https://doi.org/10.1021/ie2013532.

[39] H. Yang, X. Fang, Z. Li, H. Sun, H. Chen, Copper-Doped Small Pore Zeolites for CO_2 Capture by Honeycomb Rotor with Low Temperature Regeneration, ACS Sustain. Chem. Eng. 10 (2022) 1759–1764. https://doi.org/10.1021/acssuschemeng.1c08347.

[40] C. Zhao, Y. Guo, C. Li, S. Lu, Removal of low concentration CO_2 at ambient temperature using several potassium-based sorbents, Appl. Energy. 124 (2014) 241–247. https://doi.org/10.1016/j.apenergy.2014.02.054.

[41] S.C. Lee, Y.M. Kwon, S.Y. Jung, J.B. Lee, C.K. Ryu, J.C. Kim, Excellent thermal stability of potassium-based sorbent using ZrO_2 for post combustion CO_2 capture, Fuel. 115 (2014) 97–100. https://doi.org/10.1016/j.fuel.2013.07.007.

[42] S.M. Varghese, A.R. Chowdhury, D.N. Arnepalli, G. Ranga Rao, Crosslinked hydrogel-derived carbons activated by trace amounts of aqueous potassium carbonate for carbon dioxide adsorption, Bioresour. Technol. 403 (2024) 130851. https://doi.org/10.1016/j.biortech.2024.130851.

[43] S.C. Lee, B.Y. Choi, T.J. Lee, C.K. Ryu, Y.S. Ahn, J.C. Kim, CO_2 absorption and regeneration of alkali metal-based solid sorbents, Catal. Today. 111 (2006) 385–390. https://doi.org/10.1016/j.cattod.2005.10.051.

[44] J.B. Lee, C.K. Ryu, J.-I. Baek, J.H. Lee, T.H. Eom, S.H. Kim, Sodium-Based Dry Regenerable Sorbent for Carbon Dioxide Capture from Power Plant Flue Gas, Ind. Eng. Chem. Res. 47 (2008) 4465–4472. https://doi.org/10.1021/ie0709638.

[45] N.N.A.H. Meis, A.M. Frey, J.H. Bitter, K.P. de Jong, Carbon Nanofiber-Supported K_2CO_3 as an Efficient Low-Temperature Regenerable CO_2 Sorbent for Post-Combustion Capture, Ind. Eng. Chem. Res. 52 (2013) 12812–12818. https://doi.org/10.1021/ie4017072.

[46] R.R. Kondakindi, G. McCumber, S. Aleksic, W. Whittenberger, M.A. Abraham, Na_2CO_3-based sorbents coated on metal foil: CO_2 capture performance, Int. J. Greenh. Gas Control. 15 (2013) 65–69. https://doi.org/10.1016/j.ijggc.2013.01.038.

[47] S. Sengupta, S.A. Reddy, R. Dongara, A.K. Das, H. Bhunia, P.K. Bajpai, Improvement in Regeneration Properties and Multicycle Stability for K_2CO_3/Al_2O_3 Adsorbents for CO_2 Removal from Flue Gas, Energy & Fuels. 28 (2014) 5354–5362. https://doi.org/10.1021/ef501174m.

[48] S.T. Bararpour, D. Karami, N. Mahinpey, Investigation of the effect of alumina-aerogel support on the CO_2 capture performance of K_2CO_3, Fuel. 242 (2019) 124–132. https://doi.org/10.1016/j.fuel.2018.12.123.

CHAPTER 2

Materials and Methods, Theories, and Models

Chapter 2

Materials and Methods, Theories, and Models

After inferring upon the methodology adopted for the selection of the best commercial zeolite adsorbent for CO_2 capture, the chapter elucidates the synthesis procedures and associated characterization methods that were followed for the amine-functionalized zeolites and cation-exchanged and carbonate-loaded zeolites. Thereafter, the methodology followed for the gas adsorption characteristics assessment was delineated along with a brief account of the physical properties and purity of the gases considered. In brief, the chapter summarizes the materials and methods that were followed for (a) the selection of commercial zeolite for subsequent functionalization to enhance CO_2 adsorption, (b) synthesis and characterization of amine-functionalized Zeolite-Y adsorbents, (c) synthesis and characterization of cation-exchanged and carbonate-loaded Zeolite-Y adsorbents, and (d) synthesis and characterization of loading altered potassium-carbonate loaded Zeolite-Y adsorbents. Finally, the last section presents a summary of the chapter. The characterization methodology involved the consideration of a few adsorption isotherm theories and the evaluation of important thermodynamics parameters such as Henry's constant and adsorption enthalpy.

2.1 Selection of commercial zeolite

Zeolite-Y, β-Zeolite, and ZSM-5 commercial zeolites were selected for the assessment of the best commercial adsorbent for CO_2, CH_4, and N_2 capture. This is based on structural and chemical characteristics (such as pore diameter, basicity, and pore volume). Thereby the best adsorbent was chosen for gas adsorption studies. The structural characteristics contribute to the maximum availability of adsorption sites for interaction with CO_2 molecules.

2.1.1 Precursors

Commercial-grade Zeolite-Y, β-Zeolite, and ZSM-5 were obtained from Alfa Aesar company, Hyderabad, and were utilized in their as-received form and without further treatment-based

purification. The CO_2 (99.9%), CH_4 (99.9%), N_2 (99.9%), and helium (99.9%) gas cylinders were purchased from Assam Air Products, Guwahati.

2.1.2 Characterization Techniques

Several characterization techniques were deployed to analyze the chosen commercial adsorbents. Through the findings of such characterization studies, the physical and chemical properties of the adsorbents can be assessed for their sensitive influence on the efficiency and effectiveness of the CO_2 adsorption processes. Through a comprehensive characterization of the chosen adsorbents, such properties can be further tailored and customized for optimal adsorbent performance in specific applications.

2.1.2.1 X-ray Diffraction (XRD) Studies

Powder X-ray diffraction (PXRD) is an effective technique for the elucidation of the structure of materials. In crystalline substances, atoms are arranged in parallel planes known as crystallographic planes. These are identified with the Miller indices (h, k, and l). Constructive interference, which results in diffraction maxima, occurs in a scenario in which these planes satisfy the conditions outlined by the Bragg's law. Such an analysis will infer upon the crystalline structure of the assessed material. The Bragg's law is defined as:

$$2d \sin\theta = n\lambda \tag{2.1}$$

In the above equation, d denotes the distance between consecutive crystal planes, θ is the angle between the incident beam and the crystallographic planes, n is an integer, and λ represents the wavelength of the incident radiation. During X-ray diffraction (XRD) analysis, while the X-ray tube remains stationary, the detector being mounted on the goniometer circle rotates at twice the angular speed of the sample. However, the rotational axes remain aligned. During the analysis, while the detector is positioned at an angle of 2θ, the sample surface maintains a

relative angle of θ with respect to the incident beam. Thus, the detector with scanning around the sample in predetermined 2θ intervals, facilitates the recording of both angle and intensity of the diffracted X-ray radiation [1].

In the conducted PXRD study, the samples were prepared through their even distribution on a flat glass plate. This ensured upon the creation of a smooth and flat surface. The powder XRD measurements were performed using the instrument supplied by Rigaku Technologies, Japan. The instrument is equipped with Johansson Kα1 optics and is operated with a 9kW rotating anode X-ray source. The PXRD analysis was conducted in the 2θ range from 2-50°.

2.1.2.2 FESEM Imaging and Analysis

Field Emission Scanning Electron Microscope (FESEM) was employed to characterize the surface morphology of the materials. The technique utilizes a high-energy electron beam, which is raster-scanned across the sample surface in a high-vacuum environment. Thereby, primary electrons are focused and deflected by electronic lenses to form a narrow scan beam that bombards the analyzed sample. The interaction between the beam and the sample surface results in the emission of secondary electrons. The angle and velocity of these secondary electrons provide information for the surface structure of the sample. A detector captures the emitted secondary electrons and converts them into an electronic signal. This signal is then amplified and transformed into a video scan image. Subsequently, the image can be viewed on a monitor or can be saved as a digital file for further analysis [2].

The FESEM analyses were conducted with the Zeiss Sigma 300 instrument. It was operated at a magnification of 50,000x and an accelerating voltage of 5 kV. For sample preparation, the drop-casting method was utilized with isopropanol as the solvent. Thereafter, the samples were dried in a vacuum oven at 120°C and for overnight time duration. To ensure adequate

conductivity and prevent charge build-up on the sample surface during imaging, the samples were mounted on metal stubs and with a sticky carbon disc. Additionally, to enhance conductivity, the samples were coated with a thin layer of gold with a sputter coater setup. Thereafter, the sample was introduced into the FESEM instrument environment for the analysis.

2.1.2.3 FTIR Spectroscopic Analysis

Fourier-transform infrared (FTIR) spectroscopy was utilized to investigate bonding mechanisms in solids and on surfaces. Infrared spectra are used to illuminate the bonding of molecules on solid surfaces or within solid phases. This is based on the relationship between molecular vibrations and their symmetry.

The FTIR system employs features such as an interferometer composed of a beam splitter, a fixed mirror, and a movable mirror. The beam splitter, made of a specialized material, divides the incoming radiation into two beams namely a one transmitted and a reflected beam. While the transmitted beam travels to the fixed mirror, the reflected beam is directed at the moving mirror. Both mirrors reflect the radiation to a beam splitter, where it is again split. This results in one beam proceeding to the detector and another beam returning to the source [3].

The FTIR analysis was conducted with the PerkinElmer Spectrum Two system, and for a wavenumber range of 4000 to 400 cm^{-1}. For sample preparation, approximately 2-5 mg of the sample was placed directly onto the infrared plates.

2.1.2.4 BET Surface Area and Porosity Characterization

The Brunauer–Emmett–Teller (BET) theory is a widely used method for the determination of the surface area of porous materials. The method provides critical insights into the physical

structure of materials, as the surface area significantly influences their interaction with the environment. Key material properties such as material activity, moisture retention, and shelf life are often correlated with the surface area. The BET analysis is essential for the design and manufacturing of materials. Thus, the analysis is a fundamental tool in material characterization. Through the assessment of the surface area, BET analysis assists in understanding various material behaviors. Thereby, the performance of the material can be optimized in different applications.

In the BET apparatus, to measure the surface area of a solid sample, the sample is first cooled to cryogenic temperatures with the liquid nitrogen and under vacuum conditions. Nitrogen gas, commonly used as adsorbate, is then introduced in controlled increments to contact with the solid sample (adsorbent). After each increment, the relative pressure (P/P_0) is allowed to equilibrate, and the amount of nitrogen adsorbed (W) is measured.

The BET method involves the construction of a linear plot of $1/W\left(\frac{P_0}{P}-1\right)$ versus P/P_0. Thereby, the intercept $I= 1/(W_mC)$ and slope $A=(C-1)/(W_mC)$, expressions can be used for the determination of surface area of the adsorbent. In these terms, P is the equilibrium pressure and P_0 is the saturation pressure of nitrogen. For most solids, such a linear relationship is valid within a specific range of the adsorption isotherm. This is typically valid in the P/P_0 range of 0.05 to 0.35. From the linear plot, the weight of nitrogen that corresponds to a monolayer of surface coverage (W_m) is determined. Thereafter, the total surface area of the sample is determined from the slope and intercept of the BET plot (using the BET equation) and the known molecular cross-sectional area of the nitrogen molecule. The BET linearized expression is:

$$\frac{1}{W\left(\frac{P_0}{P}-1\right)} = \frac{1}{W_m C} + \frac{C-1}{W_m C}\left(\frac{P}{P_0}\right) \tag{2.2}$$

In the above expression, C is the BET constant. The constant reflects the energy of adsorption in the first adsorbed layer and conveys the strength of the adsorbent-adsorbate interactions. The following equations can be used for the determination of BET constant and monolayer adsorbed quantity:

$$C = 1 + \frac{A}{I} \tag{2.3}$$

$$W_m = \frac{1}{A+I} \tag{2.4}$$

The total surface area and specific surface area can be determined with the following expressions:

$$S_{total} = \frac{W_m N_{av} S}{V} \tag{2.5}$$

$$S_{BET} = \frac{S_{total}}{m} \tag{2.6}$$

In the above equations, N_{av} is Avogadro's number, S is the single adsorb molecule coverage, V is the adsorbate gas molar volume and m is the mass of the adsorbent.

To determine the pore volume and pore size distribution, the gas pressure is incrementally increased to fill all pores with nitrogen. Following this, the pressure is reduced incrementally to evaporate the condensed nitrogen from the system. Thereby, an analysis of the resulting adsorption and desorption isotherms provides information for the pore volume and pore size distribution [4].

The BET surface area of the samples was determined with the Quantachrome Instruments Autosorb IQ MP. Prior to the measurement, an empty cell was prepared by ensuring that it was

clean and dry. Thereby, the cell was evacuated and was filled back with inert gas as per the requirement. Given that some samples exhibit significant nitrogen absorption even at room temperature, helium was used in the weighing stages. This accounts to any potential absorption. The weight measurement procedure involved weighing the empty cell, loading the sample by avoiding sample accumulation in the stem of the cell, and then weighing of the loaded cell. Prior to the subsequent outgassing step, the system was checked for leaks, and the sample was degassed at 423 K to remove moisture and pre-adsorbent gases.

Using the Brunauer–Emmett–Teller (BET) method, the specific surface area was calculated from nitrogen adsorption data and for a relative pressure range (P/P_0) of 0.05 to 0.30. The pore size distribution was determined using the Barrett–Joyner–Halenda (BJH) method. Similarly, the total pore volume of the adsorbents was evaluated based on the maximum adsorbed volume of nitrogen gas at $P/P_0 \approx 0.99$.

2.1.3 Assessment of Gas adsorption capacity

The pure gas adsorption isotherm describes the equilibrium relationship between the quantity of a single gas adsorbed onto a solid surface and the pressure of the gas at a constant temperature. Such an isotherm is fundamental for an insight into the interaction between a specific gas and an adsorbent material and without interference from other gases. Parameters being obtained from such pure gas adsorption isotherms include the maximum adsorption capacity, energy, and adsorption constants, that characterize the affinity between the gas and the adsorbent. For the obtained data, graphical representations of the relationship between gas quantity and applied pressure in adsorption can be visualized [5]. Thereby, the amount of gas adsorbed on a solid surface depends upon the two degrees of freedom (pressure and temperature):

$$N = f(P, T) \tag{2.7}$$

where N is the amount adsorbed (mmol g^{-1}), P is the pressure (bar), and T is the temperature (K).

In the design of adsorption mechanisms, three primary factors are to be considered. These are physical adsorption (being governed by van der Waals forces); chemical adsorption (being facilitated by chemical bonding); and ion exchange processes. Adsorption isotherms are determined by several factors. These include the nature of the adsorbate and adsorbent, the species being adsorbed, and various physical properties [6].

In CO_2 adsorption studies that especially target flue gas applications, the accurate measurement of CO_2 adsorption capacity is very important. For such needs, two predominant techniques can be used for the measurement of gas adsorption isotherms. These are volumetric and gravimetric methods [7,8]. A brief account of these are as follows:

i. Volumetric Method: The technique enables the measurement of the volume or gas pressure of the adsorbent. The method requires precise determination of cell and void volumes. The amount of absorbed gas is quantified by monitoring changes in gas pressure or volume. Thus, the method provides detailed data with respect to gas volume or pressure changes [9]. However, it does not provide kinetic information about the adsorption process, is ineffective for small quantities of adsorbent (e.g., several milligrams), and is not practical at extremely low or high pressures due to difficulties in pressure measurements and for scenarios in which equations of state (EoS) could not be applied for the adsorbed gases [10].

ii. Gravimetric Method: The method enables the measurement of the amount of sorbed gas. This is conducted through the recording of the sample's weight alterations at constant pressure. To do so, the sample is either mechanically suspended or held via the magnetic coupling in a high-pressure vessel. Thereby, buoyancy effects are minimized. An accurate

balance is used to detect alterations in the sample weight [11]. The method allows for real-time observation of the adsorption system approach to reach equilibrium. This state is confirmed through the data display setup of the balance system. Thus, the method enables the definition of technical adsorption equilibrium based on a chosen fraction of the sample mass and a specified time interval. The method is less effective for very small amounts of adsorbent and can be challenging at extreme pressures.

In summary, while the volumetric method is useful for the measurement of gas volume or pressure changes, the gravimetric method is advantageous for the observation that prompts upon the approached equilibrium. Thus, the later can provide more information in certain research applications [7].

2.1.3.1 Gravimetric Adsorption Setup

Rubotherm^{TM} Magnetic Suspension Balance was used for the gravimetric gas adsorption measurements. To do so, firstly, gas cylinders were connected to the balance with the stainless-steel tubes (Figure 2.1). The temperature transducers, mass flow controllers, and pressure transducers were all installed at appropriate locations.

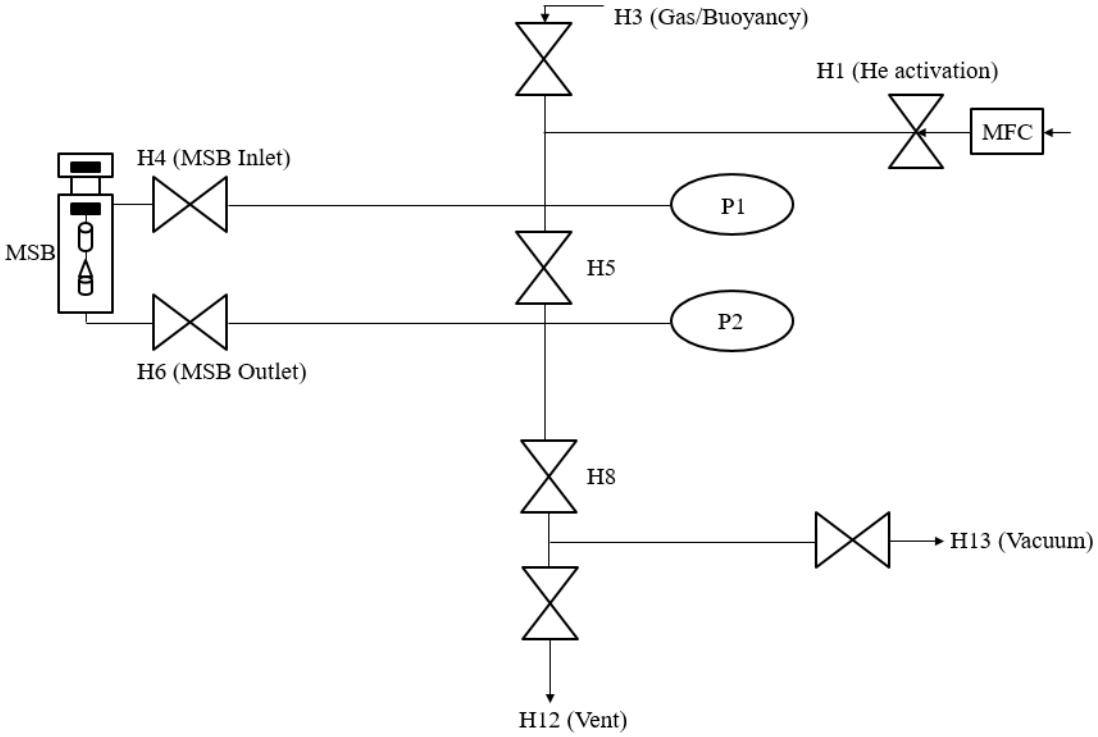

Figure 2.1: Schematic representation of gravimetric adsorption system for gas adsorption studies. (Nomenclature: *MSB: Magnetic Suspension Balance, MFC: Mass Flow Controller, P1 & P2: Pressure transducers, H1: Helium inlet valve, H3: Adsorbate inlet valve, H4: Balance inlet valve, H6: Balance outlet valve, H5 & H8: Bypass valve, H12: Vent valve, H13: Vacuum valve*)

The magnetic suspension balance (MSB) is a gravimetric device that enables to weigh samples in a contactless arrangement in almost all environments. Instead of hanging directly on the balance, the sample to be assessed is linked to a so-called suspension magnet. Such a system consists of a permanent magnet, a sensor core, and a device for the decoupling of the measured load (sample). An electromagnet, which is attached to the underfloor weighing hook of a balance, maintains the freely suspended state of the suspension magnet via an electronic control unit. Using such magnetic suspension coupling system, the measuring force is transmitted in a contactless format from the measuring chamber to the microbalance, which is located outside the chamber under ambient atmospheric conditions. A controlled suspended state is achieved

by utilizing a direct analogous control circle (PID controller and position transducer). This modulates the voltage on the electromagnet in such a way that the suspension magnet is held constantly in a vertical position. A microcontroller-driven digital set point controller being superimposed on the direct PID controller allows various positions of the suspension magnet. The distinct merit of the Rubotherm magnetic suspension balance is that the microbalance can be tared and calibrated during measurements.

The balance can be configured with a second load coupling and sample position. This enables the weight measurement of two samples during a single experiment. Such a function can be used for comparative measurements of two samples (e.g., comparison of reactive and reference samples). In other words, both sorption and density of the gaseous atmosphere in the reactor can be determined. The second coupling and sample position create in total three vertical positions. At these conditions, the MSB can be controlled. These positions refer to Zero Point, Tare, Measuring Point 1, and Measuring Point 2. A brief account of these are as follows:

Zero Point (ZP): Only the permanent magnet is suspended to tare and/or calibrate the microbalance.

Measuring Point 1 (MP1): For the first sorption measurement, the permanent magnet is raised. This engages the first coupling, and determines the weight of the first reactive sample.

Measuring Point 2 (MP2): The permanent magnet is raised further to engage the second coupling. This lifts and weighs together both the samples.

The weight of the second sample for sorption measurement 2 is determined by subtracting the weight measured at measuring point 1 from the combined weight. A known-volume inert sinker is used as the second sample for the determination of the density of the fluid phase in the

reactor. Using the Archimedes principle, the buoyancy force acting on the sinker precisely determines the density of the gas phase in the reactor.

2.1.3.2 Adsorption measurements

A gravimetric gas adsorption analyzer was used to evaluate the gas adsorption capacity of the adsorbents in the temperature range of 303-343K. In a standard measurement procedure, ~600mg of adsorbent is placed in a sample holder that is fitted with an analysis port. The sample was degassed at 523 K with helium gas (30 cm^3min^{-1}) for 180 minutes to remove the pre-adsorbent gases. A sample is considered to be activated in a scenario in which it does not loose significant weight with respect to the time. After activation, the sample was cooled under vacuum condition to reach the experimental temperature. Using a recirculation bath, the sample was maintained at the respective analysis temperature (303 K, 323 K, and 343). The adsorbed gas quantity was calculated based on the alteration in the adsorbent weight. The stability of the adsorbent was examined by determining its adsorption capacity at the applied pressure alteration. The equilibrium adsorption was measured at approximately 13 points within the measured pressure range. Thereby, more reliable isotherm model parameters have been obtained. After each cycle, the sample was degassed under vacuum at 523 K for 180 min. Thereafter, gas cyclic adsorption-desorption performance was evaluated. The excess amount of adsorption was calculated from raw measurements and with buoyancy corrections. According to non-adsorbing helium assumptions, the impenetrable solid volume of the adsorbent for buoyancy correction was determined from helium measurements at 293K and in the pressure range of 0 - 25 bar.

2.1.3.3 Adsorption Calculations

After activation, the pressure chamber of the balance was completely evacuated and was cooled down to reach to the experimental temperature. The evacuated sample weight is calculated with the following expression:

$$N_{t0} = N_{bucket,0} + N_{sample,0} \tag{2.8}$$

The activated samples are equilibrated with a gas at a particular temperature and pressure. Thereby, the excess amount adsorbed (N_t) is calculated with the expression:

$$N_t = N_{eq} - N_{t0} + V_{buo}\rho^{gas} \tag{2.9}$$

where, V_{buo} is the buoyancy volume and ρ^{gas} is the density of gas at equilibrium pressure and temperature. The balance reading taken during the experiment can directly be used to determine N_{eq} and with the expression:

$$N_{eq} = MP1 - ZP\ (at\ equilibrium) \tag{2.10}$$

To determine the excess amount adsorbed from the balance, it is necessary to know the buoyancy volume. This is determined with the expression:

$$V_{buo} = V_B + V_S \tag{2.11}$$

where, V_B is the volume of the bucket and V_s is the volume of the impenetrable solid

Usually, buoyancy volume is calculated through a base run of the adsorbent system at different pressures. The experiments are usually conducted at room temperature. Since helium is not an adsorbing gas, the excess amount adsorbed for helium was zero, and the excess amount in eq. (2.10) was reduced to

$$N_{eq} = N_{t0} - V_{buo}\rho^{gas} \tag{2.12}$$

Thus, the eq. (2.12) can be rewritten as:

$$MP1 - ZP = N_{t0} - V_{buo}\rho^{gas} \tag{2.13}$$

At different pressures, the density of helium was plotted against alterations in equilibrium conditions. The buoyancy volume was determined from the slope of the plot of the equilibrium readings and helium density.

Based on the virial equation of state, the bulk density was obtained with the expression:

$$\rho^{gas} = \frac{-1 + \sqrt{1 + 4\frac{B^{gas} \times P}{R \times T}}}{2B^{gas}} \tag{2.14}$$

where, B^{gas} is the second virial coefficient of the gas phase, P is the pressure (bar), R is the gas constant ($JK^{-1}mol^{-1}$), and T is the temperature (K).

The B^{gas} is temperature dependent parameter and is evaluated as:

$$B^{gas} = B_1 + \frac{B_2}{T} + \frac{B_3}{T^3} + \frac{B_4}{T^8} + \frac{B_5}{T^9} \tag{2.15}$$

The values of B_1, B_2, B_3, B_4, and B_5 parameters are given in Table 2.1.

Table 2.1: A summary of second-virial coefficients of various gases.

Gas	$B_1 \times 10^2$	$B_2 \times 10^{-1}$	$B_3 \times 10^{-5}$	$B_4 \times 10^{-15}$	$B_5 \times 10^{-17}$
	m^3kmol^{-1}	$m^3kmol^{-1}K$	$m^3kmol^{-1}K^3$	$m^3kmol^{-1}K^8$	$m^3kmol^{-1}K^9$
He	1.40	-3.54	-5.95×10^{-6}	3.61×10^{-13}	-7.94×10^{-15}
CO_2	5.44	-3.64	-14.96	85.90	-139.70
CH_4	5.44	-2.71	-2.14	0.92	-0.79
N_2	4.67	-1.50	-0.61	0.08	-0.05

Finally, the adsorbed gas amount (mmol g^{-1}) was calculated with the expression:

$$N = \frac{\left(N_{eq} - N_{t0} + V_{buo}\rho^{gas}\right)}{N_{t0} \times M_w} \tag{2.16}$$

where, M_w is the molar mass of the gas

It is well known that the adsorption capacity of the synthesized adsorbents is very likely to alter with the variation in the composition of the gaseous mixture. Factors such as the partial pressure of the components, competitive adsorption, and adsorbent affinity for each constituent

gas would profoundly influence the CO_2 adsorption process. For the assessment of the adsorbent's performance under standard conditions, the conducted Ph.D. thesis research works were devoted to a specific gas mixture composition. Accordingly, the consistent performance of alternate sorbents was ascertained as per the objectives set for the thesis research works. However, additional compositions also need to be considered for obtaining a comprehensive understanding of the adsorbent's behavior under diverse scenarios. Such research works could be considered as future research works and as an excellent extension of the conducted research works in the Ph.D. thesis. Accordingly, the performance of the best-assessed adsorbents can be further assured for real-world applications.

2.1.3.4 Purity of Gases

Three different gases were utilized for gas adsorption studies. Helium was employed to activate the sample. The minimum purity of the gases used in the experiments exceeded 99.9%, and no additional purification was performed after purchasing the gases.

Table 2.2 provides information with respect to the percentage purity of all gases and their respective suppliers.

Table 2.2: A summary of deployed gases and their purities in the conducted experimental investigations.

Supplier	Gas	Minimum Gas Purity (%)
Assam Air Products	He	99.995
Assam Air Products	CO_2	99.99
Assam Air Products	N_2	99.99
Vadilal Gases Limited	CH_4	99.95

2.1.3.5 Adsorption Process Conditions

The equilibrium adsorption isotherms of three gases were assessed for various adsorbents with the gravimetric adsorption method. The assessments were conducted at a wide temperature range and were extended to atmospheric pressure conditions. The selection of temperature and pressure conditions in the Ph.D. thesis research works was based on their relevance for typical industrial applications. The adsorption experiments were conducted at 303 K, 323 K, and 343 K and upto 1 bar pressure. Such conditions simulate the conditions relevant to the post-combustion carbon capture systems in which CO_2 is present at low partial pressures in flue gases. These conditions are widely studied and provide a benchmark for the comparison of the performance of various sorbents.

The undertaken experimental investigations did not involve experiments at pressures beyond 1 bar. However, the consideration of higher pressures in experimental investigations, as encountered in pre-combustion or natural gas sweetening processes, could provide valuable insights into the adsorbent's performance under variant operational conditions. Such investigations to be undertaken in the future could extend the pressure range and the associated influence assessment in terms of the behavior of the adsorbents under high-pressure environments and their associated applicability. The experimental conditions at which adsorption measurements were conducted have been detailed in Table 2.3.

Table 2.3: A summary of various investigated adsorbents in the Ph.D. thesis and their range of operating conditions.

Adsorbent	Adsorbate	T (K)	Pressure Range (bar)
Zeolite-Y	CO_2	303	0-1
	CH_4	303	
	N_2	303	
Beta	CO_2	303	0-1
	CH_4	303	
	N_2	303	
ZSM-5	CO_2	303	0-1
	CH_4	303	
	N_2	303	
MEOH1	CO_2	303	0-1
MEOH5	CO_2, CH_4, N_2	303	
MEOH10	CO_2	303	
DEOH1, DEOH5, DEOH10	CO_2	303	0-1
TEOH1, TEOH5, TEOH10	CO_2	303	0-1
HYZC, LiYZC, NaYZC, KYZC	CO_2, CH_4, N_2	303, 323, 343	0-1
KYZC5	CO_2	303	0-1
KYZC10	CO_2, CH_4, N_2	303, 323, 343	
KYZC15	CO_2	303	

2.1.3.6 Physical Properties of Gases

The physical properties of gases are important to understand and predict their behavior. They as well influence the interaction of the gases with surfaces and external fields. Based on gas laws, the molecular weight of gas molecules affects their average kinetic energy at a given

temperature. Thereby, this property influences other key properties such as pressure and temperature. Gas molecules can adsorb onto surfaces and traverse porous materials. This is based on the size of gas molecules. Higher polarizability produces stronger London dispersion forces (van der Waals forces) between molecules. Polarizable gases interact more strongly with electric fields and other dipolar or charged species. This affects their chemical reactivity and interactions with the surfaces. Gases with significant quadrupole moments interact with non-uniform electric fields. This aspect influences their behavior in electrostatic adsorption processes. The physical properties of the gases deployed in the conducted research have been listed in Table 2.4.

Table 2.4: A summary of the adsorption-related molecular properties of various gases.

Gas	Molecular Weight ($gmol^{-1}$)	Kinetic Diameter (Å)	Polarizability ($\times 10^{25}$ cm^3)	Quadrupole Moment ($\times 10^{40}$ Cm^2)
He	4	2.58	2.06	0
CO_2	44	3.3	26.3	14.3
CH_4	16	3.8	26	0
N_2	28	3.64	17.6	1.52

2.1.4 Ranking methodology for the selection of the best commercial adsorbent

To evaluate upon the effectiveness of commercial zeolites as support materials for amine-functionalization and cation loading, a ranking methodology was deployed based on the data of the carbon dioxide adsorption studies. The three alternate zeolites (Zeolite-Y, β-Zeolite, and ZSM-5) were assessed for their CO_2 adsorption capacities. The findings conveyed that the Zeolite-Y exhibited the highest CO_2 adsorption capacity. This is attributed to its large pore diameter within the supercage structure that facilitates greater CO_2 uptake. Following Zeolite-Y, β-Zeolite demonstrated a commendable CO_2 adsorption capacity. ZSM-5, while effective,

exhibited the lowest CO_2 adsorption capacity among the selected zeolites. Consequently, Zeolite-Y was identified as the most suitable candidate for further studies that prompt upon the assessment of amine-functionalized or cation-loaded adsorbents.

2.2 Synthesis and characterization of amine-functionalized Zeolite-Y adsorbents

2.2.1 Base Materials

The materials used in this study were methanol (99.5%) (supplied by Sigma Aldrich), monoethanolamine, diethanolamine, and triethanolamine (98%) (provided by Sigma Aldrich), and Zeolite-Y (provided by Alfa Aesar). The CO_2 (99.9%), CH_4 (99.9%), N_2 (99.9%), and helium (99.9%) gas cylinders were purchased from Assam Air Products, Guwahati.

2.2.2 Adsorbent Synthesis

Three alternate amine loadings were considered to prepare amine-functionalized adsorbents (1 wt.%, 5 wt.%, and 10 wt.%). Monoethanolamine, diethanolamine, and triethanolamine were deployed as alternate amines. Firstly, high-temperature calcination was conducted for 4h for the Zeolite-Y support. This removed volatile materials. Thereafter, the synthesis process involved two separate sub-processes. In the first sub-process, the Zeolite-Y support was mixed with methanol for 20 min and a 1:2 solid-to-liquid loading ratio choice. Thereafter, the mixture was allowed to air dry for 180 min at room temperature. Such a mixture is termed as air-dried zeolite. In the second sub-process, amine with respective loading was added to methanol and was stirred for 20 min. This solution is termed as amine-solution. Subsequently, the air-dried zeolite from first sub-process and amine-solution from second sub-process were mixed for 120 min in a separate conical flask. Subsequently, the mixture was subjected to filtration and the adsorbent from the process was dried at 140°C in a vacuum oven for 180 min [12]. The

modified Zeolite-Y with monoethanolamine loading of 1 wt.%, 5 wt.%, and 10 wt.% have been designated as MEOH1, MEOH5, and MEOH10. Similarly, diethanolamine (DEOH) and triethanolamine (TEOH) were used to produce respective amine-loaded adsorbents (DEOH1, DEOH5, DEOH10, TEOH1, TEOH5, TEOH10). The visual representation of commercial Zeolite-Y and synthesized amine-functionalized adsorbent is represented in Appendix A2.1.

2.2.3 Adsorbent Characterization

The characterization of the materials was carried out with various analytical techniques such as X-ray diffraction (XRD), field emission scanning electron microscopy (FESEM), Fourier-transform infrared spectroscopy (FTIR), and Brunauer-Emmett-Teller (BET) surface area analyses. These have been detailed in section 2.1.2 of the Ph.D. thesis.

2.2.3.1 XPS Spectral Analysis

X-ray photoelectron spectroscopy (XPS) is a surface-sensitive, non-destructive technique being used to analyze the outermost layer of 10 nm approximate size (~30 atomic layers) of the assessed material. XPS is employed to determine the composition of material surfaces, perform semi-quantitative analyses of the relative abundances of surface components, and assess upon the chemical states of polyvalent ions. These are analyzed through the measured binding energies, which are indicative of the nature and strength of their chemical bonds.

XPS operates based on the photoelectric effect. As per this principle, electrons are emitted from atoms in response to incident electromagnetic radiation. When the energy of the incident photons exceeds the binding energy of the electrons in the material, photoelectrons are ejected. The energy of the incident photons ($h\vartheta$), which is fixed, influences the emission of photoelectrons. The kinetic energy ($E_{kinetic}$) of the emitted electrons is related to their binding

energy. Thus, XPS spectrum is produced and is characterized with a range of binding energies due to the prevalent multiple atomic orbitals.

The relationship between the kinetic energy of the emitted electrons and their binding energy is expressed as:

$$E_{kinetic} = E_{photon}(h\vartheta) - E_{binding} - \emptyset \quad (2.17)$$

where $E_{kinetic}$ is the kinetic energy of the photoelectron measured by the instrument, E_{photon} is the energy of the incident photon (1486.7 eV for the X-ray source used), $E_{binding}$ is the binding energy of the electron, and Ø is the work function that represents the energy difference between the vacuum level (E_ϑ) and the Fermi level (E_f) of the solid [13].

The XPS data were collected with a PHI 5000 Versa Probe III (Physical Electronics, USA) equipped with a micro-focused monochromatic K-Alpha X-ray source at 1486.7 eV. To ensure accurate spectral acquisition, the instrument provided charge compensation using low-energy electrons and positive ions. The samples were mounted on double-stick carbon tape. However, it was ensured that the powder is secure to avoid contamination of the sample chamber and degradation of the detectors.

2.2.4 Gas Adsorption Studies

In the conducted study, CO_2, CH_4, and N_2 adsorption on amine-functionalized Zeolite-Y were assessed to determine the sensitive influence of various amine groups and their loadings on the adsorption data. Zeolite-Y samples were functionalized with three types of amine groups—primary, secondary, and tertiary—at three different loadings: 1 wt.%, 5 wt.%, and 10 wt.%. The adsorption performance was assessed in terms of the CO_2 uptake capacity of these functionalized materials.

Among the amine groups tested, the Zeolite-Y functionalized with primary amines demonstrated the highest CO_2 adsorption capacity. Such a superior performance is attributed to the simpler molecular structure of primary amines. This enhanced their effectiveness in capturing CO_2 with respect to the secondary and tertiary amines. The findings convey that the primary amine functionalization favors CO_2 adsorption in this context.

2.3 Synthesis and characterization of cation-loaded Zeolite-Y adsorbents

2.3.1 Raw Materials

Zeolite-Y was purchased from Alfa Aesar, Hyderabad. The lithium carbonate, sodium carbonate, and potassium carbonate (≥98%) were obtained from Merck India Limited, Mumbai. The gas cylinders for carbon dioxide (99.99%), nitrogen (99.99%), methane (99.99%), and helium (99.995%) were purchased from Assam Air Products, GuwahatiThe Analytical-grade chemicals were used without any further purification.

2.3.2 Material Synthesis

The adsorbents were prepared using the wet-impregnation method and lithium, sodium, and potassium as cations. To do so, in the first step, Zeolite-Y was calcined for four hours at 600°C. To achieve a homogeneous mixture, sodium, potassium, or lithium carbonate (0.10g) was added to distilled water (5.0ml) and stirred for 20 minutes. Zeolite-Y (1g) was subsequently added to the solution and was stirred for 60 minutes. As a final step, activated adsorbents at different cation-loading were produced by drying the prepared adsorbents for 24 hours at 120°C [14]. Thereby, adsorbents with lithium, sodium, and potassium ions were synthesized and were labeled as LiYZC, NaYZC, and KYZC. The visual representation of synthesized adsorbents is presented in Appendix A2.1.

2.3.3 Material Characterization

The materials were characterized with a range of analytical techniques. Detailed descriptions of X-ray diffraction (XRD), Fourier-transform infrared spectroscopy (FTIR), and Brunauer-Emmett-Teller (BET) surface area analyses have been provided in section 2.1.2 of the Ph.D. thesis. Additionally, X-ray photoelectron spectroscopy (XPS) analysis as described in section 2.2.3.1 of the Ph.D. thesis has been conducted.

2.3.3.1 FETEM Structural Analysis

Transmission electron microscopy (TEM) is a high-resolution analytical technique being used to visualize structures at the atomic scale. TEM achieves magnification of nanometer-scale structures up to 50 million times. This surpasses the resolution capabilities of visible light microscopy due to the shorter wavelength of electrons, which is approximately 100,000 times smaller than that of visible light.

The TEM operates by generating a high-energy electron beam with a heated tungsten filament within the electron gun. This beam is focused onto the specimen through the condenser lenses and magnetic lenses. The electron column, maintained under vacuum, prevents interactions with air molecules. Thereby, it reduces deflections and ensures a clear image. As the electron beam interacts with the specimen, electrons are scattered. This creates variations in the image density. While denser regions of the specimen scatter more electrons and appear darker on the final image, thinner and more transparent regions allow more electrons to pass through and appear brighter.

To eventually form a TEM image, the electron beam is accelerated through an extremely thin, "electron transparent" sample, which is typically less than 100 nm in thickness. The beam is

then focused and magnified through a series of electromagnetic lenses and apertures. Thereby, the resultant image is projected onto a phosphor screen or specialized camera for visualization. Such a process allows for a detailed examination of structural features at the atomic scale [15].

High-resolution imaging was conducted with a 200 kV Field Emission Transmission Electron Microscope (FETEM) (JEOL, Model: JAM-2100F), and for a magnification range of 100-200 nm. The sample preparation involved a drop-casting method with isopropanol as the solvent. Precisely, two drops of the sample were deposited onto a TEM grid. The grid was then placed in a vacuum oven and was heated at 120°C for the overnight duration. This ensured complete solvent evaporation. Following the sample preparation process, the TEM grid was directly mounted into the TEM instrument for the imaging analysis.

2.3.4 Evaluation of Best Isotherm Model for Pure Gas

Isotherm models are often used to model adsorption equilibrium data. They are widely used to assess the pertinent adsorption mechanisms [16]. The conducted study primarily utilized two alternate adsorption isotherm models i.e. the Langmuir adsorption isotherm model and the Virial adsorption isotherm model.

2.3.4.1 Langmuir Isotherm Model

Langmuir developed a theoretical equilibrium isotherm that correlates the amount of gas adsorbed on the surface of an adsorbent with the gas pressure. The model is particularly suitable as the experimental adsorption isotherms being obtained from adsorption analysis are typically Type I isotherms [17]. The Langmuir isotherm model assumes a homogeneous distribution of reactive sites on the adsorbent surface and no lateral interactions between adsorbed molecules. The model applies to the case in which adsorption occurs in a monolayer. Thus, the surface has a fixed number of identical adsorption sites, and no migration of adsorbate molecules occurs

across the surface [18]. The non-linearized form of the Langmuir isotherm model, as proposed by Langmuir in 1918, is expressed as follows:

$$N = \frac{N^{max}\beta P}{1 + \beta P} \tag{2.18}$$

where P is the pressure (bar), N is the amount of adsorbed gas on the support (mmol g^{-1}), N^{max} is the saturation adsorption capacity (mmol g^{-1}), and β is Henry's constant (mmol g^{-1} bar^{-1}). The Henry's constant is represented as:

$$\beta = \beta^0 \exp\left(\frac{\beta^1}{T}\right) \tag{2.19}$$

where T is the temperature (K), β^0 and β^1 are denoted as entropy and enthalpy of adsorption at zero loading condition, respectively.

2.3.4.2 Virial Isotherm Model

The Virial adsorption isotherm model is another important model for providing an insight into the gas adsorption on solid surfaces. It is based on the virial equation of state. The equation determines the pressure of a gas for a given volume and temperature. It incorporates coefficients that account for intermolecular interactions. The model is represented as:

$$P = \frac{N}{\beta} exp(bN + cN^2) \tag{2.20}$$

where P (bar) is the pressure, and N (mmol g^{-1}) is the amount of adsorbent. Additionally, Henry's constant, β (mmol g^{-1} bar^{-1}), as well as two Virial coefficients (b, $mmol^{-1}$ g and c, $mmol^{-2}$ g^2) are included in the above expression. It is considered that these parameters are temperature-dependent, i.e.

$$b = b^0 \exp\left(\frac{b^1}{T}\right) \tag{2.21}$$

$$c = c^0 \exp\left(\frac{c^1}{T}\right) \tag{2.22}$$

where T represents adsorption temperature (K)

A Virial isotherm model is particularly useful for the adsorption data being measured at a wide range of pressures. The model enables a useful analysis of the adsorbate molecules and adsorbent surfaces. Unlike the Langmuir model, which assumes a homogeneous surface with identical adsorption sites, the Virial model can account for heterogeneity on the adsorbent surface. A Virial coefficient is determined experimentally and provides an insight into the nature of the interactions between an adsorbent and the adsorbed species.

2.3.4.3 Henry's constant

Henry's law describes the relationship between the partial pressure of the adsorptive fluid and the amount of adsorbate [5]. Henry constant is defined as the slope of the isotherm at zero pressure. This constant, which appears in linear adsorption isotherms, is analogous to Henry's gas law. Derived from Gibbs adsorption, it is used to determine the equilibrium state of adsorption for adsorbates at low and constant temperatures. According to Henry's adsorption isotherm, the equilibrium amount of adsorbate in the fluid is related to the partial pressure of the adsorptive fluid. This is expressed as:

$$\beta = \left(\frac{N}{P}\right)_{P \to 0} \tag{2.23}$$

where N is the amount of adsorbate (mmol g^{-1}), β is Henry's adsorption constant, and P is the pressure (bar) of the adsorbate on the adsorbent.

Henry's isotherm is not suitable for adsorption experiments being conducted at high temperatures and pressures. For such conditions, the molecular motion and significant interaction forces might result in large fluctuations in the potential energy [19].

2.3.4.4 Adsorption Enthalpy

The isosteric enthalpy of adsorption (Δh_{ads}) is an important parameter for an insight into the adsorption process of an adsorptive agent on an adsorbent. It describes the strength of the binding energy created between the adsorbate and the adsorbent. This exists due to an adsorptive agent's binding to an adsorbent's solid surface. An adsorbate with a high enthalpy of adsorption has a high affinity for an adsorbent. This facilitates a greater concentration of the adsorbed species under the same conditions.

Low pressures typically facilitate the highest affinity for the adsorbate for occupancy at the adsorption sites. This corresponds to higher $-\Delta h_{ads}$ values at very low loadings. The enthalpy of adsorption at zero coverage represents the interaction energy between initially adsorbed molecules. In the zero to low coverage range, the magnitude of the isosteric enthalpy of adsorption is primarily determined by the binding strength of the most favorable binding sites within the material. As these preferred sites become occupied, the enthalpy of adsorption usually decreases with increasing uptake [20]. The enthalpy of adsorption is typically determined either through experimental measurements or by using model-derived parameters based on the following equation:

$$\Delta h_{ads} = -R \left. \frac{\ln P}{1/T} \right|_N \tag{2.24}$$

where R is the universal gas constant ($JK^{-1}mol^{-1}$), P is the pressure (bar), T is the temperature (K), and N is the amount adsorbed (mmol g^{-1}). The slope of this equation can be fitted to a plot of lnP and 1/T at various loadings to determine the heat of adsorption. Statistically relevant

linear fits can only be made from measurements of isotherms at three alternate temperatures. The enthalpy of adsorption for Langmuir (eq. 2.18) and Virial (eq. 2.20) adsorption isotherm models are represented as:

$$\Delta h_{ads} = -\beta^1 R \tag{2.25}$$

$$\Delta h_{ads} = -R(\beta^1 + b^1 N + c^1 N^2) \tag{2.26}$$

Two adsorption isotherm models, Langmuir and Virial, were employed to characterize the adsorption of CO_2, CH_4, and N_2 gases. Thereby, Henry's constant and the heat of adsorption were determined for both cases.

2.3.5 Ideal Adsorbed Solution Theory for Gas Mixture Selectivity Estimation

The Ideal Adsorbed Solution Theory (IAST) is a predictive model being utilized to estimate multicomponent adsorption equilibrium and selectivity without experimental mixture data. The model is particularly valuable in gas purification and separation processes, and for cases that leverage upon the single-component adsorption isotherms for the prediction of the behavior of mixtures. According to IAST, the adsorbed phase is considered to be ideal. Thus, with no interactions among adsorbate molecules, the phase follows the principles of Raoult's law for vapor-liquid equilibrium [21]. In such a scenario, an ideal solution is assumed to have formed in the adsorbed phase. This is characterized by the equal spreading of pressures for all components at constant temperatures.

The spreading pressure (π) is an intensive variable being used to describe the state of the adsorbed phase and is calculated with the following integral expression [22]:

$$\frac{\pi A}{RT} = \int_0^{P_i^0} \frac{n_i}{P_i} dP_i \tag{2.27}$$

where A is the specific surface area of the adsorbent ($m^2\ g^{-1}$), R is the gas constant (8.314 $J\ K^{-1}\ mol^{-1}$), T is the temperature (K), and n_i represents the adsorption amount of component i. The

partial pressure (P_i) of a component is related to its spreading pressure π and can be expressed using Raoult's law:

$$P_i = y_i P = x_i P_i^0(\pi) \tag{2.28}$$

where $P_i^0(\pi)$ is the partial pressure of the pure component i, P is the total pressure (bar), and x_i and y_i are the mole fractions of component i in the adsorbed and gas phases, respectively. The total amount of adsorbed species is calculated with the expression:

$$\frac{1}{n_T} = \sum_{i=1}^{N_0} \frac{x_i}{n_i^0} \tag{2.29}$$

where N_0 is the number of components in the mixture, and n_i^0 is the standard loading state (mmol g^{-1}). The adsorption amount of component i is determined with the expression:

$$n_i = x_i n_T \tag{2.30}$$

The adsorption selectivity (S_{ij}) based on IAST is defined with the expression:

$$S_{ij} = \frac{x_i/x_j}{y_i/y_j} \tag{2.31}$$

where x_i and x_j are the mole fractions of components i and j in the adsorbed phase, and y_i and y_j are their respective mole fractions in the gas phase.

Based on experimental single-component adsorption isotherms, the Ideal Adsorbed Solution Theory (IAST) was employed to assess upon the selectivity of CO_2/CH_4 and CO_2/N_2 mixtures at 303 K. The gas mixture of CO_2, CH_4, and N_2 was chosen for its industrial relevance and the assessment of the practical selectivity of the adsorbent. CO_2 is a major greenhouse gas, CH_4 represents natural gas, and N_2 is a significant component of the flue gas. While CO_2 separation from CH_4 is highly desired in natural gas purification schemes, the CO_2/N_2 separation is highly desired in carbon capture and storage frameworks. Since these gases also exhibit diverse

adsorption characteristics, their utilization as the test gases prompts a comprehensive evaluation of the adsorbent's performance and selectivity under real-time scenarios.

For the CO_2/CH_4 system, while a CO_2 concentration of 5 mol% was used, a CO_2 concentration of 13 mol% was chosen for the CO_2/N_2 system and the utilized gas mixture compositions were as per a relevant prior art [23]. These concentrations were selected to simulate the typical compositions being found in natural gas and flue gas streams, respectively. The selected concentrations were as per the typical compositions being reported in the relevant prior art for natural gas and flue gas streams. While the gas mixtures used in this study do not fully replicate real-world industrial conditions due to the absence of additional contaminants, they do provide fundamental insights into the adsorption behavior of zeolites under controlled conditions.

2.3.6 Gas Adsorption Assessment Inference

A comprehensive study was carried out to evaluate the gas adsorption properties of alkali-cation-loaded Zeolite-Y and for CO_2, CH_4, and N_2 gases. The cation sources used were Li^+, Na^+, and K^+.

2.4 Influence of Potassium Carbonate Loading on the Cation-Loaded Zeolite-Y Adsorbent CO_2 Capture Characteristics

2.4.1 Materials

The raw materials utilized in this study have been detailed in Section 2.3.1. For cation loading studies with Zeolite-Y, only potassium carbonate (K_2CO_3) was employed. Such a choice was to assess upon the loading effect on the adsorption characteristics of the potassium-loaded Zeolite-Y adsorbent. Other raw materials discussed in Section 2.3.1 were not utilized in this

particular section, as potassium loading has been the sole objective for its sensitivity assessment.

2.4.2 Synthesis

All adsorbents were synthesized with the impregnation method and for variant potassium carbonate loadings of 5 wt.%, 10 wt.%, and 15 wt.% on Zeolite-Y. Initially, Zeolite-Y was calcined at 600°C for 4 h. Thereafter, firstly, potassium carbonate (either of 0.10 g, 0.20 g, and 0.30 g) was dissolved in 5 mL of distilled water and the mixture stirred for 20 minutes. Subsequently, 1 g of Zeolite-Y was added to the potassium carbonate solution, and the mixture was stirred for 60 minutes. This ensured complete impregnation. The adsorbents were then activated by drying at 120°C for 24 h. The adsorbents prepared with different potassium carbonate loadings were designated as KYZC5, KYZC10, and KYZC15. These respectively correspond to 5%, 10%, and 15% K_2CO_3 loadings [14].

2.4.3 Characterization

The materials were characterized with a variety of analytical techniques such as the X-ray diffraction (XRD), Fourier-transform infrared spectroscopy (FTIR), Brunauer-Emmett-Teller (BET) surface area analyses (details provided in section 2.1.2 of the Ph.D. thesis), X-ray photoelectron spectroscopy (XPS) (details provided in section 2.2.3.1 of the Ph.D. thesis), and the Field Emission Transmission Electron Microscopy (FETEM) analyses (detailed presented in section 2.3.3.1 of the Ph.D. thesis).

2.4.3.1 Thermal Stability Assessment

Thermogravimetric analysis (TGA) is a thermal analysis technique being used to monitor changes in the physical and chemical properties of materials and as a function of temperature.

The method involves the usage of a high-temperature furnace and a precise mass balance to track mass alterations in the sample being kept in a controlled purge gas stream. As the temperature of the system is incrementally increased, the TGA records the change in mass. Thereby, a plot can be generated for the weight loss versus temperature data. Such a plot provides valuable information with respect to the activation and decomposition temperatures of the material.

In the conducted TGA study, a Netzsch STA449F3A00 thermogravimetric analyzer was employed to evaluate the thermal properties of the adsorbent and for a temperature range of 25 to 900°C. To do so, firstly, approximately 10 mg of the sample was placed in a covered crucible. Thereafter, sample was the inserted into the TGA instrument. The analysis was carried out in an argon atmosphere and for a heating rate of 10°C/min. The resultant TGA data provided insights into the thermal behavior of the adsorbent.

2.4.4 Modelling Studies

The modeling studies for gas adsorption isotherms of CO_2, CH_4, and N_2 have been discussed in detail in section 2.3.4 of the Ph.D. thesis. The section provided an in-depth analysis of the adsorption behavior of the gases and for two alternate isotherm models. The theoretical framework and computational methods deployed for fitness studies with the experimental data and subsequent interpretation of the adsorption characteristics have been thoroughly described. The modeling approach referred to the application of Langmuir and Virial adsorption isotherms for the evaluation of the adsorption capacity of the adsorbents. Additionally, the section addresses the parameters (Henry's constant and heat of adsorption) derived from the models and their implications for an insight into the interaction between the gases and the adsorbent materials.

2.4.5 Application of IAST for Selectivity Prediction

The selectivity of the optimized material for CO_2 over CH_4 and N_2 has been addressed in detail. To do so, a comprehensive explanation of the Ideal Adsorbed Solution Theory (IAST) provided in section 2.3.5 of the Ph.D. thesis has been adopted. The section highlights the utility of IAST for the prediction of the adsorption selectivity of CO_2 to CH_4 and N_2.

2.4.6 Gas Adsorption Studies

The gas (CO_2, CH_4, and N_2) adsorption studies were conducted with the synthesized materials at temperatures of 303 K, 323 K, and 343 K.

2.5 Summary

The chapter provides a comprehensive analysis of the characterization and evaluation of various adsorbents for CO_2 capture. Initially, commercial adsorbents were characterized, and their CO_2 adsorption capacities were assessed to select a suitable support material for further studies. Based on these assessments, a support material with an optimal CO_2 adsorption capacity was chosen.

The chapter then details upon the synthesis and characterization of amine-functionalized adsorbents, including monoethanolamine, diethanolamine, and triethanolamine. CO_2 adsorption studies on these amine-functionalized adsorbents were conducted to evaluate their efficacy. Following this, the focus shifted to alkali-cation-loaded adsorbents, specifically incorporating Li^+, Na^+, and K^+. These adsorbents were synthesized, characterized, and subjected to gas adsorption studies involving CO_2, CH_4, and N_2.

Modeling studies using the Langmuir and Virial adsorption isotherm models were performed to understand the adsorption behavior and derive thermodynamic parameters such as Henry's

constant and the heat of adsorption. Additionally, the selectivity of gas mixtures was evaluated using the Ideal Adsorbed Solution Theory (IAST). Based on the comprehensive analysis, the best-performing cation-loaded adsorbent was selected for further optimization. This included synthesizing adsorbents with various weight percentages of the cation and characterizing them through multiple techniques. Gas adsorption studies for CO_2, CH_4, and N_2 were carried out, and the adsorption behavior was modeled to provide insights into the adsorbents' performance and selectivity for practical applications in gas separation.

References

[1] C.F. Holder, R.E. Schaak, Tutorial on Powder X-ray Diffraction for Characterizing Nanoscale Materials, ACS Nano. 13 (2019) 7359–7365. https://doi.org/10.1021/acsnano.9b05157.

[2] H. Jaksch, J.-P. Vermeulen, New Developments in Gemini® Fesem Technology, Micros. Today. 13 (2005) 8–11. https://doi.org/10.1017/S1551929500051397.

[3] S.A. Khan, S.B. Khan, L.U. Khan, A. Farooq, K. Akhtar, A.M. Asiri, Fourier Transform Infrared Spectroscopy: Fundamentals and Application in Functional Groups and Nanomaterials Characterization, in: Handb. Mater. Charact., Springer International Publishing, Cham, 2018: pp. 317–344. https://doi.org/10.1007/978-3-319-92955-2_9.

[4] F. Ambroz, T.J. Macdonald, V. Martis, I.P. Parkin, Evaluation of the BET Theory for the Characterization of Meso and Microporous MOFs, Small Methods. 2 (2018). https://doi.org/10.1002/smtd.201800173.

[5] M.A. Al-Ghouti, D.A. Da'ana, Guidelines for the use and interpretation of adsorption isotherm models: A review, J. Hazard. Mater. 393 (2020) 122383. https://doi.org/10.1016/j.jhazmat.2020.122383.

[6] X.-F. Yan, X.-R. Fan, Q. Wang, Y. Shen, An adsorption isotherm model for adsorption performance of silver-loaded activated carbon, Therm. Sci. 21 (2017) 1645–1649. https://doi.org/10.2298/TSCI151202048Y.

[7] M. Abunowara, M.A. Bustam, S. Sufian, U. Eldemerdash, Measurement techniques for carbon dioxide sorption capacity on various coal samples: critical review, IOP Conf. Ser. Earth Environ. Sci. 36 (2016) 012059. https://doi.org/10.1088/1755-1315/36/1/012059.

[8] D.P. Broom, Challenges in characterizing adsorbents for gas storage and separation, Adsorption. (2023). https://doi.org/10.1007/s10450-023-00424-9.

[9] S. Harpalani, B.K. Prusty, P. Dutta, CH_4/CO_2 Sorption Modeling for Coalbed Methane Production and CO_2 Sequestration, Energy & Fuels. 20 (2006) 1591–1599. https://doi.org/10.1021/ef050434l.

[10] M. Sudibandriyo, Z. Pan, J.E. Fitzgerald, R.L. Robinson, K.A.M. Gasem, Adsorption of Methane, Nitrogen, Carbon Dioxide, and Their Binary Mixtures on Dry Activated Carbon at 318.2 K and Pressures up to 13.6 MPa, Langmuir. 19 (2003) 5323–5331. https://doi.org/10.1021/la020976k.

[11] S. Ottiger, R. Pini, G. Storti, M. Mazzotti, R. Bencini, F. Quattrocchi, G. Sardu, G. Deriu, Adsorption of pure carbon dioxide and methane on dry coal from the sulcis coal province (SW Sardinia, Italy), Environ. Prog. 25 (2006) 355–364. https://doi.org/10.1002/ep.10169.

[12] M. Babaei, M. Anbia, M. Kazemipour, Improving CO_2 adsorption with new amine-functionalized Y-type zeolite, J Adv. Env. Heal. Res. 5 (2017) 70–77. https://doi.org/https://doi.org/10.22102/jaehr.2017.71674.

[13] F.A. Stevie, C.L. Donley, Introduction to x-ray photoelectron spectroscopy, J. Vac. Sci. Technol. A Vacuum, Surfaces, Film. 38 (2020). https://doi.org/10.1116/6.0000412.

[14] S. Sengupta, V. Amte, R. Dongara, A.K. Das, H. Bhunia, P.K. Bajpai, Effects of the Adsorbent Preparation Method for CO_2 Capture from Flue Gas Using K_2CO_3 /Al_2O_3 Adsorbents, Energy & Fuels. 29 (2015) 287–297. https://doi.org/10.1021/ef501792c.

[15] D.J. Flannigan, A.H. Zewail, 4D Electron Microscopy: Principles and Applications, Acc. Chem. Res. 45 (2012) 1828–1839. https://doi.org/10.1021/ar3001684.

[16] J. Wang, X. Guo, Adsorption isotherm models: Classification, physical meaning, application and solving method, Chemosphere. 258 (2020) 127279. https://doi.org/10.1016/j.chemosphere.2020.127279.

[17] S.R. Olsen, F.S. Watanabe, A Method to Determine a Phosphorus Adsorption Maximum

of Soils as Measured by the Langmuir Isotherm1, Soil Sci. Soc. Am. J. 21 (1957) 144. https://doi.org/10.2136/sssaj1957.03615995002100020004x.

[18] R.K. Gautam, A. Mudhoo, G. Lofrano, M.C. Chattopadhyaya, Biomass-derived biosorbents for metal ions sequestration: Adsorbent modification and activation methods and adsorbent regeneration, J. Environ. Chem. Eng. 2 (2014) 239–259. https://doi.org/10.1016/j.jece.2013.12.019.

[19] Z. Wang, Y. Li, P. Guo, W. Meng, Analyzing the Adaption of Different Adsorption Models for Describing the Shale Gas Adsorption Law, Chem. Eng. Technol. 39 (2016) 1921–1932. https://doi.org/10.1002/ceat.201500617.

[20] A. Nuhnen, C. Janiak, A practical guide to calculating the isosteric heat/enthalpy of adsorption via adsorption isotherms in metal-organic frameworks, MOFs, Dalt. Trans. 49 (2020) 10295–10307. https://doi.org/10.1039/D0DT01784A.

[21] K.S. Walton, D.S. Sholl, Predicting multicomponent adsorption: 50 years of the ideal adsorbed solution theory, AIChE J. 61 (2015) 2757–2762. https://doi.org/10.1002/aic.14878.

[22] R. Krishna, J.M. van Baten, How Reliable Is the Ideal Adsorbed Solution Theory for the Estimation of Mixture Separation Selectivities in Microporous Crystalline Adsorbents?, ACS Omega. 6 (2021) 15499–15513. https://doi.org/10.1021/acsomega.1c02136.

[23] A. Khademi, E.G. Babakhani, J.T. Darian, H.R. Mahdipoor, M. Pourkhalil, Adsorption study of CO_2/CH_4 and CO_2/N_2 binary mixtures on titanosilicates ETS-10 and SrETS-10; industrial application aspects, Results in Surfaces and Interfaces. 16 (2024) 100259. https://doi.org/10.1016/j.rsurfi.2024.100259.

CHAPTER 3

Exploring the Synergistic Impact of Amine-Functionalization on Zeolite-Y for Gas Adsorption

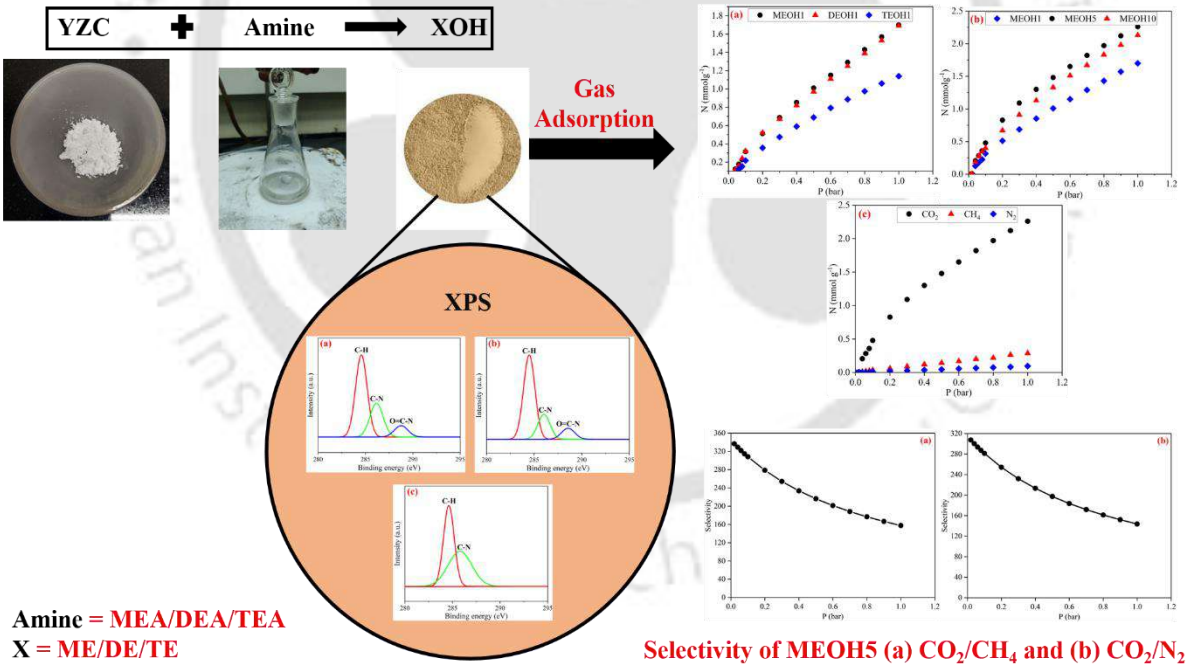

Chapter 3

Exploring the Synergistic Impact of Amine-Functionalization on Zeolite-Y for Gas Adsorption

In the pursuit of enhancing gas adsorption capacities for industrial applications, the selection of optimal zeolites plays a pivotal role. This chapter discusses the performance comparison of three zeolites available commercially: Zeolite-Y, Beta, and ZSM-5. A series of rigorous evaluations identifies the best-performing zeolite based on its adsorption efficiency. The chapter explores further the functionalization of the selected zeolite with amine groups to enhance its adsorption capabilities. The investigation is substantiated by comprehensive gas adsorption studies, complemented by thermodynamic analyses, to elucidate amine functionalization's underlying mechanisms and efficacy in improving gas adsorption performance.

3.1 Background

Zeolites are crystalline aluminosilicates with a porous structure, which makes them ideal for adsorption applications such as gas capture. Zeolites exhibit high thermal stability, chemical resistance, and large surface areas, crucial for efficient gas adsorption. Among the wide array of zeolites, three commercially significant types—Zeolite-Y, Beta, and ZSM-5—are frequently studied for their CO_2 adsorption capacities.

A comparative study was conducted on the CO_2 adsorption capacities of Zeolite-Y, Beta, and ZSM-5 to identify effective CO capture materials. These three zeolites were selected based on their structural diversity and previously reported potential for gas adsorption applications. Zeolite-Y is known for its large pore size and high adsorption capacity, making it suitable for capturing larger molecules such as CO_2. Zeolite Beta exhibits high surface area and microporosity, which can potentially enhance adsorption efficiency. Zeolite ZSM-5 features a

medium pore size and a unique channel structure, offering distinctive adsorption characteristics. The term "medium pore size" for ZSM-5 typically refers to a pore size range of 5–6 Å. Such a value range arises from its unique MFI framework structure. This framework consists of the intersection of the straight and sinusoidal channels with 10-membered ring openings and contributes to its distinct adsorption characteristics. The mentioned pore size range allows the ZSM-5 sorbent to exhibit selective adsorption for molecules with kinetic diameters within the mentioned range. Such molecules include the CO_2. The CO_2 adsorption capacities of the three zeolites were systematically evaluated under controlled conditions. The adsorption studies revealed that Zeolite-Y outperformed Zeolite Beta and ZSM-5 in terms of CO_2 uptake.

The superior adsorption capacity of Zeolite-Y is attributed to its larger pore volume and higher affinity for CO_2 molecules. Given its exceptional performance in CO_2 adsorption, Zeolite-Y was CO_2 capture and sequestration applications in CO_2 capture and sequestration.

The selection of the best zeolite for CO_2 adsorption was determined through a comparative study of Zeolite-Y, Beta, and ZSM-5, with Zeolite-Y demonstrating the highest adsorption capacity. The promising results for Zeolite-Y have led to its further enhancement via amine-functionalization, which is anticipated to elevate its performance in practical CO_2 capture scenarios. This research contributes to the ongoing development of efficient materials for mitigating the environmental impact of CO_2 emissions.

3.2 Commercial Zeolite Assessment

3.2.1 Characterization

Figure 3.1 (a) shows the XRD pattern of Zeolite-Y, Beta, and ZSM-5 in the 2θ range of 5-45°. The XRD peaks of Zeolite-Y exhibited at 6.28°, 10.26°, 12°, 15.78°, 18.84°, 20.5°, 23°, 23.84°, 27.22°, 29.88°, 30.96°, 31.6°, and 34.3°. The appearance of all sharp peaks is due to the

topology structure of the Zeolite-Y framework. Beta zeolite peaks at 7.92°, 14.64°, 22.64°, and 25.62° are broad peaks which is due to the amorphous nature of the material. The beta zeolite does not possess the periodicity and atoms are randomly distributed in the space. ZSM-5 revealed the characteristic diffraction peaks at 2θ values around 7.88°, 8.78°, 14.74°, 23.02°, 23.86°and 29.86°. These values were completely indexed to the structure of MFI topology and sharp peaks showed good crystallinity.

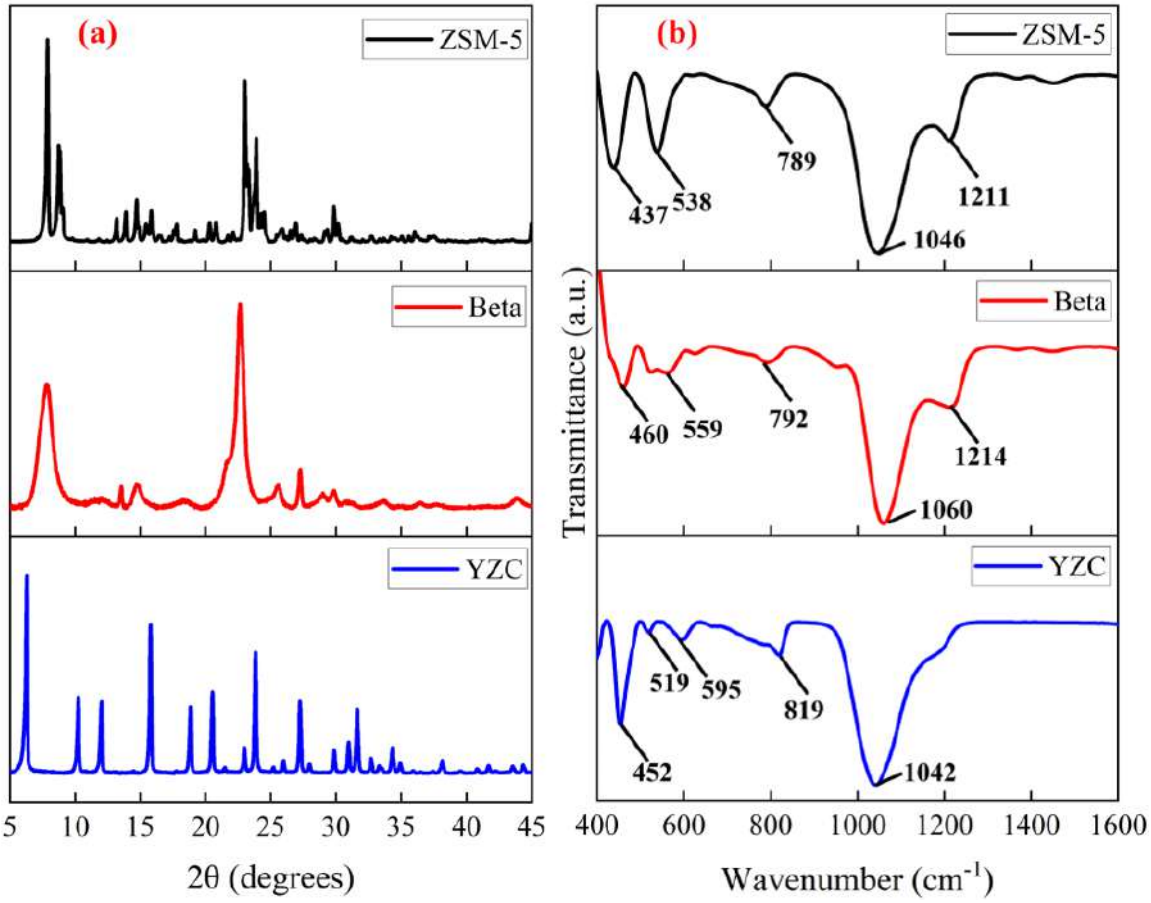

Figure 3.1: (a) XRD pattern and (b) FTIR spectra of commercial zeolites.

The functional groups and surface acidity of the adsorbents were characterized using Fourier Transform Infrared Spectroscopy (FTIR). Figure 3.2(b) presents the FTIR spectra of the studied zeolites, highlighting key vibrational modes that provide insights into their structural properties. For Zeolite-Y, the absorption band at 452 cm^{-1} corresponds to the O-T-O bending

vibrations. The internal TO_4 tetrahedral bending vibrations for zeolites generally occur in the range of 437-519 cm^{-1}, indicating the presence of the tetrahedral framework structure.

All zeolites exhibited an absorption band in the range of 538-595 cm^{-1}, which is attributed to variations in the five- or six-membered ring structures of the composite building units (CBU). This range highlights the structural diversity among the different zeolites. The external symmetric stretching vibrations of the zeolite framework are observed in the range of 789-819 cm^{-1}. Additionally, a strong band in the range of 1042-1060 cm^{-1} indicates the internal asymmetric stretching of the T-O-T bond, a crucial characteristic of the zeolite framework. Beta and ZSM-5 zeolites also show bending vibrations in the range of 1211-1214 cm^{-1}, which are assigned to the external asymmetric stretching of the T-O-T bond. These observations confirm the presence of specific functional groups and the integrity of the zeolite structure, which are essential for their performance in CO_2 adsorption [1].

The morphologies of all raw zeolites were analyzed by SEM and results are presented in Figure 3.2 at a magnification of 20 KX with a particle size in the range of 100-200 nm. The SEM image of Zeolite-Y exhibits a typical crystal-like structure with a tetrahedral and hexagonal structure. It is seen from both SEM images of beta zeolite possessing almost spherical-shaped morphologies. The SEM images of ZSM-5 confirmed that it has high crystallinity, uniform in size and shape. It could be seen that it exhibited a typical hexagonal morphology characteristic of MFI-type zeolites.

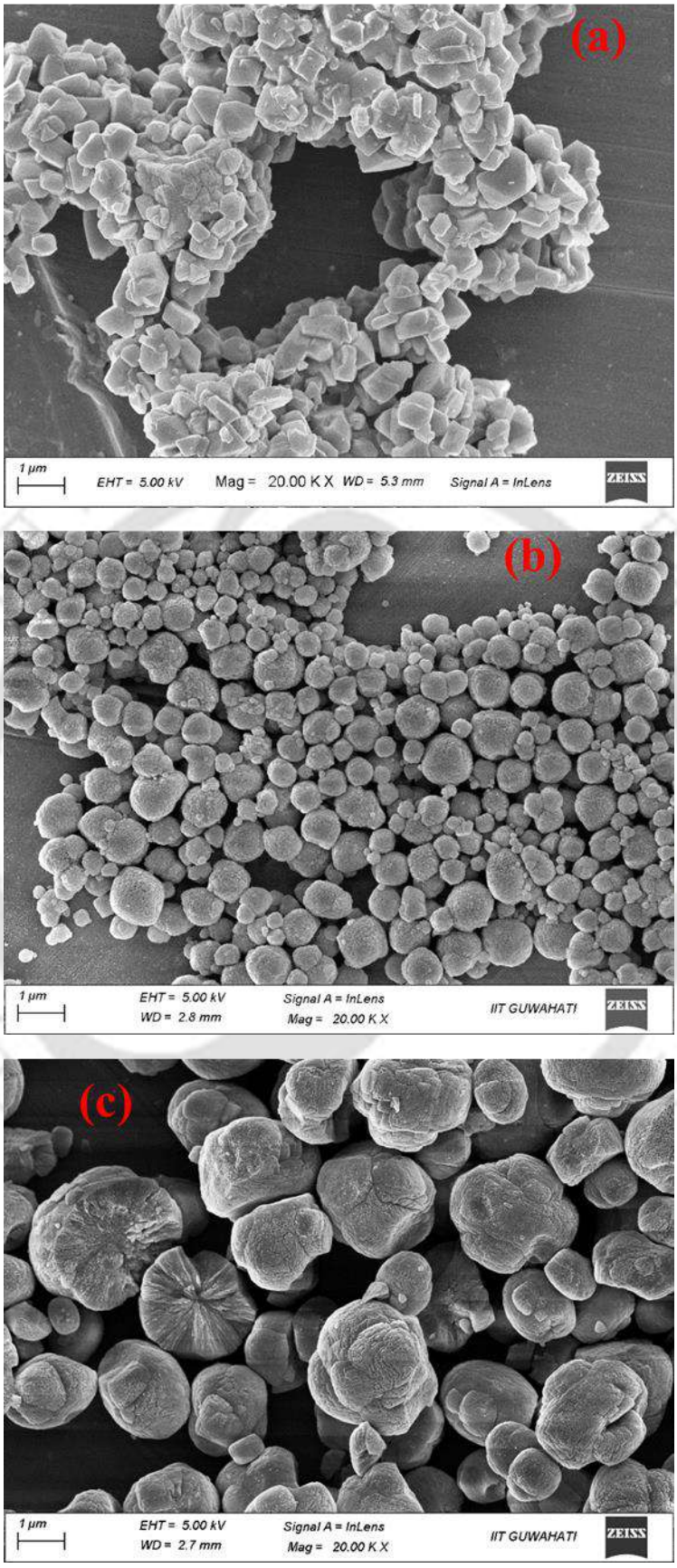

Figure 3.2: FESEM images of (a) YZC, (b) Beta, and (c) ZSM-5 at 20kX magnification.

In this study, the BET isotherms (Figure 3.3) for N_2 adsorption/desorption on three zeolites—Zeolite-Y, Beta, and ZSM-5—are presented to compare their pore structures and surface areas. The N_2 adsorption/desorption isotherm for Zeolite-Y shows a Type I isotherm, characteristic of microporous materials. The initial steep rise at low relative pressures indicates a high affinity for N_2 adsorption due to the presence of micropores. The plateau at higher relative pressures suggests that the micropores are filled, and there is limited mesoporosity. This behavior is typical of materials with a large surface area and significant micropore volume.

The N_2 adsorption/desorption isotherm for Beta zeolite exhibits a combination of Type I and Type IV isotherms. The initial steep rise at low relative pressures indicates the presence of micropores, while the subsequent increase at higher relative pressures suggests the presence of mesopores. This dual behavior indicates that Beta zeolite has both microporous and mesoporous structures, providing a moderate surface area and pore volume suitable for various adsorption applications.

The N_2 adsorption/desorption isotherm for ZSM-5 also shows a combination of Type I and Type IV isotherms, similar to Beta zeolite. The initial rise at low relative pressures indicates the presence of micropores, while the increase at higher relative pressures and the hysteresis loop in the desorption branch indicate mesoporosity. This suggests that ZSM-5 has a mixed pore structure with both micropores and mesopores but with a lower surface area and pore volume compared to Zeolite-Y and Beta.

These findings are crucial for selecting the appropriate zeolite for specific applications, particularly in the context of gas adsorption. The superior properties of Zeolite-Y make it a prime candidate for further functionalization and optimization to enhance its adsorption capabilities.

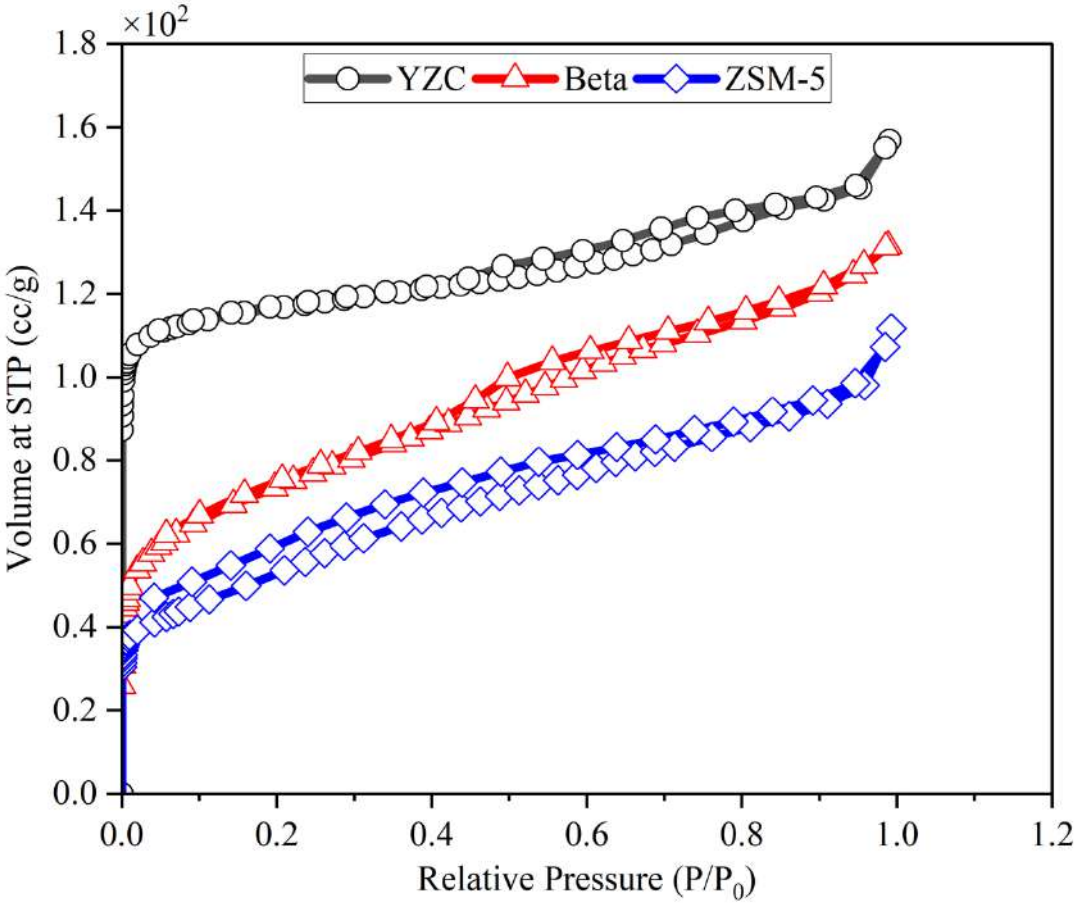

Figure 3.3: N_2 adsorption-desorption isotherm plot of commercial zeolites.

3.2.2 Adsorption Study

Zeolite Y is a Faujasite [FAU] framework and thus has the crystalline structure channels run in three perpendicular dimensions and intersect to form large and spherical internal cavities. The FAU framework consists of sodalite building blocks that are connected through double 6 rings (D6Rs), forming a super cage with a 12MR window. Beta zeolite has a large pore size and complex structure. It has a three-dimensional pore network with intersecting channels having 12 tetrahedral atom apertures, giving rise to large internal cavities similar to those in Zeolite-Y but the third channel is tortuous [2].

ZSM-5[MFI] is a medium pore zeolite with interconnected channels. The framework contains straight 10MR channels that are intersected by sinusoidal 10MR channels. The structure was

geometrically optimized, which resulted in one cation being located in a 5MR adjacent to the wall of the 10MR main channel, and the other cation in the 10MR channel. This study showed that the interaction of CO_2 occurs only with the cation site located in the 10MR channel because this is the only site accessible to CO_2. The cation that is situated in a 5MR adjacent to the wall is not accessible to CO_2 because the kinetic diameter of CO_2 (3.3Å) is much larger than the pore size of the 5MR (approximately1.5Å) through which the cation is accessed [3].

Figure 3.4 illustrates the CO_2, CH_4, and N_2 adsorption performance of Zeolite-Y, beta, modernite, and ZSM-5 zeolites as a support material at 303 K. The reduction of adsorption capacity depends on the pore size of the support. In Zeolite-Y, the other sites except supercage are also available for adsorption. The double six-membered rings are available for the adsorption which is also a factor to enhance the adsorption. Zeolite-Y's carbon dioxide adsorption capacity (1.869 mmol g^{-1}) is high compared to the remaining three zeolites because of the high supercage pore diameter.

The adsorption capacity of carbon dioxide (CO_2) is notably higher compared to methane (CH_4) and nitrogen (N_2) due to several intrinsic properties of CO_2 and the corresponding interactions with the adsorbent surface. CO_2 possesses a relatively high quadrupole moment, which contributes to stronger van der Waals forces and significant electrostatic interactions with the adsorbent, particularly when the adsorbent surface contains active sites capable of engaging in such interactions. These interactions are further enhanced in adsorbents with cation exchange sites, which preferentially attract and bind CO_2 molecules.

In contrast, CH_4 and N_2 exhibit lower quadrupole moments, resulting in predominantly weaker van der Waals interactions with the adsorbent surface. Consequently, the adsorption capacities for CH_4 and N_2 are considerably lower compared to CO_2. Additionally, the smaller kinetic diameter of CO_2 allows it to be more efficiently accommodated within the micropores of the

adsorbent, compared to the larger kinetic diameters of CH_4 and N_2. This size exclusion effect further enhances the selectivity of adsorbents towards CO_2 over CH_4 and N_2, leading to a higher overall adsorption capacity for CO_2.

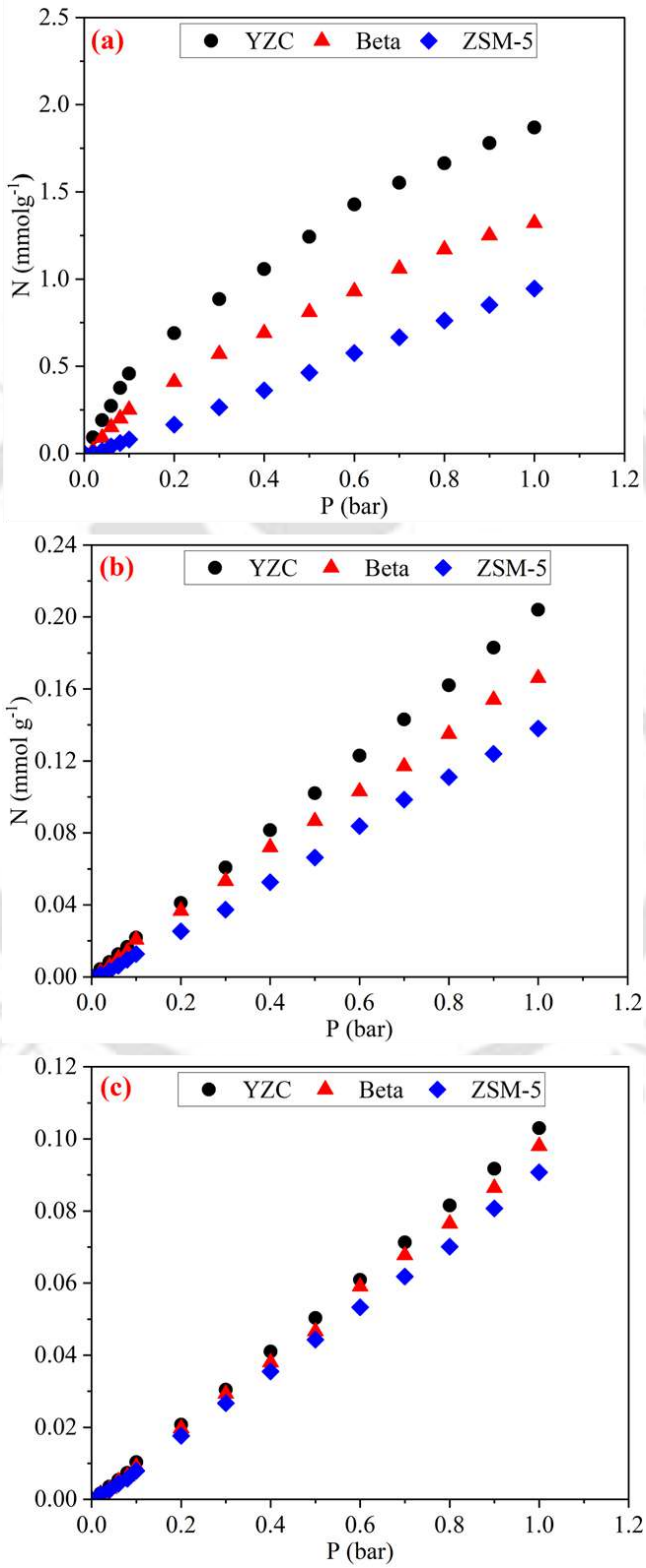

Figure 3.4: (a) CO_2, (b) CH_4, and (c) N_2 adsorption capacities at 303K for commercial zeolites.

3.3 Amine-functionalized Zeolite

The amine-loaded Zeolite-Y adsorbents were evaluated to enhance carbon dioxide adsorption capacity through synthesis, characterization, and the adsorption of carbon dioxide, within the context of current trends in separation technology. This study aims to study the ability of amine-loaded Zeolite-Y to adsorb carbon dioxide using three different loadings ethanolamine, diethanolamine, and triethanolamine.

3.3.1 Characterization

Figure 3.5(a) shows the thermal behavior of all the amine-loaded zeolites. They were obtained with the TGA instrument under N_2 conditions. The characterization was carried out in a temperature range of 25 to 600°C and at a heating rate of 10°C/min. It was observed that a two-step decomposition process occurred in the synthesized adsorbents (between 25 and 200°C and 200 and 600°C). The TGA profile indicated that the physically adsorbed water molecules got desorbed in the first step. The second region in the range of 200°C and 600°C can be attributed to the volatilization of the entrapped amine material. The heat treatment of materials from 160°C to 600°C did not result in significant weight loss. This confirmed the high thermal stability of all the synthesized samples. The mass loss profile showed a larger variation in the order of MEOH<DEOH<TEOH loaded zeolite adsorbents, which follows the boiling point order (MEOH<DEOH<TEOH).

X-ray diffraction was used for the determination of crystallinity in functionalized and commercial samples. Figure 3.5(b) shows the XRD patterns of Zeolite-Y and amine-functionalized Zeolite-Y. Based on the X-ray powder diffraction of amine-functionalized Zeolite-Y, it appears that the crystal structure of Zeolite-Y was retained even after the modification. This conveys that the impregnation process did not affect crystallinity in any of the synthesized samples. Also, the diffraction peaks located at 2θ values of 6.28°, 15.82°, and

23.86° can be seen in all the samples. This indicates the presence of an ordered hexagonal structure.

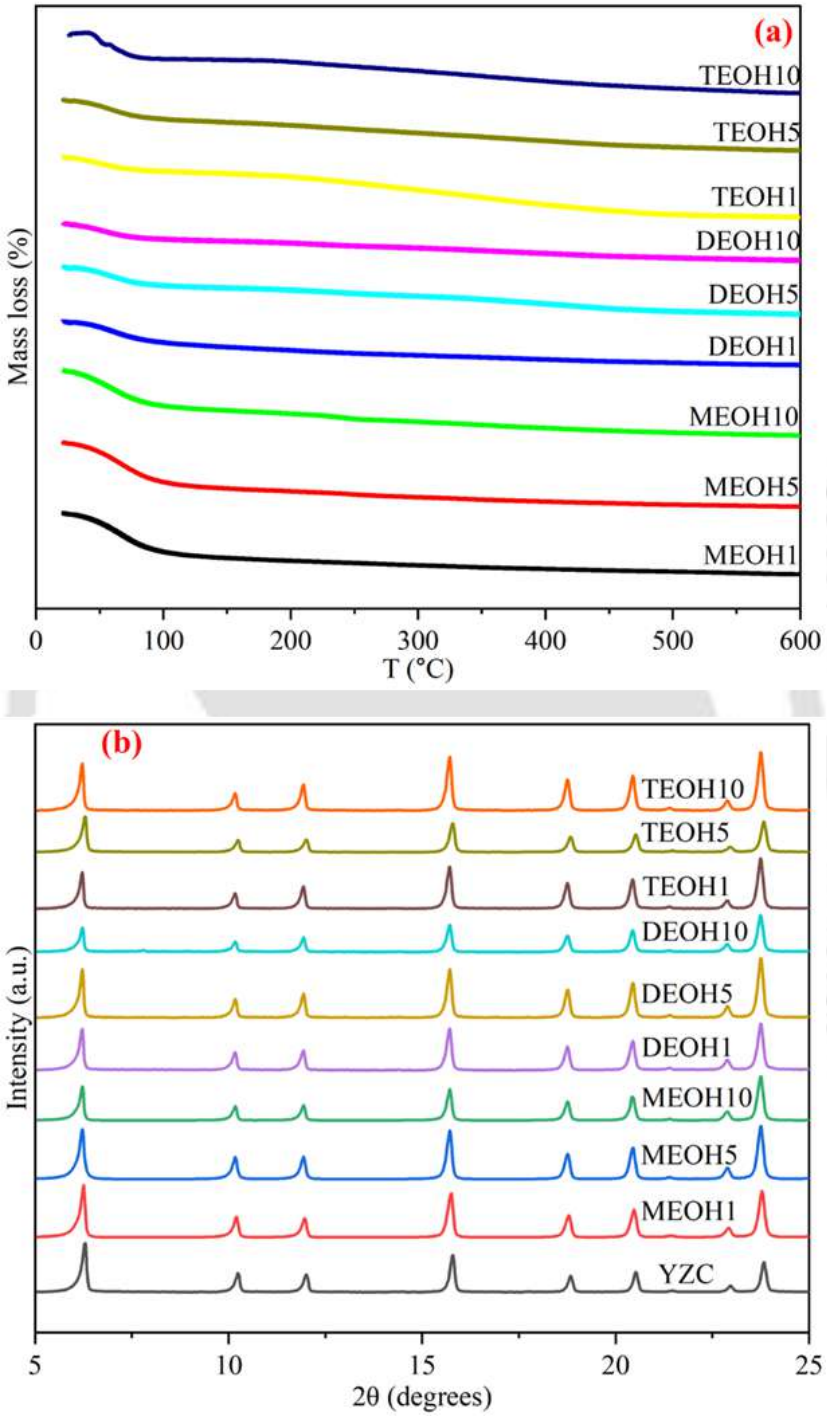

Figure 3.5: (a) TGA curve and (b) XRD pattern of amine-functionalized Zeolite-Y samples.

Figure 3.6 depicts nitrogen adsorption-desorption isotherms of amine-functionalized Zeolite-Y samples. For this case, a typical type-IV adsorption isotherm exists along with a hysteresis

loop. This conveyed a uniform mesoporous structure since the high volume of nitrogen got adsorbed at very low relative pressures. Therefore, marginally higher nitrogen uptake observed at lower pressures, in the range of 0.0-0.1, can be probably attributed to the fact that amine groups added to the pure Zeolite-Y occupy the surface and pore openings of the support. The relative pressure in the range between 0.3 and 0.4 has a steep capillary condensation inflection. This was confirmed by the narrow pore size distribution in mesoporous materials. A sharp increase of relative pressures in the range of 0.9-1.0 was prevalent in some isotherms. This is probably due to multi-layer adsorption. The Zeolite-Y being impregnated with other amine groups and at various amine loadings, affirmed progressive decline in the nitrogen uptake with the increasing loading.

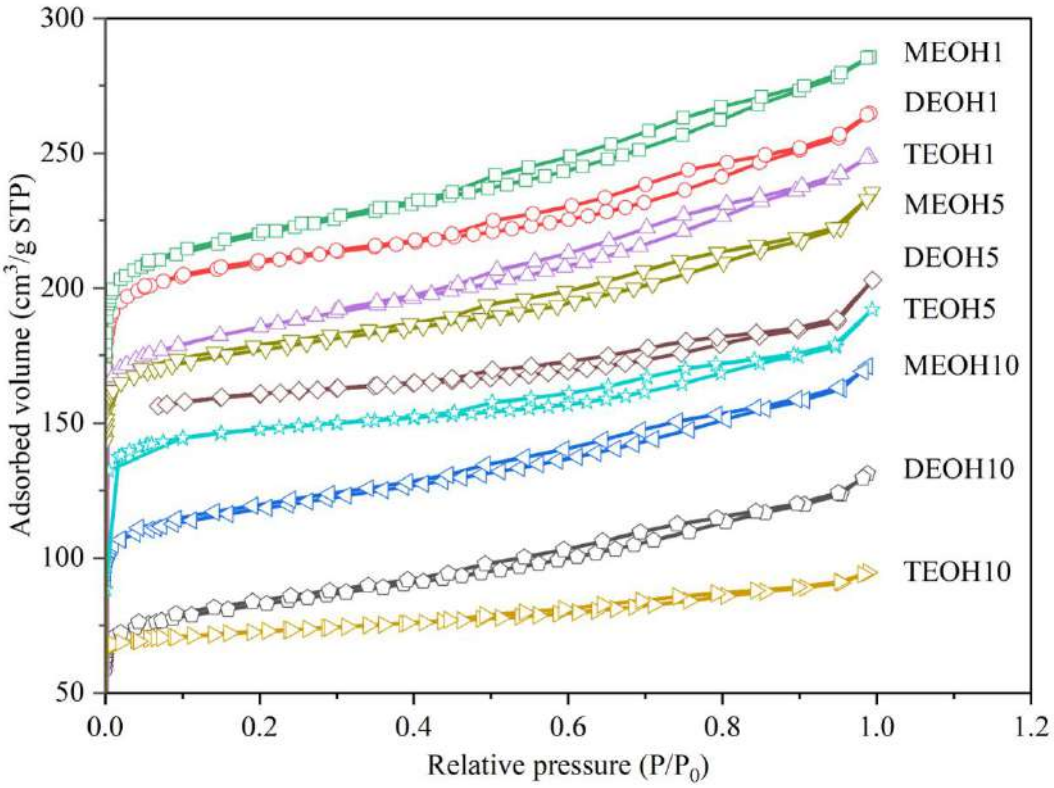

Figure 3.6: Nitrogen adsorption isotherms at 77 K of the amine-functionalized Zeolite-Y.

Table 3.1 shows the surface properties of amine-functionalized Zeolite-Y. The surface area, pore volume, and pore size were determined using N_2 isotherms. For enhanced amine loading, the specific surface area and pore volume are reduced at a progressive rate. This indicated that

the amine groups filled the pores and prevented nitrogen from being adsorbed. Zeolite-Y loaded with the lowest amine wt.% and the commercial Zeolite-Y had similar surface characteristics.

Table 3.1: Textural properties of amine-functionalized Zeolite-Y.

Adsorbent	S_{BET} (m^2/g)	V_t (cc/g)	$P.D._{avg}$ (nm)
YZC	355.26	0.24	2.73
MEOH1	308.08	0.22	1.88
MEOH5	286.60	0.20	2.03
MEOH10	212.75	0.15	2.60
DEOH1	280.29	0.18	2.01
DEOH5	269.82	0.17	2.73
DEOH10	192.61	0.13	3.27
TEOH1	266.82	0.16	2.68
TEOH5	206.83	0.14	3.90
TEOH10	101.02	0.11	4.48

Figure 3.7 shows the FTIR spectra of Zeolite-Y and the amine-functionalized Zeolite-Y adsorbents. All the samples exhibited symmetric T-O bands at 450 cm^{-1} (T: Si or Al) resulting from internal vibrations of the TO_4 (SiO_4 and AlO_4) tetrahedron framework. Additionally, the spectrum suggests that the tetrahedral units are externally linked at 590 cm^{-1}, and confirmed secondary building units (SBU) and external linkage. The IR spectrum of samples conveyed

significant bands at 810 cm^{-1}, which are related to T-O-T (Si-O-Si or Si-O-Al) symmetry stretching (external linkage to symmetric stretch reflecting structure). The strongest vibration at 1029 cm^{-1} occurred due to an asymmetric stretching mode O-T-O that involved motions primarily associated with oxygen atoms. The sample's IR spectra affirmed a peak at 1633 cm^{-1} related to O-H stretching, which is due to the existence of water molecules. The peak intensities of synthesized samples corresponding to the Zeolite-Y structure reduced after amine loading. The peaks found in the region 3387 cm^{-1} provide important information on impregnated amine groups [4]. In comparison to Zeolite-Y and amine-functionalized samples, the presence of an additional peak can be observed for amine-loading with N-H stretching on the surfaces of adsorbents.

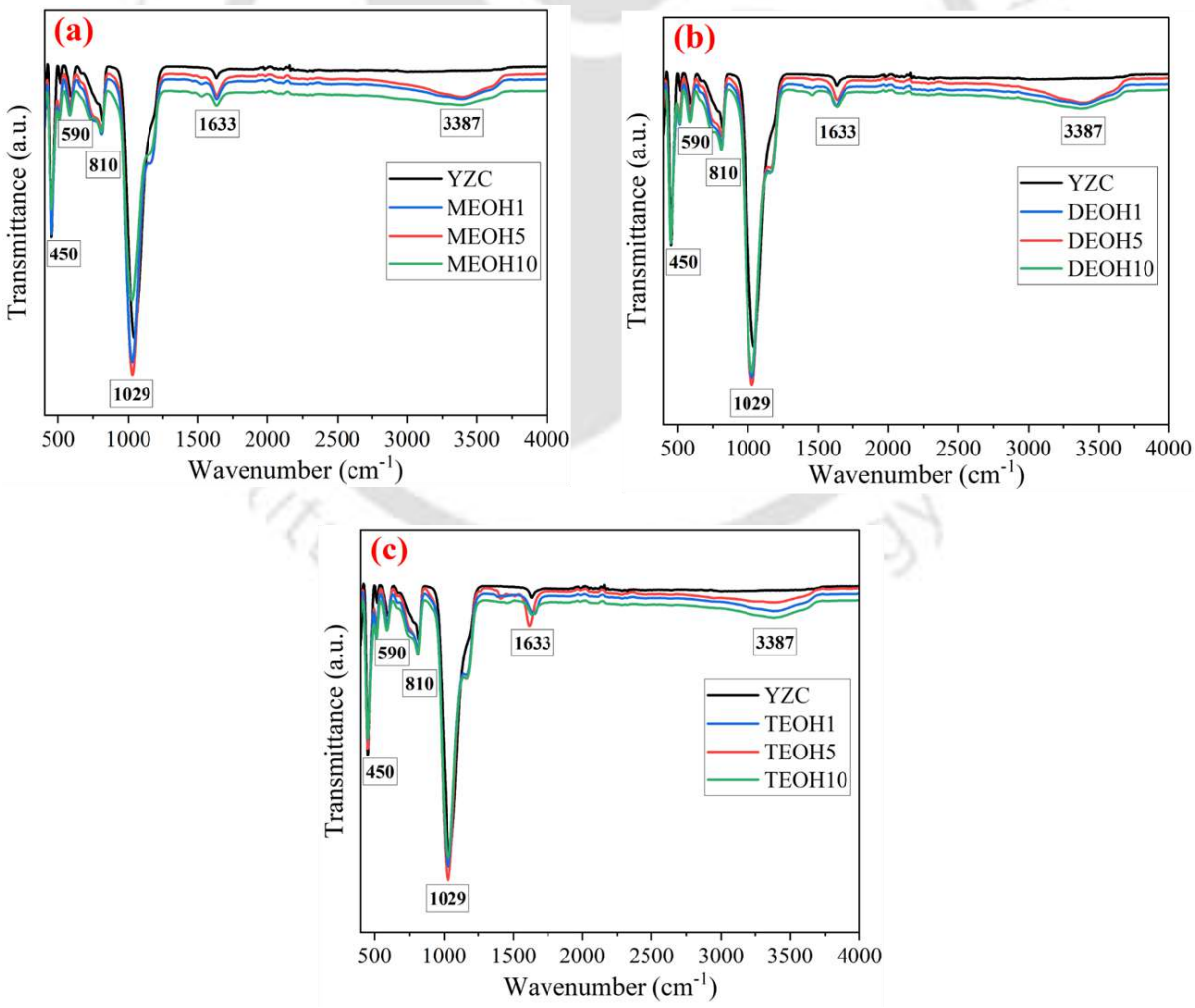

Figure 3.7: FTIR spectra of Zeolite-Y and amine-functionalized Zeolite-Y adsorbents.

Figure 3.8, Figure 3.9, Figure 3.10, and Figure 3.11 shows the SEM images of Zeolite-Y before and after amine loading. All the samples being characterized at 5kV acceleration voltages have been presented at a magnification of 50KX. The primary tetrahedral and secondary hexagonal structures of Zeolite-Y were intact even in the amine-modified samples. This indicates that the morphology of Zeolite-Y support did not change even after amine loading, which is also in alignment with the literature [5].

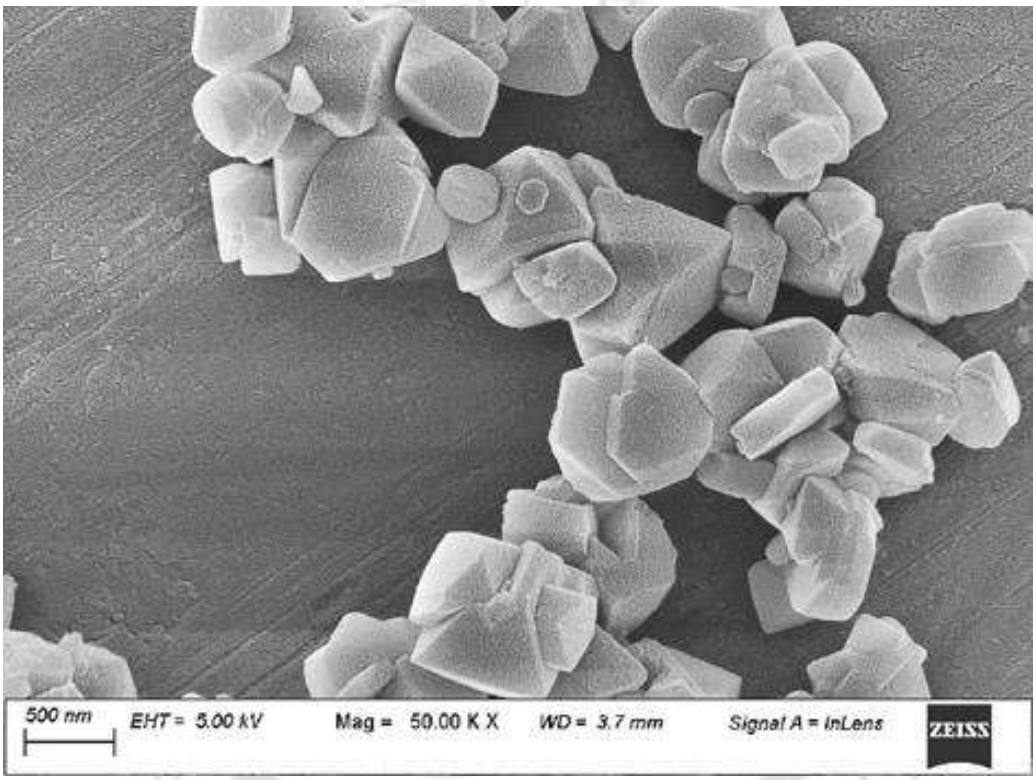

Figure 3.8: FESEM image of pure Zeolite-Y adsorbent.

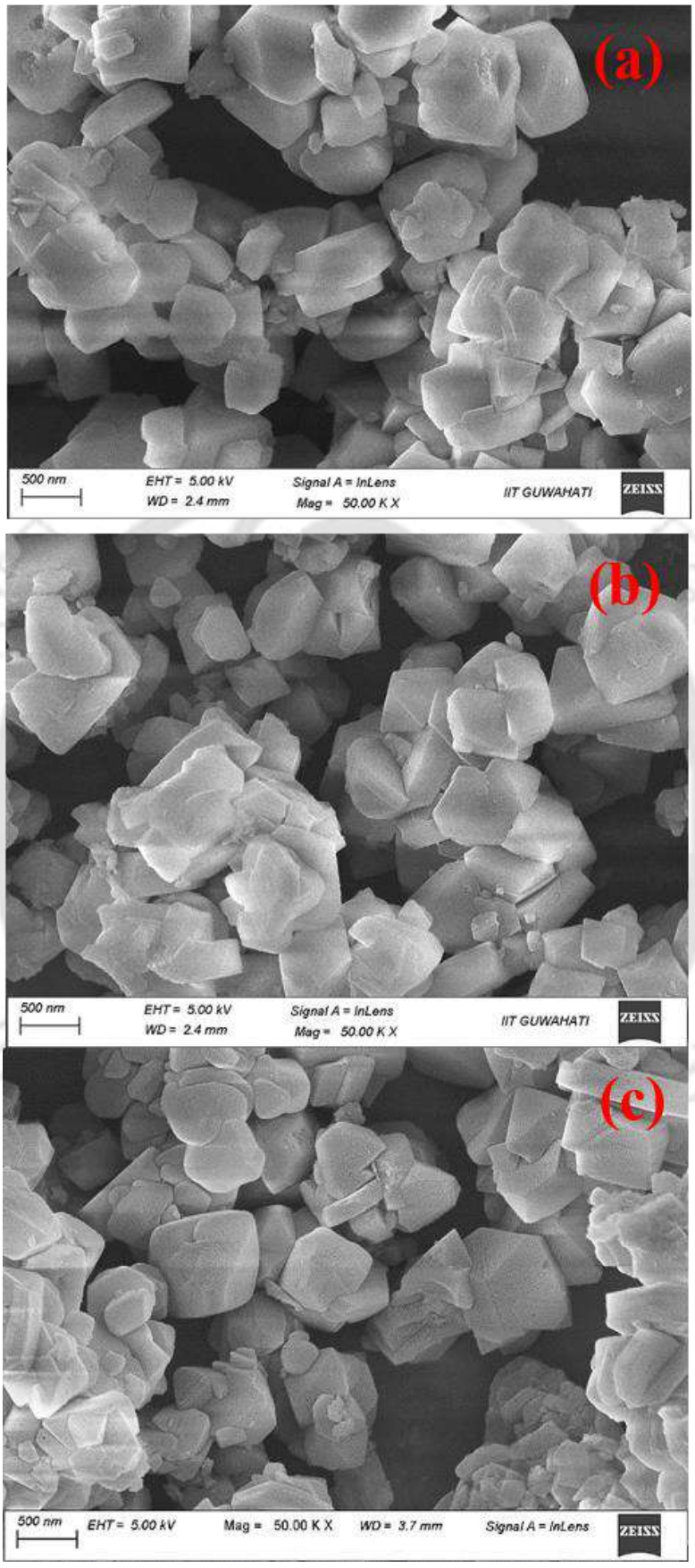

Figure 3.9: FESEM images of (a) MEOH1, (b) MEOH5, and (c) MEOH10 adsorbents.

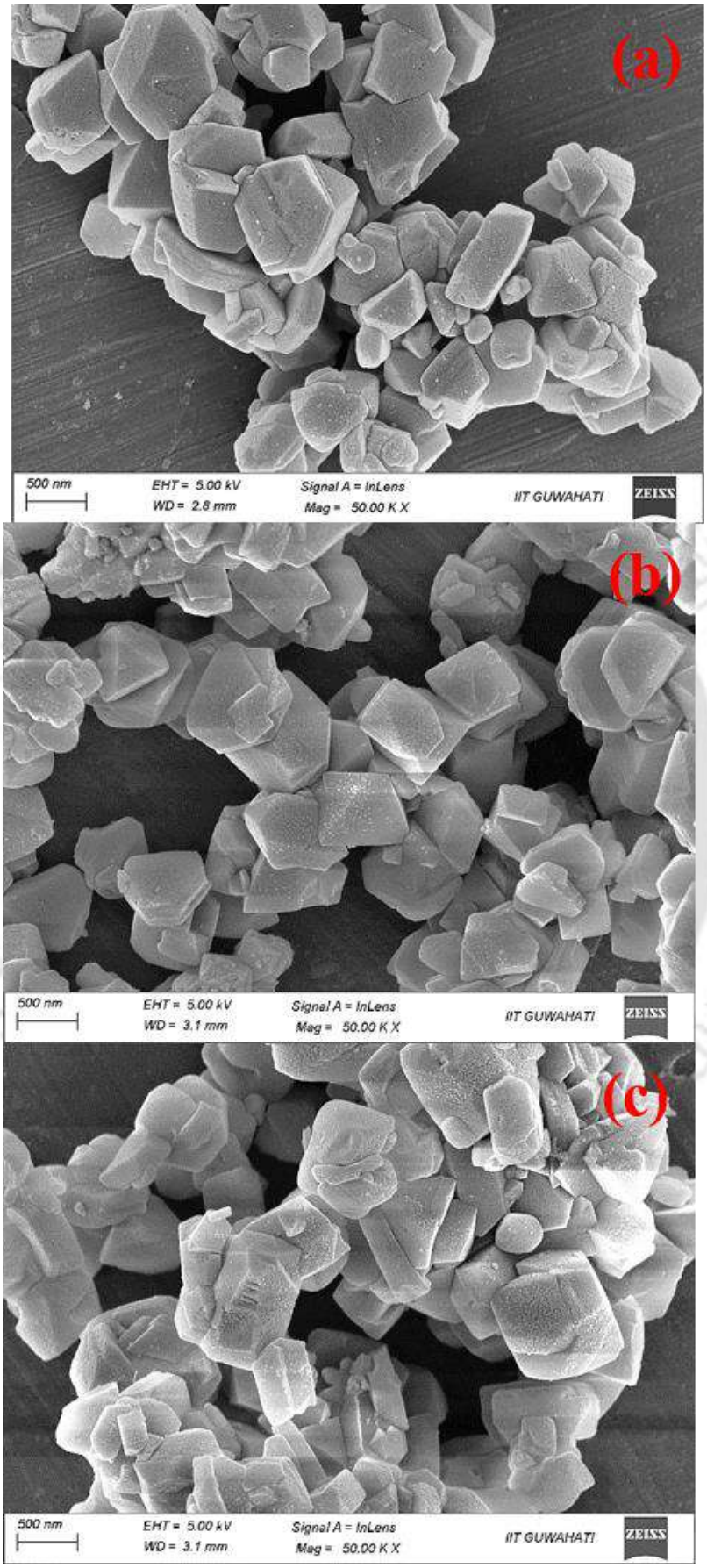

Figure 3.10: FESEM images of (a) DEOH1, (b) DEOH5, and (c) DEOH10 adsorbents.

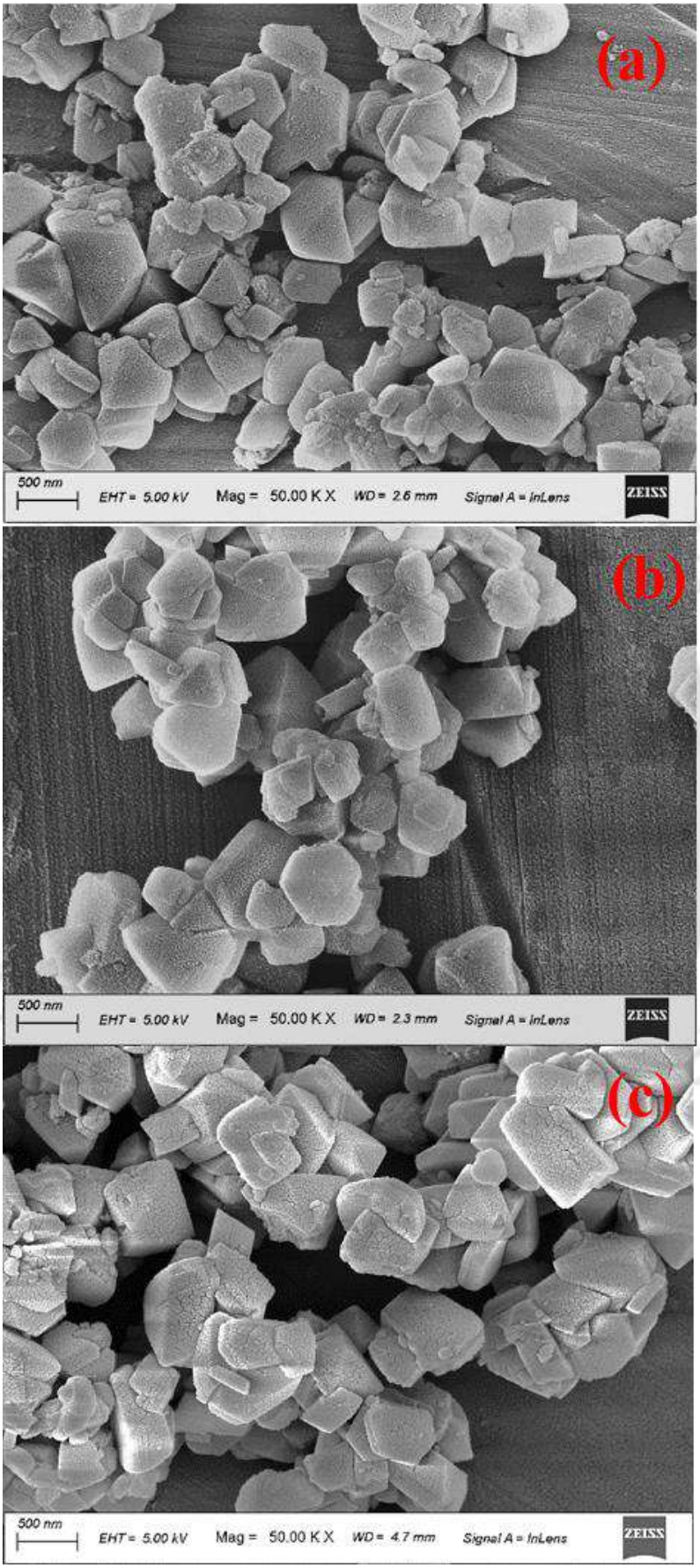

Figure 3.11: FESEM images of (a) TEOH1, (b) TEOH5, and (c) TEOH10 adsorbents.

3.3.2 Parameters Effect for CO_2 Adsorption

During adsorption equilibrium measurements, 99.9% pure carbon dioxide gas was used. Using a gravimetric adsorption system, the adsorption equilibrium of carbon dioxide gas on synthesized adsorbents was determined at 303 K. Before each isotherm measurement the sample was degassed by heated to 423 K under vacuum before the measurement. Gravimetric adsorption systems include a section of the system with a known volume, called the manifold. Using high-sensitivity pressure sensors, the exact amount of gas enclosed in these areas can be determined at any given time with the pneumatic valves connected to the system.

3.3.2.1 Effect of amine groups

In this study, the amine-loaded Zeolite-Y was used to adsorb carbon dioxide. During such sorption, some of the CO_2 diffused into the adsorbent pores (physisorption), and the remainder reacted with the active amino sites. In empirical studies, it was affirmed that both Zeolite-Y and amine contribute to CO_2 adsorption. FTIR spectra of the synthesized samples indicated the presence of amine groups and these functional amine groups act as active sites for CO_2 adsorption. The Si-OH-Al clusters on Zeolite-Y surfaces serve as a link to connect amine molecules.

Figure 3.12 illustrates the molecular structures of the amines and their reactions with CO_2. MEOH exhibited good adsorption capacity due to its simple molecular structure and a terminal $–NH_2$ group which easily reacted with CO_2. The steric hindrance of DEOH and TEOH limits molecular contact with CO_2. Hence, DEOH has a lower adsorption capacity than MEOH due to the relatively larger molecules. In addition to steric hindrance, TEOH reacts with CO_2 only in water, resulting in its lowest adsorption capacity [6]. The BET analysis of the samples discussed in **section 3.3.1**, also supports the decreasing adsorption capacity of the synthesized samples. During the amine modification of the zeolite using the wet impregnation method, the

amine molecules occupy the surface and pores of the zeolite sample which could be confirmed by the decrease in surface area and average pore size of the sample. As a result of the combined effect of steric hindrance and decreasing surface area the CO_2 adsorption capacities of the synthesized samples decreased in the order of MEOH<DEOH<TEOH. The CO_2 adsorption tests carried out in this study were performed under anhydrous conditions. Under these circumstances, CO_2 binding to tertiary amines is very difficult.

$$CO_2 + 2RNH_2 \leftrightarrow RNH_3^+ + RNHCOO^- \quad (3.1)$$

$$CO_2 + 2R_2NH \leftrightarrow R_2NH_2^+ + R_2NCOO^- \quad (3.2)$$

The reaction of primary and secondary amine groups with carbon dioxide results in the formation of carbamate ions as shown in equations (3.1) and (3.2).

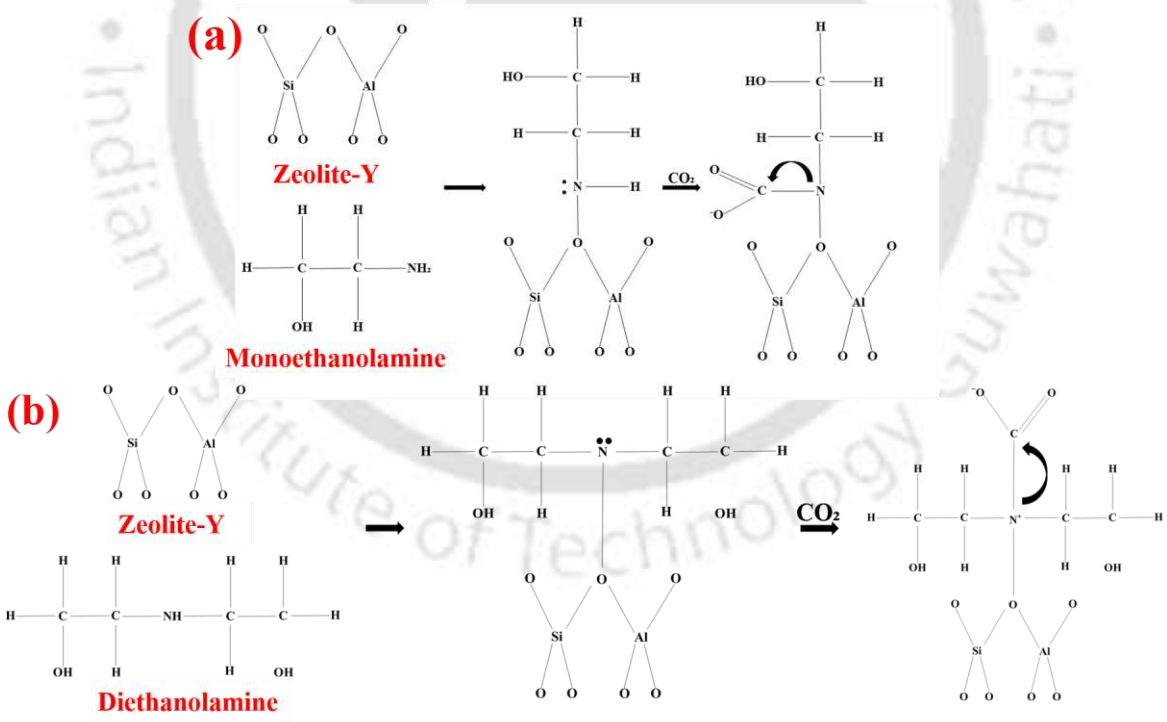

Figure 3.12: Adsorption mechanism of CO_2 with (a) MEOH, and (b) DEOH.

XPS measurements were performed on synthesized adsorbents after carbon dioxide adsorption to evaluate the adsorption mechanism of carbon dioxide on amine-loaded adsorbents. In the

high-resolution XPS analysis of the C1s spectrum, three distinct peaks were observed at 284.49 eV, 286 eV, and 288.54 eV, as illustrated in Figure 3.13(a) and (b). These peaks are associated with the C-H, C-N, and O=C-N species, respectively [7,8]. However, in Figure 3.13(c), the C1s spectrum displays only two peaks at 284.49 eV and 286 eV, corresponding to C-H and C-N species, respectively. Therefore, both primary and secondary amine-loaded adsorbents exhibited adsorption mechanisms. Figure 3.13(c) shows a lack of adsorption peak for O=C-N, which may indicate that there is no adsorption between tertiary amines and carbon dioxide.

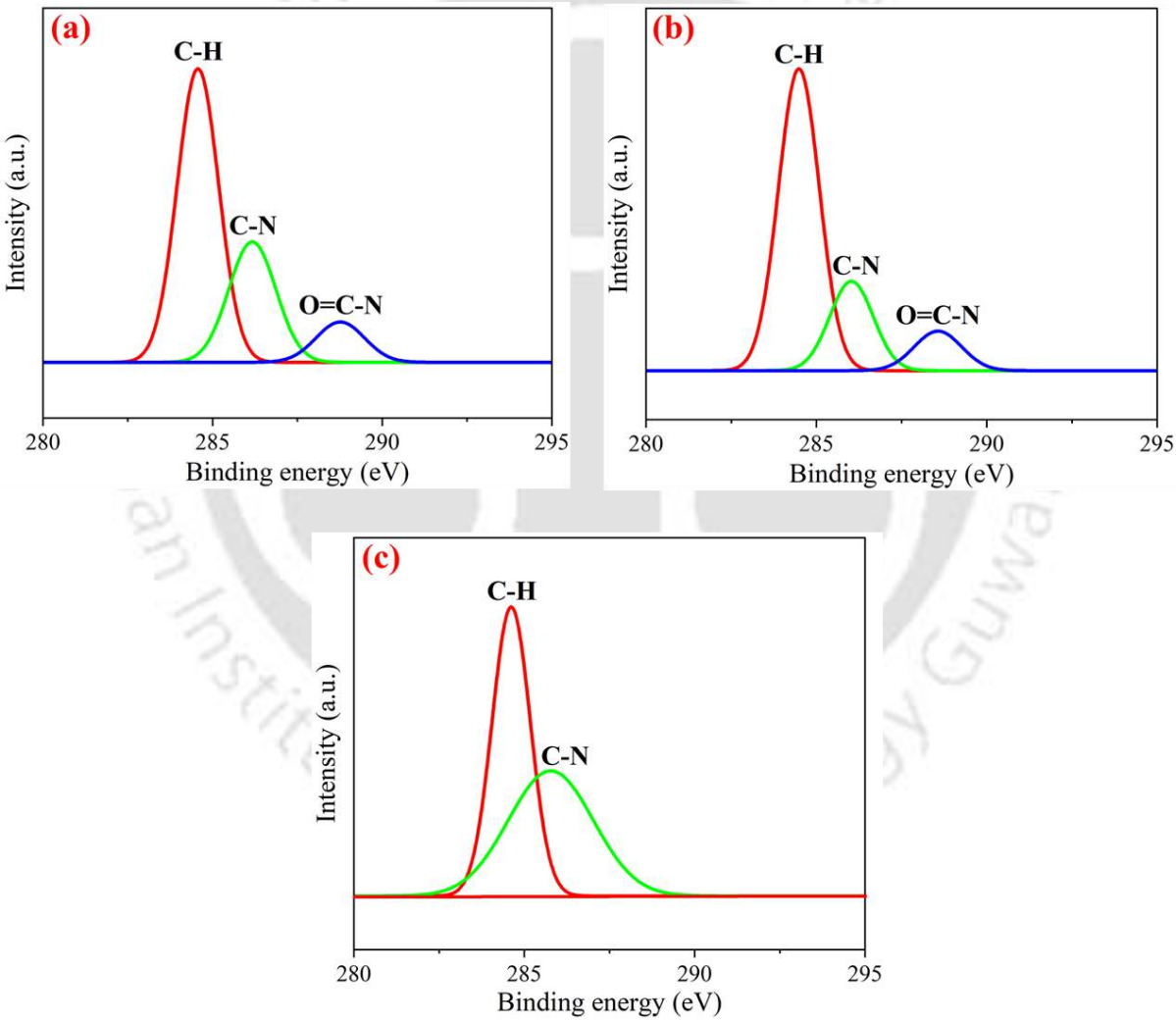

Figure 3.13: High-resolution XPS spectra of C1s for (a) monoethanolamine, (b) diethanolamine, and (c) triethanolamine-loaded adsorbents.

3.3.2.2 Effect of amine loading

Using a gravimetric adsorption system, the adsorption capacity of CO_2 for modified Zeolite-Y adsorbents at 303 K has been depicted in Figure 3.14 (a), (b), and (c). According to the obtained results, CO_2 adsorption capacity increased from 1 wt.% to 5 wt.% amine loading (2.13 - 2.26 mmol g^{-1}) but decreased for 10 wt.% amine loading case (1.7 mmol g^{-1}). A higher MEOH loading (<5 wt.%) resulted in the maximum pore blocking of the zeolite structure. As a result of this, the zeolite surface available to adsorb CO_2 decreased greatly and the diffusion barrier also increased. Therefore, support pore structure is not the only factor to influences CO_2 adsorption capacity. However, MEOH supported on mesoporous Zeolite-Y barely adsorbs CO_2 at room temperature at such a higher loading of the amine. Thus, adsorbents with low loadings will circumvent the adverse effect of diffusion limitation at room temperature. MEOH loading of 5 wt.% affirmed a maximum CO_2 adsorption capacity of 2.26 mmol g^{-1} at 303 K and 1 bar pressure for pure CO_2. The MEOH dispersion within the support cage-like structure can significantly enhance the CO_2 adsorption capacity.

The CO_2 adsorption capacities of the synthesized samples in the present work are compared with the existing literature data in Table 3.2. All the synthesized samples, exhibited superior surface area, pore volume, and CO_2 adsorption capacities. The MEOH-modified zeolite (MEOH5) sample exhibited the highest adsorption capacity and the effects of amine loading were discussed above**.** The determination of gas adsorption capacity for commercial Zeolite-Y as a sample has been explained in Appendix 3.1 and remaining gas adsorption capacity has been calculated by using similar steps.

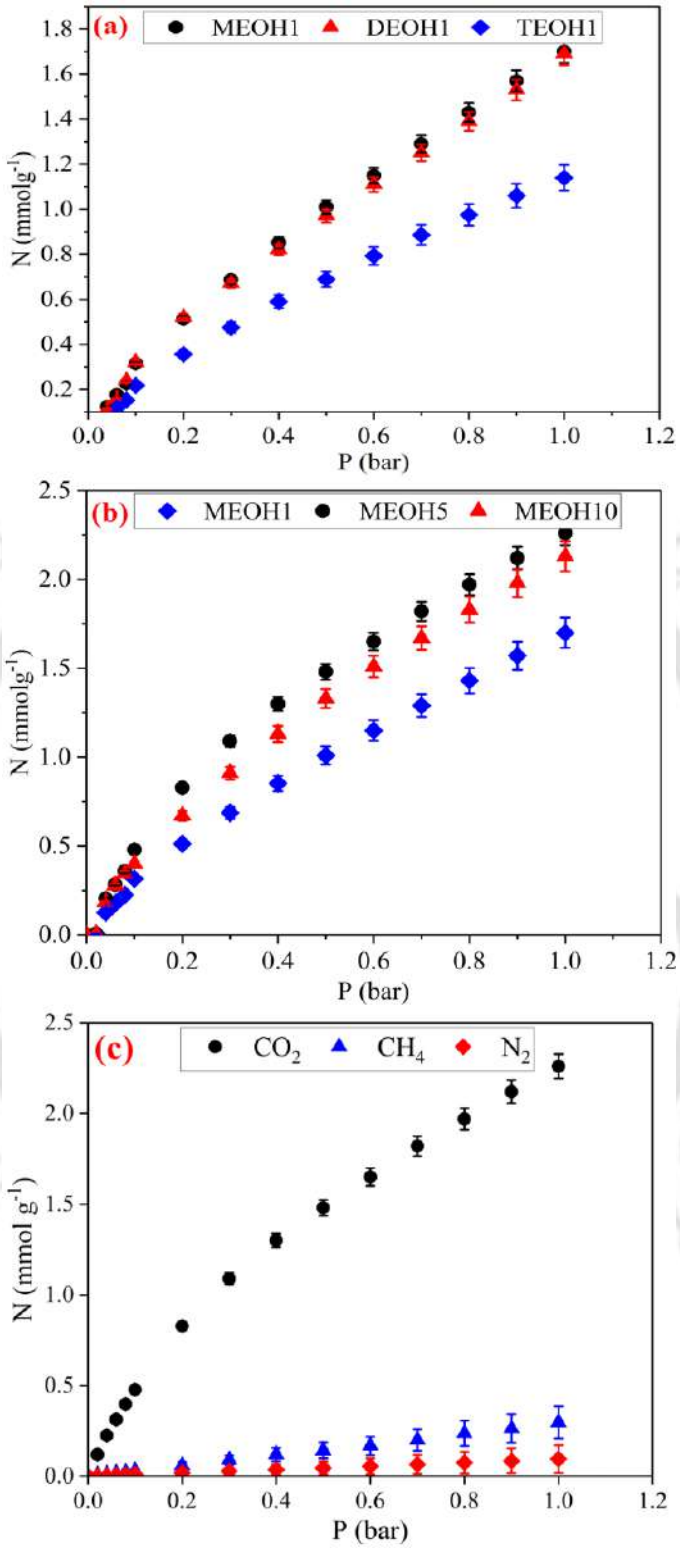

Figure 3.14: (a) Effect of primary, secondary, and tertiary amine groups CO_2 adsorption at 303K, (b) Effect of 1 wt.%, 5 wt.%, and 10wt.% monoethanolamine loading on CO_2 adsorption at 303K, and (c) CO_2, CH_4, and N_2 adsorption of MEOH5 adsorbent at 303K.

Table 3.2: Comparative evaluation of amine loading adsorbents for pure CO_2 adsorption at atmospheric pressure.

Support	Amine group	Amine loading (wt.%)	T (°C)	S_{BET} ($m^2\ g^{-1}$)	V_{total} ($cm^3\ g^{-1}$)	CO_2 Capacity (mmol g^{-1})	Ref.
NaY	TEPA	50	75	172	0.148	2.11	[9]
NaY	DEA	50	75	-	-	1.77	[10]
NaY	2-MAE	50	75	-	-	1.94	[10]
Zeolite-13X	DETA	40	75	35.43	0.993	1.05	[11]
Zeolite-13X	TEA	40	75	30.75	0.995	0.11	[11]
Zeolite-13X	MEA	40	75	-	-	0.37	[11]
Zeolite 4A	TEA	40	75	-	-	0.37	[11]
Zeolite 4A	MEA	40	75	-	-	0.24	[11]
Zeolite 5A	TEA	40	75	-	-	0.24	[11]
Zeolite 5A	MEA	40	75	-	-	0.04	[11]
Zeolite-Y	MEOH	5	30	286.60	0.20	2.26	Present work
Zeolite-Y	DEOH	5	30	269.82	0.17	1.84	Present work
Zeolite-Y	TEOH	5	30	206.83	0.14	1.62	Present work

3.3.2.3 Adsorption isotherm

A virial adsorption isotherm model was used to analyze the CO_2 adsorption behavior of amine-functionalized adsorbents as shown in Figure 3.15 (a), (b), and (c). The isotherm model has been used to determine the adsorbent's affinity and thermodynamic properties for the design of

an adsorption system. The virial isotherm model used for fitting experimental CO_2 adsorption data is represented in Equation 3.3. Accordingly, the isotherm plot illustrates the model data at 303 K and 0.1-1 bar pressure intervals.

$$P = \frac{N}{\beta}\exp(bN + cN^2) \tag{3.3}$$

where P stands for pressure (bar), and N stands for amount adsorption (mmol g^{-1}). Apart from Henry's constant (β) (mmol g^{-1} bar^{-1}), two virial coefficients b ($mmol^{-1}$ g) and c ($mmol^{-2}$ g^2) are also included in the above expression. Generally, these parameters depend upon temperature as,

$$\beta = \beta^0 \exp\left(\frac{\beta^1}{T}\right) \tag{3.4}$$

$$b = b^0 \exp\left(\frac{b^1}{T}\right) \tag{3.5}$$

$$c = c^0 \exp\left(\frac{c^1}{T}\right) \tag{3.6}$$

In the above expressions, T represents the system temperature in Kelvin. The model was used to obtain Type I CO_2 isotherm with good fitting at ambient temperatures (303 K).

The expression revealed that the virial isotherm was independent of saturation capacity. In the literature [12], a different version of the equation exists that incorporates saturation capacity. Virial isotherms with a second or third truncated virial coefficient are capable of correlating gas-solid equilibrium data with high accuracy. Virial adsorption isotherms can very effectively describe heterogeneous surfaces of adsorbents which possess many types of adsorption sites.

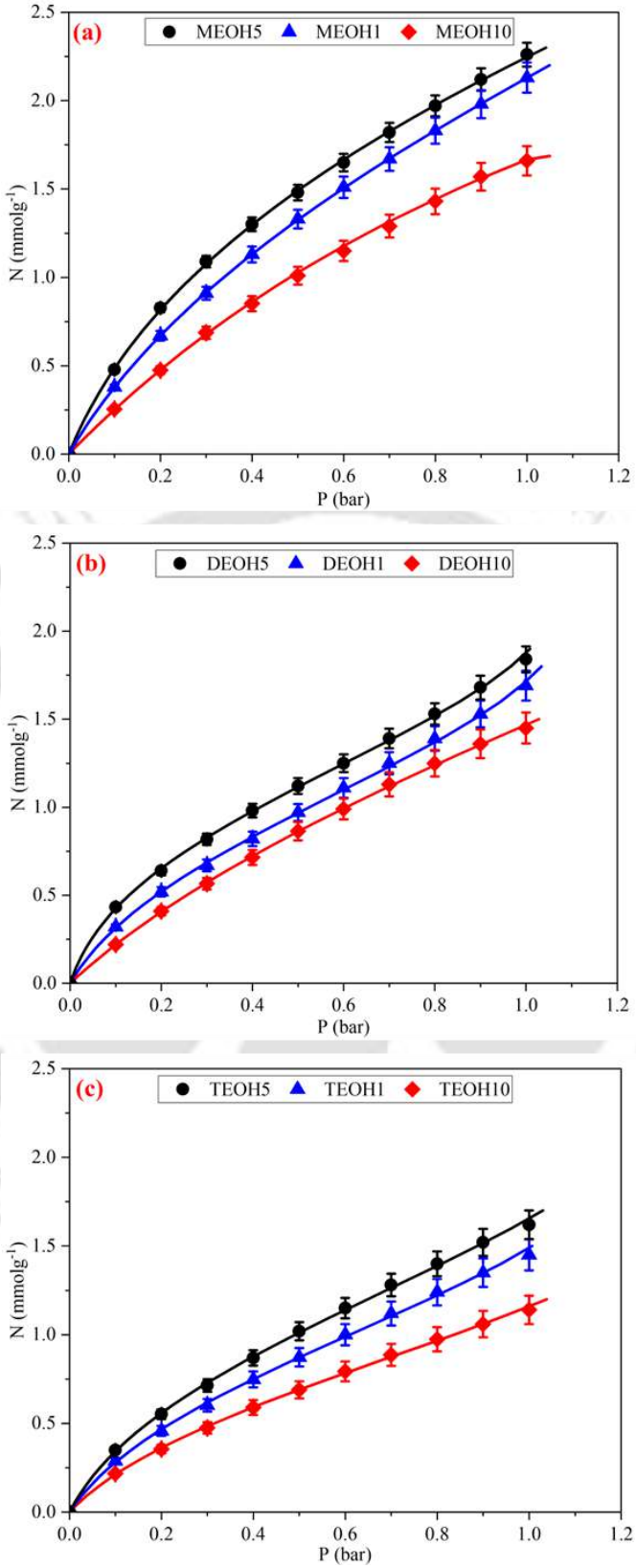

Figure 3.15: (a) Monoethanolamine, (b) Diethanolamine, (c) Triethanolamine adsorption isotherms for (▲) 1 wt.%, (●) 5 wt.%, and (◆) 10 wt.%. Symbols are experimental data; lines are fits obtained using the Virial model parameter.

The CO_2 adsorption of all synthesized adsorbents increased gradually with increasing pressure. Adsorbents with a 5 wt.% amine loading affirmed the best CO_2 adsorption capacity at 303K and 1 bar. This is due to the large number of amine functionalities that act as CO_2-affinity sites on the sorbent. The gradual increase in CO_2 adsorption could be due to the initial packing of CO_2 molecules in monolayers and then in multilayers. CO_2 adsorption can also occur inside amine-loaded pores, or on their external surfaces. This is because most exposed amine sites are already occupied by CO_2. The larger molecular structure of DEOH molecules possessing two alkyl groups connected to the central "N," may contribute less to the CO_2 adsorption capacity of the sorbent and accordingly reported low CO_2 uptake in comparison to MEOH functionalized adsorbents. The structure or type of an amine molecule influences CO_2 adsorption on the adsorbent. In comparison to MEOH and DEOH, TEOH has a larger molecular structure with three alkyl groups on the central atom. CO_2 adsorption capacity is lower for TEOH-functionalized adsorbents than for either MEOH or DEOH-functionalized adsorbents. It could be due to the presence of three bulky alkyl groups on the central "N" atom causing steric hindrance for CO_2 adsorption.

Figure 3.16 (a), (b), and (c) present the adsorption isotherms of CO_2, CH_4, and N_2, along with their respective model fits using the Virial model for CO_2 and the Langmuir model for CH_4 and N_2. The adsorption data indicate that the quantity of gas adsorbed increases with an increase in partial pressure and decreases. The MEOH5 adsorbent exhibited adsorption capacities of 2.26, 0.297, and 0.095 mmol g^{-1} for CO_2, CH_4, and N_2, respectively. The isotherms underscore MEOH5's pronounced preference for CO_2 over CH_4 and N_2, which can be attributed to CO_2's large linear quadrupole moment and its robust interaction with the intra-crystalline charge density frameworks of the adsorbent. The Langmuir model, as shown by the best-fit curves in Figure 3.16 (b) and (c), accurately describes the adsorption behavior of CH_4 and N_2. Despite

CH_4's zero quadrupole moment, it demonstrates a higher adsorption capacity than N_2 due to its greater polarizability.

The Langmuir model, represented by the equation

$$N = \frac{N^{max}\beta P}{1 + \beta P} \tag{3.7}$$

where N is the amount of adsorbed gas (mmol g^{-1}), P is the pressure (bar), Nmax is the saturation adsorption capacity (mmol g^{-1}), and β is Henry's constant (mmol g^{-1} bar^{-1}), provides an excellent fit for the experimental data of CH_4 and N_2. The adsorption isotherm model parameters are presented in Appendix A3.2.

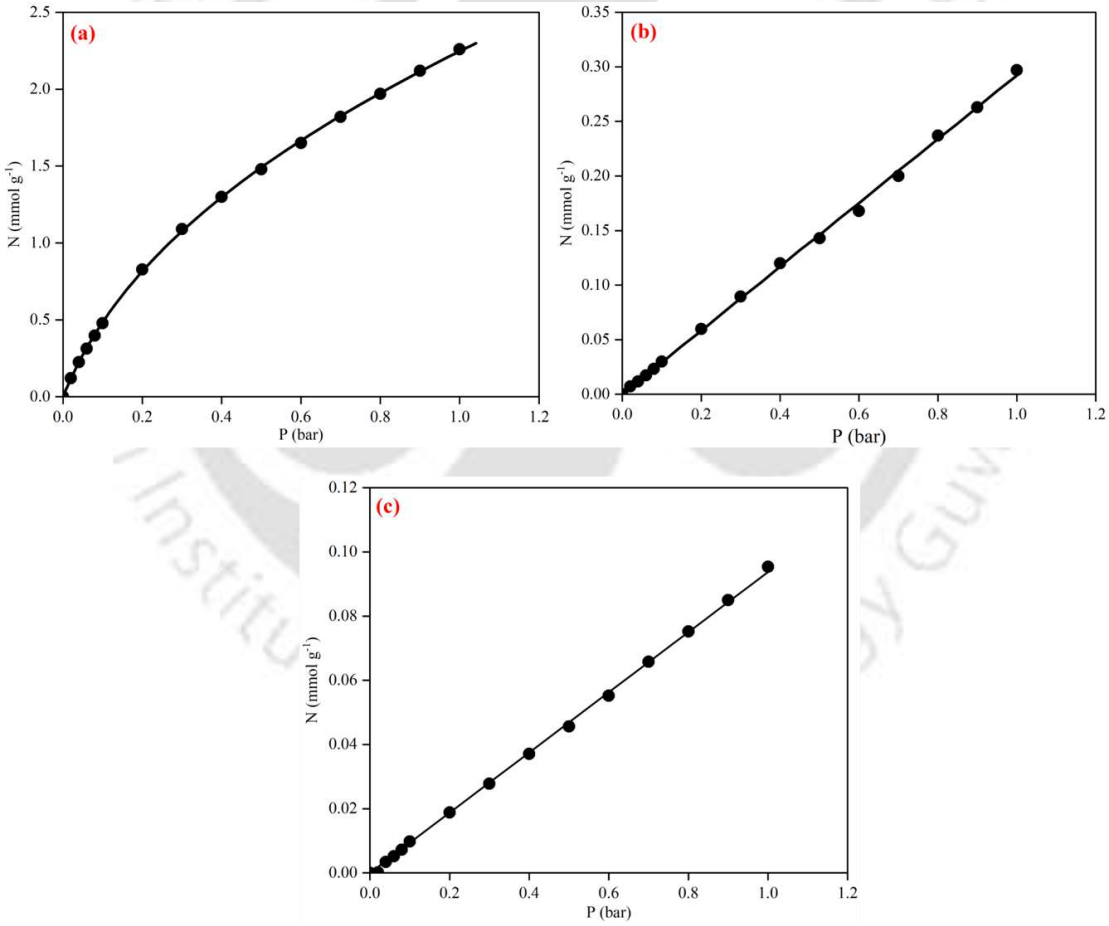

Figure 3.16: (a) CO_2 adsorption isotherms, (b) CH_4 adsorption isotherms, (c) N_2 adsorption isotherms on MEOH5 at 303 K. Symbols are experimental data; lines are fits obtained using Virial and Langmuir model parameters.

3.3.2.4 Adsorption enthalpy

Based on the Virial adsorption isotherm, the following equation relates to the total amount of heat generated due to reactions between absorbent and CO_2. For the heat of adsorption, the enthalpy of the standard state is computed with the determination of the heat of adsorption generated per mole of CO_2. Amine structure is one of the main factors that affect heat adsorption [13].

$$\frac{-\Delta h_{ads}}{R} = \beta_1 + b_1 N + c_1 N^2 \quad (3.8)$$

Figure 3.17 depicts the heat of absorption ($-\Delta h_{ads}$) generated by amine-functionalized adsorbent at 303K. The heat adsorption at initial loading is extremely important as it represents the adsorption enthalpy at the strongest site and confirms its surface heterogeneity. At nearly zero loading, all graphs show relatively high adsorption enthalpy, which decreases with increasing amine loading. The negative values of $-\Delta h_0$ confirm the exothermic adsorption of CO_2. According to the thermodynamic analysis, the higher heat of adsorption value for MEOH-loaded adsorbents conveyed that they have a higher CO_2 interaction potential.

While MEOH5 is considered to be the most efficient absorbent in the absorption process, it assured the highest heat of absorption value of 22.59 kJ mol^{-1} CO_2. The lowest absorption rate was achieved for TEOH10, a tertiary amine (lowest heat of absorption value of 21.09 kJ mol^{-1} CO_2). The heat of adsorption was observed to be as per the order of TEOH < DEOH < MEOH in the synthesized sorbents. Adsorption processes generally involve physical adsorption with enthalpy changes in the range of 20-40 kJ mol^{-1}. Similarly, chemical adsorption assures enthalpy changes in the range of 40-400 kJ mol^{-1} [14]. Thus, the amine-loaded adsorbents are likely to strongly physisorbed carbon dioxide.

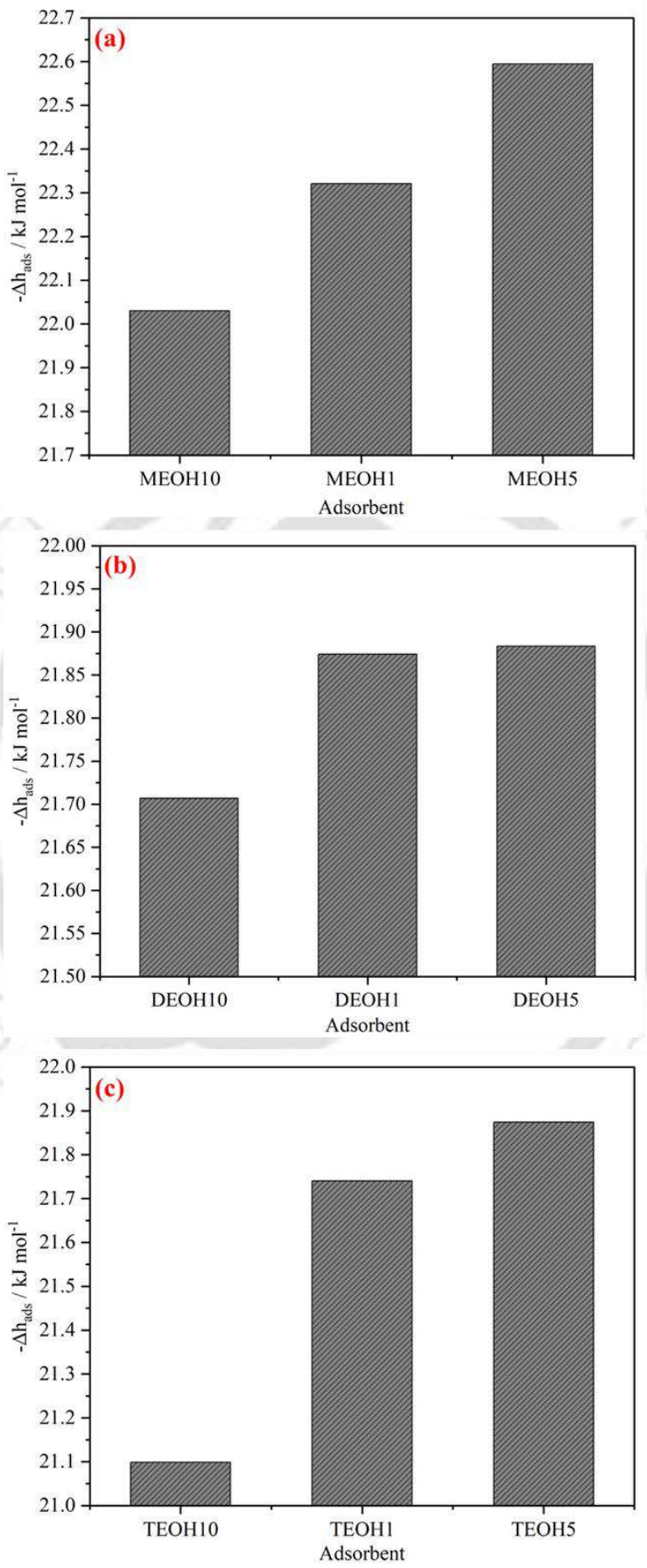

Figure 3.17: Heat of adsorption at zero loading of amine-functionalized Zeolite-Y.

3.3.2.5 IAST Application

Based on the experimental single-component adsorption isotherms, the selectivity of CO_2/CH_4 and CO_2/N_2 mixtures at 303 K was evaluated using the Ideal Adsorbed Solution Theory (IAST), as depicted in Figure 3.18 (a) and (b). For the IAST calculations, 5 mol% CO_2 in CO_2/CH_4 and 13 mol% CO_2 in CO_2/N_2 were chosen to reflect typical concentrations found in natural gas and flue gas streams, respectively.

At low pressures, CO_2 molecules in MEOH5 experience strong electrostatic interactions, leading to high initial selectivity. However, as these sites become progressively occupied, the strength of these interactions diminishes, resulting in a notable decrease in CO_2 selectivity over CH_4 and N_2. For the MEOH5 material, the calculated IAST selectivity at 0.02 bar was remarkably high, reaching values of 330 for the CO_2/CH_4 mixture and 300 for the CO_2/N_2 mixture. As pressure increases, the selectivity for both CO_2/CH_4 and CO_2/N_2 mixtures decreases, eventually reaching a saturation point at 1 bar with still substantial values of 157.59 and 143.77, respectively. This decline in selectivity was attributed to the kinematic diameter of the adsorbate molecules, with CO_2 having a smaller kinematic diameter compared to methane and nitrogen. A smaller kinematic diameter of MEOH5 at lower pressures facilitates the occupancy of the narrow pores with the CO_2. This is due to the higher adsorption selectivity. With increasing pressure, adsorption shifted to the lesser selective surfaces of the adsorbent. This prompted a reduction in the selectivity.

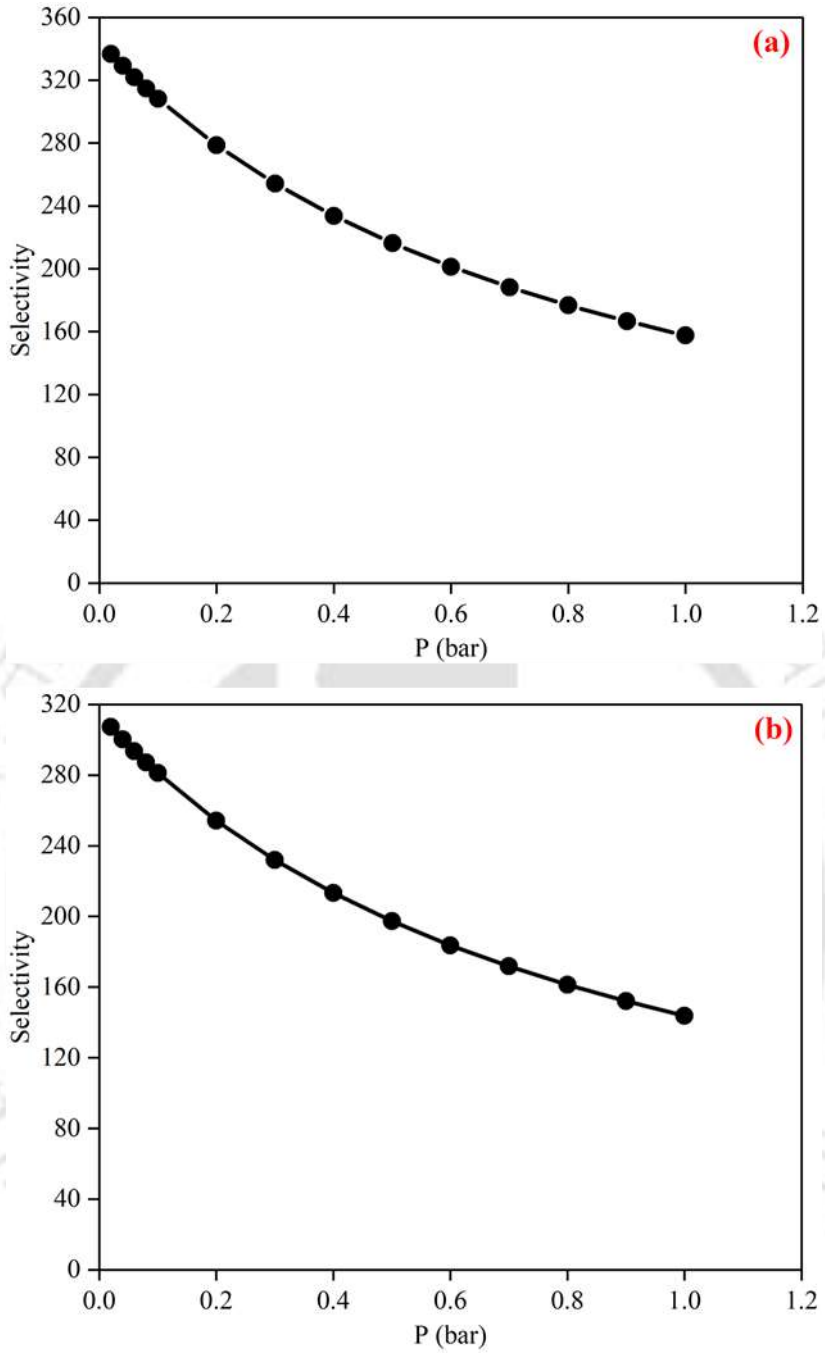

Figure 3.18: IAST predicted binary adsorption isotherms with pressure on MEOH5 for (a) 5 mol% for the CO_2/CH_4 mixture and (b) 13 mol% for the CO_2/N_2 mixture.

3.3.2.6 Cyclic study

A series of four continuous adsorption-desorption cycles have been performed in the adsorption setup to investigate the cyclic performance of the optimized adsorbent (MEOH5). During each cycle, the adsorption process is performed at 303 K and up to 1 bar with pure carbon dioxide

gas. Regeneration of the adsorbent was performed at 423 K in a pure helium atmosphere under vacuum conditions to remove strongly adsorbed water molecules and make free adsorption sites available in small cages.

Figure 3.19 shows the CO_2 adsorption capacity of the adsorbent in the first cycle at 2.26 mmol g^{-1}. As a result, the CO_2 adsorption capacity of MEOH5 decreased to 2.19 mmol g^{-1} after four cycles, indicating that MEOH5 may be used for longer-term processes without major adsorption loss. All adsorption-desorption cycles had similar behavior with a small deviation over the four cycles studied. According to these results, it is mainly a physisorption process in which the adsorbent structure remains mechanically stable and there was oxidative degradation of the amine component to form amide, nitrite, and imine phases, which results in the deactivation of the adsorbent, resulting in a decrease in the CO_2 adsorption capacity [15].

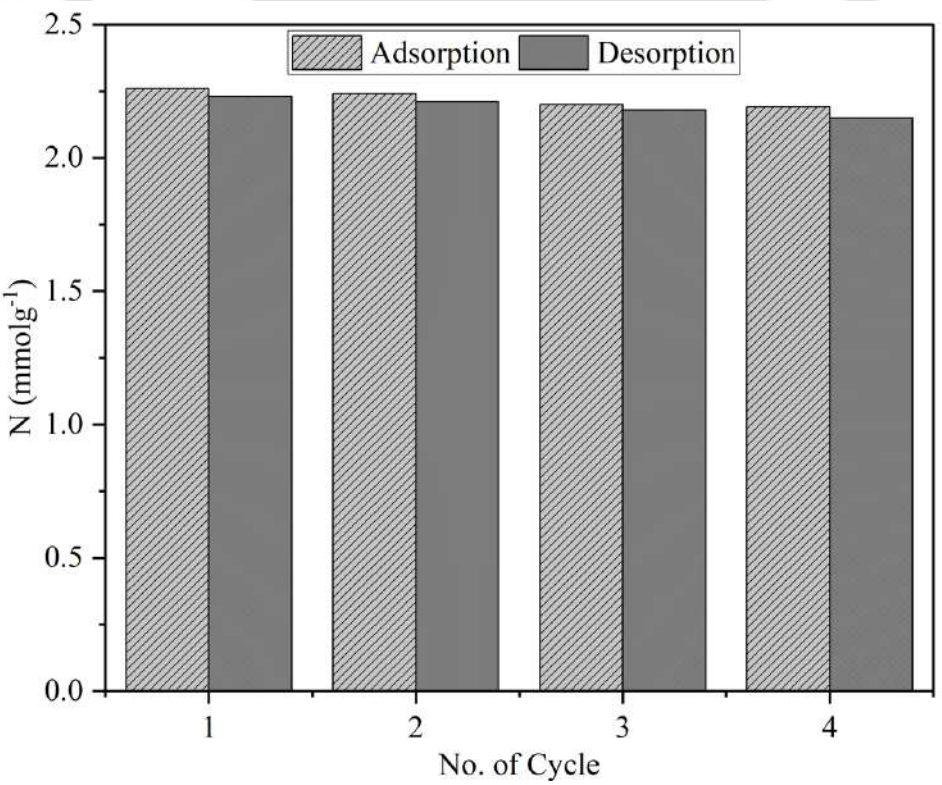

Figure 3.19: Cyclic adsorption-desorption performance of MEOH5 adsorbent.

3.3.3 Summary

The effects of monoethanolamine (MEOH), diethanolamine (DEOH), and triethanolamine (TEOH) functionalization on highly ordered mesoporous Zeolite-Y adsorbent was compared for the pure CO_2 case using a gravimetric adsorption system. Various characterization techniques and CO_2 adsorption thermodynamics models were used to verify the results. The amines were well distributed on the surface and also effectively filled the Zeolite-Y pore space. Amine loading higher than 5 wt.% was probably effective in coating the external surface of the support material. In this study, MEOH5, DEOH5, and TEOH5 showed maximum adsorption capacities of 2.26, 1.84, and 1.62 mmol of CO_2 per g adsorbents, respectively. Hence, MEOH-loaded adsorbent was the suitable CO_2 adsorbent. Physical adsorption was the primary mechanism for CO_2 adsorption and the functional $–NH_2$, -NH, and -N groups of the amines served as active sites. According to a thermodynamic perspective, the experimental results for CO_2 adsorption were well concordant with the Virial, and CH_4 and N_2 were well fitted with Langmuir adsorption isotherm. Based on thermodynamic analysis, the corresponding heat of adsorption increased in the order MEOH > DEOH > TEOH. This is consistent with affirming a higher interaction potential between the adsorbate and adsorbent molecules. The selectivity of optimized amine-functionalized adsorbent (MEOH5) for two binary mixtures CO_2/CH_4 (157.59) and CO_2/N_2 (143.77) has been predicted by using IAST at 303 K and 1 bar condition. The monoethanolamine functionalized Zeolite-Y adsorbent can effectively mitigate well-known issues associated with high carbon capture costs, thus offering a promising application for future CO_2 capture procedures. Following these findings, the next chapter explores the enhancement of gas adsorption capacity through the use of cation-loaded Zeolite-Y, aiming to increase the material's performance in gas capture.

References

[1] B. Fareed, F. Sher, S. Sehar, T. Rasheed, F. Zafar, M. Ameen, E.C. Lima, Tailor-made Functional Zeolite as Sustainable Potential Candidates for Catalytic Cracking of Heavy Hydrocarbons, Catal. Letters. 152 (2022) 732–744. https://doi.org/10.1007/s10562-021-03657-x.

[2] Y. Li, L. Li, J. Yu, Applications of Zeolites in Sustainable Chemistry, Chem. 3 (2017) 928–949. https://doi.org/10.1016/j.chempr.2017.10.009.

[3] D.G. Boer, J. Langerak, P.P. Pescarmona, Zeolites as Selective Adsorbents for CO_2 Separation, ACS Appl. Energy Mater. 6 (2023) 2634–2656. https://doi.org/10.1021/acsaem.2c03605.

[4] F. Su, C. Lu, S.C. Kuo, W. Zeng, Adsorption of CO_2 on amine-functionalized Y-type zeolites, Energy and Fuels. 24 (2010) 1441–1448. https://doi.org/10.1021/ef901077k.

[5] V. Tejavath, V. Kasarabada, S. Gonuguntla, V. Perupoga, S. V. Nandury, S. Bojja, U. Pal, Technoeconomic Investigation of Amine-Grafted Zeolites and Their Kinetics for CO_2 Capture, ACS Omega. 6 (2021) 6153–6162. https://doi.org/10.1021/acsomega.0c05397.

[6] Y.G. Ko, S.S. Shin, U.S. Choi, Primary, secondary, and tertiary amines for CO_2 capture: Designing for mesoporous CO_2 adsorbents, J. Colloid Interface Sci. 361 (2011) 594–602. https://doi.org/10.1016/j.jcis.2011.03.045.

[7] M. Liu, W. Li, J. Rong, C. Zhou, Novel polymer nanocomposite hydrogel with natural clay nanotubes, Colloid Polym. Sci. 290 (2012) 895–905. https://doi.org/10.1007/s00396-012-2588-z.

[8] R.A. Zangmeister, T.A. Morris, M.J. Tarlov, Characterization of Polydopamine Thin Films Deposited at Short Times by Autoxidation of Dopamine, Langmuir. 29 (2013) 8619–8628. https://doi.org/10.1021/la400587j.

[9] M.K. Majideh Babaei, Mansoor Anbia, Improving CO_2 adsorption with new amine-functionalized Y-type zeolite, J. Adv. Environ. Heal. Res. 5 (2017) 70–77. https://doi.org/https://doi.org/10.22102/jaehr.2017.71674.

[10] M. Babaei, M. Anbia, M. Kazemipour, Improving CO_2 adsorption with new amine-functionalized Y-type zeolite, J Adv. Env. Heal. Res. 5 (2017) 70–77. https://doi.org/https://doi.org/10.22102/jaehr.2017.71674.

[11] V. Tejavath, V. Kasarabada, S. Gonuguntla, V. Perupoga, S. V. Nandury, S. Bojja, U. Pal, Technoeconomic Investigation of Amine-Grafted Zeolites and Their Kinetics for CO_2 Capture, ACS Omega. 6 (2021) 6153–6162. https://doi.org/10.1021/acsomega.0c05397.

[12] R.M. Barrer, J.A. Lee, Hydrocarbons in zeolite L II. Entropy, physical state and isotherm model, Surf. Sci. 12 (1968) 354–368. https://doi.org/10.1016/0039-6028(68)90135-0.

[13] I. Kim, H.F. Svendsen, Heat of absorption of carbon dioxide (CO_2) in monoethanolamine (MEA) and 2-(aminoethyl)ethanolamine (AEEA) solutions, Ind. Eng. Chem. Res. 46 (2007) 5803–5809. https://doi.org/10.1021/ie0616489.

[14] X. Zhou, H. Yi, X. Tang, H. Deng, H. Liu, Thermodynamics for the adsorption of SO_2, NO and CO_2 from flue gas on activated carbon fiber, Chem. Eng. J. 200–202 (2012) 399–404. https://doi.org/10.1016/j.cej.2012.06.013.

[15] P. Huang, J. Fu, D. Qiu, Z. Gu, J. Sun, Y. Guo, C. Zhao, Experimental and kinetic study on the cyclic removal of low concentration CO_2 by amine adsorbents in confined spaces, Process Saf. Environ. Prot. 180 (2023) 417–427. https://doi.org/10.1016/j.psep.2023.10.032.

CHAPTER 4

Influence of Cation Exchange on the Gas Adsorption Efficiency of Zeolite-Y

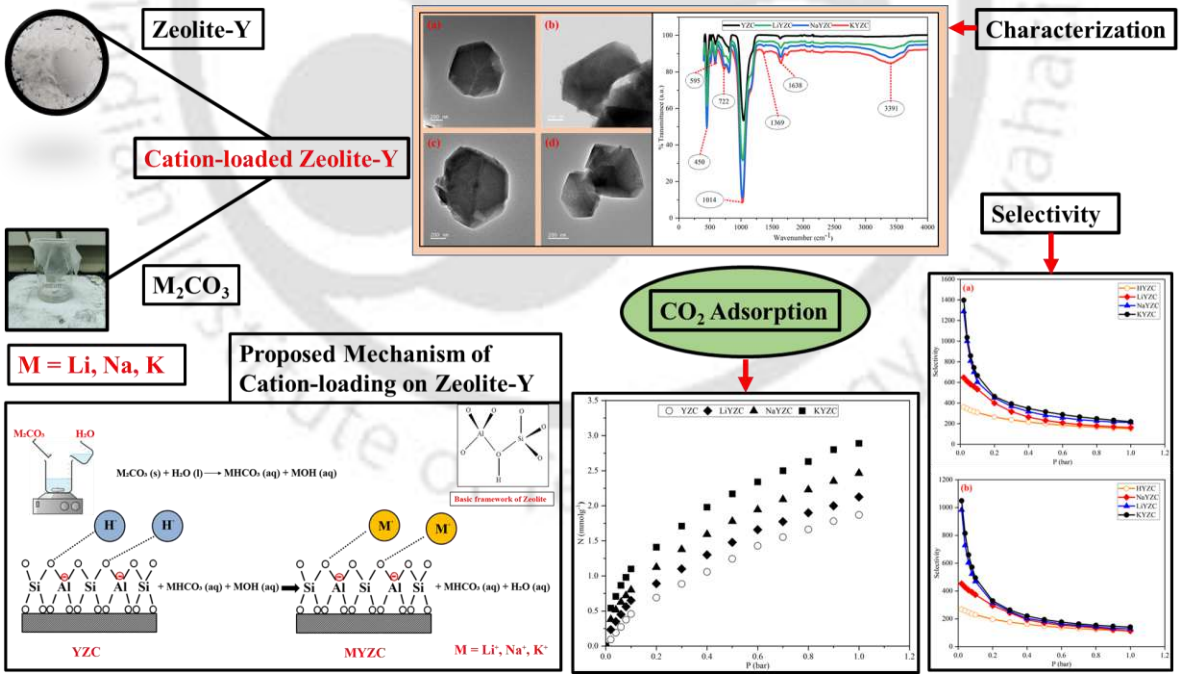

Chapter 4

Influence of Cation Exchange on the Gas Adsorption Efficiency of Zeolite-Y

This chapter presents the synthesis and characterization of Zeolite-Y loaded with various cations, aiming to enhance its adsorption properties. The chapter begins with an overview of the methods used for the incorporation of different cations into the Zeolite-Y framework and the subsequent characterization techniques employed to evaluate the structural and chemical modifications. Following the synthesis and characterization, comprehensive gas adsorption studies are conducted using CO_2, CH_4, and N_2 to assess the performance of the cation-loaded zeolites. The adsorption data is analyzed using two distinct modeling approaches to interpret the adsorption behavior. Additionally, the Ideal Adsorbed Solution Theory (IAST) is applied to determine the selectivity of the cation-loaded zeolites for CO_2 relative to other gases, providing valuable insights into their potential for gas separation applications.

4.1 Background

Zeolite-based adsorbents contain both Lewis and Bronsted acid sites used as active sites that play a key role in various processes in refineries and petroleum technologies [1–4]. A zeolite with large pore apertures and 12 oxygen atoms connected by a silicon or aluminum atom (Faujasite Zeolite) adsorbs CO_2 more readily at low pressures than CH_4 or N_2 [5]. Zeolites can be tailor-made for specific adsorption properties by manipulating their charge-balancing cations. Zeolites are distinguished by both negatively charged frameworks and charge-balancing cations that can serve as effective adsorption sites [6]. In Zeolite-Y, all the cations are located in the supercage, which is located above the hexagonal window between the supercage and the sodalite cage. Furthermore, larger cations easily fit in the Zeolite-Y structure on another side of hexagonal windows that also contain counteractions [7].

In the framework, aluminium atoms have a net negative charge of one due to their less positive charge than silicon atoms. The negative charge is balanced by exchangeable ions at each aluminium atom. Cations induce high electricity gradients within cavities, and the framework itself can be acidic or basic. The gas adsorption on alkali metal cations in Zeolite-Y may be related to the coordination of the cations to oxygen in the structure, which is highly dependent on the basicity of the associated cation and the location of the cation in framework channels [8]. The supercage contains the most preferred cationic site. Once the supercage is fully occupied, the remaining cations are distributed between the double-6-ring (D6R) connecting the two sodalite cages and another site within the sodalite cage [9].

4.2 Characterization

In Figure 4.1, the FTIR spectrum indicates the formation of hydroxide and bicarbonate in the synthesized samples. There are two FTIR peaks for all adsorbents at 450 cm^{-1} and 586 cm^{-1}. The peaks correspond to the tetrahedral bend of Si & Al and the stretching vibration of double six rings (D6R) [10]. The FT-IR spectrum of all the samples shows two peaks at 722 cm^{-1} and 1014 cm^{-1} associated with TiO_4 symmetric stretching and Si-O-Si asymmetric stretching. Compared to the support material, the carbonate-loaded samples showed a distinct peak at 1369 cm^{-1}, indicating the presence of CO_3^{2-} ions because of the formation of bicarbonate [11]. In the IR spectrum, the peak at 1638 cm^{-1} is caused by the stretching vibrations of the –OH group of the hydroxide molecule. As a result of hydroxide formation, the peak at 3391 cm^{-1} is indicated by the -OH stretching band [12]. Thus, the FT-IR spectra of carbonate-modified Zeolite-Y confirm the modification of Zeolite-Y supported with lithium, sodium, and potassium carbonates.

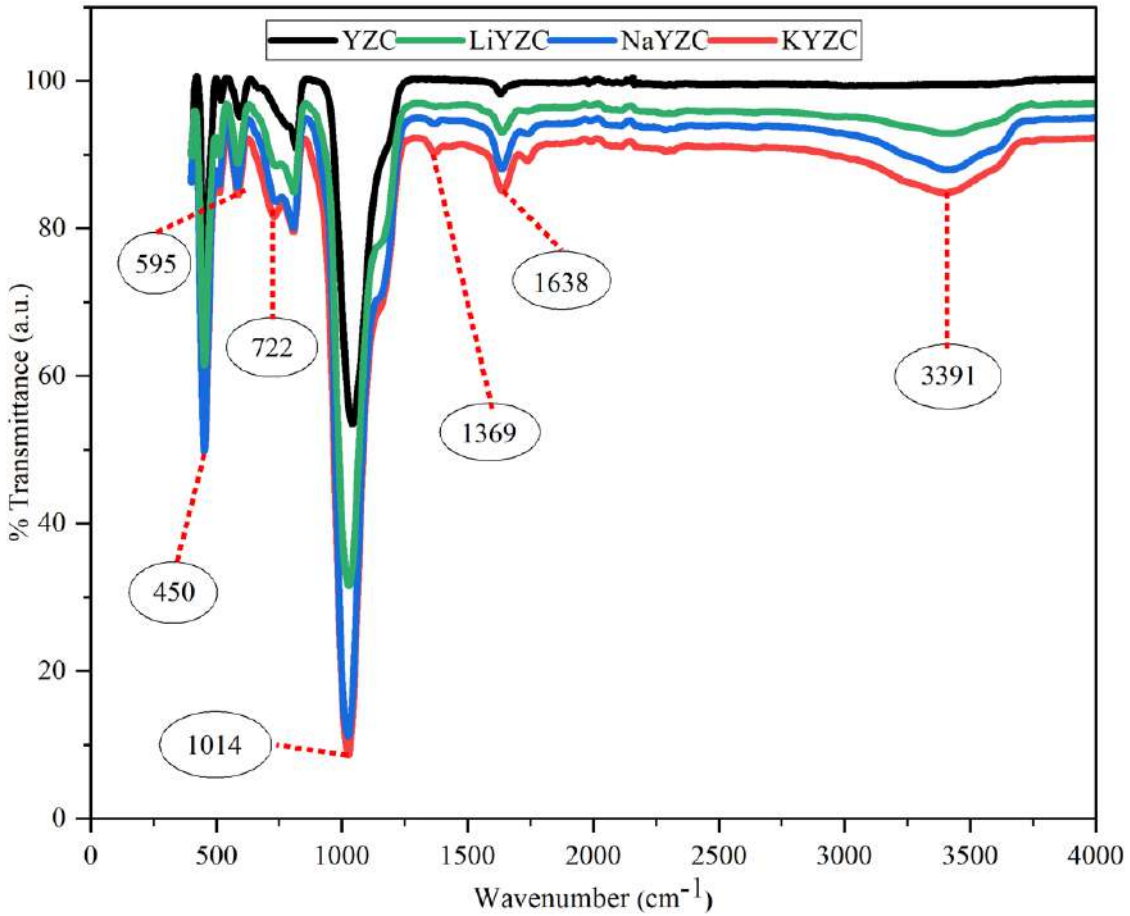

Figure 4.1: FTIR spectra of commercial Zeolite-Y and cation-loaded Zeolite-Y adsorbents.

The XRD patterns of pure Zeolite-Y and the cation-loaded adsorbents are shown in Figure 4.2. The similarity between XRD patterns of the synthetic and commercial adsorbents indicates that the original Zeolite-Y structure has been preserved [13]. No shift in peak positions and no significant diffraction peak was assigned to the cations. These results demonstrate that the wet-impregnation method did not significantly affect Zeolite-Y structure. All the synthesized samples had sharp peaks due to their crystalline structure. Peak intensities decrease with carbonate loading due to a decrease in crystallinity of Zeolite-Y. There was also the possibility that secondary scattering may have occurred due to the presence of potassium ions on the Zeolite support.

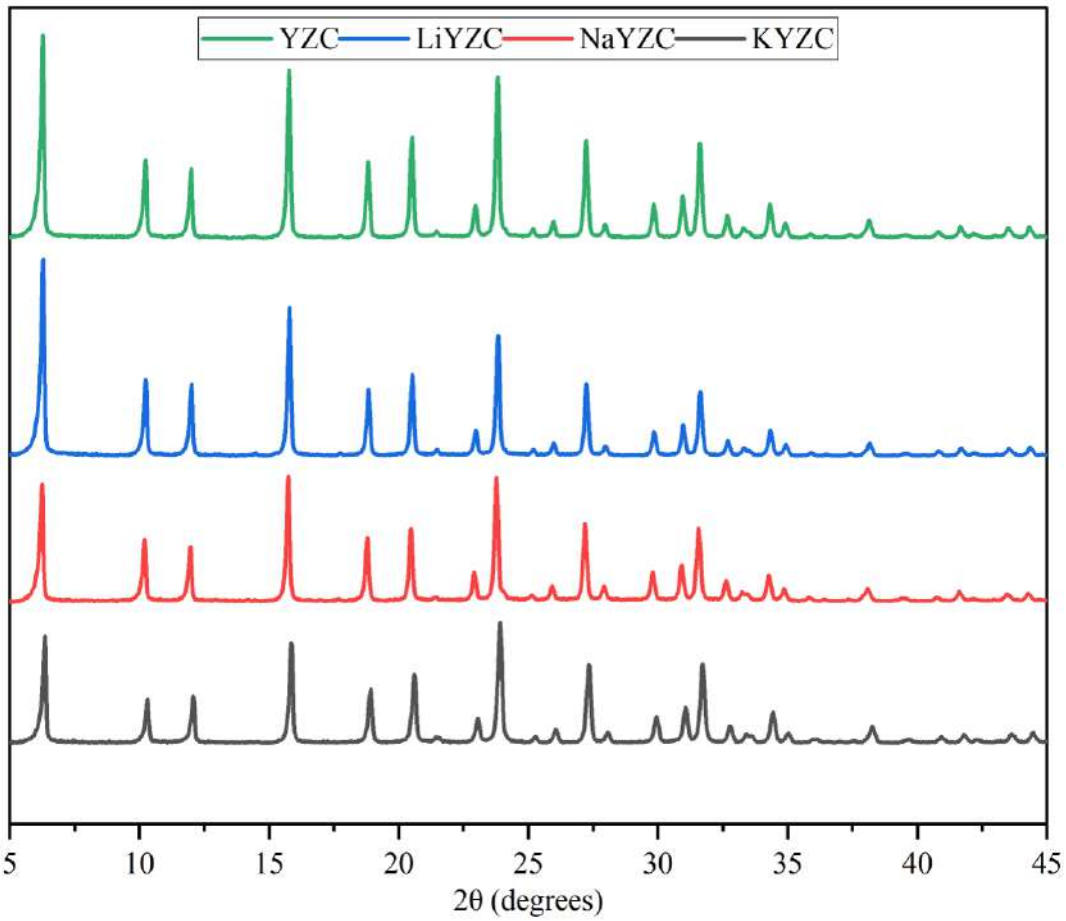

Figure 4.2: XRD pattern of commercial Zeolite-Y and cation-loaded Zeolite-Y.

Figure 4.3 (a) illustrates the nitrogen adsorption/desorption isotherm of Zeolite-Y and cation-loaded Zeolite-Y samples. A hysteresis loop of type H4 was observed in all the mesoporous adsorbents based on surface area analysis, indicating they were mesoporous. Micropores are apparent in all adsorbents when relative pressure is low, as evidenced by steep isotherms [14]. However, as pressure increases, capillary condensation is observed between the adsorption and desorption branches, and the level of hysteresis indicates the amount of mesopores present. Due to uniform internal mesoporosity, the adsorbents demonstrated a pronounced capillary condensation step between 0.4 and 0.9 relative pressure. At high relative pressures, the adsorbents revealed a sharp increase in adsorbed nitrogen volume, which was consistent with the large mesoporous structure of the adsorbents.

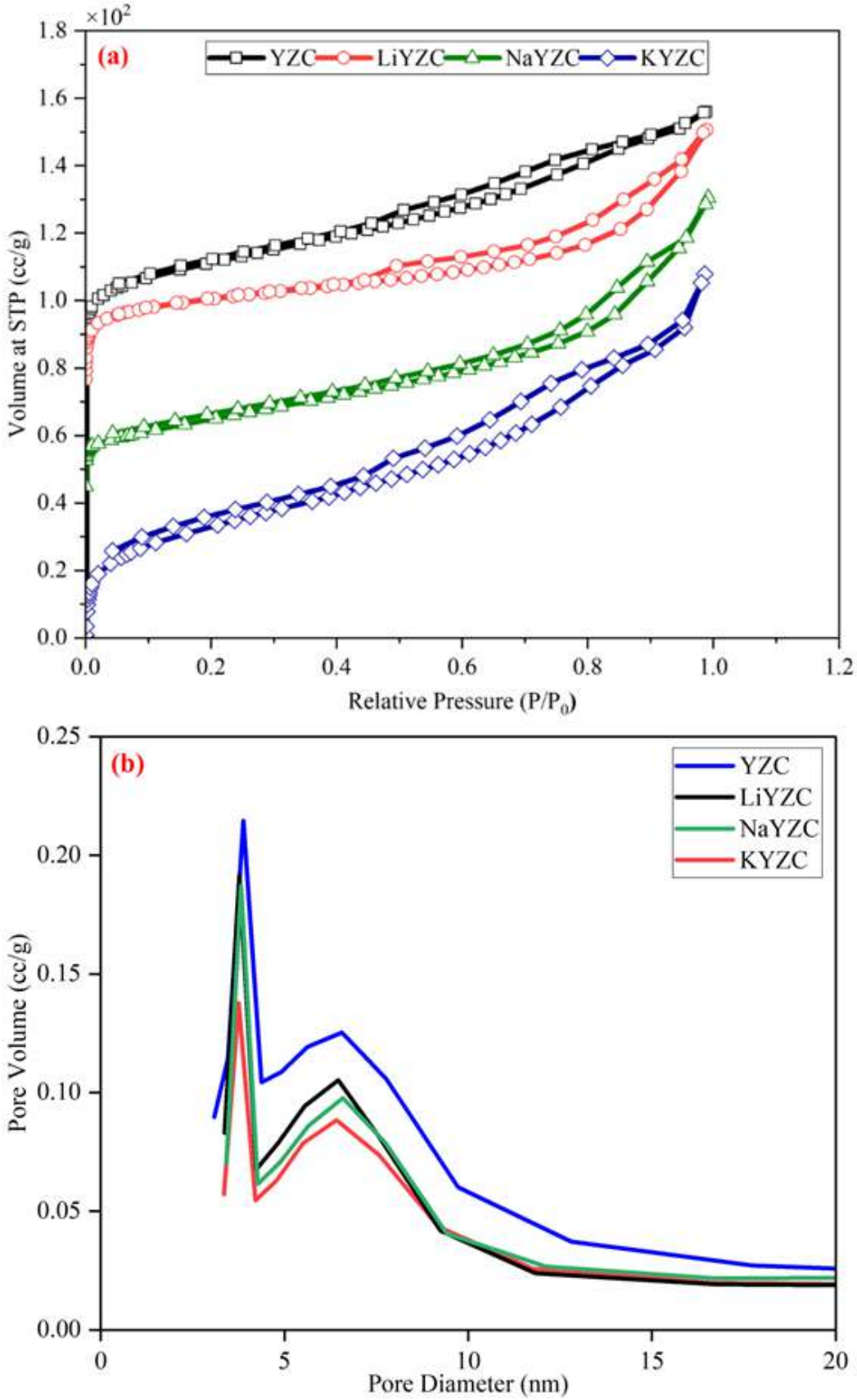

Figure 4.3: (a) N_2 adsorption-desorption isotherm, and (b) Pore size distribution of commercial Zeolite-Y and cation-loaded Zeolite-Y.

To calculate the pores in the samples, a classical BJH model was used based on the Kelvin equation corrected for multiple layers of adsorption. According to Figure 4.3 (b), BJH desorption patterns reveal the pore distribution of all adsorbents. The pore sizes range from 3 to 10 nm with the most possible value being 3 nm which confirms the mesoporous nature of the adsorbents.

Table 4.1: Physiochemical properties of adsorbents.

Adsorbent	S_{BET} (m^2/g)	d_{BJH} (nm)	V_t (cc/g)
YZC	432.11	2.23	0.24
LiYZC	401.03	2.24	0.21
NaYZC	333.36	2.26	0.19
KYZC	294.29	2.27	0.17

Table 4.1 shows the BET surface area, pore size, and pore volume of commercial and cation-loaded adsorbents. In comparison with commercial adsorbent, cation-loaded Zeolite-Y has lesser surface areas (S_{BET}) and total pore volumes (V_{total}) sequentially. In addition, a proportion of the cations entered the pores, and another proportion was incorporated into the zeolite's framework during cation loading [15].

Figure 4.4 (a), (b), (c), and (d) shows TEM images of commercial Zeolite-Y and cation-loaded adsorbents. The commercial adsorbent contains zeolite agglomerates consisting of nanosized zeolite crystallites. The cation-based adsorbents were prepared by impregnation and all the adsorbents possessed hexagonal structures with a particle size of 200 nm. A uniform distribution of cations was observed between the micropores and the exterior surface of the zeolite. Although cation loading changed texture properties, morphology remained unchanged. It was possible that this would result in a higher fraction of cations inside the micropores of the

zeolite. Moreover, more cations were immobilized on the zeolite due to higher cation loading (Li^+, Na^+, and K^+) in the channels of H-modified Zeolite-Y.

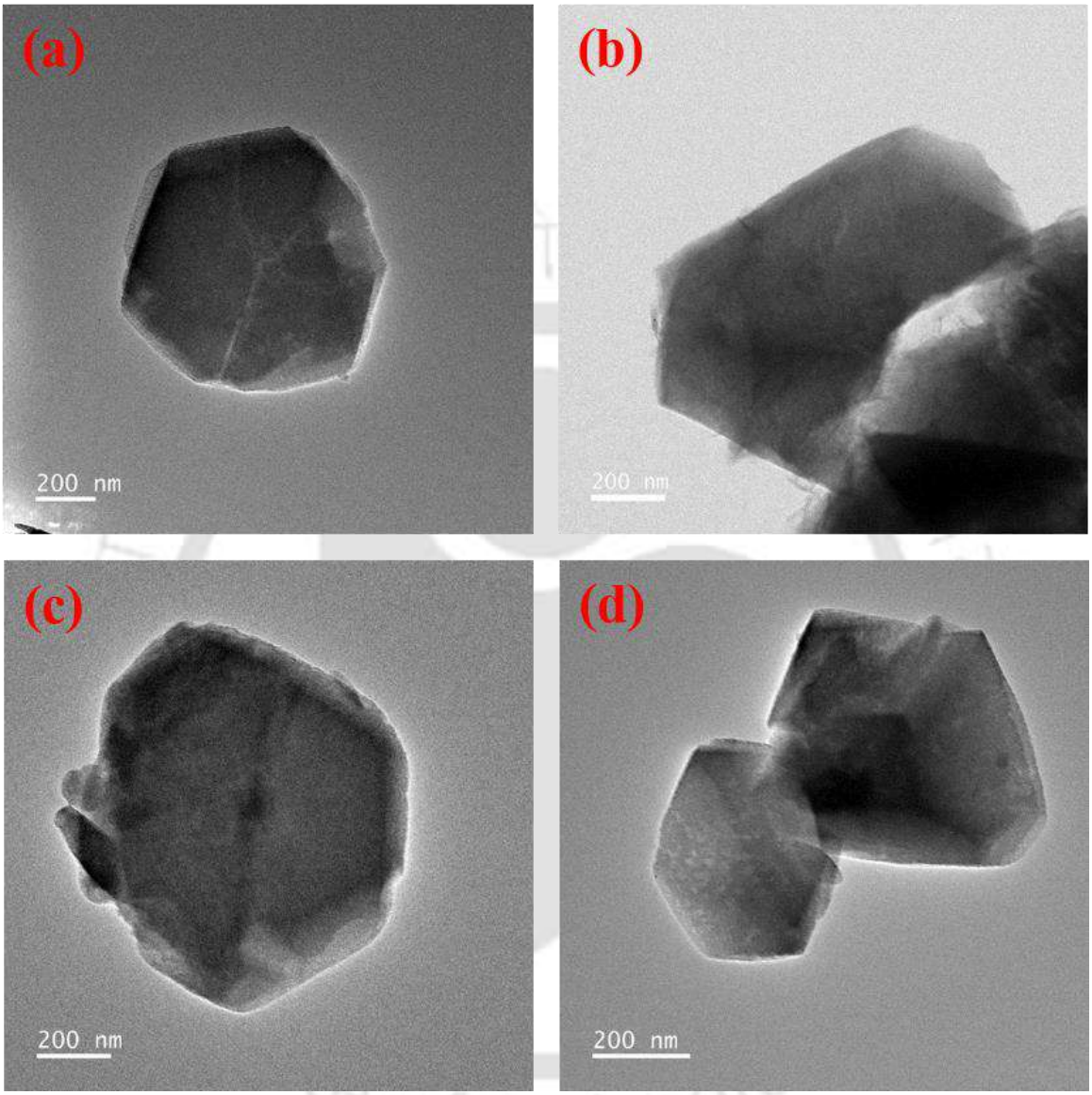

Figure 4.4: FETEM images of (a) Zeolite-Y, (b) LiYZC, (c) NaYZC, and (d) KYZC.

A detailed XPS spectrum of the C1s, Li1s, Na1s, and K2p regions is shown in Figure 4.5. To facilitate comparison, the intensity of each synthesized adsorbent is scaled equally in each figure. All adsorbents exhibited C1s spectrum peaks at 285 eV, consistent with C-C bonded carbon. This peak was attributed to the reference peak. A further position of the C1s peak was observed for carbonate in synthesized materials. A 288 eV peak in synthesized materials was

attributed to a carbonate compound, which may be the result of bicarbonate formation [16]. In the case of the Li1s, Na1s, and K2p peaks, peak fit results are included as a means of displaying the state of the metal. There was a clear peak at 54 eV for lithium, a peak at 1071.12 eV for sodium, and a peak at 293.88 eV for potassium in its metallic state [17,18]. The presence of cations confirmed Zeolite-Y cation loading.

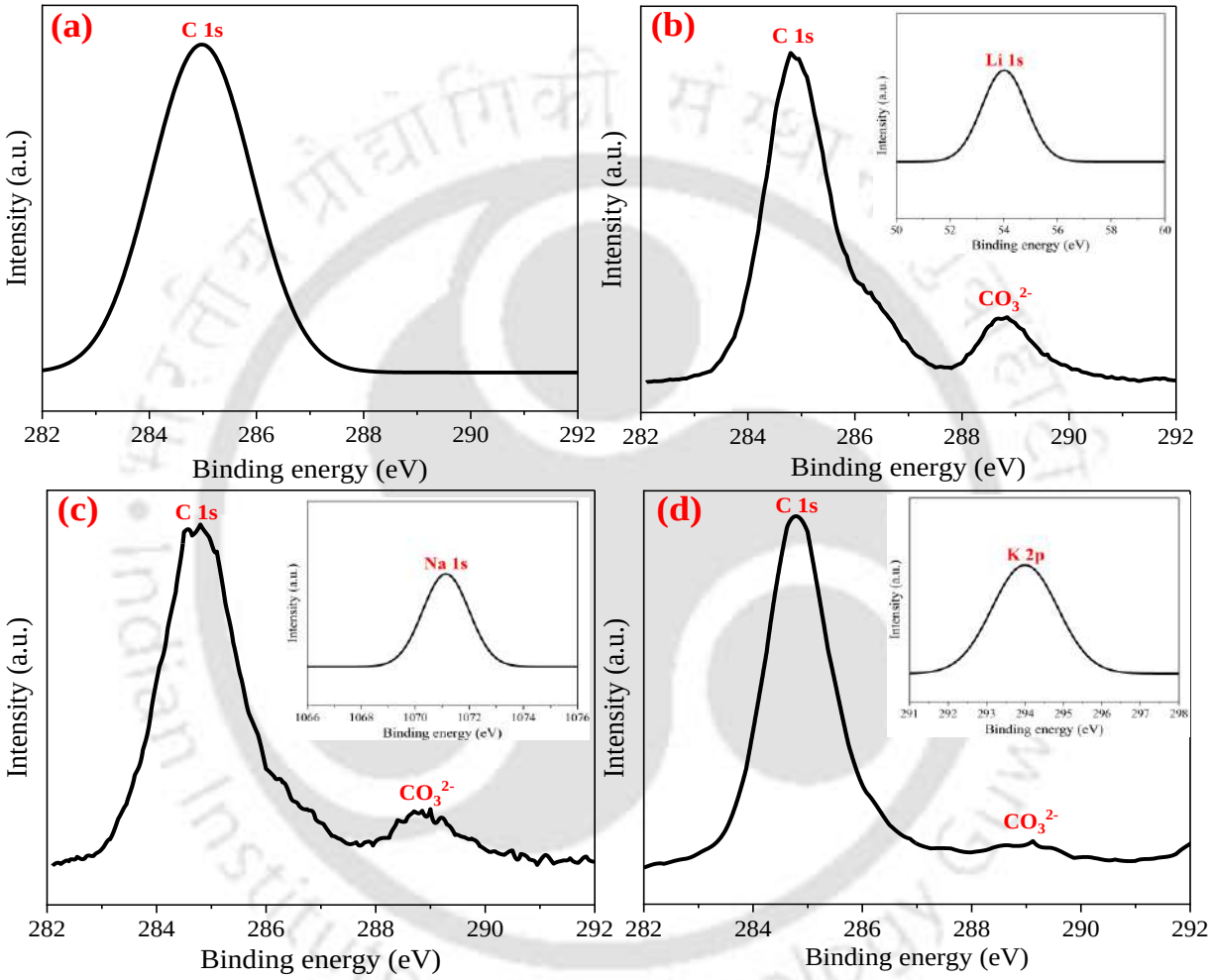

Figure 4.5: High-resolution XPS spectrum of (a) YZC, (b) LiYZC, (c) NaYZC, and (d) KYZC.

4.3 Gas adsorption performance

The gas adsorption performance of different cation loadings (Li^+, Na^+, and K^+) on Zeolite-Y was measured at 303 K, 323 K, and 343 K. A Rubotherm Magnetic Suspension balance was used to measure the adsorption isotherm. The adsorbent was thoroughly activated at a high temperature (423 K) for 180 min. In this process, helium flows over the sample at 30 cc min^{-1} under vacuum and the sample is cooled down to an experimental temperature. The jacket

surrounding the balance assembly circulated water from the water bath to maintain a constant temperature. The gas of interest was introduced to the desired experimental pressure after the desired temperature had been established in the system. A controlled increase in pressure in the system resulted in equilibrium measurements at intermediate pressures. To desorb the adsorbate from the solid, the system was evacuated and regenerated with heating and helium purging. In equilibrium, the excess amount adsorbed, M_{ex}, is correlated with the microbalance reading, M_t, and the buoyancy force acting on the bucket and sample.

$$M_{ex} = M_t - M_{t0} + M_{buoyancy}\rho^{gas} \quad (4.1)$$

Where the M_{t0} signal is a result of the sample evacuated weight and the sample holder weight. $V_{buoyancy}$ is the buoyancy volume and ρ_{gas} is the bulk gas density at equilibrium pressure and temperature. A buoyancy volume can be determined using helium run on an adsorbent at varying pressures. The experiments are usually carried out at room temperature.

4.3.1 Effect of Cation Loading

As shown in Figure 4.6, CO_2 adsorption isotherms were measured on cation-loaded Zeolite-Y at 303 K. In zeolites, cations enhance the electron density of the framework oxygen to enhance the capitation of acidic molecules [19,20]. For all the adsorbents, cations act as Lewis acid sites, whereas oxygen atoms in the framework, bearing partial negative charges, act as basic sites. The metal cations Li, Na, and K neutralized the negative charge of the framework. The electropositivity of exchangeable cations increases the basic strength of these sites [21]. The basicity of framework oxygen atoms of cation-loaded Zeolite-Y is in the order of $H^+ < Li^+ < Na^+ < K^+$ based on local hard–soft acid–base (HSAB) descriptors[22]. This principle indicates that the Lewis acid site (the carbon in CO_2) and basic Zeolite-Y oxygen atoms interact the most in K^+ and the least in H^+. Based on this observation, KYZC had the highest CO_2 occupancy in the middle of the 12-membered oxygen ring, while HYZC had the lowest [23]. There is

evidence that electrostatic and van der Waals interactions are crucial to the interactions between metal ions, zeolite, and carbon dioxide [24].

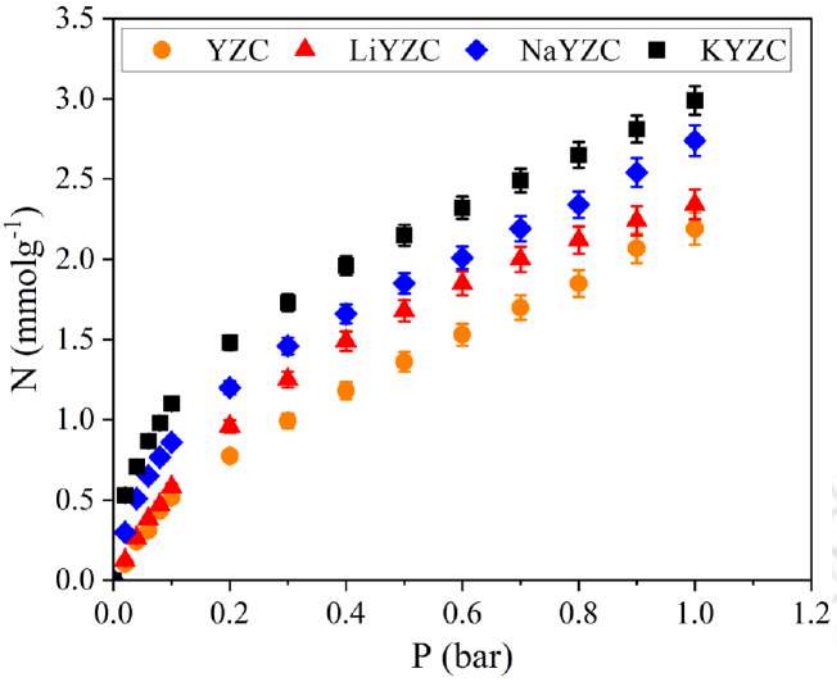

Figure 4.6: Carbon dioxide adsorption isotherm of commercial Zeolite-Y and cation-loaded Zeolite-Y at 303K.

The high sorption capacity of K^+-loaded Zeolite-Y is primarily due to the basicity of the potassium ion. However, the ionic radius and charge/radius ratio also play a very important role in this regard. The potassium's relatively large ionic radius reduces framework distortion and maintains favorable electrostatic interactions within the Zeolite supercage. Such a feature enhances CO_2 adsorption but shall not detriment upon the desired pore accessibility or structural integrity. While smaller cations may increase charge density and interaction strength, they can also cause greater framework distortion. This prompts a reduction in the overall adsorption performance. In the conducted investigations, the structural stability of Zeolite-Y Post-K^+ inclusion was verified and confirmed. As per this observation, it can be inferred that the ionic radius and charge/radius ratio of potassium are optimal for the enhancement of the CO_2 sorption capacity.

4.3.2 Effect of temperature

The effect of temperature on CO_2 adsorption has been investigated with cation-loaded Zeolite-Y as shown in Figure 4.7. Adsorbents enhanced their CO_2 adsorption capacity with increasing partial CO_2 pressure and decreased their adsorption capacity with rising temperatures. The decrease of CO_2 adsorption with the increase of the temperature has been associated with a decrease in adsorbent-adsorbate interactions (site–adsorbate) caused by the increasing mobility of adsorbed molecules into the zeolites cavities due to an increase in thermal agitation [25]. At higher adsorption temperatures, CO_2 molecules have greater kinetic energy. This leads to faster diffusion and shorter equilibrium times. However, due to the exothermic nature of physisorption, higher temperatures tend to reduce the interaction strength between CO_2 and the adsorbent surface. This phenomenon results in a lower adsorption capacity.

In addition, fixed energy sites reduce the possibility of CO_2 being retained on the adsorbent surface [26]. The highest adsorption capacity was obtained for all adsorbents at 303 K. This pattern is attributed to the exothermic nature of the adsorption process.

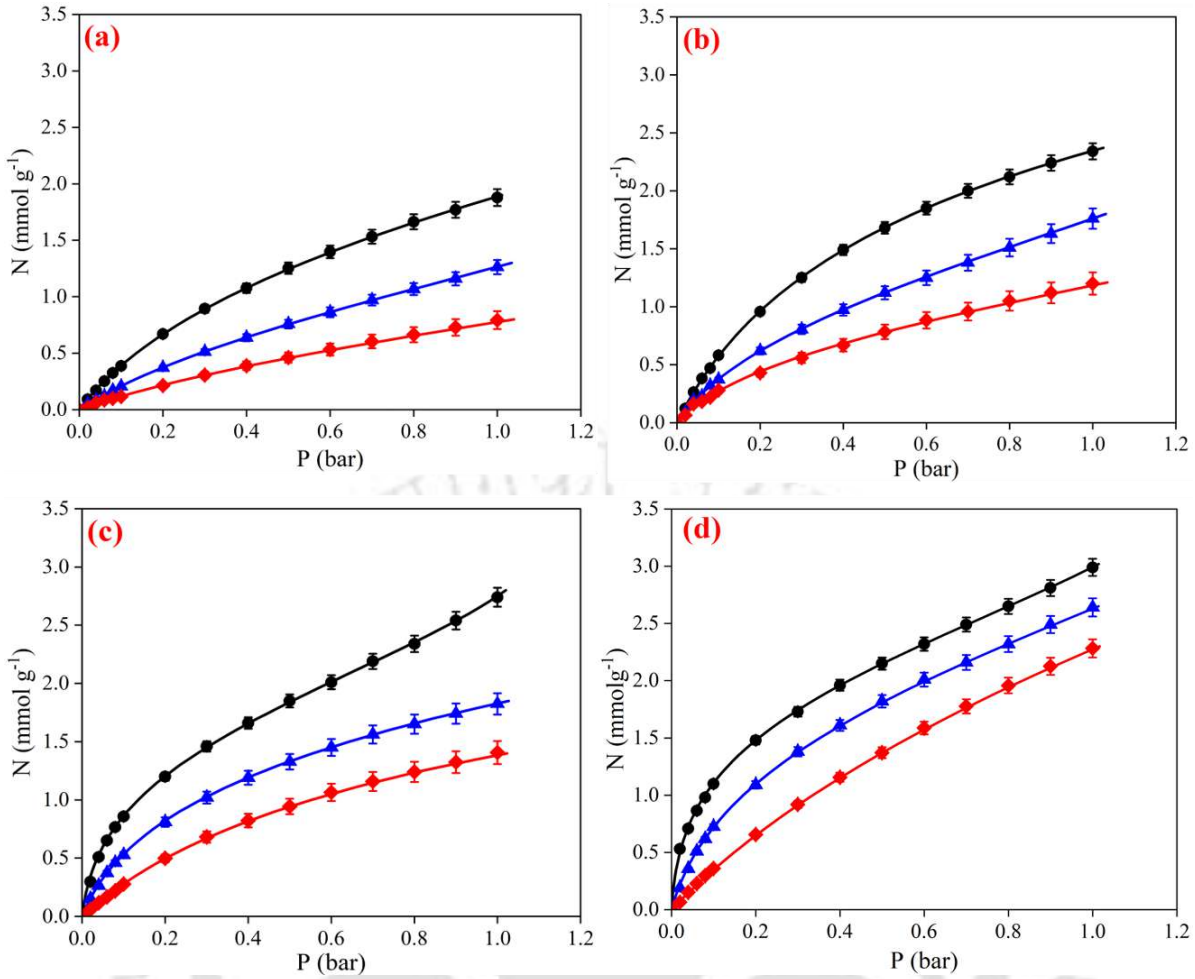

Figure 4.7: Carbon dioxide adsorption isotherm of (a) HYZC, (b) LiYZC, (c) NaYZC, and (d) KYZC at (●) 303 K, (▲) 323 K, and (◆) 343 K.

4.3.3 Adsorption isotherm model

The adsorption isotherms were modelled to gain insight into the adsorption process. The accuracy of the models is generally determined by the independent variables in the equation. The Virial model was used to fit carbon dioxide experimental data and the Langmuir model was used to fit CH_4 and N_2 gases with good statistical significance. As shown in Figure 4.7, Figure 4.8, and Figure 4.9, equilibrium adsorption isotherms of CO_2, CH_4, and N_2 on cation-loaded adsorbents were well described by their respective isotherm models at 303 K, 323 K, and 343 K.

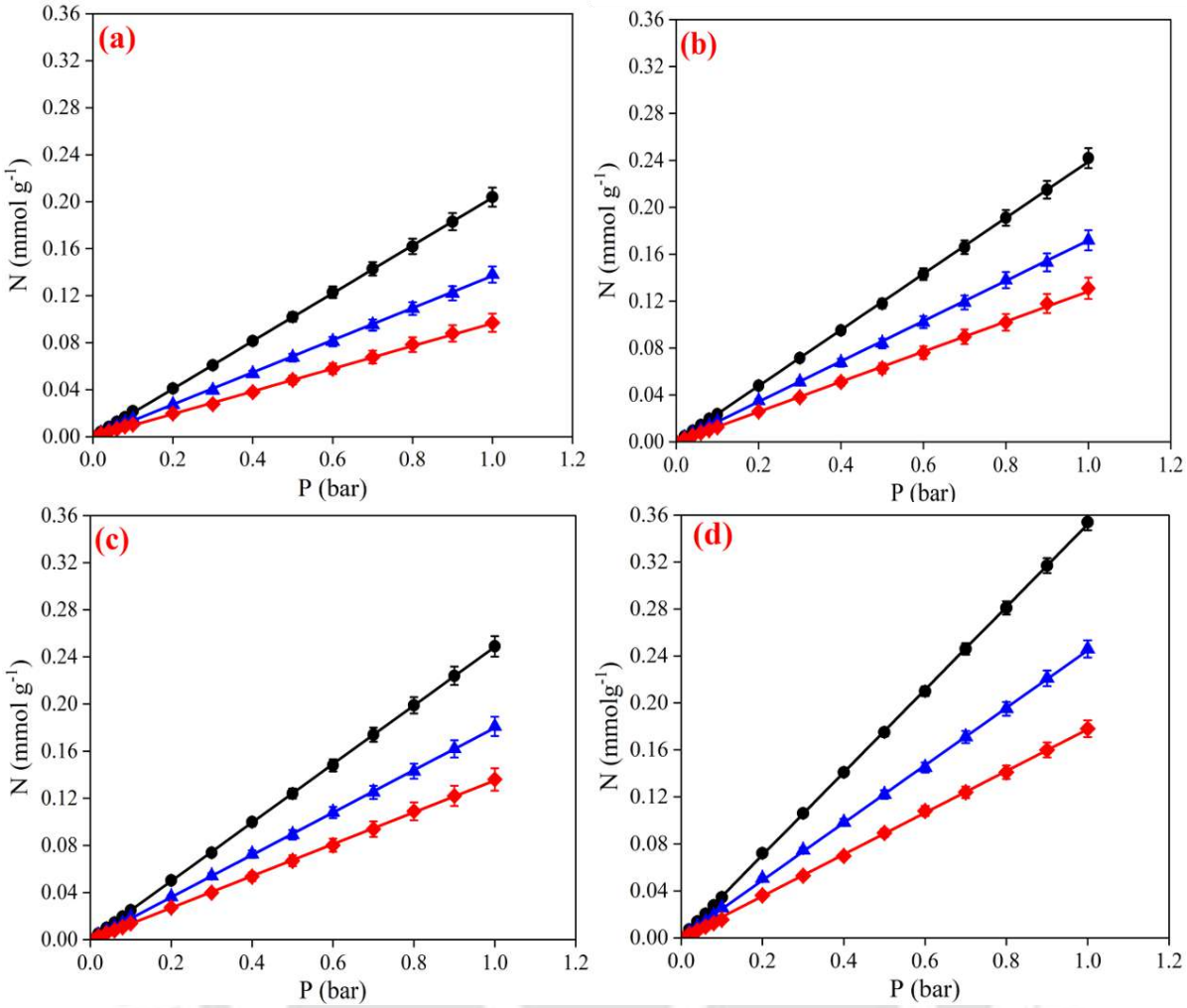

Figure 4.8: Methane adsorption isotherm of (a) HYZC, (b) LiYZC, (c) NaYZC, and (d) KYZC at (●) 303 K, (▲) 323 K, and (◆) 343 K.

The Virial adsorption isotherm model equation for the carbon dioxide gas fit was

$$\ln\left(\frac{P}{N}\right) = bN + cN^2 - \ln(\beta) \tag{4.2}$$

where P and N indicate pressure (bar) and adsorption capacity (mmol g^{-1}). The Henry's constant (mmol g^{-1} bar^{-1}) is represented by the symbol β whereas b and c are virial coefficients. The parameters are temperature-dependent

$$b = b^0 + \frac{b^1}{T} \tag{4.3}$$

$$c = c^0 + \frac{c^1}{T} \tag{4.4}$$

$$\beta = \beta^0 \, exp\left(\frac{\beta^1}{T}\right) \tag{4.5}$$

T represents temperature in K. There are two parameters β^0 and β^1, which are related to entropy and enthalpy of adsorption at zero loading, respectively.

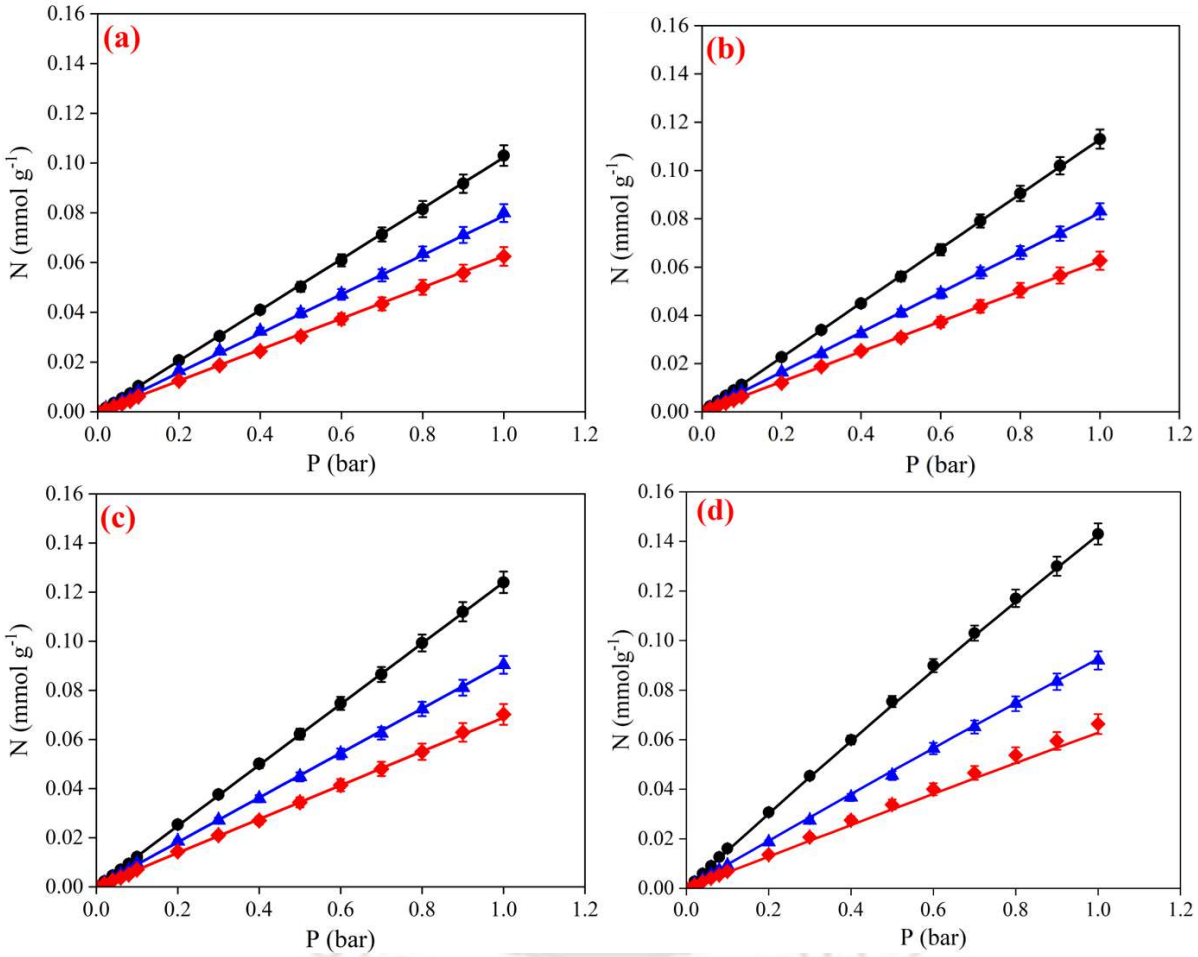

Figure 4.9: Nitrogen adsorption isotherm of (a) HYZC, (b) LiYZC, (c) NaYZC, and (d) KYZC at (●) 303 K, (▲) 323 K, and (◆) 343 K.

In this study, CO_2 loading on KYZC at 303 K and 1 bar was measured to be 2.99 mmol g^{-1}, which is higher than the loadings on NaYZC (2.74 mmol g^{-1}), LiYZC (2.37 mmol g^{-1}), and HYZC (1.87 mmol g^{-1}) which are due to the existence of larger pores and channel structures that hold adsorbate in place without steric effects. It is due to the cationic nature of the

adsorbent surface that alternatives have higher adsorption capacities. The CO_2 loadings were higher than those of CH_4 and N_2 in all adsorbents despite carbon dioxide having a large linear quadrupole moment, polarizability, smaller kinetic diameter, and stronger interaction between CO_2 molecules and cations. The high polarizability of methane gas makes it more adsorbent than nitrogen even though it has a zero quadrupole moment.

The Langmuir adsorption isotherm model for methane and nitrogen fit was

$$N = \frac{N^{max}\beta P}{1 + \beta P} \tag{4.6}$$

In the above equation, N, N_{max}, β, and P represent the amount adsorbed (mmol g^{-1}), maximum loading (mmol g^{-1}), Henry's constant (mmol g^{-1} bar^{-1}), and Pressure (bar). The adsorption isotherm model parameters are mentioned in Appendix A 4.1, 4.2, 4.3, and 4.4 for all the adsorbents with three different gases.

4.3.4 Heat of Adsorption

In the adsorption process, adsorption heat is a thermodynamic parameter that reflects adsorption behavior, and it is often used to identify the type of adsorption [27]. Viral and Langmuir's parameters were used to calculate the enthalpy of adsorption at zero loading for CO_2, CH_4, and N_2 using experimental data at 303 K, 323 K, and 343 K as shown in Figure 4.10. Based on these parameters, enthalpies were calculated as follows [28]:

Langmuir Model:
$$\Delta h_{ads} = \beta_1 R \tag{4.7}$$

Virial Model:
$$\Delta h_{ads} = -R(\beta_1 + b_1 N + c_1 N^2) \tag{4.8}$$

where, R is the gas constant ($Jmol^{-1}K^{-1}$)

A negative enthalpy change $-\Delta h_{ads}$ value for three gases confirms exothermic adsorption on synthesized adsorbents. All three Δh_{ads} values are smaller than 40 $kJmol^{-1}$, which indicates that physisorption occurred on all three adsorbents.

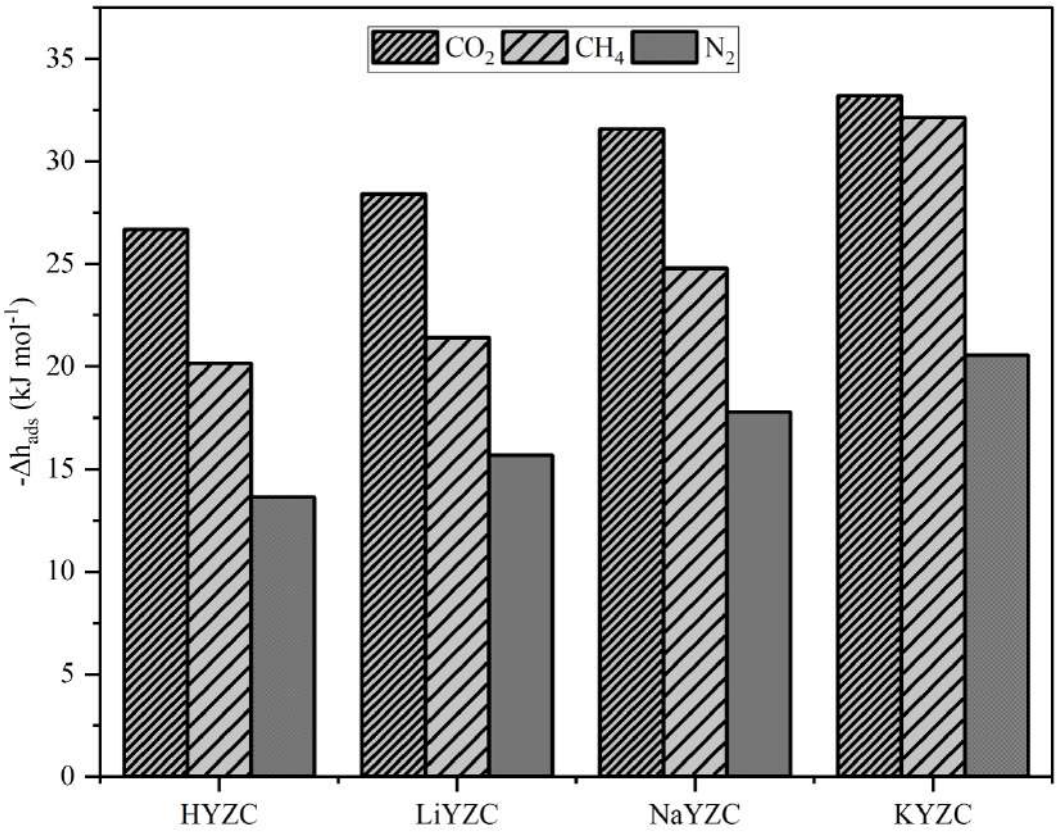

Figure 4.10: Heat of adsorption at zero loading of cation-loaded adsorbents for three different gases.

KYZC has a CO_2 enthalpy of adsorption of 33.19 $kJmol^{-1}$ at zero coverage. The value of this adsorbent is higher than other synthesized adsorbents. At zero loading, the enthalpy of adsorption of CH_4 and N_2 on KYZC10 is 32.13 kJ mol^{-1} and 20.56 kJ mol^{-1}, respectively. A comparison of the enthalpy of adsorption for CH_4 and N_2 with CO_2 indicates that the enthalpy of adsorption for CO_2 is among the highest among all the adsorbents. These molecules' polarity doesn't significantly affect their interactions and only dispersion interactions with the surface control the adsorption process. However, CH_4 has greater polarizability (even though it is non-polar), resulting in a slightly higher adsorption enthalpy than N_2. As shown by the largest -

Δh_{ads}, CO_2-adsorbents had the strongest interaction. Since the quadrupole moment strengthens the interaction between CO_2 and the adsorbent, CO_2 adsorption generates more heat. A combination of increasing pore curvature and increasing pore diameter positively affects $-\Delta h_{ads}$ [29]. A larger amount of heat is released when CO_2 migrates into small pores, which makes CO_2 adsorption more effective.

4.3.5 IAST Applications

The selectivity of two binary mixtures was calculated using Ideal Adsorbed Solution Theory (IAST) to investigate the influence of adsorbate properties and the role of cations in the Zeolite-Y framework on binary adsorption. Figure 4.11 (a) and (b) illustrates the variation in CO_2 selectivity over CH_4 and N_2 with pressure, starting from 5 mol% for the CO_2/CH_4 mixture and 13 mol% for the CO_2/N_2 mixture at 303 K. At atmospheric pressure and 303 K, CO_2 selectivity over CH_4 was significantly higher in KYZC (219.59) compared to HYZC (150.11), LiYZC (161.51), and NaYZC (211.11) adsorbents. This enhanced selectivity was attributed to the strong electrostatic interactions between K^+ ions and CO_2 molecules, owing to the higher basicity of KYZC. At low pressures, CO_2 molecules experience strong electrostatic interactions with the cations in the Zeolite-Y framework. However, as these adsorption sites became increasingly occupied, the electrostatic interactions weakened, leading to a notable decrease in CO_2 selectivity with increased pressure. The extent of this selectivity decreased under pressure varies among different adsorbents. For instance, the CO_2/N_2 selectivity was reduced for HYZC (111.79), LiYZC (113.50), and NaYZC (128.56) adsorbents at 1 bar pressure is less pronounced than KYZC (140.62) due to the weaker electrostatic interactions of CO_2 with the Zeolite-Y framework.

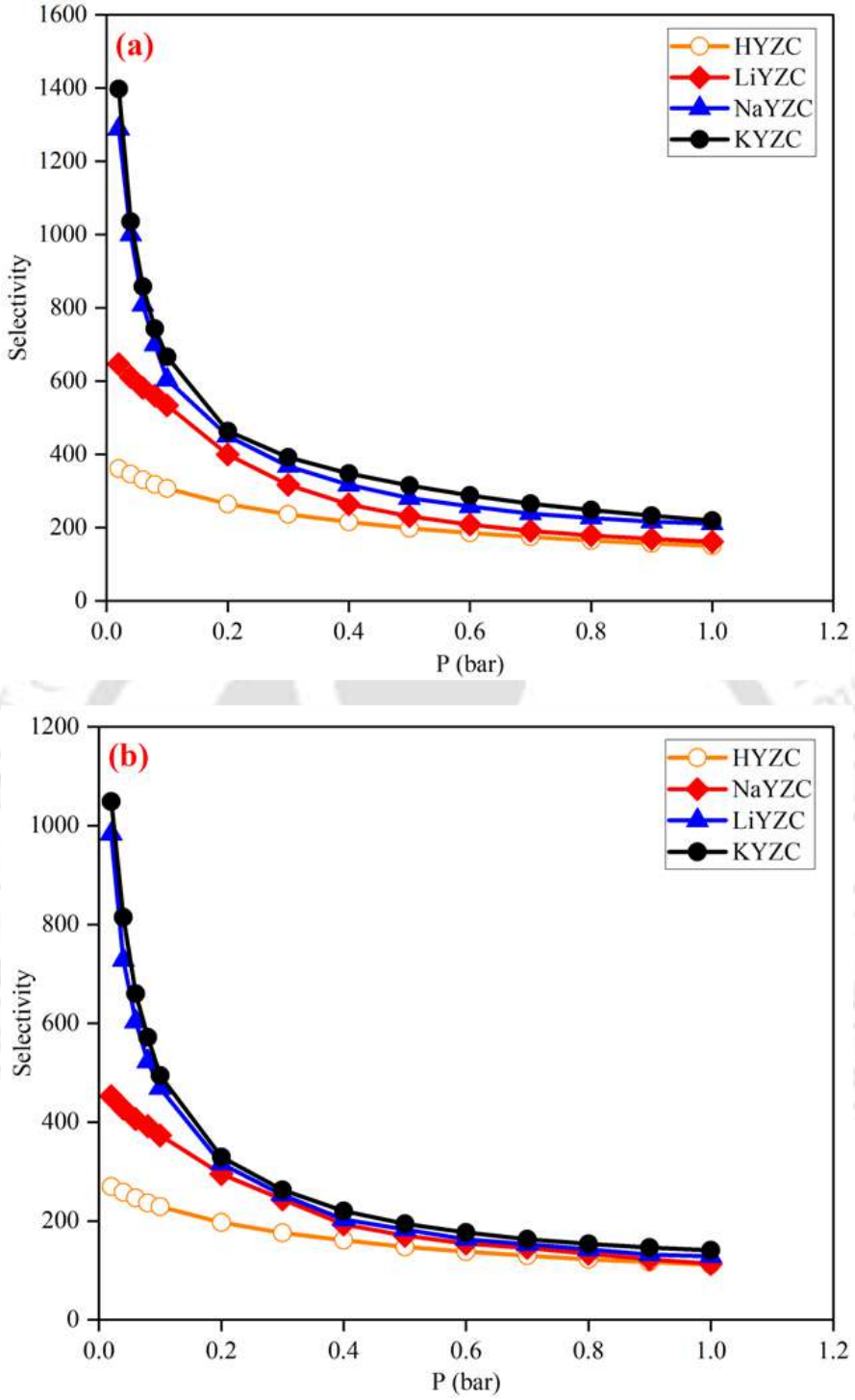

Figure 4.11: IAST predicted binary adsorption isotherms at 303K with pressure on cation-loaded Zeolite-Y for (a) 5 mol% for the CO_2/CH_4 mixture and (b) 13 mol% for the CO_2/N_2 mixture.

4.4. Summary

A systematic study of the relationship between physiochemical properties and adsorption of cation-loaded Zeolite-Y (1.87 mmol g^{-1}) adsorbents was conducted using Li^+ (2.37 mmol g^{-1}), Na^+ (2.74 mmol g^{-1}), and K^+ (2.99 mmol g^{-1}) as cation sources. CO_2 adsorption was predominantly affected by isosteric heat, while potassium-loaded samples had the highest adsorption factor due to their increased basicity. The equilibrium adsorption data for carbon dioxide have been obtained for all four materials at 303 K and up to 1 atmosphere. A Virial adsorption isotherm model was successfully used to model CO_2 data. Based on the results, CO_2 simultaneously interacts with the cation and neighbouring lattice oxygen atoms in the adjacent 12-MR window. The interaction strongly stabilizes CO_2 adsorption on KYZC, but not on LiYZC and NaYZC. This trend can be explained by the basicity (charge) of the oxygen atoms within the framework. The interaction of a cation-oxygen dipole with a CO_2 quadrupole allows the more basic lattice oxygen atoms to provide more charge to the carbon atom. The IAST was conducted to predict the selectivity of the two binary mixtures of gases. The selectivity of KYZC for CO_2/CH_4 (219.59) and CO_2/N_2 (140.62) mixtures was higher as compared to the other synthesized adsorbents at 303 K and 1 bar. As a result of these promising results, the following chapter focuses on optimizing this adsorbent to refine and maximize its efficiency for gas capture by using various potassium loadings on Zeolite-Y at different temperatures.

References

[1] A. Corma, Inorganic Solid Acids and Their Use in Acid-Catalyzed Hydrocarbon Reactions, Chem. Rev. 95 (1995) 559–614. https://doi.org/10.1021/cr00035a006.

[2] G. Busca, Acid Catalysts in Industrial Hydrocarbon Chemistry, Chem. Rev. 107 (2007) 5366–5410. https://doi.org/10.1021/cr068042e.

[3] R. Weingarten, G.A. Tompsett, W.C. Conner, G.W. Huber, Design of solid acid catalysts for aqueous-phase dehydration of carbohydrates: The role of Lewis and Brønsted acid sites, J. Catal. 279 (2011) 174–182. https://doi.org/10.1016/j.jcat.2011.01.013.

[4] W.O. Haag, R.M. Lago, P.B. Weisz, The active site of acidic aluminosilicate catalysts, Nature. 309 (1984) 589–591. https://doi.org/10.1038/309589a0.

[5] K.S. Walton, M.B. Abney, M. Douglas LeVan, CO_2 adsorption in Y and X zeolites modified by alkali metal cation exchange, Microporous Mesoporous Mater. 91 (2006) 78–84. https://doi.org/10.1016/j.micromeso.2005.11.023.

[6] D. Fu, M.E. Davis, Carbon dioxide capture with zeotype materials, Chem. Soc. Rev. 51 (2022) 9340–9370. https://doi.org/10.1039/D2CS00508E.

[7] D.G. Boer, J. Langerak, P.P. Pescarmona, Zeolites as Selective Adsorbents for CO_2 Separation, ACS Appl. Energy Mater. 6 (2023) 2634–2656. https://doi.org/10.1021/acsaem.2c03605.

[8] A. Pulido, P. Nachtigall, A. Zukal, I. Domínguez, J. Čejka, Adsorption of CO_2 on Sodium-Exchanged Ferrierites: The Bridged CO_2 Complexes Formed between Two Extraframework Cations, J. Phys. Chem. C. 113 (2009) 2928–2935. https://doi.org/10.1021/jp810038b.

[9] V. Mauer, C. Bläker, C. Pasel, D. Bathen, Energetic Characterization of Faujasite Zeolites Using a Sensor Gas Calorimeter, Catalysts. 11 (2021) 98. https://doi.org/10.3390/catal11010098.

[10] B. Fareed, F. Sher, S. Sehar, T. Rasheed, F. Zafar, M. Ameen, E.C. Lima, Tailor made Functional Zeolite as Sustainable Potential Candidates for Catalytic Cracking of Heavy Hydrocarbons, Catal. Letters. 152 (2022) 732–744. https://doi.org/10.1007/s10562-021-03657-x.

[11] S. Manadee, O. Sophiphun, N. Osakoo, N. Supamathanon, P. Kidkhunthod, N. Chanlek, J. Wittayakun, S. Prayoonpokarach, Identification of potassium phase in catalysts supported on zeolite NaX and performance in transesterification of Jatropha seed oil, Fuel Process. Technol. 156 (2017) 62–67. https://doi.org/10.1016/j.fuproc.2016.09.023.

[12] B. Fareed, F. Sher, S. Sehar, T. Rasheed, F. Zafar, M. Ameen, E.C. Lima, Tailor made Functional Zeolite as Sustainable Potential Candidates for Catalytic Cracking of Heavy Hydrocarbons, Catal. Letters. 152 (2022) 732–744. https://doi.org/10.1007/s10562-021-03657-x.

[13] M. Xue, R. Chitrakar, K. Sakane, T. Hirotsu, K. Ooi, Y. Yoshimura, Q. Feng, N. Sumida, Selective adsorption of thiophene and 1-benzothiophene on metal-ion-exchanged zeolites in organic medium, J. Colloid Interface Sci. 285 (2005) 487–492. https://doi.org/10.1016/j.jcis.2004.12.031.

[14] J. Liu, X. Yang, C. Wang, L. Ye, H. Sun, Synthesis of hierarchical 5A zeolites to improve the separation efficiency of n-paraffins, Adsorpt. Sci. Technol. 37 (2019) 530–544. https://doi.org/10.1177/0263617419850226.

[15] C. Huang, A. Li, Z.-S. Chao, Heterogeneous catalytic synthesis of quinoline compounds

from aniline and C1 – C4 alcohols over zeolite-based catalysts, RSC Adv. 7 (2017) 48275–48285. https://doi.org/10.1039/C7RA08442K.

[16] A.M. Andersson, D.P. Abraham, R. Haasch, S. MacLaren, J. Liu, K. Amine, Surface Characterization of Electrodes from High Power Lithium-Ion Batteries, J. Electrochem. Soc. 149 (2002) A1358. https://doi.org/10.1149/1.1505636.

[17] S. Oswald, Binding energy referencing for XPS in alkali metal-based battery materials research (I): Basic model investigations, Appl. Surf. Sci. 351 (2015) 492–503. https://doi.org/10.1016/j.apsusc.2015.05.029.

[18] Z. Zhang, M. Hu, B. Lv, J. Kang, J. Tang, Z. Fei, X. Chen, Q. Liu, M. Cui, X. Qiao, Solvent-Assisted Stepwise Redox Approach To Generate Zeolite NaA-Supported KO as Strong Base Catalyst for Michael Addition of Ethyl Acrylate with Ethanol, ACS Omega. 3 (2018) 10188–10197. https://doi.org/10.1021/acsomega.8b00704.

[19] A. de Mallmann, D. Barthomeuf, Four Different States of Benzene Adsorbed in Faujasites, in: 1986: pp. 609–615. https://doi.org/10.1016/S0167-2991(09)60926-5.

[20] G. Martra, R. Ocule, L. Marchese, G. Centi, S. Coluccia, Alkali, and alkaline-earth exchanged faujasites: strength of Lewis base and acid centers and cation site occupancy in Na- and BaY and Na- and BaX zeolites, Catal. Today. 73 (2002) 83–93. https://doi.org/10.1016/S0920-5861(01)00521-1.

[21] E.J. Doskocil, R.J. Davis, Spectroscopic Characterization and Catalytic Activity of Zeolite X Containing Occluded Alkali Species, J. Catal. 188 (1999) 353–364. https://doi.org/10.1006/jcat.1999.2676.

[22] R.C. Deka, R. Kinkar Roy, K. Hirao, Local reactivity descriptors to predict the strength of Lewis acid sites in alkali cation-exchanged zeolites, Chem. Phys. Lett. 389 (2004)

186–190. https://doi.org/10.1016/j.cplett.2004.03.094.

[23] M.R. Hudson, W.L. Queen, J.A. Mason, D.W. Fickel, R.F. Lobo, C.M. Brown, Unconventional, Highly Selective CO_2 Adsorption in Zeolite SSZ-13, J. Am. Chem. Soc. 134 (2012) 1970–1973. https://doi.org/10.1021/ja210580b.

[24] W. Wong-Ng, J.A. Kaduk, Q. Huang, L. Espinal, L. Li, J.W. Burress, Investigation of NaY Zeolite with adsorbed CO_2 by neutron powder diffraction, Microporous Mesoporous Mater. 172 (2013) 95–104. https://doi.org/10.1016/j.micromeso.2013.01.024.

[25] D. Bonenfant, M. Kharoune, P. Niquette, M. Mimeault, R. Hausler, Advances in principal factors influencing carbon dioxide adsorption on zeolites, Sci. Technol. Adv. Mater. 9 (2008) 013007. https://doi.org/10.1088/1468-6996/9/1/013007.

[26] S.O. Akpasi, Y.M. Isa, Effect of operating variables on CO_2 adsorption capacity of activated carbon, kaolinite, and activated carbon – kaolinite composite adsorbent, Water-Energy Nexus. 5 (2022) 21–28. https://doi.org/10.1016/j.wen.2022.08.001.

[27] K.N. Son, G.E. Cmarik, J.C. Knox, J.A. Weibel, S. V. Garimella, Measurement and Prediction of the Heat of Adsorption and Equilibrium Concentration of CO_2 on Zeolite 13X, J. Chem. Eng. Data. 63 (2018) 1663–1674. https://doi.org/10.1021/acs.jced.8b00019.

[28] F.R. Siperstein, A.L. Myers, Mixed-gas adsorption, AIChE J. 47 (2001) 1141–1159. https://doi.org/10.1002/aic.690470520.

[29] D. Keffer, H.T. Davis, A. V. McCormick, The effect of nanopore shape on the structure and isotherms of adsorbed fluids, Adsorption. 2 (1996) 9–21. https://doi.org/10.1007/BF00127094.

CHAPTER 5

Exploring CO_2 Selectivity in K_2CO_3-Modified Zeolite-Y: Loading and Temperature Effects on Adsorption Performance

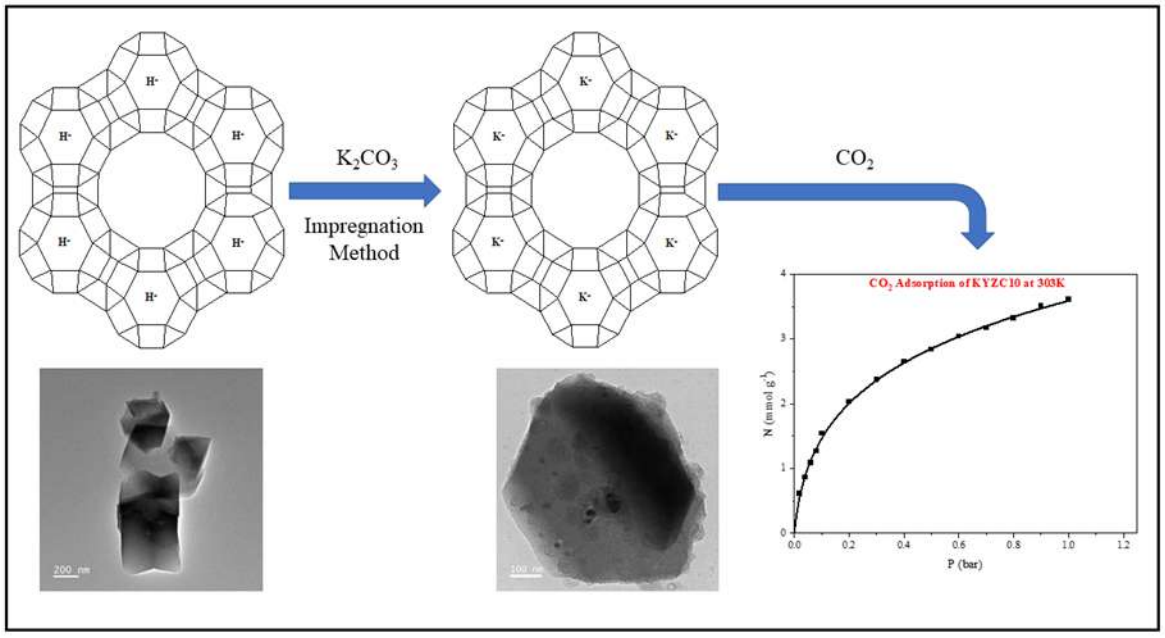

Chapter 5

Exploring CO_2 Selectivity in K_2CO_3-Modified Zeolite-Y: Loading and Temperature Effects on Adsorption Performance

This chapter focuses on the synthesis and characterization of Zeolite-Y modified with various weight percentages of potassium carbonate, aimed at enhancing its performance as an adsorbent. The synthesis process involves loading different amounts of potassium carbonate onto Zeolite-Y, followed by comprehensive characterization to assess the impact on the zeolite's structural and chemical properties. The chapter details gas adsorption studies conducted for CO_2, CH_4, and N_2 using a gravimetric system to evaluate the adsorption capabilities of these modified adsorbents. The data obtained from these studies are analyzed through modelling approaches to better understand adsorption behaviour. Additionally, the Ideal Adsorbed Solution Theory (IAST) is applied to determine the selectivity of the potassium carbonate-loaded zeolites for CO_2 relative to other gases (CH_4 and N_2). The chapter concludes with cyclic studies to assess the stability and reusability of the optimized adsorbents over multiple adsorption cycles.

5.1 Background

An innovative concept for CO_2 adsorption was investigated recently using alkali metal-based sorbents, such as potassium carbonate. Various mesoporous solid support materials based on K_2CO_3 have been demonstrated to be very promising for CO_2 capture. Adsorbents based on alkaline metals like Na_2CO_3, K_2CO_3, MgO, and CaO exhibit good potential for regenerable CO_2 adsorption due to their higher uptake, faster kinetics, higher selectivity, and wider temperature applicability range. Potassium-based adsorbents, in particular, are a cost-effective and energy-efficient solution for post-combustion CO_2 capture and separation. K_2CO_3 is thermally stable, resulting in a more stable and greener CO_2 sorbent. It has been reported that K_2CO_3 has excellent carbonation properties due to its hexagonal crystal structure and the

dispersion of K_2CO_3 in support material is affected by the porosity of the support material. Potassium carbonate-based adsorbents can adsorb CO_2 via a carbonation reaction, and they can be regenerated at a lower temperature not exceeding 150ºC [1].

5.2 Adsorbents characterization

The FTIR analysis of both the pure zeolite and synthesized samples is shown in Figure 5.1. The results revealed that the synthesized samples exhibited nearly identical FT-IR spectra, indicating that the Zeolite-Y structures were preserved. All the samples possess two FTIR peaks at 450 cm^{-1} and 586 cm^{-1} that were related to Si-O-Al stretching and the double six rings (D6R) external linkage band of the zeolite structure [2,3]. A significant peak at 1014 cm^{-1} corresponds to Si-O asymmetric stretching vibrations [4]. In addition, one peak was observed in synthesized samples between 1312-1423 cm^{-1} representing the presence of carbonate ions due to the formation of $KHCO_3$ [5]. The peak at 1638 cm^{-1} in the FT-IR spectrum of all the samples was due to the O-H stretching vibrations of water molecules [6]. The broad peaks at 3078-3629 cm^{-1} for KYZC5, KYZC10, and KYZC15 can be correlated with the –OH group of the KOH molecule [7]. Thus, the FT-IR spectra of the K_2CO_3-modified Zeolite-Y confirmed the modification of Zeolite-Y support with potassium carbonate using the impregnation method.

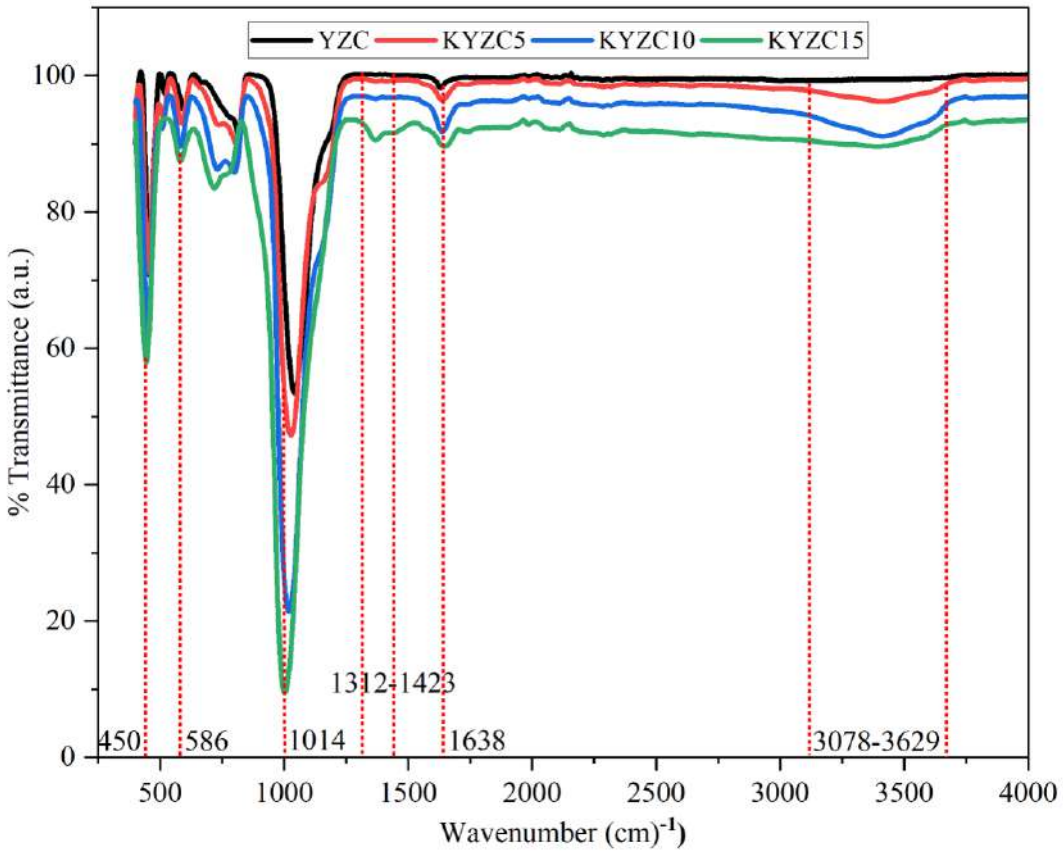

Figure 5.1: Attenuated total reflection (ATR) spectra of potassium carbonate loaded Zeolite-Y.

Figure 5.2 shows the XRD patterns of pure Zeolite-Y and the synthesized adsorbents. The peaks in Zeolite-Y occur at 2θ values of 6.3°, 10.26°, 12°, 15.78°, 18.84°, 20.52°, 22.98°, 23.82°, 26°, 27.26°, 29.84°, 31°, 31.64°, 32.7°, 34.36°, and 38.2°. It is also evident that all synthesized sample particles exhibited sharp peaks. This is due to their crystalline nature. The reduction in peak intensity occurred for enhanced potassium carbonate loading scenario. This is due to the reduced crystallinity of Zeolite-Y for the case. The change in peak intensity could also be a result of secondary scattering by the presence of potassium ions on the Zeolite-Y support [5].

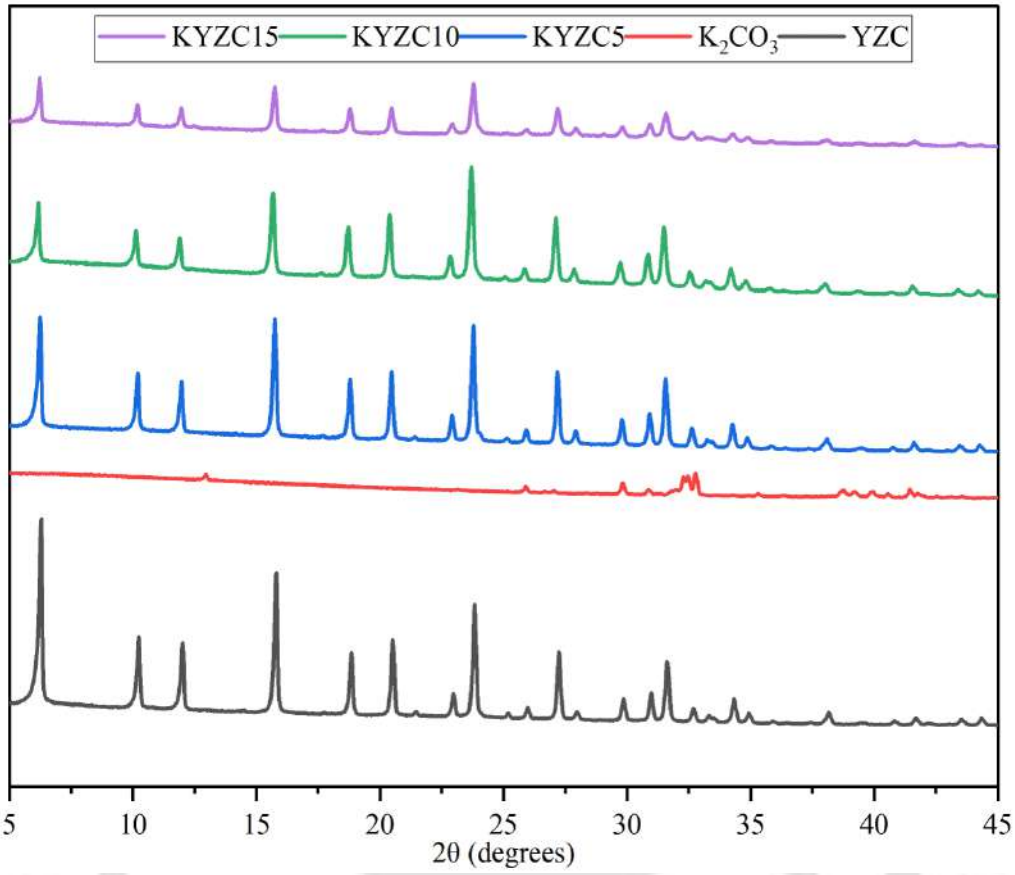

Figure 5.2: XRD patterns of Zeolite-Y, pure K_2CO_3, and synthesized adsorbents.

During large-scale applications, recyclability of the adsorbent is considered to be one of the most important parameters and TGA analysis helps in determining the stability as well as suitable regeneration temperatures of the samples. So, the thermogravimetric analysis of pure Zeolite-Y and the synthesized samples, shown in Figure 5.3, was carried out.

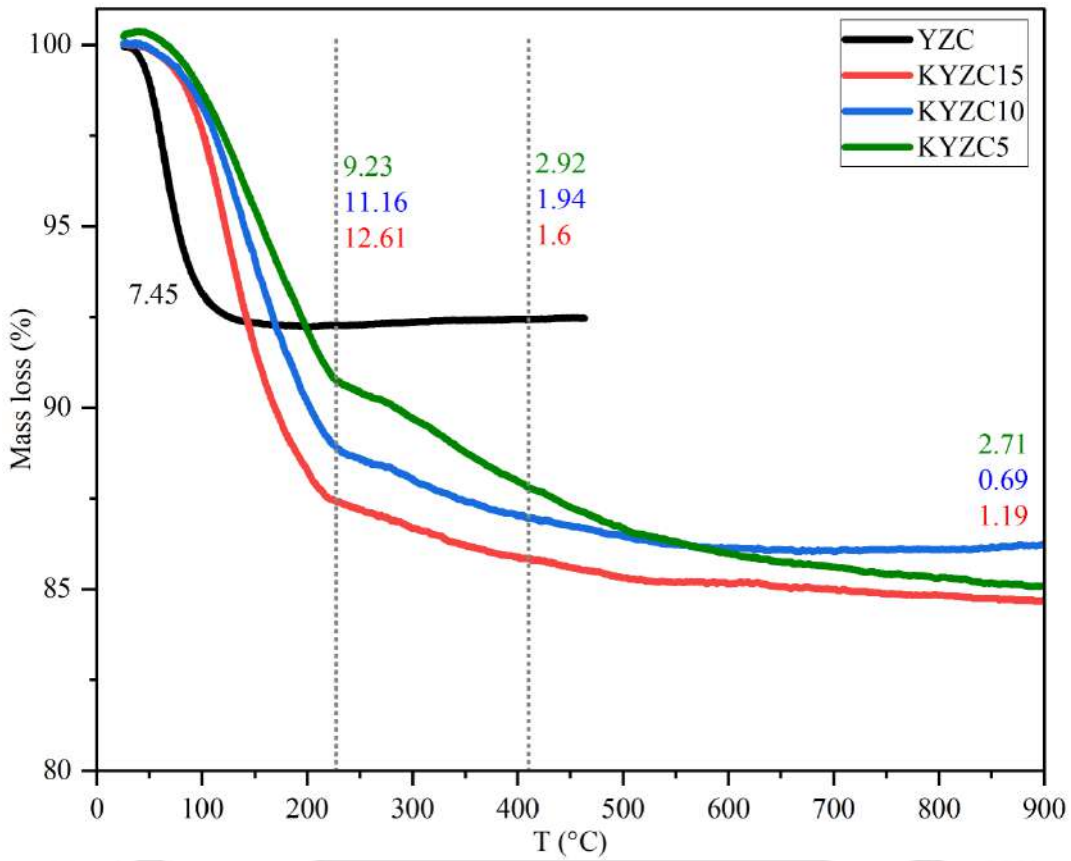

Figure 5.3: TGA analysis of Zeolite-Y, and different loading of K_2CO_3 on Zeolite-Y.

The TGA analysis of pure Zeolite-Y exhibited a single step weight (7.45 wt.%) in the temperature range of 25-120°C which was due to the moisture. For synthesized adsorbents, they were observed to have a three-stage weight loss in the temperature ranges of 25-227°C, 227-411°C, and 422-900°C as shown in Table 5.1. The first stage of weight loss was observed for all adsorbents in the temperature range 25-227°C which is due to the desorption of physically adsorbed water molecules from the adsorbent surface. A second phase of weight loss was attributed to the decomposition of $KHCO_3$ molecules in the temperature range of 227-411°C. The third phase of weight loss could be attributed to the decomposition of KOH molecules in the temperature range of 411-900°C [8].

Table 5.1: Thermal decomposition of pure Zeolite-Y and synthesized adsorbents.

Adsorbent	Temperature range (°C)	Weight loss (%)
ZYC	25-120	7.45
KZYC15	25-230	12.61
	230-410	1.6
	410-900	1.19
KZYC10	25-230	11.16
	230-410	1.94
	410-900	0.69
KZYC5	25-230	9.23
	230-410	2.92
	410-900	2.71

Figure 5.4 (a) depicts the nitrogen adsorption/desorption isotherms of Zeolite-Y and potassium carbonate-loaded Zeolite-Y adsorbents. It is evident from the surface area analysis that all the adsorbents exhibited a type IV isotherm with a H4 hysteresis loop which conveys that the adsorbents were mesoporous materials. Nitrogen adsorbed volume demonstrated a small step increment at the lower relative pressure ($0.1<P/P_0<0.4$) due to the existence of small internal pores in the adsorbents. The adsorbents displayed a pronounced capillary condensation step in the relative pressure range of 0.5 to 0.9 which was due to the uniform internal mesoporosity. However, at high relative pressure ($0.9<P/P_0<0.99$), the adsorbents affirmed a sharp increase in the adsorbed nitrogen volume which confirmed the larger mesoporous structure of the adsorbents.

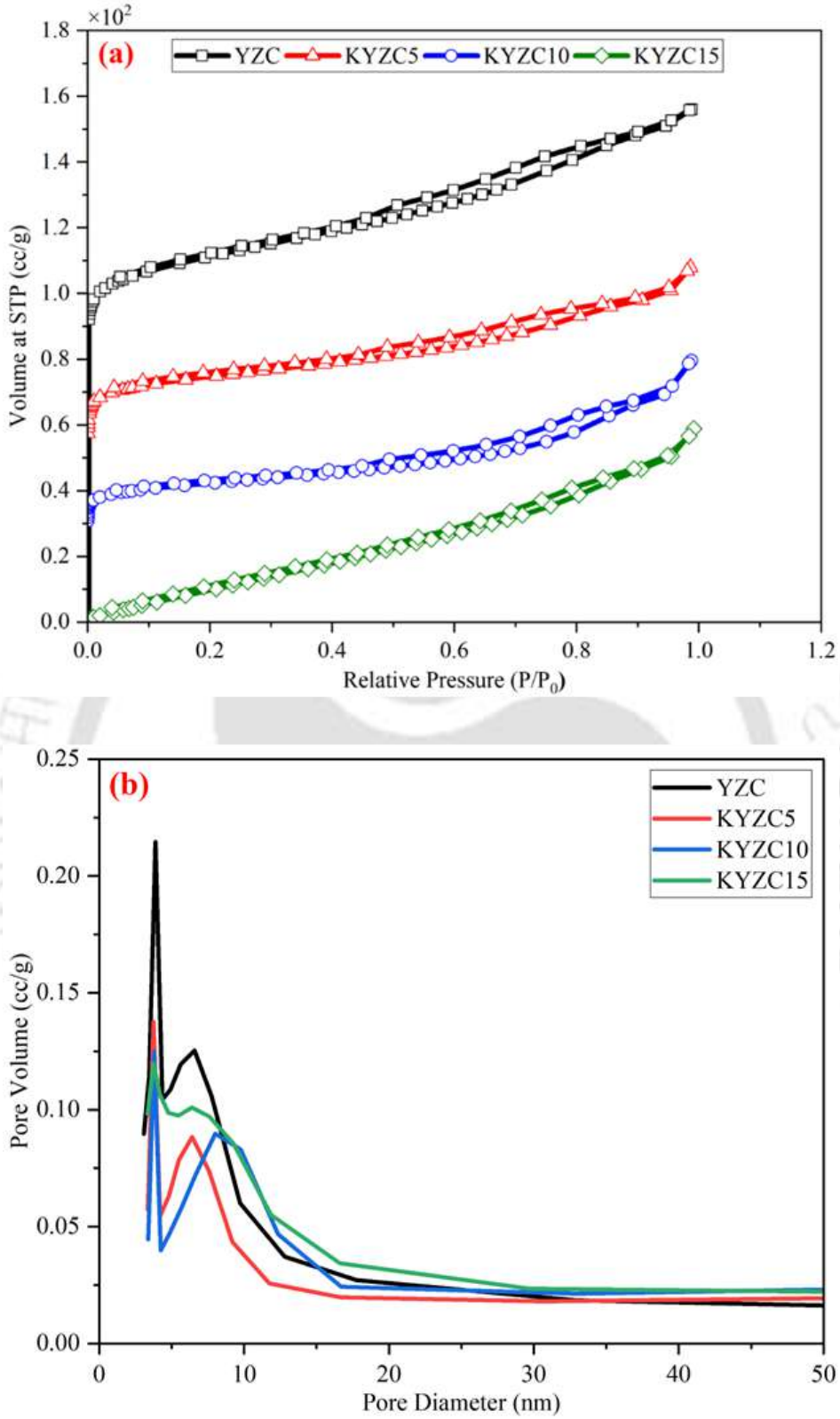

Figure 5.4: (a) Adsorption-desorption isotherm of commercial Zeolite-Y and potassium carbonate loaded Zeolite-Y with N_2 at 77K, (b) BJH pore size distribution curve for pure and loaded adsorbents.

The BET surface area and pore volume reduced with increasing K_2CO_3 loading. This implies that the potassium species ($KHCO_3$/KOH) occupied the cavities of zeolite [8].

The pore size distributions of the samples were calculated with the classical Barrett-Joyner-Halenda (BJH) model. The model is as per the corrected Kelvin equation, which is corrected for multilayer adsorption. As shown in Figure 5.4(b), the desorption pattern using BJH reveals the pore distribution of all adsorbents, indicating that the pore diameter of pure Zeolite-Y and synthesized samples ranges between 3 and 8 nm. This further confirms the presence of mesopores in the potassium-loaded samples. The pore size distribution of KYZC10 is centered around 3-8 nm whereas pure Zeolite-Y is from 3-6 nm. Table 5.2 summarizes the relevant structural properties of commercial Zeolite-Y and synthesized adsorbents.

Table 5.2: Physical properties of different adsorbents.

Adsorbent	S_{BET} (m^2/g)	PD_{avg} (nm)	V_t (cc/g)
YZC	355.26	2.73	0.24
KYZC5	294.29	3.22	0.17
KYZC10	163.83	3.80	0.12
KYZC15	62.51	3.41	0.09

A high-magnification TEM image of pure Zeolite-Y and potassium carbonate-loaded Zeolite-Y is shown in Figure 5.5 (a), (b), (c), and (d). Pure zeolite and synthesized adsorbents have a typical hexagonal sodalite cage, and their particle size is about 100–200 nm. Small spots were observed on the surface of the synthesized samples. The size and number of particles increased with potassium loading. A small amount of potassium was observed on the exterior of the KYZC15 adsorbent, which probably blocked the external pores.

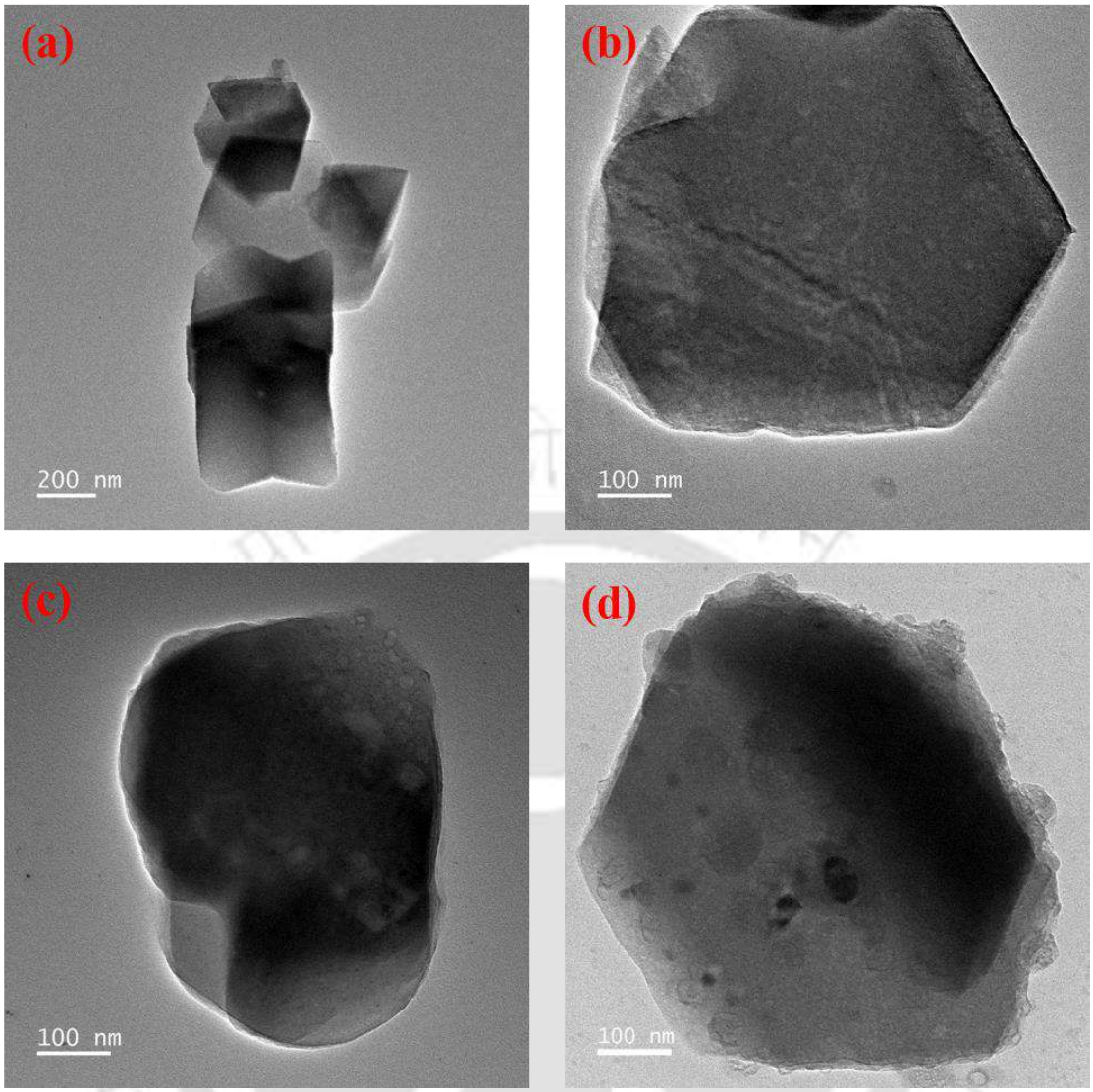

Figure 5.5: TEM images of (a) YZC, (b) KYZC5, (c) KYZC10, and (d) KYZC15.

Figure 5.6 (a), (b), (c), and (d) show the C 1s−K 2p region spectra of pure Zeolite-Y and potassium-loaded Zeolite-Y. The peaks in all the spectra appearing in the region 282.54–290.50 eV correspond to C 1s. The C 1s peak in the range 284.76-284.82eV was chosen as the reference peak, and its intensity did not change significantly. In the spectrum of the synthesized adsorbents, the C 1s peak between 289.01-289.14 eV is most likely due to a small amount of carbonate. A doublet of contributions is found in the K 2p region representing contributions in the region of 293.50-293.88 eV for the K+ group and 296.53-296.21 eV for the K-O group [9].

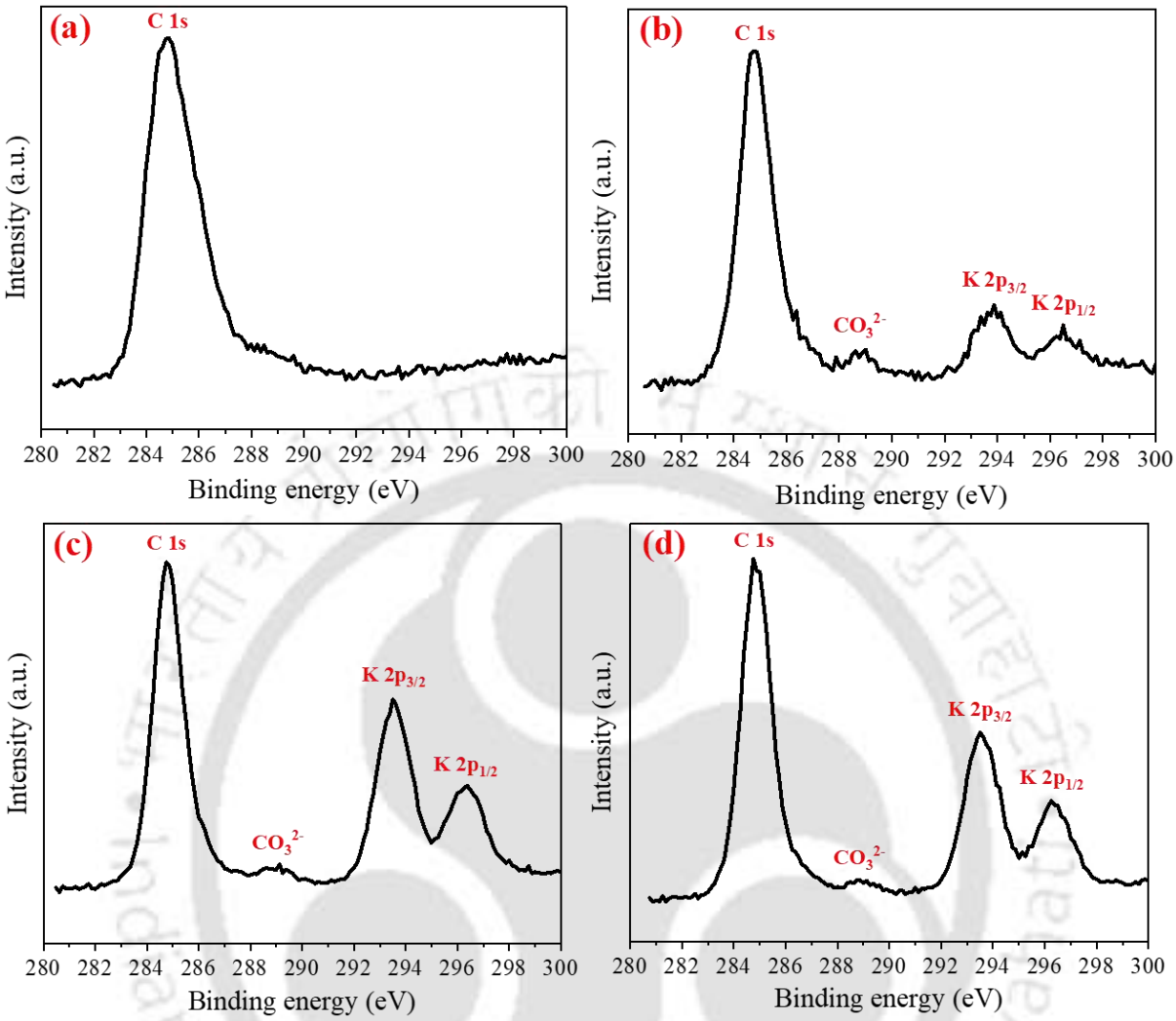

Figure 5.6: XPS spectra of (a) YZC, (b) KYZC5, (c) KYZC10, and (d) KYZC15.

5.3 Role of various parameters on gas adsorption

In a gravimetric adsorption system, the adsorption equilibria of CO_2, CH_4, and N_2 on synthesized adsorbents were determined at 303 K, 323 K, and 343 K. Before each isotherm measurement, the samples were activated by heating them to 150ºC with a 30 $cm^3\,min^{-1}$ purge flow of helium under vacuum condition. To ensure activation of the adsorbent, it was ensured that its weight did not significantly decrease over time. The activated adsorbent was cooled under vacuum to the experimental temperature. During the adsorption analysis, a sufficient amount of time was allowed for the adsorbate gas within the adsorption cell to reach

equilibrium before measuring each isotherm point. A pressure dose was increased gradually to measure the isotherm. After every adsorption process, the adsorbents were activated at a higher temperature under vacuum again for the adsorbent to be ready for the next adsorption process. The standard method for equilibrium measurement was used, and the excess amount adsorbed was estimated using buoyancy corrections [10]. The following is the equation for calculating the total amount adsorbed by the adsorbent:

$$M_t - M_{eq} - M_0 + V_{buoyancy}\rho_{gas} \quad (5.1)$$

Where M_o is the adsorbent weight under vacuum, M_{eq} is the adsorbent weight in equilibrium, $V_{buoyancy}$ is buoyancy volume, and ρ_{gas} is the density of a gas. According to the non-adsorbing helium assumption, the required buoyant volume was calculated based on helium readings at 293 K and in the pressure range of 0–25 bar.

5.3.1 Effect of K_2CO_3 loading

Figure 5.7(a) illustrates the carbon dioxide adsorption performance of sorbents prepared with three different potassium carbonate loadings ranging from 5 to 15 wt% and at 303 K. The CO_2 adsorption capacity of Zeolite-Y support was 2.19 mmol g^{-1} at 303 K and the adsorption capacity enhanced sharply after potassium carbonate loading (KYZCx). A sharp increase in the adsorption capacity was observed in the low-pressure region (≤0.30 bar) for all the synthesized samples. This is due to the physisorption between carbon dioxide and potassium carbonate on the surface of adsorbents. At 303 K and 1 bar, equilibrium adsorption capacities exhibited the following trend KYZC10 > KYXC5 > YZC > KYZC15. The potassium carbonate loading increased carbon dioxide adsorption, and the equilibrium capacity is 3.61 mmol g^{-1} (303 K and 1 bar) for 10 wt% loadings. A further increase in the loading reduced carbon dioxide adsorption capacity. This could be occurred due to the pore blocking and voids filling of zeolite based on

BET analysis. Thus, it is apparent that the active channel sites (cationic sites) overlapped and reduced the surface area of the potassium carbonate adsorbent being accessible for carbon dioxide sorption.

The lower CO_2 adsorption capacity being analyzed for the 5 wt.% potassium carbonate-loaded Zeolite-Y (KYZC5) in comparison to the 10 wt.% (KYZC10) can be attributed to insufficient active potassium cation sites for the lower loading case. For gas adsorption, the Zeolite-Y can be loaded with 10 wt.% of the potassium carbonate to ascertain a finer and optimal trade-off between the porous structural integrity and the sufficiency of active sites. Consequently, CO_2 adsorption efficiency has been higher for the later case. For the 15 wt.% loading case (KYZC15), excessive potassium carbonate may have blocked the pores and reduced the accessibility to active sites. This led to a reduced adsorption capacity. Thus, the 10 wt.% loading case that demonstrated the highest adsorption capacity can be inferred to be the best case due to its optimal loading and distribution.

5.3.2 Effect of temperature

Figure 5.7(b) depicts the adsorption capacities of KYZC10 at three different temperatures (303 K, 323 K, and 343 K). At 1 bar pressure, the adsorption capacities of KYZC10 were found to be 3.61, 2.89, and 1.73 mmol g^{-1} corresponding to 303 K, 323 K, and 343 K. Carbon dioxide adsorption was reduced with increasing temperature. This is associated with the exothermic interaction that lowers the extent of adsorption. Due to the higher kinetic energy of the adsorbate molecules, all the adsorbents possessed a lower adsorption capacity at a higher temperature. This is due to entropy enhancement with temperature that resulted in the breakage of bonds between adsorbate and adsorbent molecules. In other words, the adsorption capacity is reduced with increasing temperature.

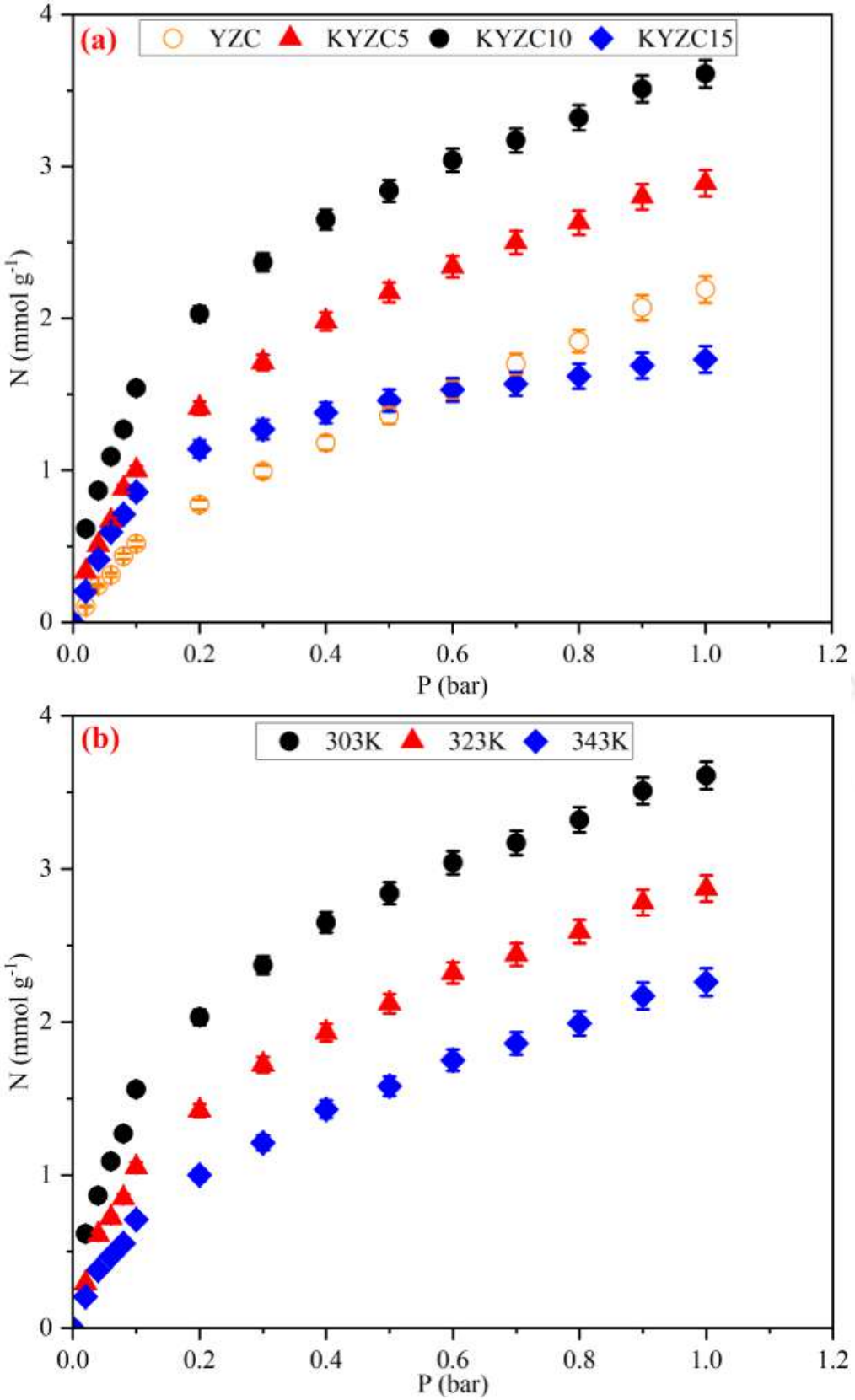

Figure 5.7: (a) CO_2 adsorption capacities at 303 K for three different K_2CO_3 loaded Zeolite-Y, and (b) Effect of KYZC10 material for CO_2 adsorption at three different temperatures.

5.3.3 Isotherm model

The adsorption energetics can be better understood with isotherm modeling. Thereby, Langmuir isotherm and dual-site Langmuir isotherm were deployed to model the experimental data of the mentioned adsorbents. Subsequently, for both models, good fitness was not assured for the carbon dioxide adsorption case. This is possibly due to the pertinent heterogeneity in the zeolite system with multiple groups. Virial isotherms, however, are versatile and can provide good statistical significance for the description of zeolite. The model is represented as:

$$P = \frac{N}{\beta} exp(bN + cN^2) \tag{5.2}$$

where, P (bar) refers to pressure, and N (mmol g^{-1}) refers to the amount adsorbed. Also, other terms in the above expression are Henry's constant β (mmol g^{-1} bar^{-1}), and two virial coefficients b ($mmol^{-1}$ g) and c ($mmol^{-2}$ g^2). These parameters are considered to be temperature dependent i.e.

$$\beta = \beta^0 \exp\left(\frac{\beta^1}{T}\right)$$

$$b = b^0 \exp\left(\frac{b^1}{T}\right)$$

$$c = c^0 \exp\left(\frac{c^1}{T}\right)$$

where T represents the system temperature (in Kelvin). Using this model, the best fit was achieved for CO_2 adsorption isotherm at all temperatures (303 K, 323 K, 343 K).

The adsorption capacities of an optimized sample (KYZC10) for other gases (CH_4 and N_2) were determined to evaluate the potential of adsorbent for flue gas separation. Each gas (CO_2,

CH_4, and N_2) possessed different polarizability and quadrupole moment (Table 5.3). Using the adsorption isotherms were modeled to determine Henry's constant and heat of adsorption.

Table 5.3: Gas adsorption properties.

Gas	M.W.	Kinetic diameter	Polarizability×10^{25}	Quadrupole moment×10^{40}
	($gmol^{-1}$)	(Å)	(cm^3)	($C.m^2$)
CO_2	44	3.3	26.3	14.3
CH_4	16	3.8	26.0	0.0
N_2	28	3.64	17.6	1.52

Figure 5.8 (a), (b), and (c) show the adsorption of CO_2, CH_4, and N_2 as well as the fit of the isotherm models with Langmuir (for CH_4 and N_2) and virial (for CO_2) models. The amount adsorbed by all gas adsorbate increases as partial pressure increases and decreases as temperature increases. In KYZC10, the adsorption capacity for CO_2, CH_4, and N_2 is 3.61, 0.13, and 0.047 mmol g^{-1}, respectively. As shown in the adsorption isotherms, KYZC10 adsorbent has a much higher affinity for carbon dioxide when compared to the other gases (N_2, CH_4) due to the large linear quadrupole moment of CO_2, and its strong interaction with intra-crystalline charge density frameworks. Considering the isotherm model fitting (lines in Figure 5.8), the Langmuir model is useful to describe CH_4 and N_2 data. Despite having zero quadrupole moment, methane gas has a higher adsorption value over nitrogen because of its high polarizability.

For CH_4 and N_2 gases, the best-fit curves representing the Langmuir isotherm for experimental adsorption data are depicted in Figure 5.8 (b) and (c) respectively.

$$N = \frac{N^{max}\beta P}{1 + \beta P} \tag{5.3}$$

where, the model considers pressure (P, bar), amount of adsorbed gas on the support (N, mmol g^{-1}), saturation adsorption capacity (N_{max}, mmol g^{-1}), and Henry's constant (β, mmol g^{-1} bar^{-1}) as the relevant terms.

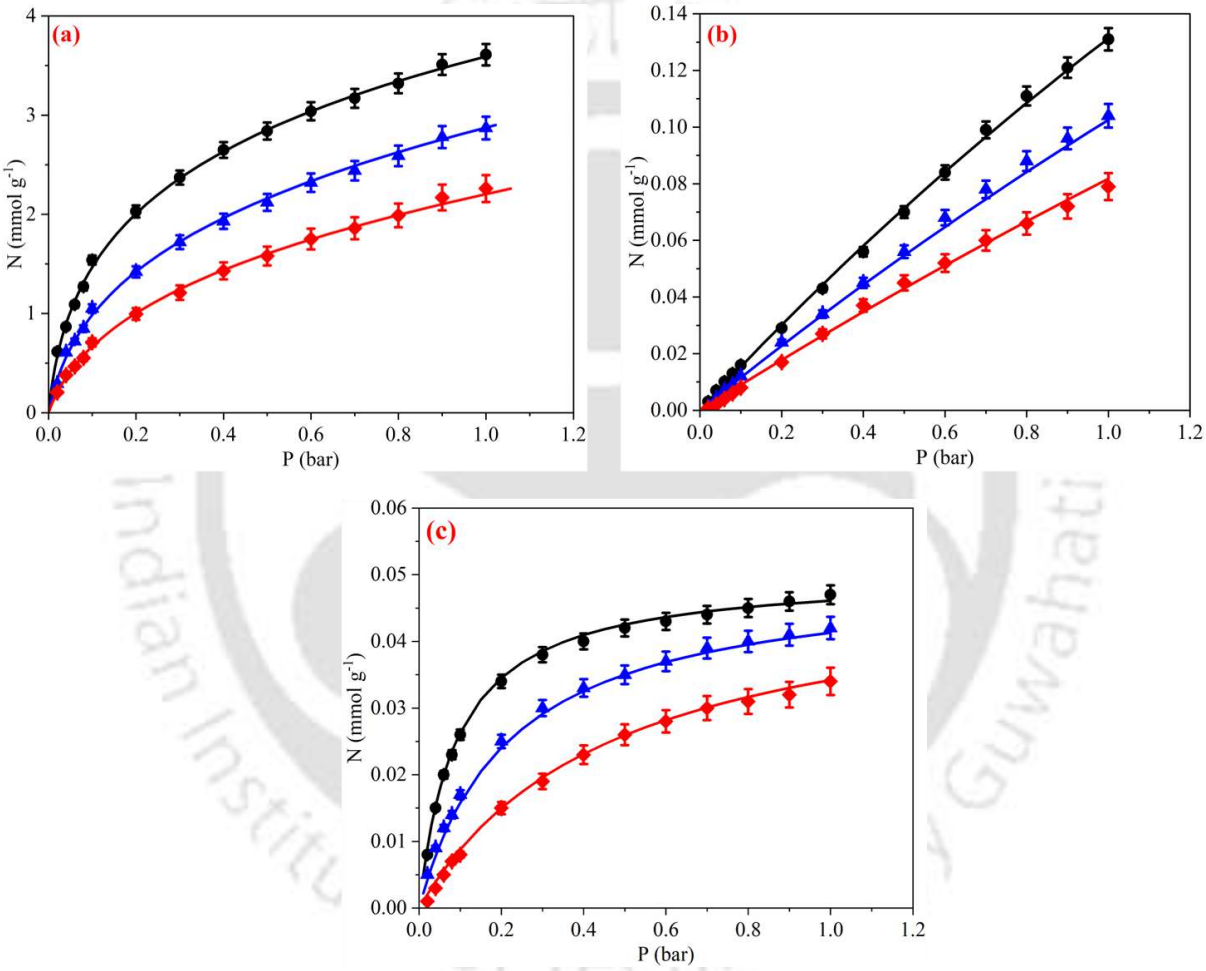

Figure 5.8: (a) CO_2 adsorption isotherms, (b) CH_4 adsorption isotherms, (c) N_2 adsorption isotherms on KYZC10 at (●) 303 K, (▲) 323 K, and (◆) 343 K. Symbols are experimental data; lines are fits obtained using Virial and Langmuir model parameters.

In comparison to CH_4 and N_2, CO_2 has a higher adsorption capacity in the entire parametric range due to high polarizability and quadrupole moments (Table 5.3). In the low-pressure

region, carbon dioxide exhibits greater loading due to the strong electrostatic interaction between CO_2 molecules and K^+ ions than CH_4 or N_2. The adsorption isotherm model parameters for KYZC10 adsorbent of all the three gases are presented in Appendix A5.1.

5.3.4 Adsorption enthalpy and Henry constant variation

Henry's constant (β) and the adsorption enthalpy of all three gases were determined at zero loading ($\Delta h_{ads,0}$) for KYZC10 adsorbent at 303 K, 323 K, and 343 K respectively. For KYZC10, CO_2 has higher values of β and $\Delta h_{ads,0}$, which confirms the importance of electrostatic interactions during the adsorption process.

5.3.4.1 Enthalpy Calculation

The isotherm models can be used to evaluate the enthalpy of adsorption. To evaluate enthalpy with the Virial and Langmuir models, the following equations can be respectively applied:

$$\frac{-\Delta h_{ads}}{R} = \beta_1 + b_1 N + c_1 N^2 \tag{5.4}$$

$$\frac{-\Delta h_{ads}}{R} = \beta_1 \tag{5.5}$$

Figure 5.9 (a) depicts the enthalpy of the material (KYZC10) at zero loading conditions which helps in understanding the ease of regeneration. The enthalpy of adsorption indicated the strength of the interactions between the adsorbate and the adsorbent molecules. The isosteric heat of adsorption for CO_2, CH_4, and N_2 at zero loading is 34.83 kJmol^{-1}, 18.54 kJmol$^{-1,}$ and 11.73 kJmol^{-1}, respectively.

5.3.5 Henry's constant calculation

Variation of Henry's constant (β) plot with temperature for all the adsorbate gases adsorbing on KYZC10 is depicted in Figure 5.9(b). Among the adsorbate gases, CO_2 exhibits stronger

van der Waals interactions at all temperatures over CH_4 and N_2. Henry's constant altered significantly in low-pressure conditions highlighting the greater role of electrostatic interactions. Further, the electrostatic interactions weakened with increasing temperature. On the other hand, due to low electrostatic interactions, Henry's constant is comparatively insensitive to CH_4 and N_2 gases and at all three alternative temperatures.

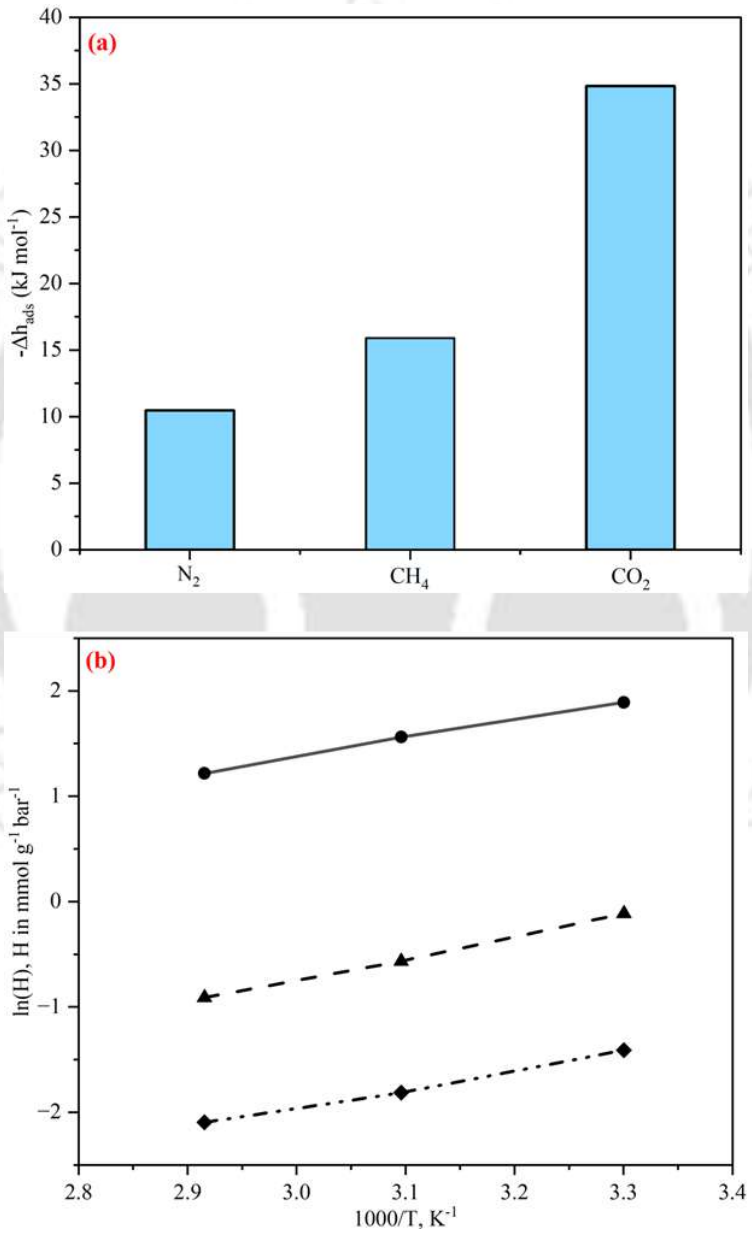

Figure 5.9: (a) Comparison of enthalpy of adsorption at zero loading of KYZC10 for three different gases, (b) Variation Henry constant with temperature for three different gases (●) CO_2, (▲) CH_4, and (◆) N_2.

Also, it shall be noted that CO_2 has a greater quadrupole moment value at 303K in comparison to the value at 323K or 343K. This is due to its electrostatic interactions with the gas molecules and K^+ metal ions. These electrostatic connections deteriorate with temperature and are replaced by dispersion interactions. In contrast to carbon dioxide, methane and nitrogen have lesser electrostatic interaction between the gas molecule and cationic group, and both gases have smaller Henry's constant. Thus, it is apparent that KYZC10 adsorbent has a high affinity for the adsorption of CO_2 due to strong ion-quadrupole interactions.

5.3.6 IAST Applications

Based on the experimental single-component adsorption isotherms, the Ideal Adsorbed Solution Theory (IAST) was utilized to determine the selectivity of CO_2/CH_4 and CO_2/N_2 mixtures at 303 K, 323 K, and 343 K as presented in Figure 5.10 (a) and (b). In the case of CO_2/CH_4, 5 mol% of CO_2 and 13 mol% of CO_2 for CO_2/N_2 were selected for IAST calculations to the composition of natural gas and flue gas streams.

A decrease in CO_2 selectivity with the rise in CO_2 pressure was less pronounced for CO_2/N_2 mixtures than for CO_2/CH_4 mixtures due to the larger difference in the polarizability between CO_2 and N_2. The selective adsorption of the gases occurs as a result of interaction between the adsorbate and adsorbent molecules. In the case of CO_2/CH_4, at 303 K and 1 bar pressure, the selectivity was 273.63, which indicates high selectivity for carbon dioxide. This could be due to the modified zeolite likely exhibiting a higher affinity for CO_2 compared to CH_4. This is due to CO_2's higher polarizability and quadrupole moment, which enhance its interaction with the surface of the zeolite. The presence of potassium ions (K^+) from K_2CO_3 may also enhance CO_2 adsorption due to increased basicity, which favors the adsorption of acidic gases like CO_2. But as the pressure of the binary mixture increased, the selectivity decreased exponentially, as the carbon dioxide now has to competitively adsorb over methane gas which has comparable

polarizability. In the case of the CO_2/N_2 system, nitrogen being a relatively bigger molecule compared to carbon dioxide, occupies the pores of the adsorbent, resulting in lower selectivity (202.74) at 303 K and 1 bar. However, as the CO_2 has more affinity for the adsorbent, the CO_2 molecules gradually replaced N_2 molecules from the pores, resulting in increased selectivity for CO_2 at higher pressures. The impact of temperature on CO_2 selectivity over CH_4 is illustrated in Figure 5.10 (a) As the temperature increases from 303 K to 343 K, a noticeable decline in CO_2 selectivity for the binary gas mixture is observed. This reduction can be attributed to the more significant decrease in electrostatic interactions for CO_2 molecules compared to CH_4 molecules at elevated temperatures. A similar trend is observed for CO_2 selectivity over N_2, as depicted in Figure 5.10 (b).

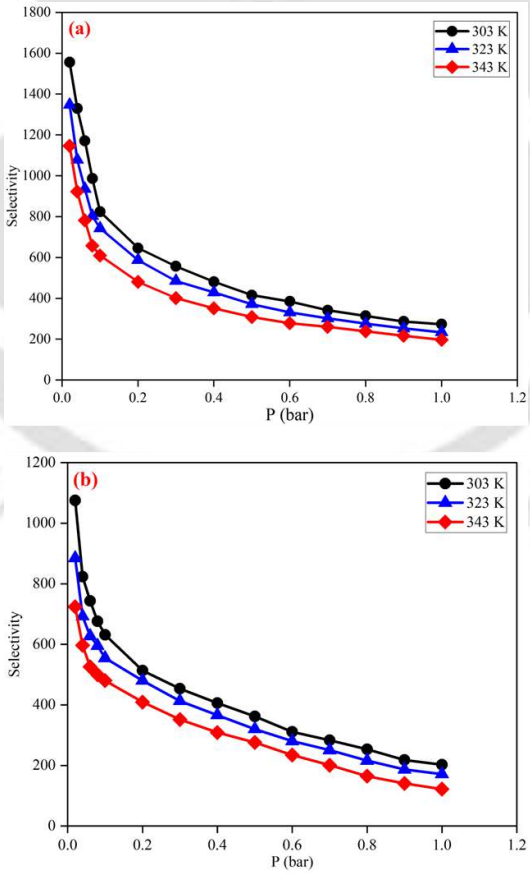

Figure 5.10: IAST predicted binary adsorption isotherms with pressure on KYZC10 for (a) 5 mol% for the CO_2/CH_4 mixture and (b) 13 mol% for the CO_2/N_2 mixture.

5.3.7 Cyclic performance

Adsorption capacity stability after regeneration of the adsorbent is a fundamental parameter for industrial application. Henceforth, cyclic studies were conducted for carbon dioxide adsorption with KYZC10. The regeneration of the KYZC10 was carried out in a helium environment at 150°C for 180 min after which the adsorption-desorption studies were carried out. KYZC10 performed well at 303 K and 1 bar and for eight cycles as shown in Figure 5.11. It was observed that the adsorbent possessed stable adsorption capacity in the range of 3.61-3.51 mmol g^{-1} for eight cycles. After the 8^{th} cycle, the adsorbent exhibited only a 3% loss of adsorption capacity in comparison to its initial capacity of 3.61 mmol g^{-1}. Thus, it can be inferred that the KYZC10 is a good adsorbent due to its stable performance during the adsorption and desorption process.

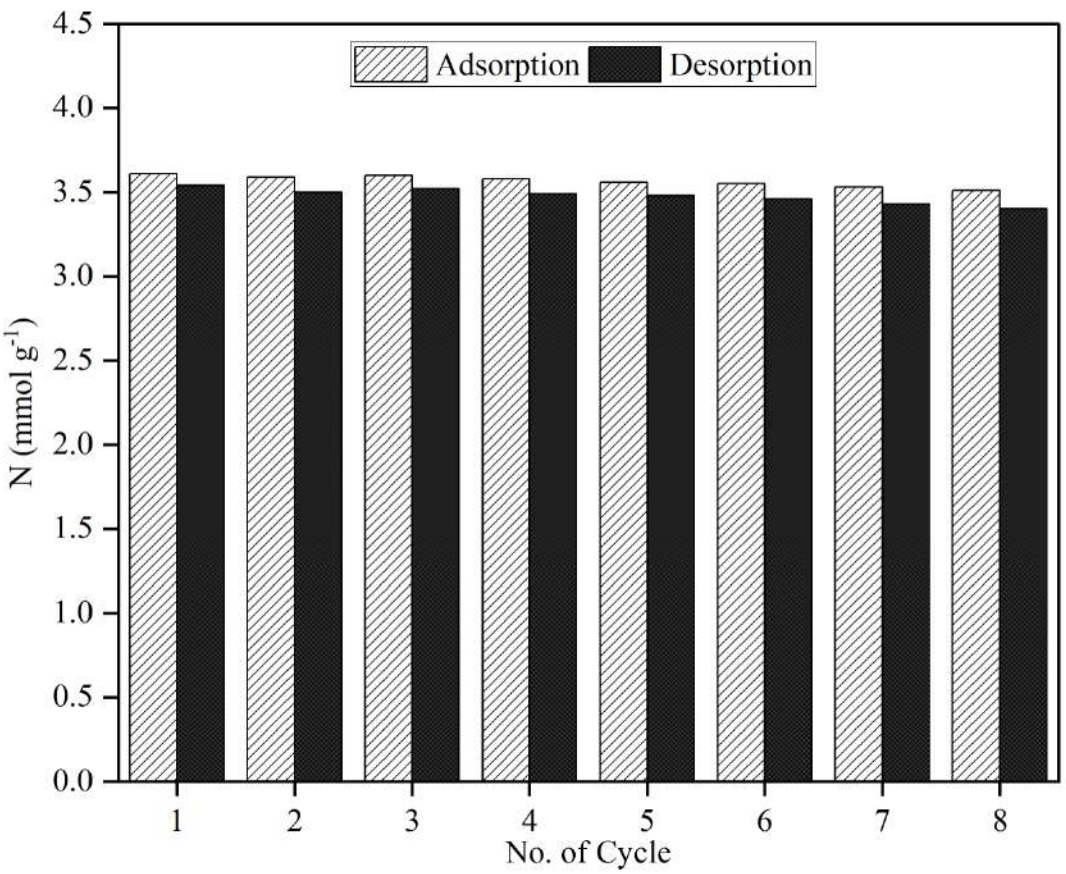

Figure 5.11: Cyclic adsorption/desorption performance of KYZC10 adsorbent for carbon dioxide adsorption.

The excellent cyclic adsorption-desorption performance and thermal stability of the KYZC10 sorbent are supported with rigorous experimental tests. The CO_2 adsorption capacity of KYZC10 was retained up to the eighth cycle and the negligible structural degradation and thermal stability up to 200°C confirms its suitability for repeated applications. These features can be attributed to the optimal potassium loading that facilitated the optimal trade-off between adsorption performance and structural integrity. Future studies could aim to enhance the cyclic performance beyond the eight cycles, and such efforts will potentially ascertain the viability of KYZC10 in long-term industrial applications.

This number of adsorption-desorption cycles was selected as eight for the conduct of the preliminary assessment of any significant loss in the CO_2 sorption capacity. While industrial applications require significantly more cycles for ascertaining the long-term viability of the tested sorbents, the Ph.D. thesis research work scope was to only affirm upon an initial assessment of the evaluated material's performance.

Furthermore, industrial gas streams often contain impurities that also affect adsorption. However, the conducted Ph.D. research works involved a fundamental evaluation under controlled conditions and with high-purity gases. Future research works in the chosen field of study can further extend the investigations to a higher number of cycles (about 10 – 15) and thereby facilitate the assessment of the adsorption performance with even more realistic conditions and with impurities-containing gas streams. Accordingly, the long-term applicability of the material in real-world scenarios can be confirmed and needful process/product alterations can be as well targeted.

In summary, KYZC10 exhibited superior adsorption capacity over pure and other synthesized adsorbents. Such data can be used very effectively for enhanced energy-efficient large CO_2 capture systems.

5.4 Comparison of synthesized adsorbents for gas adsorption

In this Ph.D. thesis, a comprehensive approach was undertaken to enhance carbon dioxide adsorption capacity using commercial Zeolite-Y as a support material. Zeolite-Y was initially selected based on its favourable pore size and inherent CO_2 adsorption capacity (1.869 mmol g^{-1}). To further augment its performance, the zeolite was functionalized with three distinct amine groups—monoethanolamine, diethanolamine, and triethanolamine—at varying loadings (1 wt.%, 5 wt.%, and 10 wt.%). Among these, monoethanolamine-functionalized Zeolite-Y (MEOH5) emerged as the most effective, exhibiting superior CO_2 adsorption (2.26 mmol g^{-1}) due to its simple molecular structure and enhanced interaction with the zeolite framework. This material maintained stability across four adsorption-desorption cycles.

For the determination of the specific influence of the cations on the CO_2 adsorption capacity of the doped Zeolite-Y sorbents, the Ph.D. thesis research works were only conducted for the alternate monovalent cations (Li^+, Na^+, and K^+). Such a choice was guided by their ionic radius, charge density, and affinity for CO_2, as well as their practical feasibility for large-scale applications. However, likely, bivalent cations (e.g., Mg^{2+}, Ca^{2+}, and Ba^{2+}) may also have a significant and sensitive influence on the CO_2 adsorption capacity. This is due to their higher charge density, which potentially enhances the electrostatic interactions between the adsorbent and CO_2 molecules. Literature reports suggest that bivalent cations could alter the zeolite framework's charge distribution and pore environment and can consequently improve the selectivity and adsorption performance. The case of bivalent cation doping is beyond the scope of the research undertaken in the Ph.D. thesis. However, it is indeed a promising direction for

future research. Accordingly, future research needs to assess and optimize the performance of bivalent cations' doped Zeolite-Y-based adsorbents in terms of enhanced CO_2 adsorption capacity.

Subsequently, the research shifted focus to cation-exchanged Zeolite-Y to explore further enhancements. Potassium-loaded Zeolite-Y demonstrated the highest CO_2 adsorption capacity (2.99 mmol g^{-1}), leading to an optimized material, KYZC10, which not only achieved the best adsorption capacity (3.61 mmol g^{-1}) but also remained stable through eight adsorption-desorption cycles. Modeling studies revealed that CO_2 adsorption was best described by the Virial adsorption isotherm model, whereas CH_4 and N_2 adsorption adhered to the Langmuir model. Additionally, the selectivity of the synthesized adsorbents was effectively predicted using Ideal Adsorbed Solution Theory (IAST). Among all the synthesized adsorbents, the KYZC10 had the highest selectivity values for two binary mixtures CO_2/CH_4 with 5 mol% of CO_2 and CO_2/N_2 with 13 mol% of CO_2 at 303 K and 1 bar. This comparative analysis highlights the systematic optimization and robust performance of the developed adsorbents, underscoring their potential for industrial applications. The comparison of the selected Zeolite-Y as a support material for gas adsorption studies, followed by its functionalization with various amine groups and subsequent cation exchange, is detailed in Table 5.4. This table presents a comprehensive overview of the performance metrics, highlighting the evolution of adsorption capacities across the different modifications.

Table 5.4: A comparison of the CO_2 adsorption capacities and selectivity of selected commercial zeolites and best synthetic adsorbents at 303 K and 1 bar conditions.

Adsorbent	Selectivity		N (CO_2)
	CO_2/CH_4	**CO_2/N_2**	**(mmol g^{-1})**
Zeolite-Y	150.11	111.78	1.87
MEOH5	157.59	143.77	2.26
KYZC10	***273.63***	***202.74***	***3.61***

The potassium compounds other than K_2CO_3 were used, such as KOH or KNO_3, the effect on CO_2 adsorption could differ due to the variant chemical properties and ion release behavior of these compounds. K_2CO_3 was selected for its ability to release K^+ ions while maintaining a moderate increase in basicity, which is essential for CO_2 interaction. KOH would release OH^- in addition to K^+. This potentially enhances CO_2 adsorption and as well modifies the framework. In contrast, KNO_3 would release NO_3^-, which is less basic and might have a lesser effect on the CO_2 adsorption for the adsorption facilitated by the K_2CO_3. Therefore, while K_2CO_3 is effective, other potassium compounds may lead to different adsorption behavior. This is due to their ionic composition and interaction with the zeolite.

Distinct mechanisms are responsible for the interactions between the CO_2 and the cations and amines. Accordingly, loading ranges are bound to alter significantly for the amines and the cations functionalized Zeolite-Y sorbents. Based on preliminary investigation and literature-reported details, the cation loadings are lower than the 5 wt.% impregnation may not either significantly alter the Zeolite-Y's basicity or increase CO_2 adsorption capacity. Henceforth, the cation loading range has been chosen to be from 5 – 15 wt.% in the conducted research works. This ascertained optimal adsorbent performance and maintenance of the structural integrity of the zeolite. In contrast, being a chemisorption process, the amine functionalization is effective even for the lower loading case. This is due to the strong interaction of amine groups with the

CO_2. Thus, a lower loading range of 1 – 10 wt.% was adopted for the amine-functionalized Zeolite-Y sorbent. However, future work needs to explore even lower cation loadings to validate their impact and sensitive influence. Needless to say, such efforts may require advanced and sensitive characterization techniques.

Theoretically, while the doping of the Zeolite-Y with K^+ ions enhances the basicity and adsorption sites, the functionalization with amines introduces chemisorptive interactions with CO_2. Accordingly, a synergistic combination of these processes will propel and substantially improve the adsorption efficiency. However, the conducted Ph.D. thesis research works did not explore this perspective. Henceforth, future research investigations can be devoted to the optimization of the sequence and degree of the associated modifications for the maximization of the CO_2 taken along with the material's stability and reusability. Additionally, the targeted research works carefully to avoid detrimental issues such as pore blockage and reduced adsorption site accessibility.

The inherent differences in the gas properties and associated interaction mechanisms are responsible for the choice of the Virial isotherm as the best-fit model for CO_2 sorption data and the Langmuir isotherm as the best-fit model for CH_4 and N_2 sorption data. The high quadrupole moment of CO_2 and its ability to interact strongly with adsorbent surfaces renders the Virial isotherm to be the most appropriate as it accounts for both adsorbate-adsorbent interactions as well as adsorbate-adsorbate interactions. However, in contrast, the non-polar CH_4 and N_2 gases with weaker and enhanced uniform interactions align well with the assumption of the monolayer adsorption on a homogenous surface i.e., with the Langmuir isotherm model. These distinctions underscore the need for model selection based on the physical characteristics of the investigated system.

Due to pertinent experimental constraints and optimization of the adsorbent performance, the PhD thesis research works were carried out upto 4 adsorption-desorption cycles. The observed stability in these cycles ascertained confidence levels with respect to the potential of the synthesized materials. However, for the assessment of the long-term reusability of the sorbents, larger cycles (upto 8) shall be considered in the testing phase. Such studies shall be addressed in future efforts and with extended cyclic studies, the adsorbents' robustness towards industrially relevant conditions can be confirmed. Thereby, apart from the longevity of the sorbents in real-time applications, the data can be analyzed for further optimization of the materials design and associated regeneration protocols.

In the Ph.D. thesis research works it has been established that the K_2CO_3 sorbent is a readily available low-cost sorbent that can serve as a highly effective cation source for improved CO_2 adsorption. However, a detailed economic analysis that infers upon the economic feasibility of the sorbent would further strengthen the argument. Such a study is beyond the scope of the objectives undertaken in the Ph.D. thesis research works. Accordingly, in the near future, based on the costs of the raw materials, processes, and performance with alternate cation sources, the economic feasibility shall be addressed in quantitative format for the relevance of the sorbent for industrial and real-time applications.

5.5 Summary

In this study, potassium-loaded Zeolite-Y was synthesized through an impregnation approach that significantly enhanced carbon dioxide adsorption capacity. The carbon dioxide gas adsorption studies were performed at 303 K, 323 K, and 343 K in a gravimetric adsorption system. Based on the experimental results, KYZC10 (10 wt.% loading of K_2CO_3 on support) was determined to be the optimized adsorbent which gives maximum equilibrium adsorption capacity (3.61 mmol g^{-1}) at atmospheric pressure (1 bar). A thermodynamic study was also conducted on the synthesized adsorbents with three potassium carbonate loading (5 wt.%, 10

wt.%, and 15 wt.%) on support. Among the three synthesized adsorbents, KYZC10 was considered to be an optimized adsorbent due to its high carbon dioxide uptake. Subsequently, the optimized adsorbent was used to carry out adsorption studies (CO_2, CH_4, and N_2) at three different temperatures (303 K, 323 K, and 343 K) along with the carbon dioxide cyclic adsorption/desorption process. This study also used the Ideal Adsorbed Solution Theory (IAST) to predict CO_2 selectivity over other gases (CH_4 and N_2). This adsorbent exhibited good stability during cyclic performance, indicating that it was a potential candidate for carbon dioxide separation. In conclusion, KYZC10 adsorbent performed better CO_2 adsorption concerning adsorption capacity and selectivity in comparison to all synthesized adsorbents.

References

[1] N. Masoud, G. Bordanaba-Florit, T. van Haasterecht, J.H. Bitter, Effect of Support Surface Properties on CO_2 Capture from Air by Carbon-Supported Potassium Carbonate, Ind. Eng. Chem. Res. 60 (2021) 13749–13755. https://doi.org/10.1021/acs.iecr.1c01229.

[2] J.A. Oyebanji, P.O. Okekunle, O.S.I. Fayomi, Synthesis, and characterization of zeolite-Y using Ficus exasperate leaf: A preliminary study, Case Stud. Chem. Environ. Eng. 2 (2020) 100063. https://doi.org/10.1016/j.cscee.2020.100063.

[3] A. Mekki, A. Benmaati, A. Mokhtar, M. Hachemaoui, F. Zaoui, H. Habib Zahmani, M. Sassi, S. Hacini, B. Boukoussa, Michael Addition of 1,3-Dicarbonyl Derivatives in the Presence of Zeolite Y as an Heterogeneous Catalyst, J. Inorg. Organomet. Polym. Mater. 30 (2020) 2323–2334. https://doi.org/10.1007/s10904-019-01424-5.

[4] B. Fareed, F. Sher, S. Sehar, T. Rasheed, F. Zafar, M. Ameen, E.C. Lima, Tailor-made Functional Zeolite as Sustainable Potential Candidates for Catalytic Cracking of Heavy Hydrocarbons, Catal. Letters. 152 (2022) 732–744. https://doi.org/10.1007/s10562-021-03657-x.

[5] S. Manadee, O. Sophiphun, N. Osakoo, N. Supamathanon, P. Kidkhunthod, N. Chanlek, J. Wittayakun, S. Prayoonpokarach, Identification of potassium phase in catalysts supported on zeolite NaX and performance in transesterification of Jatropha seed oil, Fuel Process. Technol. 156 (2017) 62–67. https://doi.org/10.1016/j.fuproc.2016.09.023.

[6] S. Sengupta, V. Amte, R. Dongara, A.K. Das, H. Bhunia, P.K. Bajpai, Effects of the Adsorbent Preparation Method for CO_2 Capture from Flue Gas Using K_2CO_3/Al_2O_3 Adsorbents, Energy & Fuels. 29 (2015) 287–297. https://doi.org/10.1021/ef501792c.

[7] B. Fareed, F. Sher, S. Sehar, T. Rasheed, F. Zafar, M. Ameen, E.C. Lima, Tailor made Functional Zeolite as Sustainable Potential Candidates for Catalytic Cracking of Heavy Hydrocarbons, Catal. Letters. 152 (2022) 732–744. https://doi.org/10.1007/s10562-021-03657-x.

[8] P. Chaiwang, B. Chalermsinsuwan, P. Piumsomboon, Thermogravimetric Analysis and Chemical Kinetics for Regeneration of Sodium and Potassium Carbonate Solid Sorbents, Chem. Eng. Commun. 203 (2016) 581–588. https://doi.org/10.1080/00986445.2015.1078796.

[9] Z. Zhang, M. Hu, B. Lv, J. Kang, J. Tang, Z. Fei, X. Chen, Q. Liu, M. Cui, X. Qiao, Solvent-Assisted Stepwise Redox Approach To Generate Zeolite NaA-Supported K_2O as Strong Base Catalyst for Michael Addition of Ethyl Acrylate with Ethanol, ACS Omega. 3 (2018) 10188–10197. https://doi.org/10.1021/acsomega.8b00704.

[10] O. Talu, Needs, status, techniques and problems with binary gas adsorption experiments, Adv. Colloid Interface Sci. 76–77 (1998) 227–269. https://doi.org/10.1016/S0001-8686(98)00048-7.

CHAPTER 6

Conclusions and Future Scope

Chapter 6

Conclusions and Future Scope

In this chapter, section 6.1 describes the major conclusions that have been summarized from the Ph.D. thesis research works. Section 6.2 summarizes recommendations for future research work in the addressed research sub-themes.

6.1 Conclusions

6.1.1 Selection of Zeolite-Y as the best commercial sorbent

The primary aim of the Ph.D. thesis was to conduct a comprehensive assessment of the adsorptive properties of commercially available zeolites, amine-functionalized best-performing commercial zeolites, and cation-loaded best-performing commercial zeolites. The initial phase of the research focused on the selection of Zeolite-Y as the support material. Subsequent research activity explored the effects of amine functionalization and cation loading on the mentioned support. Gases with industrial significance such as carbon dioxide, methane, and nitrogen, were selected for the adsorption studies. This is due to their diverse range of polarity and polarizability. The adsorption isotherms of these gases were meticulously assessed for the mentioned. Thereby, a relationship between the adsorption dynamics and the physical properties of the adsorbates was sought and achieved.

The rationale behind the specific selection of Zeolite-Y stems from its impressive structural attributes, such as high surface area, substantial pore volume, and an adaptable framework that allows for significant modifications such as amine-functionalization or cation exchange. These characteristics render Zeolite-Y to be an excellent candidate for gas adsorption applications. Furthermore, the use of Zeolite-Y and its modified counterparts within this study has been based on the proven effectiveness of the adsorbents in selectively adsorbing specific gases. Such a trait is very important for industrial applications that demand the capture of selected

gases. The research problem formulation encapsulates the pivotal achievements and converges to major conclusions. These precisely summarize the works undertaken and their findings.

6.1.2 Amine-functionalized Zeolite-Y characteristics

- The results indicated successful dispersion of amines (monoethanolamine, diethanolamine, and triethanolamine) on the adsorbent surface. Thus, the pore structure of Zeolite-Y was substantially occupied by the amines.
- The modified adsorbents, MEOH5, DEOH5, and TEOH5, reached maximum CO_2 uptake capacities of 2.26, 1.84, and 1.62 mmol g^{-1} adsorbents, respectively. Thus, MEOH5 has been the most efficient for CO_2 adsorption.
- The adsorption process was primarily governed by physical interactions, with the functional groups $–NH_2$, -NH, and -N acting as the principal active sites to facilitate the selective CO_2 sorption mechanism.
- Thermodynamic analysis confirmed that the CO_2 adsorption behavior aligned closely with the Virial adsorption isotherm model.
- The heat of adsorption values followed the sequence of MEOH (22.59 kJ mol^{-1}) > DEOH (21.88 kJ mol^{-1}) > TEOH (21.87 kJ mol^{-1}). This signified a stronger interaction between CO_2 molecules and the MEOH-functionalized adsorbent.
- Monoethanolamine (MEOH) modification demonstrated enhanced adsorptive interactions. Thus, the MEOH-functionalized Zeolite-Y is a promising candidate for the targeting of economic challenges that are linked to CO_2 sequestration.
- Four continuous adsorption-desorption cycles were performed to evaluate the cyclic performance of the optimized MEOH5 adsorbent at 303 K and up to 1 bar with pure CO_2. The CO_2 adsorption capacity marginally reduced from 2.26 mmol g^{-1} in the first cycle to

2.19 mmol g^{-1} after four cycles. This affirmed the long-term usage potential of the sorbent with minimal adsorption loss

- The IAST predicted selectivity of optimized adsorbent (MEOH5) for two binary mixtures CO_2/CH_4 and CO_2/N_2 was 157.59 and 143.77 at 303 K and 1 bar.
- In summary, the MEOH-functionalized Zeolite-Y has a significant potential for future applications in CO_2 capture technologies.

6.1.3 Cation-loaded Zeolite-Y

- Among Li^+, Na^+, and K^+ ions based alternate cation-loaded Zeolite-Y, the potassium-modified sorbent has been the best in terms of sub-sequentially higher adsorption. This is attributed to increased basicity.
- For all sorbents, CO_2 sorption was primarily influenced by the isosteric heat of adsorption (such as CO_2 has 33.19 kJ mol^{-1}, CH_4 has 32.13 kJ mol^{-1}, and N_2 has 20.56 kJ mol^{-1} for KYZC adsorbent).
- The CO_2 adsorption data was effectively described by the Virial isotherm model. However, CH_4 and N_2 adsorption data were best assessed by the Langmuir isotherm model. Thus, the mentioned models could accurately represent the adsorption mechanism of the mentioned gases at the process conditions (1 bar, 303 – 343 K).
- The CO_2 engages in a dual-point interaction. This is associated with both the exchangeable cation and the adjacent lattice oxygen atoms located in the contiguous 12-membered ring (12-MR) windows of the Zeolite-Y structure.
- Variations in CO_2 adsorption were explained by the cation-oxygen dipole coupling with the CO_2 quadrupole moment. This is influenced by the basicity or effective charge of the oxygen atoms within the Zeolite framework.

- Selectivity for the CO_2/CH_4 and CO_2/N_2 binary mixtures was determined with Ideal Adsorbed Solution Theory (IAST), with 5 mol% CO_2 for the CO_2/CH_4 mixture and 13 mol% CO_2 for the CO_2/N_2 mixture. The KYZC adsorbent exhibited higher selectivity for both cases (219.59 for CO_2/CH_4 and 140.62 for CO_2/N_2 mixtures) at 303 K and 1 bar condition. This is attributed to its enhanced basicity and stronger interactions with CO_2 in comparison with the CH_4 and N_2.

6.1.4 Optimally loaded potassium-exchanged Zeolite-Y sorbent characteristics

- KYZC10, with a 10 wt.% K_2CO_3 loading on Zeolite-Y has been the most effective sorbent, as the material achieved the highest equilibrium adsorption capacity of 3.61 mmol g^{-1} at standard atmospheric pressure and 303 – 343 K temperature range.
- Thermodynamic studies with variant potassium carbonate loadings (5 wt.%, 10 wt.%, and 15 wt.%), inferred that the KYZC10 has been the optimal adsorbent for CO_2 capture.
- Cyclic adsorption-desorption tests affirmed that the KYZC10 maintained consistent performance in successive eight adsorption-desorption cycles (3.61–3.51 mmol g^{-1}). This affirmed its stability and potential for CO_2 adsorption applications.
- Selectivity for CO_2/CH_4 and CO_2/N_2 binary mixtures was determined using Ideal Adsorbed Solution Theory (IAST), with 5 mol% CO_2 for CO_2/CH_4 (273.63) and 13 mol% CO_2 for CO_2/N_2 (202.74) at 303 K and atmospheric pressure.
- With increasing binary mixture pressure, selectivity decreased exponentially. This is due to the competitive adsorption of CO_2 with respect to CH_4. Also, comparable polarizability has been confirmed.
- For the CO_2/N_2 system, lower selectivity was observed due to nitrogen's larger molecular size, which prompts it to occupy the pores of the adsorbent.

- The reduced CO_2 selectivity for binary gas mixtures was noted with temperature alteration from 303 K to 343 K. This attributed to a significant reduction in electrostatic interactions for CO_2 in comparison to CH_4 and N_2 and at higher temperatures.

6.2 Future Scope

The following areas have been identified for possible research in the addressed sub-research themes of the Ph.D. thesis.

- Investigate the effects of other alkaline cations (such as Mg, Ca) on the adsorption performance of Zeolite-Y. Thereby, cations with even superior adsorptive characteristics can be identified along with their composition.
- Conduct comprehensive kinetic studies to assess the rate of adsorption and desorption. Such studies provide insights into the practical application of these materials in dynamic industrial processes.
- Examine the adsorption thermodynamics at different temperatures and pressures. Thereby, a comprehensive, rigorous, and versatile understanding of the best material's performance for wider process conditions can be achieved.
- Focus on the long-term stability and regeneration efficiency of cation-loaded Zeolite-Y. Thereby, ensuring economic viability for repeated use in commercial applications.
- Evaluate the performance of synthesized zeolite adsorbents using real industrial gas streams rather than idealized gas mixtures. Thereby, assess upon the selectivity of cation-loaded Zeolite-Y in more constrained and real-world scenarios.
- The CO_2 adsorption performance of the synthesized adsorbents shall be assessed at variant levels of the RH. Accordingly, the best fitness of the best-performing sorbents can be ascertained in real-world scenarios.
- Future research should focus on the evaluation of the performance of synthesized zeolite adsorbents with real industrial gas streams but not idealized gas mixtures. The presence of

impurities, such as sulphur compounds, moisture, and other trace contaminants, could affect adsorption efficiency and material stability. Henceforth, a deeper understanding of these interactions is very important for the assessment of the long-term durability and economic feasibility of zeolites for CO_2 capture applications in industrial processing schemes.

In summary, elucidating upon the foundational aspects, future investigations need to develop and evaluate Zeolite-based adsorbents for CO_2 capture and shall explore research sub-themes such as adsorbent performance optimization under variant conditions and for alternate cation modifications. Deeper explorations in the undertaken field of study shall address molecular interactions between CO_2 and adsorbents and shall eventually facilitate the effective and efficient design of tailored sorbents for CO_2 capture. Such studies shall involve advanced characterization techniques and computational modeling approaches for the assessment of competent adsorption mechanisms. Accordingly, features that govern CO_2 uptake at the molecular level can be effectively explored. Also, the influence of material aging, structural changes under long-term cycling, and the sensitive influence of multi-component gas mixtures on adsorption behavior shall be considered competent research sub-themes. In summary, the conduct of future research works with the foundational and deeper research sub-themes will ill facilitate the design and development of cost-competitive and optimal adsorbent systems with enhanced CO_2 capture in real-world applications.

Appendix A2.1: Visual representation of commercial and synthesized adsorbents

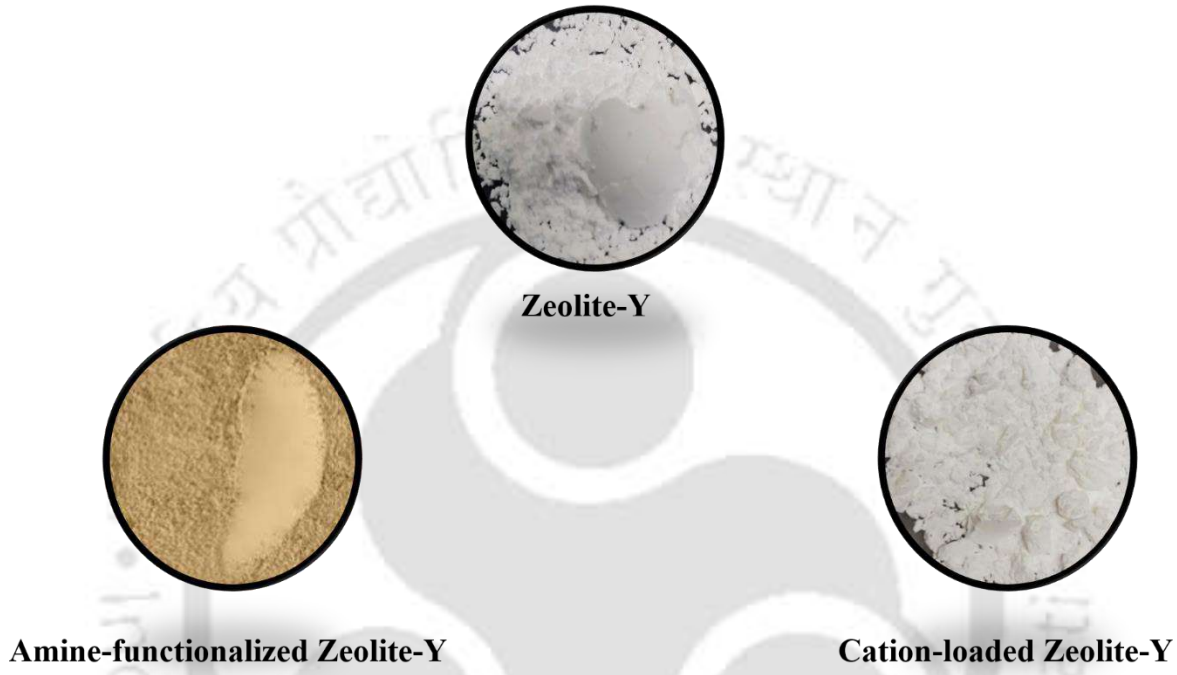

Appendix A3.1: Adsorption capacity sample calculation

The steps outlined below detail the procedure used to determine the carbon dioxide adsorption capacity of the commercial Zeolite-Y adsorbent at 303 K and 1 bar. These calculations are consistent and have been applied to all adsorbents studied to assess their gas adsorption capacities.

1. Note down the reading of ZP, MP1, MP2, temperature, and pressure from control panel

ZP = 0.00215 gm

MP1 = 9.59285 gm

MP2 = 29.12661 gm

T = 30°C

P = 751 mmHg

2. Convert the temperature into Kelvin

T = 303K

3. Calculate B^{gas}

$$B^{gas} = B_1 + \frac{B_2}{T} + \frac{B_3}{T^3} + \frac{B_4}{T^8} + \frac{B_5}{T^9}$$

$B_1 = 5.440*10^{-2}$ m^3kmol^{-1}

$B_2 = -3.635*10^{1}$ m^3kmol^{-1} K^3

$B_3 = -1.496*10^{6}$ m^3kmol^{-1} K^8

B_4 = 8.590*10^{16} m^3kmol^{-1} K^9

B^{gas} = -118.784761 cc mol^{-1}

4. Convert pressure into bar

$$P\ (bar) = \frac{-1.01325}{760} \times \left((P(mmHg) \times slope) + Intercept\right)$$

For pressure gauge = 3 (20000 torr),

Slope = 1

Intercept = 14

P = 1.02 bar

5. Density (mg cc^{-1})

$$density = \left(\frac{-1 + \sqrt{\left(1 + 4 \times B^{gas} \times 0.000001 \times P \times \frac{100000}{T \times R}\right)}}{(2 \times B^{gas} \times 0.000001) \times \frac{M.W. \times 1000}{1000000}} \right)$$

where,

M.W. = Molecular weight of carbon dioxide (44 g mol^{-1})

Density = 1.79 mg cc^{-1}

6. Difference of weights

MP1 – ZP = 9.59070 gm

MP2 – MP1 = 19.53376 gm

MP1 – ZP0 = 9.54438 gm (under vacuum condition)

MP2 – MP10 = 19.54108 gm (under vacuum condition)

7. Buoyancy correction, bucket = 1.29642 mg

$$buoyancy\ correction, bucket = density \times (volume\ of\ (bucket + hangdown))$$

where,

volume of (bucket + hang down) = 0.7242 cc

8. Weight of M_{net} and M_0

$$(M_{net} + M_0) = \left(\frac{buoyancy\ correction, bucket}{1000}\right) + (MP1 - ZP)$$

M_{net} + M_0 = 9.59200 gm

9. N_{net} (mmol g^{-1})

$$N_{net} = \left(\frac{(M_{net} + M_0)}{M.W.}\right) \times \left(\frac{1000}{Adsorbent\ wt.}\right)$$

N_{net} = 1.82966 mmol g^{-1}

10. Buoyancy correction, sinker = 2.48836 mg

$$buoyancy\ correction, sinker = V - ratio \times \big((MP2 - MP10) - (MP2 - MP1)\big) \times 1000$$

where,

$$V - ratio = \frac{slope\ of\ MP1}{slope\ of\ MP2}$$

The slope of MP1 (linear graph between density as the x-axis and (MP1-ZP) as the y-axis)

Slope of MP2 (linear graph between density as x-axis and (MP2-ZP) as y-axis)

11. Buoyancy correction, density = 2.58456 mg

$$buoyancy\ correction, density = density \times MP1\ slope$$

12. True mass in vacuum = 9.59328 gm

$$true\ mass\ in\ vacuum = \frac{buoyancy\ correction, density}{1000} + (MP1 - ZP)$$

13. Adsorption capacity, N = **1.869 mmol g^{-1}**

$$N = \frac{\left(true\ mass\ in\ vacuum - (MP1 - ZP0)\right)}{M.W.} \times \frac{1000}{Adsorbent\ wt.}$$

Appendix A3.2: Adsorption isotherm model parameters for optimized material (MEOH5)

Isotherm	Gas	Parameters	Coefficient	R^2
Virial	CO_2	$\beta^0 \times 10^3$, mmol g^{-1} bar^{-1}	7.192	0.9996
		β^1, K	-2634.2	
		b^0, $mmol^{-1}$ g	2.733	
		b^1, $mmol^{-1}$ g K	-600.4	
		c^0, $mmol^{-2}$ g^2	-1.675	
		c^1, $mmol^{-2}$ g^2 K	495.4	
Langmuir	CH_4	N^{max}, mmol g^{-1}	0.29	0.9975
		$\beta^0 \times 10^3$, mmol g^{-1} bar^{-1}	1.25	
		β^1, K	1018.3	
Langmuir	N_2	N^{max}, mmol g^{-1}	0.09	0.9726
		$\beta^0 \times 10^3$, mmol g^{-1} bar^{-1}	0.942	
		β^1, K	870.5	

Appendix A4.1: Adsorption isotherm model parameters for HYZC adsorbent

Isotherm	Gas	Parameters	Coefficient	R^2
Virial	CO_2	$\beta^0 \times 10^3$, mmol g^{-1} bar^{-1}	3.061	0.9999
		β^1, K	-1528.6	
		b^0, $mmol^{-1}$ g	2.553	
		b^1, $mmol^{-1}$ g K	-588.2	
		c^0, $mmol^{-2}$ g^2	-0.699	
		c^1, $mmol^{-2}$ g^2 K	203.9	
Langmuir	CH_4	N^{max}, mmol g^{-1}	0.21	0.9994
		$\beta^0 \times 10^3$, mmol g^{-1} bar^{-1}	1.80	
		β^1, K	1582.9	
Langmuir	N_2	N^{max}, mmol g^{-1}	0.09	0.9826
		$\beta^0 \times 10^3$, mmol g^{-1} bar^{-1}	1.48	
		β^1, K	1278.8	

Appendix A4.2: Adsorption isotherm model parameters for LiYZC adsorbent

Isotherm	Gas	Parameters	Coefficient	R^2
Virial	CO_2	$\beta^0 \times 10^3$, mmol g^{-1} bar^{-1}	8.572	0.9999
		β^1, K	-3416.2	
		b^0, $mmol^{-1}$ g	8.434	
		b^1, $mmol^{-1}$ g K	-3059.8	
		c^0, $mmol^{-2}$ g^2	-1.823	
		c^1, $mmol^{-2}$ g^2 K	630.6	
Langmuir	CH_4	N^{max}, mmol g^{-1}	0.192	0.9998
		$\beta^0 \times 10^3$, mmol g^{-1} bar^{-1}	6.46	
		β^1, K	1613.1	
Langmuir	N_2	N^{max}, mmol g^{-1}	0.09	0.9908
		$\beta^0 \times 10^3$, mmol g^{-1} bar^{-1}	2.10	
		β^1, K	1411.4	

Appendix A4.3: Adsorption isotherm model parameters for NaYZC adsorbent

Isotherm	Gas	Parameters	Coefficient	R^2
Virial	CO_2	$\beta^0 \times 10^3$, mmol g^{-1} bar^{-1}	9.709	0.9999
		β^1, K	-4260.2	
		b^0, $mmol^{-1}$ g	10.497	
		b^1, $mmol^{-1}$ g K	-3062.1	
		c^0, $mmol^{-2}$ g^2	-2.994	
		c^1, $mmol^{-2}$ g^2 K	995.9	
Langmuir	CH_4	N^{max}, mmol g^{-1}	0.24	0.9998
		$\beta^0 \times 10^3$, mmol g^{-1} bar^{-1}	7.033	
		β^1, K	1779.9	
Langmuir	N_2	N^{max}, mmol g^{-1}	0.12	0.9986
		$\beta^0 \times 10^3$, mmol g^{-1} bar^{-1}	2.42	
		β^1, K	1526.6	

Appendix A4.4: Adsorption isotherm model parameters for KYZC adsorbent

Isotherm	Gas	Parameters	Coefficient	R^2
Virial	CO_2	$\beta^0 \times 10^3$, mmol g^{-1} bar^{-1}	15.506	0.9999
		β^1, K	-5720.4	
		b^0, $mmol^{-1}$ g	11.025	
		b^1, $mmol^{-1}$ g K	-3247.4	
		c^0, $mmol^{-2}$ g^2	-4.159	
		c^1, $mmol^{-2}$ g^2 K	1241.9	
Langmuir	CH_4	N^{max}, mmol g^{-1}	0.24	0.9998
		$\beta^0 \times 10^3$, mmol g^{-1} bar^{-1}	7.43	
		β^1, K	1939.6	
Langmuir	N_2	N^{max}, mmol g^{-1}	0.14	0.9992
		$\beta^0 \times 10^3$, mmol g^{-1} bar^{-1}	4.52	
		β^1, K	1536.4	

Appendix A5.1: Adsorption isotherm model parameters for optimized material (KYZC10)

Isotherm	Gas	Parameters	Coefficient (Std. Error)	R^2
Virial	CO_2	$\beta^0 \times 10^3$, mmol g^{-1} bar^{-1}	19.053	0.9999
		β^1, K	-6994.9	
		b^0, $mmol^{-1}$ g	11.193	
		b^1, $mmol^{-1}$ g K	-3872.1	
		c^0, $mmol^{-2}$ g^2	-6.526	
		c^1, $mmol^{-2}$ g^2 K	1489.4	
Langmuir	CH_4	N^{max}, mmol g^{-1}	0.82	0.9999
		$\beta^0 \times 10^3$, mmol g^{-1} bar^{-1}	9.63	
		β^1, K	3280.3	
Langmuir	N_2	N^{max}, mmol g^{-1}	0.05	0.9998
		$\beta^0 \times 10^3$, mmol g^{-1} bar^{-1}	5.43	
		β^1, K	2232.4	